50376
1992
5

BIBLIOTHEQUE INTERUNIVERSITAIRE
SECTION DE SCIENCES
LILLE

61591

50376
1992
5

N° d'ordre : H 34

Université des Sciences et Technologies de Lille

Travaux présentés par

Colette BROGNIEZ

en vue de l'obtention de

L'HABILITATION A DIRIGER DES RECHERCHES EN SCIENCES PHYSIQUES

Soutenance le 5 février 1992

devant le jury composé de :

J. LENOBLE	Professeur à l'Université de Lille,	rapporteur
W.P. CHU	Research Scientist à la NASA,	rapporteur
H. JAGER	Docteur Rerum Naturarum au Fraunhofer-Institut, Garmisch-Partenkirchen, RFA	rapporteur
M. ACKERMAN	Directeur de l'Institut d'Aéronomie Spatiale de Belgique	examinateur
A. BAUER	Chargée de Recherches au CNRS,	examinateur
M.L. CHANIN	Directeur de Recherches au CNRS,	examinateur
M. HERMAN	Professeur à l'Université de Lille,	examinateur
R. SANTER	Maître de Conférences à l'Université de Lille,	examinateur

U. F. R. de Physique Fondamentale
Laboratoire d'Optique Atmosphérique

A mon mari,

A Philippe, Hélène, Stéphane,

A mes parents.

Remerciements

J'adresse mes sincères remerciements à Madame Lenoble, Professeur à l'Université de Lille, qui m'a accueillie dans son équipe et qui m'a suivie et conseillée efficacement pendant toutes ces années.

Monsieur Chu, Research Scientist à la NASA, nous a permis de comparer notre inversion des données SAGE II à la sienne et me fait l'honneur d'être rapporteur, je l'en remercie vivement.

J'exprime tout particulièrement ma reconnaissance à Monsieur Jäger, Docteur Rerum Naturarum au Fraunhofer-Institut à Garmisch-Partenkirchen , pour son étroite collaboration et pour avoir accepté de rapporter sur mon travail.

Monsieur Ackerman, directeur de l'Institut d'Aéronomie Spatiale de Belgique, nous a transmis ses mesures au limbe et a bien voulu juger mon travail, je l'en remercie sincèrement.

Madame Chanin, directeur de Recherches au CNRS, et Madame Bauer, chargée de Recherches au CNRS ont accepté d'examiner cette thèse, je leur en suis reconnaissante.

Je voudrais également remercier Monsieur Herman, Professeur à l'Université de Lille et directeur du Laboratoire, pour l'intérêt qu'il a pris aux différentes parties de ce travail.

J'exprime toute ma gratitude à Monsieur Santer, Maître de Conférences à Lille, pour ses nombreuses discussions concernant l'expérience RADIBAL.

Messieurs Pruvost et Diallo ont contribué au succès de l'analyse des mesures SAGE II et RADIBAL, je les en remercie.

Enfin je n'oublierai pas de remercier Madame Deroo, informaticienne, pour l'aide précieuse qu'elle m'a apportée.

SOMMAIRE

Introduction

Le travail présenté dans cette thèse constitue mon activité de recherche effectuée sous la direction de Madame Lenoble au Laboratoire d'Optique Atmosphérique de l'Université des Sciences et Technologies de Lille.

Les aérosols stratosphériques, dont l'origine est principalement volcanique, jouent un rôle important dans les études climatiques, ce qui nous a conduits à nous intéresser à leurs caractéristiques (nature des particules, spectre dimensionnel, abondance) et aux variations aussi bien temporelles que spatiales de ces paramètres.

Une première approche a consisté en l'étude comparative des différents modèles d'aérosols troposphériques et stratosphériques proposés par la Commission Radiation de IAMAP (International Association of Meteorology and Atmospheric Physics).

L'opportunité d'appliquer les résultats obtenus s'est rapidement présentée, le laboratoire ayant eu accès, grâce à J. Lenoble, tout d'abord aux données SAGE (Stratospheric Aerosol and Gas Experiment) qui était une expérience d'occultation solaire menée par la NASA de février 1979 à novembre 1981, puis aux données SAGE II qui est une expérience du même type ayant débuté en Octobre 1984 et qui se poursuit actuellement.

J'ai étudié les coefficients d'extinction des aérosols stratosphériques ainsi que les possibilités de détermination des caractéristiques de ces aérosols à partir des mesures spectrales de coefficients d'extinction. Des expériences corrélatives (mesures au sol, mesures ballon) ont été menées afin de procéder à la validation des résultats obtenus.

Parallèlement à cette analyse des données journalières je me suis intéressée aux coefficients d'extinction moyennés sur des bandes de latitude de 10° pendant des périodes voisines de un mois. L'intérêt d'une telle étude réside dans le fait qu'elle permet d'élaborer des modèles qui ne sont plus seulement valables à un instant donné et en un endroit précis. On aboutit à la description d'une atmosphère "moyenne" utile pour des études climatiques à grande échelle.

1 Etude des modèles d'aérosols

Les nombreux modèles d'aérosols troposphériques et stratosphériques existant ont été analysés et comparés afin de déterminer un modèle réaliste simple permettant de retrouver les caractéristiques radiatives des aérosols. On a pu ainsi montrer qu'une distribution log-normale de la taille des particules avec 2 paramètres ajustables convenait très bien pour représenter les aérosols stratosphériques et surtout qu'elle était d'un emploi souple (1).

J'ai contribué à l'étude des possibilités de détermination des caractéristiques des aérosols stratosphériques d'acide sulfurique à partir des mesures de coefficient d'extinction des aérosols à deux longueurs d'onde (1,02 et 0,45 μm qui sont les canaux SAGE). La conclusion de ce travail a été que les variations spectrales du coefficient d'extinction traduites par la loi d'Angström, permettent d'accéder à l'un des paramètres de la distribution de taille des particules en supposant connus leur forme, leur composition et le deuxième paramètre intervenant dans l'expression de la granulométrie.

Ces résultats ont été appliqués à l'étude des profils verticaux de coefficients d'extinction obtenus dans l'expérience SAGE après l'éruption du Mont S^t Helens en mai 1980, profils qui nous avaient été communiqués par la NASA. La comparaison directe à des coefficients d'extinction obtenus avant éruption en période non perturbée a montré que les expériences d'occultation du type SAGE étaient parfaitement adaptées à la mise en évidence de phénomènes volcaniques. Aussi bien sur des profils individuels que sur des profils moyennés, l'augmentation notable de l'extinction a été corrélée à une augmentation de la taille des aérosols et une structure en couches de particules de tailles différentes a pu également être mise en évidence avec particulièrement une région de petites particules au dessus d'une couche de grosses particules (2)(3)(4).

L'expérience SAGE ayant pris fin en 1981, une autre expérience du même type, SAGE II, a été lancée en octobre 1984 par la NASA et est toujours opérationnelle. Des canaux ont été ajoutés au spectromètre afin de permettre notamment une meilleure détermination des caractéristiques des aérosols. Pour cette expérience à laquelle le LOA est également associé, j'ai repris l'algorithme d'inversion des transmissions que J. Lenoble et P. Pruvost avaient amorcé pour l'expérience SAGE et je l'ai adapté et affiné. Cette étape s'est avérée très fructueuse puisqu'elle nous a permis d'évaluer l'importance relative des divers constituants de l'atmosphère et de mieux appréhender les différentes causes d'erreur dans la détermination des coefficients d'extinction. Cette inversion, menée en parallèle avec celle effectuée à la

NASA, a permis d'éclaircir différents points délicats dans chaque inversion, et donne des résultats en excellent accord avec les leurs, conduisant ainsi à la détermination des zones où les données fournies sont crédibles et celles où leur utilisation doit être faite avec prudence (6).

Par rapport à l'expérience SAGE, les deux longueurs d'onde suppémentaires pour lesquelles on obtient les coefficients d'extinction des aérosols (0,385 et 0,525 μm), permettent d'établir les variations spectrales de ce coefficient avec plus de précision. J'ai pu mettre au point un algorithme simple basé sur une loi d'Angström modifiée, permettant d'obtenir le rayon effectif de la granulométrie des aérosols comme précédemment, et une information supplémentaire : un ordre de grandeur de la variance effective. La restitution de la granulométrie est malheureusement limitée aux moyennes altitudes (16-23 km) en raison de la médiocre qualité du canal de courte longueur d'onde (5).

J'ai, en collaboration avec J. Lenoble, dirigé le travail de DEA de C. N'Doumé qui consistait à étudier les profils d'extinction aux dessus des zones désertiques et sahéliennes d'Afrique. L'altitude de la couche d'aérosols peut facilement se déceler sur les profils d'extinction à 1,02μm, et le transport vertical et horizontal des aérosols a pu être mis en évidence en sélectionnant des profils d'extinction qui descendaient assez bas. Néanmoins les dimensions des aérosols n'ont pu être déterminées de façon satisfaisante étant donnée l'absence des mesures aux courtes longueurs d'onde en basse altitude.

A Comparative Review of Radiation Aerosol Models

J. Lenoble[1]), C. Brogniez

Laboratoire d'Optique Atmosphérique ERA 466, Université des Sciences et Techniques de Lille, 59655 Villeneuve d'Ascq Cedex, France

(Manuscript received 22.04.1983, in revised form 04.07.1983)

Abstract:

The problem of aerosol modeling for radiative transfer computation is considered, with a purpose of homogenization. The main characteristics to be introduced into the model are recalled and some currently used "complete models" are reviewed. Comparison of the global TOON and POLLACK (1976) model with the set of the Standard Radiation Atmosphere (SRA) models (McCLATCHEY et al., 1980) leads to some suggestions for building an average global model with the SRA components. The "size distribution models" are also reviewed and compared concerning their main characteristics; a slight modification of the SRA stratospheric models is suggested.

Résumé: Revue comparative des modèles d'aérosols pour les calculs de transfert radiatif

On considère le problème de la modélisation des aérosols pour les calculs de transfert radiatif dans un but d'homogénéisation. Les principales caractéristiques à introduire dans le modèle sont rappelées et on passe en revue quelques «modèles complets» couramment utilisés. La comparaison du modèle global de TOON et POLLACK (1976) avec la série de modèles de la Standard Radiation Atmosphere (SRA) (McCLATCHEY et al., 1980) conduit à quelques suggestions pour bâtir un modèle global moyen avec les composantes SRA. On passe en revue aussi les «modèles de répartition dimensionnelle» et on compare leurs principales caractéristiques; une légère modification des modèles SRA pour la stratosphère est suggérée.

Zusammenfassung: Ein vergleichender Überblick über die Aerosol-Modellierung in Strahlungsübertragungsrechnungen

Das Problem der Aerosol-Modellierung für Strahlungsübertragungsrechnungen wird im Hinblick auf eine Vereinheitlichung dargestellt. Die Arbeit beschreibt die wesentlichen Modelleigenschaften und gibt einen Überblick über einige zur Zeit benutzte „vollständige Modelle". Der Vergleich des globalen Modells von TOON und POLLACK (1976) mit den Modellen der Strahlungs-Norm-Atmosphäre (SRA) (McCLATCHEY et al., 1980) führen zu einigen Anregungen für ein mittleres globales Modell mit den SRA Komponenten. Ebenso werden die „Modelle der Größenverteilung" behandelt und in ihren Haupteigenschaften verglichen; dabei wird eine kleine Modifikation der stratosphärischen SRA Modelle vorgeschlagen.

1 Introduction

In order to introduce aerosols into radiative transfer computations, it is necessary to fix their characteristics and when possible to represent them by analytical expressions. These aerosol models have of course to be as realistic as possible, but the necessity of having some standard models, used by the different authors in order to make their results comparable, has long been recognized. Recently the Radiation Commission of IAMAP has proposed a set of aerosol models within the framework of a Standard

---

[1]) This work was partly done when one of us (J.L.), was visiting the Institute for Atmospheric Optics and Remote Sensing as a senior scientist under a NASA contract NASI-17032.

Beitr. Phys. Atmosph. Vol. 57, No. 1, February 1984

0005-8173/84/01 0001–20 $ 03.00/0 © 1984 Friedrich Vieweg & Sohn Verlagsgesellschaft mbH

Radiation Atmosphere (McCLATCHEY et al., 1980). However, many different aerosol models have been and are still currently used and some clarification seems useful.

In the next section we will review the aerosol characteristics to be introduced into the models and try to clarify the terminology currently used in the modeling. Section 3 will be devoted to the comparison of models, with the main purpose to reconciliate the TOON and POLLACK (1976) global model with the Standard Radiation Atmosphere (SRA) models; the suggestion is being done to modify slightly the SRA profile VI. Section 4 reviews and compares the size distributions used in the different models; an homogeneization of the size distributions used in the SRA models is suggested.

2 Aerosol Characteristics and Different Kinds of Models

2.1 Physical Characteristics

The atmospheric aerosols are completely described by the total aerosol loading into a unit volume, their chemical composition, their shape, and their size distribution, given at each point within the atmosphere.

The shape is approximately spherical for liquid particles, but very irregular and variable for solid particles. Numerous studies, both experimental and theoretical (POLLACK and CUZZI, 1980) have been devoted to non-spherical particles and their radiative characteristics. However, their modeling still remains difficult and all current aerosol models assume spherical particles, relying on the hope that a large quantity of irregular particles behave on the average approximately as spherical ones. The size is therefore characterized by the particle radius r, and the size distribution by n(r), where Nn(r)dr holds for the number of particles per unit volume with a radius between r and r + dr; we have here normalized n(r) by

$$\int_0^\infty n(r)dr = 1, \qquad (1)$$

and we will retain this normalization throughout this paper. The particle number density N is a measure of the aerosol loading which can also be expressed by the aerosol mass or aerosol volume per unit volume of air.

The chemical composition is very variable, and many particles are probably complex and even non-homogeneous. The composition is of major importance and has to be known for a better understanding of the atmospheric processes of aerosol formation and removal (TWOMEY, 1977). However, it impacts on the radiative characteristics only by the aerosol refractive index $m = m' - im''$, where the imaginary part m'' is directly proportional to the absorption coefficient of the aerosol substance. The knowledge of the chemical composition may not lead directly to the value of m, even if the bulk refractive index of the aerosol substance is known, this being probably due to the particulate and inhomogeneous structure, as well as to the impurity inclusions which are not detected by chemical analysis. All models which are built for radiative studies have therefore to fix the refractive index of the aerosol, the composition being given only as informative.

In an air sample the aerosol particles can generally be classified into groups; within each group the refractive index is the same (m_i) for all the N_i particles, and the size distribution associated to this group will be referred to as $n_i(r)$. The total particle number density is $N = \Sigma_i N_i$, the sum being taken over all existing groups, and the number concentration is N_i/N for each group.

2.2 Radiative Characteristics

The radiative characteristics of a spherical particle of radius r, refractive index m, at a wavelength λ derive from the Mie theory. They are the extinction cross-section $Q_{ext}(\lambda, r, m)$, the scattering cross-section $Q_{scatt}(\lambda, r, m)$ and the angular distribution of the scattered light, characterized by a phase function $p(\lambda, r, m; \theta)$ where θ is the scattering angle; the phase function is normalized to 4π when integrated over a sphere. Instead of the scattering cross-section, we will preferably use the single scattering albedo $\bar{\omega}(\lambda, r, m) = Q_{scatt}/Q_{ext}$. We will not consider here the polarization effects of scattering, which can be taken care of by replacing the phase function by a 4 x 4 phase matrix. For N particles of the same kind with the normalized size distribution n(r) we will define the extinction coefficient as

$$\beta(\lambda) = N\int_0^\infty \pi r^2 Q_{ext}(\lambda, r, m)\, n(r)\, dr, \tag{2}$$

the scattering coefficient

$$\sigma(\lambda) = N\int_0^\infty \pi r^2 Q_{scatt}(\lambda, r, m)\, n(r)\, dr, \tag{3}$$

the single scattering albedo

$$\bar{\omega}(\lambda) = \frac{\sigma(\lambda)}{\beta(\lambda)}, \tag{4}$$

and the phase function

$$p(\lambda; \theta) = \frac{N}{\sigma(\lambda)}\int_0^\infty \pi r^2 p(\lambda, r, m; \theta) Q_{scatt}(\lambda, r, m)\, n(r)\, dr. \tag{5}$$

If the phase function is expanded into Legendre series, each of the expansion coefficient $\beta_\ell(\lambda)$ derives from the $\beta_\ell(\lambda, r, m)$ for each individual particle by an equation similar to Equation (5). Of particular interest is the asymmetry factor $g(\lambda) = \frac{1}{2}\int_0^\pi \cos\theta\, p(\lambda; \theta)\, d(\cos\theta)$, which is used in most of the approximate methods to solve the problem of radiative transfer and has a commanding influence on the results; as $g = \beta_1/3$, it can be generated from the individual $g(\lambda, r, m)$ by

$$g(\lambda) = \frac{N}{\sigma(\lambda)}\int_0^\infty \pi r^2\, g(\lambda, r, m)\, Q_{scatt}(\lambda, r, m)\, n(r)\, dr. \tag{6}$$

The single scattering albedo and the phase function (and the g factor) are specific characteristics of the kind of aerosols depending only on the size distribution and refractive index, whereas the extinction coefficient is proportional to the particle density number. However, its spectral variation, defined by $\beta(\lambda)/\beta(\lambda_0)$, where λ_0 is some reference wavelength is again a specific property of the aerosol type. For a mixture of different types of particles, the extinction and scattering coefficients, the single scattering coefficient, the phase function and the asymmetry factor derive respectively from

$$\beta(\lambda) = \sum_i N_i \beta_i(\lambda), \tag{7}$$

$$\sigma(\lambda) = \sum_i N_i \sigma_i(\lambda), \tag{8}$$

$$\bar{\omega}(\lambda) = \frac{\sum_i N_i \sigma_i(\lambda)}{\sum_i N_i \beta_i(\lambda)}, \tag{9}$$

$$p(\lambda;\theta) = \frac{\sum_i N_i \sigma_i(\lambda)\, p_i(\lambda;\theta)}{\sum_i N_i \sigma_i(\lambda)}, \tag{10}$$

$$g(\lambda) = \frac{\sum_i N_i \sigma_i(\lambda)\, g_i(\lambda)}{\sum_i N_i \sigma_i(\lambda)}, \tag{11}$$

where the subscript i refers to the parameters derived from Equations (2) to (6) for the particles of type i, and the sum is taken over all groups of particles.

The extinction coefficient is generally variable with altitude z, due to the aerosol profile N(z); we will define the optical thickness of an atmospheric layer between z_1 and z_2 by

$$\delta(\lambda) = \int_{z_1}^{z_2} \beta(\lambda, z)\, dz \tag{12}$$

where $\beta(\lambda, z)$ is the value of $\beta(\lambda)$ at the altitude z.

2.3 Radiation Aerosol Models

A "complete aerosol model" for radiation computations must give the size distribution n(r), the refractive index $m = m' - im''$ versus wavelength and the number density N, eventually for each type of particles ($n_i(r)$, m_i, N_i), including the vertical variations of n(r), m and N. As all horizontal variations are much smoother in the atmosphere than the vertical ones, the model will be assumed valid over some area around the considered location. A further simplification arises from the fact that the aerosol material defined by $n_i(r)$, m_i and N_i/N for each type of particles, can be assumed to remain constant within a finite (more or less thick) atmospheric layer, leaving within each layer N(z) to be the only parameter varying with the altitude z.

A first rough complete model has been proposed by McCLATCHEY et al. (1971) and has been intensively used. TOON and POLLACK (1976) have worked out a global average model based on a detailed review of existing experimental data. More recently, an effort has been made to obtain a series of models able to give at least an approximate description of most of the situations encountered in the real atmosphere. Based on the preliminary work of SHETTLE and FENN (1979), these models have been first described and their use recommended in a report of the International Radiation Commission working group on a Standard Radiation Atmosphere (McCLATCHEY et al., 1980). These complete models will be compared in the next section.

The term "aerosol model" is frequently used to name incomplete models, such as "size distribution models" or "material models" or "number density or extinction profile models." The most popular profile model is ELTERMAN's profile, which is based on an average of many experimental measures (ELTERMAN et al., 1969). Many different analytical expressions have been proposed to describe the size distribution and they will be reviewed in Section 4. They generally leave two, three or even more parameters to be adjusted to the particular problem or to an experimental set of data. When numerical values are attributed to the parameters, one can really speak of an aerosol size distribution model, such as the DEIRMENDJIAN's size distribution models (1969).

A lot of work has been recently and is currently done to measure aerosol characteristics and to build model by seeking a best fit with the data either at the stratosphere level (BIGG, 1976; GRAS and MICHAEL, 1979; PINNICK et al., 1976), or at the troposphere level (PATTERSON and GILLETTE, 1977; GOROCH et al., 1982). These studies will probably lead to an improvement of the existing models in a near future but their review is outside the scope of this paper.

3 Complete Radiation Models

3.1 Review of the Models

The most comprehensive set of models is the one recommended by the Radiation Commission working group on a Standard Radiation Atmosphere (McCLATCHEY et al., 1980), henceforth referred to as SRA. For the troposphere it comprises four basic components (type i) defined by their size distributions $n_i(r)$ and their refractive index $m_i(\lambda)$ between 0.2 and 40 μm, from which three "material models" are built by giving the volume concentration c_i^j of each component i in the material j; the number density concentration derives from

$$\frac{N_i^j}{N^j} = \frac{c_i^j/v_i}{\sum\limits_i c_i^j/v_i}, \quad \text{with} \quad v_i = \int_0^\infty r^3\, n_i(r)\, dr \qquad (13)$$

The size distributions are normalized in the SRA models, in order to fix the extinction coefficient of the material $\beta(0.55) = 1$ at $\lambda = 0.55\ \mu$m; we have found it more convenient and general to keep the normalization of Equation (1).

For the stratosphere two "material models" are proposed, each built of one single component. A complete description of the SRA models, including references to the sources of data used is given by the Radiation Commission of IAMAP (1983).

Table 1 gives the composition and the size distributions with the c_i^j values; for example, values of the refractive index are shown at 0.4 μm and 1 μm; the size distributions are described with more details in Section 4. The associated vertical extinction profiles lead to a set of six "complete aerosol models" for the low troposphere (0–6 km), two for the high troposphere (6–12 km), one for the unperturbed stratosphere, plus a variable model (over 30 years) for the volcanic stratosphere (12–30 km), and one model for the upper atmosphere (30–100 km). Figure 1 shows the different profiles for the extinction coefficient at

Table 1 Main Characteristics of the Aerosol Models (see text)
LND = Log Normal Distribution; MGD = Modified Gamma Distribution; TPL = Truncated Power Law.

	i	Component	$n_i(r)$ = LND					Material C_i^j %				
			r_m (μm)	σ		m_i(0.4 μm)	m_i(1.06 μm)	j = 1	j = 2	j = 3	j = 5	j = 6
SRA Materials	1	Water soluble	0.005	0.475		$1.53-5 \cdot 10^{-3}i$	$1.52-1.7 \cdot 10^{-2}i$	29	5	61		
	2	Dust-like	0.50	0.475		$1.53-8 \cdot 10^{-3}i$	$1.52-8 \cdot 10^{-3}i$	70		17		
	3	Soot	0.0118	0.301		$1.75-0.46i$	$1.75-0.44i$	1		22		
	4	Oceanic	0.30	0.400		$1.385-9.9 \cdot 10^{-9}i$	$1.367-6 \cdot 10^{-5}i$		95			
			$n_i(r)$ = MGD									
			α	β	γ							
	5	75 % H_2SO_4	1	18	1	$1.44-1 \cdot 10^{-8}i$	$1.42-1.5 \cdot 10^{-6}i$				100	
	6	Volcanic	1	16	0.5	$1.50-8 \cdot 10^{-3}i$	$1.50-8 \cdot 10^{-3}i$					100

j = 1 Continental
j = 2 Maritime
j = 3 Urban
j = 5 Stratosphere background
j = 6 Stratosphere volcanic

	i	Component	m_i(0.4 μm)	m_i(1.00 μm)	Material C_i^j %			
					j = 1	j = 2	j = 3	j = 4
TP Materials	1	Basalt	$1.52-9 \cdot 10^{-4}i$	$1.51-1.6 \cdot 10^{-3}i$	40	35		
	2	$(NH_4)2\,SO_4$	$1.54-1 \cdot 10^{-7}i$	$1.51-3.5 \cdot 10^{-7}i$	60	50		
	3	Sea Salt	$1.57-1 \cdot 10^{-7}i$	$1.53-1 \cdot 10^{-7}i$		15		
	4	75 % H_2SO_4	$1.44-1 \cdot 10^{-8}i$	$1.42-1.5 \cdot 10^{-6}i$			100	100

	$n_j(r)$ = TPL								$n_j(r)$ = zold			
ℓ	1	2	3	4	1	2	3	4	r_m(μm)	σ	r_m(μm)	σ
r_ℓ(μm) v_ℓ	0 − 1	0.045 2.6	5 4.6	30	0 − 1	0.1 2	5 4	50	0.035	2	0.1 to 1	1.8

j = 1: 3–12 km – j = 2: 0.3 km –
j = 4: Stratosphere background – j = 5: Stratosphere volcanic

	n(r) = TPL				m_i(0.4 μm)	m_i(1.06 μ)
MC Material	ℓ	1	2	3		
	r_ℓ(μm) v_ℓ	0.02 − 1	0.1 3	10	1.50−0.i	$1.50-3.29 \cdot 10^{-2}i$

Figure 1 Aerosol extinction profiles at λ = 0.55 μm for SRA (——), TP (— · —) and MC (•) models (see text) with ELTERMAN's profile (– – –) Notice the change of altitude scale at 12 km.
Some profiles have been shifted a little in order to make the different profiles appear clearly.
Circled numbers refered to the material (table 1)
Roman numbers refered to the different SRA tropospheric models.

▶

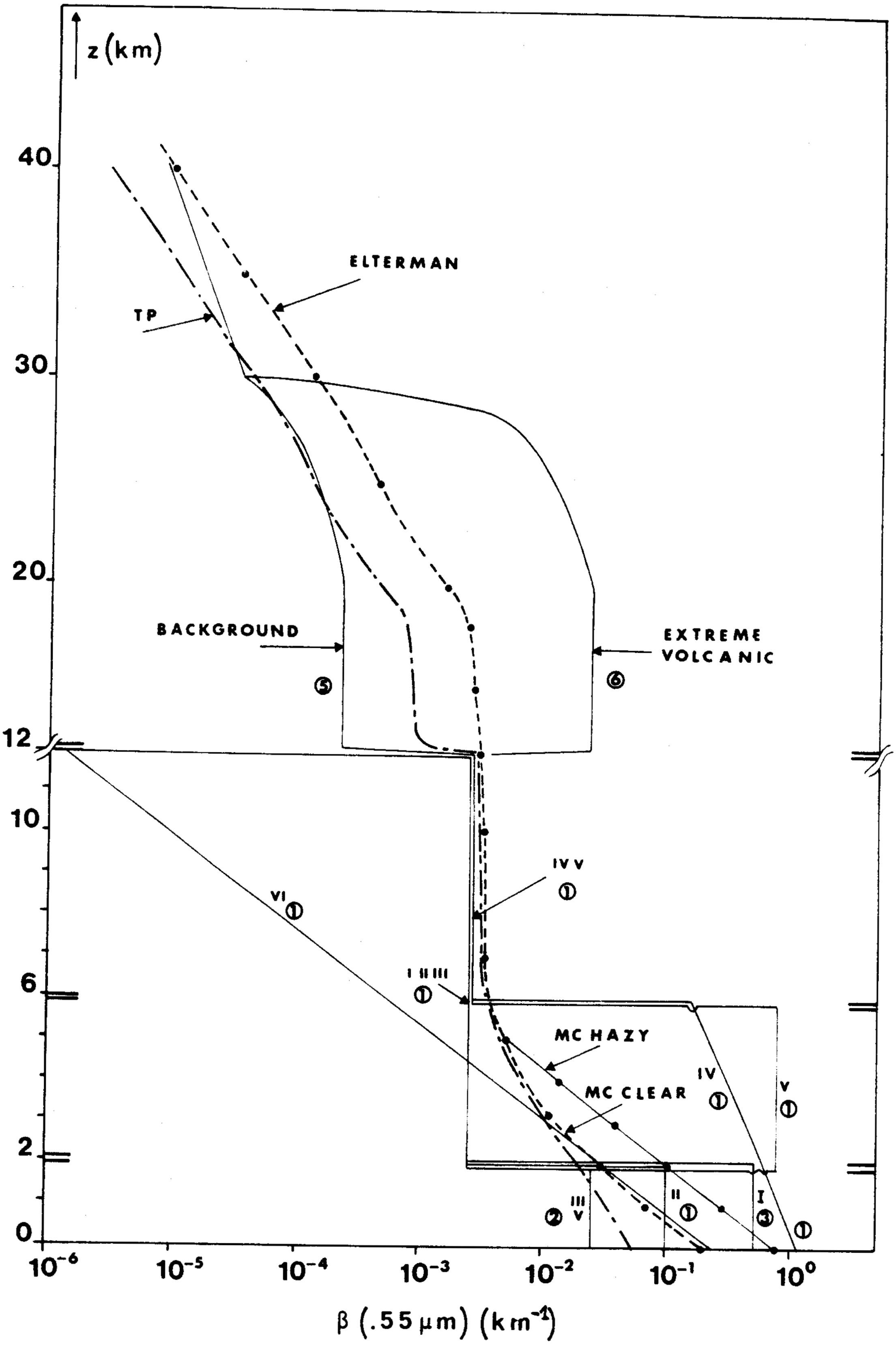
z (km)
40
30
20
12
10
6
2
0
ELTERMAN
TP
BACKGROUND
⑤
EXTREME VOLCANIC
⑥
IV V
①
VI ①
I II III
①
MC HAZY
MC CLEAR
IV
①
V
①
III
V
②
II
①
I
③
①
10^{-6}
10^{-5}
10^{-4}
10^{-3}
10^{-2}
10^{-1}
10^{0}
β (.55 μm) (km^{-1})

0.55 μm; the material to be associated with each profile is indicated by its reference number (see Table 1). The SRA profiles have been intended to give representation of some extreme cases and exhibit strong discontinuities at the boundary layer limit (2 km) and at the tropopause level (12 km); profiles IV and V include a dust layer limited by a discontinuity at 6 km.

We will not consider here the SHETTLE and FENN (1979) models, as they are now to be replaced by the SRA models, which were derived from them. It should be mentioned however, that they included the influence of relative humidity both on the size distribution and on the refractive index (HÄNEL, 1976). It may be too early to consider this influence, but it should certainly be taken into account for further improvement.

The TOON and POLLACK global model (referred to as TP) comprises three basic components for the troposphere and one for the stratosphere, each characterized by their refractive index to be taken from POLLACK et al. (1973) for basalt, PALMER and WILLIAMS (1975) for 75 % H_2SO_4, TOON and POLLACK (1976) for sea salt and $(NH_4)_2SO_4$. Two material models are built and defined by the volume concentration of each component, one for the low troposphere (0–3 km) and one for the high troposphere (3–12 km). The size distribution is given for the material itself, as if the mixing of components was done inside each particle; in other terms, we can also consider that each component of the material has the same size distribution. For the stratosphere only one component is considered, 75 % H_2SO_4, with one fixed size distribution for the background stratosphere and one variable between two extreme values for the volcanic stratosphere.

The tropopause level is fixed at 12 km as in the SRA models. The extinction profile is a slight modification of ELTERMAN's profile (Figure 1), but it implies a discontinuity at the tropopause level; only a background stratosphere profile is considered.

The McCLATCHEY et al. (1971) model (referred to as MC) is also shown on Table 1 and Figure 1. It is simply defined by a size distribution and an imaginary part of the refractive index which is zero for wavelengths shorter than 0.6 μm and 0.1 above 2 μm, with a linear variation between these values. The real part is not given, but has been taken by different authors as 1.50 (TANRE et al., 1979). Two vertical profiles are proposed for the low troposphere corresponding respectively to ground visibility of 5 km, and 23 km; they join at 5 km leading to only one profile for the high troposphere and the stratosphere. The clear atmosphere profile is actually the ELTERMAN's profile.

3.2 Comparison Between the TP and SRA Models

As it has been pointed out above, the TP model provides an average description of the aerosol over the global scale, whereas the SRA models aim at giving a more detailed description of the different aerosols adaptable to various local conditions. For the sake of homogeneity, it would be satisfying to add to the SRA set of models a global model, built with the same components. Actually the tropospheric profile VI was intended to be possibly used for this purpose. As the global TP model has been widely used, it seems worthwhile to compare it with the SRA models or to try to build a model with similar radiative characteristics from the SRA components. Such a comparison should involve a comparison of the extinction profiles at 0.55 μm, which is generally chosen as a reference wavelength, and a comparison of the specific radiative characteristics (single scattering albedo, phase function, spectral variation of extinction).

3.2.1 Extinction profile at 0.55 μm

Figure 1 shows the comparison between the different extinction profiles. TOON and POLLACK have modified ELTERMAN's original profile in order to have a total optical thickness of 0.125 (or $\delta_t = 0.120$ for the troposphere optical thickness) instead of 0.250 (or $\delta_t = 0.224$) for ELTERMAN's. The SRA model VI fixes $\delta_t = 0.2$; although it agrees reasonably with ELTERMAN's in the low levels, it becomes completely

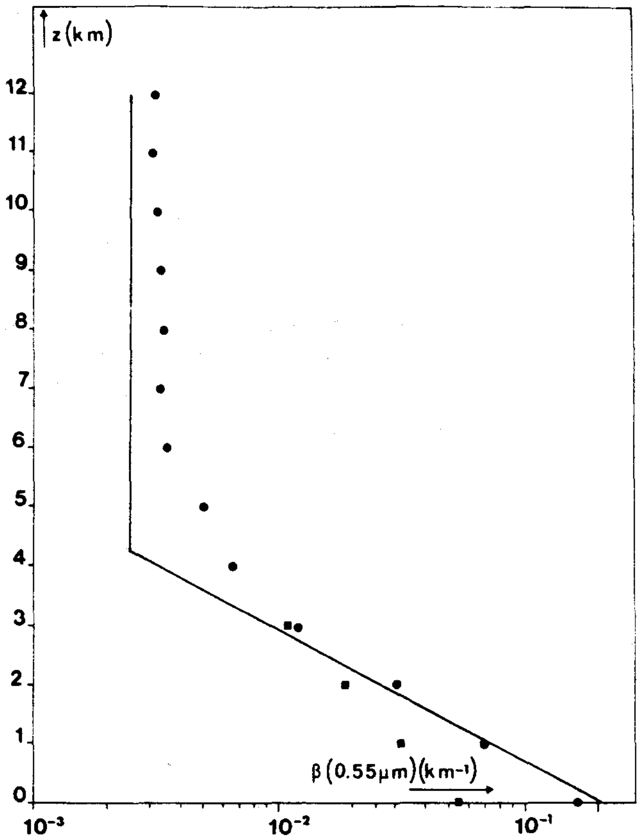

● **Figure 2**

Comparison of SRA modified extinction (0.55 μm) profile VI (——) with TP's (■) and ELTERMAN's (●) profiles.

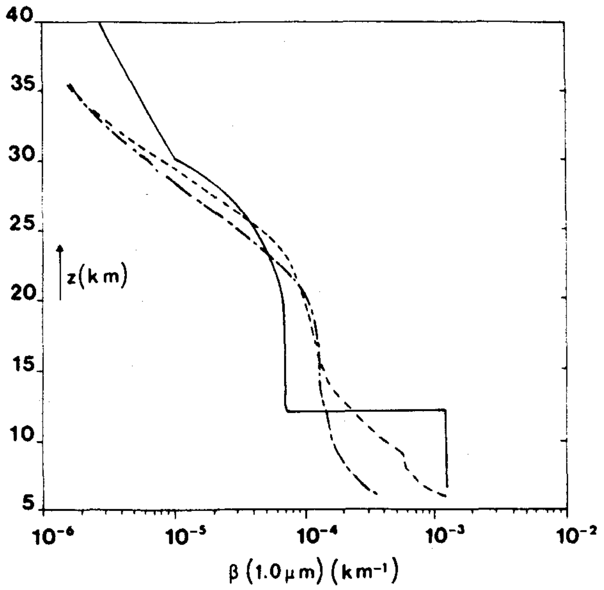

● **Figure 3**

Comparison of SRA background stratosphere and free troposphere extinction profile at 1.0 μm (——) with SAGE profiles averaged over latitude bands 40–50 °N (– – –) and 40–50 °S (—·—) during May 1979.

unrealistic in the high troposphere, leading to an optical thickness $\delta(6-12) = 0.00049$ for the layer 6–12 km, instead of $\delta(6-12) = 0.015$ for all other SRA models, and $\delta(6-12) = 0.019$ for both ELTERMAN's and TP. The simplest modification which can be suggested to SRA profile VI to make it more realistic and more coherent with others is to stop the exponential decrease at the level $z = 4.382$ km where the extinction reaches the value $\beta = 0.0025\ \text{km}^{-1}$ which is the high troposphere value in all other SRA models; this leads to a total troposphere optical thickness $\delta_t = 0.217$. This modified profile VI could be used as an average global profile for the troposphere. It is compared with TP's and ELTERMAN's profile with an enlarged scale on Figure 2.

Above 12 km we will consider only the unperturbed stratosphere, as the volcanic models are time varying. Both TP and SRA models include a strong unrealistic discontinuity at the tropopause level (see Figure 1). They respectively lead to a stratospheric optical thickness $\delta_s = 0.005$ and 0.003, which are very close values. The ELTERMAN model does not exhibit this discontinuity, but as pointed out by TP, it corresponds to a perturbed stratosphere ($\delta_s = 0.026$); it cannot therefore be used for our purpose of a global modelisation of the unperturbed atmosphere. However, further improvement of the SRA models must urgently aim at smoothing the discontinuity at the tropopause level; the many profiles provided by the SAM II and SAGE experiments (McCORMICK et al., 1981) could certainly be used for this purpose. Figure 3 compares the SRA background extinction profile at 1.0 μm with May 1979 SAGE data averaged over a 10° latitude belt between 40°–50° N and 40°–50° S, where the main tropopause level is close to 12 km. Another necessary improvement of the models will include the seasonal and latitudinal variation of the tropopause height rather than to fix it everywhere at 12 km.

3.2.2 Albedo for Single Scattering

The single scattering albedo depends mainly on the imaginary part of the refractive index (or of the absorption) of the aerosol material. At a first look the material used to build the troposphere models are very similar in TP and SRA, except for the strong absorbing soot component in SRA. But the soil particles in TP are assumed to be basalt with an imaginary part of refractive index m″ between 0.0009 to 0.0016 in the visible spectrum (POLLACK et al., 1973), whereas the dust-like particles in SRA have a value of m″ close to 0.008. More important, the sulfates in TP are $(NH_4)_2SO_4$ with $m'' \simeq 10^{-7}$ (TOON and POLLACK, 1976), whereas the water soluble particles in SRA have $m'' \simeq 0.005$ to 0.017. Only the sea salt (TP) and the oceanic component (SRA) have similar low values of $m'' \simeq 10^{-6}$ to 10^{-9}, leading to $\overline{\omega} \simeq 1$. These large differences are due to the fact that TP use refractive index measured for pure material, whereas SRA values came from direct aerosol measurements including impurities; references to the measurements can be found in (Radiation Commission of IAMAP, 1983). Due to the difficulty of measuring m″ accurately (GERBER, 1982) the values chosen in SRA models have to be treated with some reservations and certainly need improvement; they are in any case more realistic than the TP's values. The free troposphere of the TP's model has a single scattering albedo of 0.994, almost constant in the solar spectrum; the boundary layer value is slightly higher due to the sea salt component. Such a high value cannot be achieved with the SRA component unless one uses an almost pure oceanic aerosol, which is unrealistic on the global scale. The continental and maritime SRA models have respectively $\overline{\omega} = 0.891$ and $\overline{\omega} = 0.989$ at 0.55 µm. For the background stratosphere both SRA's and TP's models assume non-absorbing H_2SO_4 particles leading to a single scattering albedo $\overline{\omega} = 1$.

3.2.3 Phase Function and Spectral Variation of Extinction

The phase function depends slightly on the refractive index (real and imaginary parts) and mainly on the size distribution. For the sake of simplicity, we will limit our comparison to the asymmetry factor g which increases from 0 to 1 when the particles' size increases. Similarly the spectral variation of the extinction coefficient depends mainly on the size distribution and we will characterize it by the ratio $\beta(\lambda)/\beta(1.03)$ within the visible and near IR spectrum; this ratio increases when particles are getting smaller. Table 2 shows $g(\lambda)$ and Table 3 $\beta(\lambda)/\beta(1.03)$ for the TP model and for the SRA components and materials. In the stratosphere, both TP and SRA use only one component, which is the same. The differences are due to smaller particles in TP, and both models could be reconciliated only by varying the size distribution.

Table 2 Asymmetry factor g

λ	Troposphere									Stratosphere	
	TP		SRA Components				SRA Materials		Mixture $^{(x)}$ $c_1 = 7.2\,\%$ $c_2 = 92.8\,\%$	TP	SRA background
(µm)	3–12 km	0–3 km	1	2	3	4	Continental	Maritime			
0.385	0.661	.712	0.644	.900	0.407	0.795	0.650	0.744	0.685	0.688	.735
0.450	.659	.710	.636	.894	.374	.792	0.644	0.746	.680	.672	.738
0.525	.661	.708	.630	.880	.344	.785	0.639	0.747	.686	.651	.732
0.550	.662	.707	.628	.877	.336	.781	0.638	0.745	.686	.645	.726
0.600	.663	.705	.624	.872	.321	.781	0.636	0.746	.688	.632	.716
0.800	.661	.698	.612	.850	.267	.779	0.633	0.754	.698	.581	.667
1.03	.664	.698	.600	.832	.219	.778	0.632	0.760	.711	.527	.602

TP = TOON and POLLACK
SRA = Standard Radiation Atmosphere
1 – Water-soluble, 2 – Dust-like, 3 – Soot, 4 – Oceanic
(x) see text

■ **Table 3** Relative spectral variation of the extinction coefficient $\beta(\lambda)/\beta(1.03)$

λ	Troposphere									Stratosphere	
	TP		SRA Components				SRA Materials		Mixture (x) $c_1 = 7.2\ \%$ $c_2 = 92.8\ \%$	TP	SRA background
(µm)	3–12 km	0–3 km	1	2	3	4	Continental	Maritime			
0.385	1.937	1.228	3.568	0.939	3.875	0.920	3.146	1.241	2.193	6.425	4.487
0.450	1.756	1.197	3.021	0.945	3.131	0.935	2.675	1.189	1.927	5.098	3.954
0.525	1.583	1.162	2.502	0.954	2.530	0.945	2.255	1.139	1.695	3.948	3.338
0.550	1.537	1.152	2.368	0.958	2.323	0.962	2.142	1.132	1.628	3.667	3.158
0.600	1.442	1.132	2.150	0.960	2.061	0.965	1.943	1.108	1.520	3.098	2.833
0.800	1.195	1.065	1.458	0.977	1.395	0.994	1.379	1.046	1.210	1.724	1.753
1.03	1.	1.	1.	1.	1.	1.	1.	1.	1.	1.	1.

TP = TOON and POLLACK
SRA = Standard Radiation Atmosphere
1 – Water-soluble, 2 – Dust-like, 3 – Soot, 4 – Oceanic
(x) see text.

In the free troposphere one can try to fit the $g(\lambda)$ or $\beta(\lambda)/\beta(1.03)$ of TP's model by a mixture of water soluble (N_1 particles) and dustlike (N_2 particles); fitting $g\ (0.55\ \mu m)$ leads to $N_2/N_1 = 6.671\ 10^{-6}$ and fitting $\beta(.385)/\beta(1.03)$ to $N_2/N_1 = 1.919\ 10^{-5}$. Tables 2 and 3 show the results for a mixture with the average value $N_2/N_1 = 1.293\ 10^{-5}$ (which corresponds to volume concentrations $c_1 = 7.2\ \%$ and $c_2 = 92.8\ \%$) to be compared with TP's values for the layer 3–12 km; as a reference value let us recall that $c_1 = 29\ \%$, $c_2 = 70\ \%$ in the continental SRA material, which includes also 1 % of soot particles. Fitting both $g(0.55)$ and $\beta(.385)/\beta(1.03)$ with addition of some soot component is not possible. In the boundary layer, the TP's values of $g(0.55)$ and $\beta(.385)/\beta(1.03)$ are very close to those of the SRA maritime material and a better fit cannot be achieved by varying the concentrations of the water soluble and oceanic components.

4 Size Distribution Models

Analytical expressions with two, three or four parameters suitable for representing aerosol size distributions have been reviewed by DEEPAK and BOX (1979); they describe a catalog depicting the parametric behavior of the functions, which can be used to find the best fitting to experimental data. A review of the currently used size distribution models can be found in RUSSELL et al. (1981). Recently ABELE and CLEMENT (1980) have emphasized the flexibility of a Chebyshev polynomials expansion to represent the size distribution; the JUNGE and the Log-Normal distributions can be reduced exactly to such an expansion. We will limit our review here to the most popular functions, which are actually used as "models" with assigned values of the parameters.

The size distribution $n(r)$ is often characterized by its mode radius r_M defined by

$$\frac{d\,n(r)}{dr} = 0 \quad \text{for} \quad r = r_M\,, \tag{14}$$

or its average radius

$$\bar{r} = \int_0^\infty r\,n(r)\,dr. \tag{15}$$

The cumulative oversize distribution represents the number of particles that have radii greater than r

$$N(r) = \int_r^\infty n(r)\,dr\,. \tag{16}$$

As the extinction coefficient for a particle is derived from the Mie theory as $\pi r^2 Q_{ext}$ and similarly the scattering coefficient as $\pi r^2 Q_{scatt}$, it is probably more sensible to define an effective radius as weighted by $r^2 n(r)$, as done by HANSEN and HOVENIER (1974)

$$r_{eff} = \frac{\int_0^\infty r^3 n(r)\,dr}{\int_0^\infty r^2 n(r)\,dr}\,; \tag{17}$$

they also characterize the width of the distribution by an effective variance

$$V_{eff} = \frac{\int_0^\infty (r - r_{eff})^2\, r^2 n(r)\,dr}{r_{eff}^2 \int_0^\infty r^2 n(r)\,dr}\,. \tag{18}$$

In terms of the moments

$$M_k = \int_0^\infty r^k n(r)\,dr \tag{19}$$

of the size distribution, we have

$$\bar{r} = M_1\,, \tag{20}$$

$$r_{eff} = M_3/M_2\,, \tag{21}$$

$$v_{eff} = \frac{M_4}{r_{eff}^2 M_2} - 1 = \frac{M_2 M_4}{M_3^2} - 1; \tag{22}$$

the normalization of $n(r)$ imposes

$$M_0 = 1. \tag{23}$$

4.1 JUNGE Power Law

The power law (PL) was originally proposed by JUNGE (1953, 1963) to represent his continental aerosol data; it is given by

$$\begin{aligned} n(r) &= Cr^{-\nu-1} \text{ for } r_1 \leqslant r \leqslant r_2\,, \\ &= 0 \text{ for } r < r_1 \quad , \\ &\qquad\quad\;\; r < r_2 \quad , \end{aligned} \tag{24}$$

where C is defined by the normalization (Equation 23). The moments are

$$
\begin{aligned}
M_k &= \frac{C}{\nu - k}\left(\frac{1}{r_1^{\nu-k}} - \frac{1}{r_2^{\nu-k}}\right) && \text{for} \quad k < \nu, \\
M_k &= \frac{C}{k-\nu}\left(r_2^{k-\nu} - r_1^{k-\nu}\right) && \text{for} \quad k > \nu, \qquad (25) \\
M_k &= C \ln \frac{r_2}{r_1} && \text{for} \quad k = \nu.
\end{aligned}
$$

A modification is the truncated power law (TPL):

$$
\begin{aligned}
n(r) &= C_i r^{-\nu_i - 1} \quad \text{for} \quad r_i \leqslant r \leqslant r_{i+1},\ i = 1, 2, \ldots, p, \\
&= 0 \quad \text{for} \quad r < r_1, \qquad (26) \\
&\qquad\qquad\quad r > r_{p+1},
\end{aligned}
$$

where the C_i's are defined by the conditions of continuity of n(r) at $r = r_i$, $i = 1 \ldots p$, and by the normalization condition (Equation 23). The parameters to be adjusted to fit an experimental curve are the r_i and the ν_i. The moments are

$$
M_k = \sum_{i=1}^{p} M_k^i , \qquad (27)
$$

where the M_k^i's derive from Equation (25) where C_1, r_1, r_2 are replaced respectively by C_i, r_i, r_{i+1}, with the proper choice according to the respective values of ν_i and k.

The size distribution used in their complete models by McCLATCHEY et al (1971) and by TOON and POLLACK (1976) for the troposphere belong to this category (see Table 1). The values of r_M, $\bar{r}$, r_{eff} and v_{eff} for these models are given in Table 4; we have also added the ratio N(.15)/N(.25) which is used in (RUSSELL et al., 1981) to compare the size distributions; values of r = 0.15 μm and 0.25 μm were chosen in connection with dustsonde measurements. Figure 4a shows the curves n(r).

4.2 Modified Gamma Distribution

The modified gamma size distribution (MGD) is defined by

$$
n(r) = C r^{\alpha} \exp(-\beta r^{\gamma}), \qquad (28)
$$

where from the moments derived as

$$
M_k = \frac{C}{\gamma} \beta^{-(k+\alpha+1)/\gamma}\, \Gamma\left(\frac{k+\alpha+1}{\gamma}\right), \qquad (29)
$$

where Γ is the gamma function; the constant C is given by the normalization equation (23). A variety of size distribution models, using Equation (28) have been proposed by DEIRMENDJIAN (1969). Their respective characteristics are for Haze M: $\alpha = 1, \gamma = 0.5, \beta = 8.9443$; for Haze L: $\alpha = 2, \gamma = 0.5, \beta = 15.1186$; For Haze H: $\alpha = 2, \gamma = 1, \beta = 20$. The MGD is also used in the two SRA stratospheric models (see Table 1). Table 4 shows r_M, $\bar{r}$, r_{eff} and v_{eff} and N(.15)/N(.25) for the DEIRMENDJIAN's and the SRA models. The size distributions are given on Figure 4b.

As a two parameter size distribution is often sufficient to represent most of the aerosols radiative characteristics, it has been suggested (KURIYAN, 1974) to limit the choice of the MGD's to those with $\gamma = 1$. If

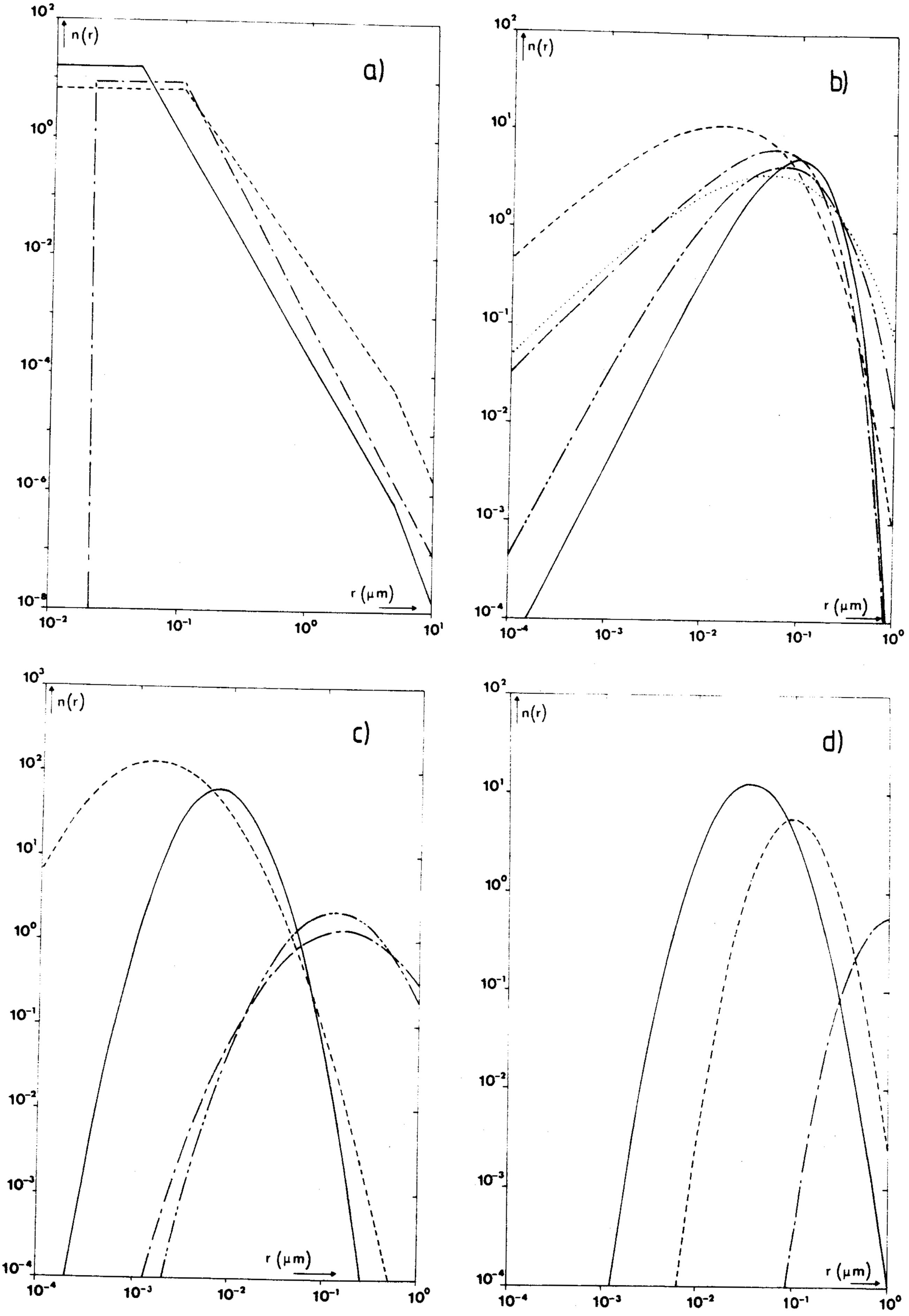
a)
n(r)
r (μm)
10²
10⁰
10⁻²
10⁻⁴
10⁻⁶
10⁻⁸
10⁻²
10⁻¹
10⁰
10¹
b)
n(r)
r (μm)
10²
10¹
10⁰
10⁻¹
10⁻²
10⁻³
10⁻⁴
10⁻⁴
10⁻³
10⁻²
10⁻¹
10⁰
c)
n(r)
r (μm)
10³
10²
10¹
10⁰
10⁻¹
10⁻²
10⁻³
10⁻⁴
10⁻⁴
10⁻³
10⁻²
10⁻¹
10⁰
d)
n(r)
r (μm)
10²
10¹
10⁰
10⁻¹
10⁻²
10⁻³
10⁻⁴
10⁻⁴
10⁻³
10⁻²
10⁻¹
10⁰

Table 4 Characteristics of different size distribution models (see text)

Model	Size distribution	r_M (μm)	$\bar{r}$ (μm)	r_{eff} (μm)	v_{eff}	$\frac{N(.15)}{N(.25)}$
MC	Truncated power law	.02	.0865	.368	4.56	4.78
TP (0–3 km)			.0991	1.614	3.60	2.78
TP (3–12 km)			.0366	.423	6.79	3.78
Haze M	Modified Gamma	0.05	0.250	0.900	0.528	1.57
Haze L		0.07	0.184	0.481	0.418	2.00
Haze H		0.10	0.150	0.250	0.2	3.39
SRA (Stratosphere background)		0.0555	0.111	0.222	0.250	4.07
SRA (Stratosphere volcanic)		0.0156	0.0781	0.281	0.528	3.17
SRA (Water soluble)	Log Normal	0.00152	0.00908	0.0994	0.307	5.39
SRA (Dust-like)		0.152	0.908	9.94	2.307	1.17
SRA (Soot)		0.0073	0.0150	0.0392	0.617	23.1
SRA (Oceanic)		0.129	0.458	2.49	1.33	1.34
Equivalent SRA						
Stratosphere (background)		0.102	0.142	0.222	0.250	4.77
Stratosphere (volcanic)		0.0637	0.120	0.281	0.528	3.44
TP (Stratosphere background)	Zold	0.035	0.072	0.188	0.617	4.99
(Stratosphere volcanic)		0.1	0.168	0.335	0.413	2.77
		1.0	1.68	3.35	0.413	1.00

MC = McCLATCHEY et al.
TP = TOON and POLLACK
SRA = Standard Radiation Atmosphere

Figure 4 Size distribution models

a Truncated Power Law
—— TP 3–12 km
– – – TP 0–3 km
—·— MC

b Modified Gamma Distribution
—·— SRA background stratosphere
– – – SRA volcanic stratosphere
······ Haze M
—··— Haze L
—— Haze H

c Log Normal Distribution
– – – SRA water-soluble
—— SRA soot
—··— SRA oceanic
—·— SRA dust-like

d Zold distribution
—— TP background stratosphere
– – – TP volcanic stratosphere (r_m = 0.1 μm)
—·— TP volcanic stratosphere (r_m = 1 μm)

we try to fit the r_{eff} and v_{eff} values of a given $n(r)$ by adjusting the α and β parameters in a MGD with $\gamma = 1$, it leads to

$$\alpha = \frac{1 - 3v_{eff}}{v_{eff}}\ , \quad \beta = \frac{1}{r_{eff}\ v_{eff}}\ ; \tag{30}$$

as α must be positive, this MGD with $\gamma = 1$ can only represent size distributions with $v_{eff} < \frac{1}{3}$; which is too restrictive for many cases with a wide range of particles.

4.3 Log Normal Distribution

The Log Normal Distribution (LND) is given by

$$n(r) = \frac{C}{r \ln \sigma} \exp\left(-\frac{\ln^2 r/r_m}{2\ln^2 \sigma}\right)\ ; \tag{31}$$

where r_m and σ are the parameters to be adjusted; r_m is sometimes considered as a mode radius for a logarithmic distribution $rn(r) = f(\ell nr)$; keeping to the definition of Equation (14) the mode radius is

$$r_M = r_m \exp(-\ln^2 \sigma), \tag{32}$$

and the cumulative oversize distribution

$$N(r) = \frac{1}{2}\left[1 - \theta\left(\frac{1}{\sqrt{2}\ln\sigma}\ \ln\frac{r}{r_m}\right)\right]\ , \tag{33}$$

where θ is the error function defined by

$$\theta(x) = \frac{2}{\sqrt{\pi}}\int_0^x \exp(-t^2)\,dt. \tag{34}$$

The moments are

$$M_k = C\sqrt{2\pi}\, r_m^k \exp\left(\frac{k^2}{2}\ln^2\sigma\right)\ , \tag{35}$$

leading to

$$C = 1/\sqrt{2\pi}, \tag{36}$$

$$\bar{r} = r_m \exp\left(\frac{\ln^2\sigma}{2}\right)\ , \tag{37}$$

$$r_{eff} = r_m \exp\left(\frac{5}{2}\ln^2\sigma\right)\ , \tag{38}$$

$$v_{eff} = \exp(\ln^2\sigma) - 1 \tag{39}$$

The tropospheric components in SRA models are LND type; they are shown on Figure 4c, and their characteristics are listed in Table 4.

From a practical point of view, it is convenient to use the same type of size distribution at all levels and for all components within a complete model. It can be considered as a drawback of the SRA models to use the log-normal distribution for the tropospheric aerosols and the modified gamma distribution for the stratospheric aerosols. The effective radius and variance are probably the parameters to which the radiative characteristics are the most sensitive. Therefore, one can try to change the size distribution keeping r_{eff} and v_{eff} at the values fixed for SRA components, either for the troposphere or for the stratosphere, in order to keep the same formalism within both layers without changing too much the radiative characteristics of the original models.

The two parameter LND is a little easier to handle than the MGD and the fitting of r_{eff} and v_{eff} by varying σ and r_m is straightforward from Equations (38) and (39). We have therefore sought for stratospheric LND leading to the same r_{eff} and v_{eff} as the SRA stratospheric MGD; we will refer to these size models as "equivalent" SRA stratospheric models. The σ and r_m value are found respectively as $\sigma = 1.6038$, $r_m = 0.1271$ μm for the background aerosols and $\sigma = 1.9177$, $r_m = 0.09736$ μm for the vocanic aerosols; these "equivalent" SRA model characteristics are listed on Table 4. Figure 5a shows the comparison of both the original and "equvalent" SRA size distributions for background stratospheric aerosols. Figure 5b is the same for volcanic aerosols. The original SRA models contain many more small particles than the "equivalent" ones, which reflects into a smaller value of the average radius $\bar{r}$ (Table 4) for the original SRA models. This excess of small particles could also have an important influence on the radiative characteristics. Therefore, the original and the "equivalent" models could behave differently, although they have the same r_{eff} and v_{eff}. Table 5 compares the extinction coefficients at 0.45 μm and 1.03 μm and their ratio, the asymmetry factor and the single scattering albedo for the same wavelengths. It appears that the differences between the original SRA and the "equivalent" models are not significant as long as the main specific quantities are concerned. Differences would certainly show up in the details of the phase

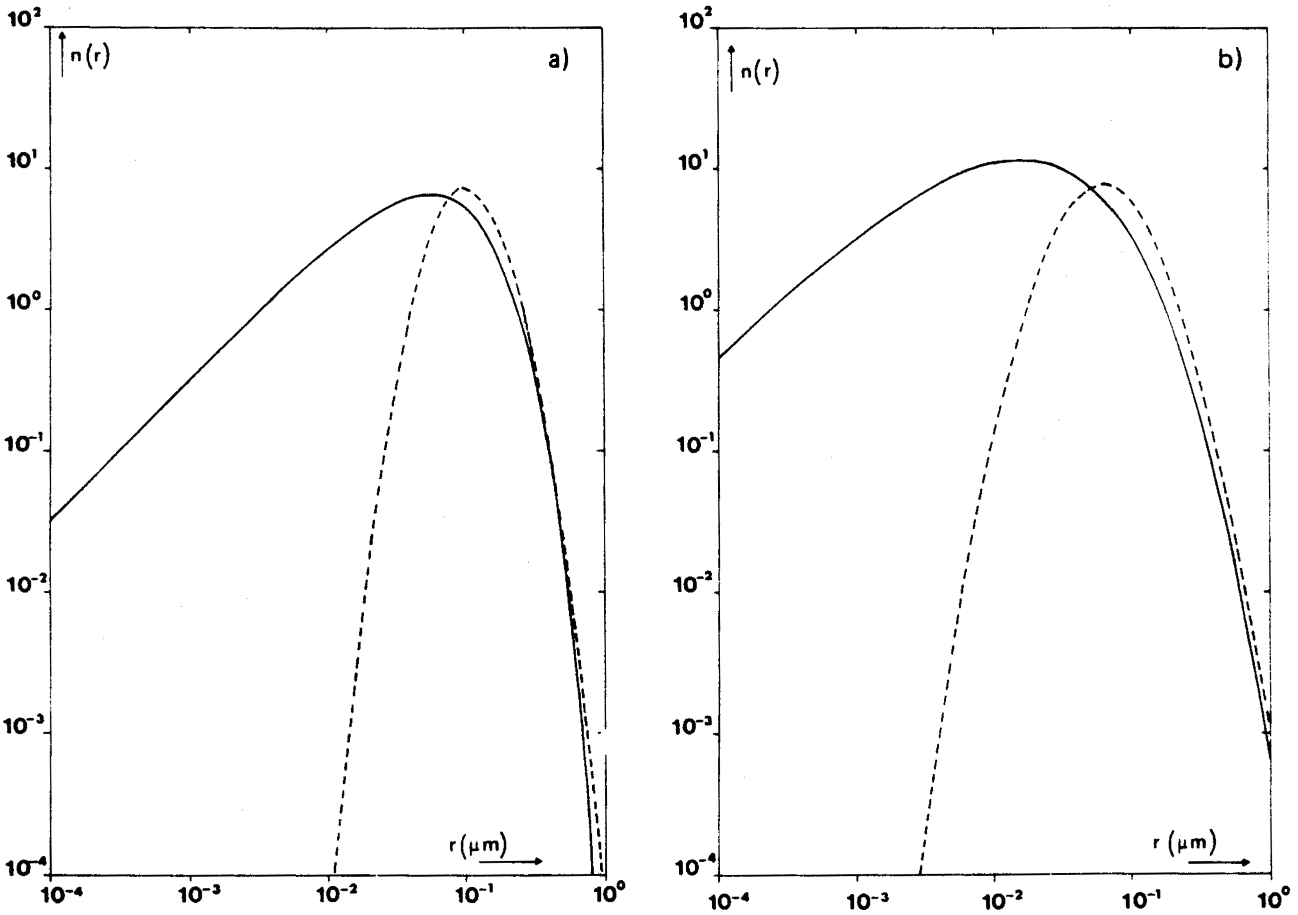

- **Figure 5** Comparison of the size distribution for the SRA stratospheric models (MGD) (——) and the "equivalent SRA" (LND) (– – –)

a background

b volcanic

Table 5
Comparison of SRA stratospheric models (MGD) and equivalent SRA (LND) (see text).
The extinction coefficient is normalized to $\beta(.55\ \mu m) = 1$.

Radiative parameters	Stratosphere background		Stratosphere volcanic	
	SRA	SRA equivalent	SRA	SRA equivalent
$\beta(1.03)$	0.312	.311	.554	.524
$\beta(.45)$	1.238	1.265	1.096	1.110
$\beta(.45)/\beta(1.03)$	3.954	4.067	1.978	2.144
g(1.03)	.602	.593	.660	.649
g(.45)	.738	.737	.703	.705
$\omega(1.03)$	1	1	.946	.953
$\omega(.45)$	1	1	.938	.941

function, but they have a minor influence on the radiative transfer computations. Differences in the absolute extinction values for the same total number of particles are of no concern, as the model profiles are given in terms of the extinction coefficient.

4.4 Zold Distribution

The Zold distribution is given by

$$n(r) = C \exp\left(\frac{-\ln^2 r/r_m}{2\ln^2\sigma}\right) \; ; \tag{40}$$

where C is fixed by the normalization equation (23); $r_m = r_M$ is the mode radius. The moments are

$$M_k = C\sqrt{2\pi}\,\ln\sigma\, r_m^{k+1} \exp\left(\frac{(k+1)^2}{2}\ln^2\sigma\right) \tag{41}$$

This Zold distribution is used in the TP's model for the stratospheric aerosols; the characteristics are shown in Table 4 and the curves n(r) given on Figure 4d.

5 Conclusion

Some currently used aerosol models have been reviewed and compared to the set of models recently proposed by the Radiation Commission of IAMAP as a Standard Radiation Atmosphere (SRA). It is suggested to modify the SRA profile VI in order to make it more realistic; then it comes very close to the ELTERMAN's profile modified in TOON and POLLACK's (TP) global model and can be reasonably used on a global average basis. The discontinuity at the tropopause level, rigidly fixed at 12 km, for all the SRA models, is also underlined and this requires further improvement.

The TP materials for the troposphere have a single scattering albedo which is too close to 1 and unrealistic. The value of the asymmetry factor and the extinction spectral variation in the TP boundary layer are very close to those of the SRA maritime material; in the free troposphere the TP's values can be reasonnably approximated by a mixture of 7.2 % of the water soluble and 92.8 % of the dust-like SRA components. At the stratosphere level for unperturbed conditions both TP and SRA models have a single scattering albedo of 1, but TP model has smaller particles leading to a smaller value of the asymmetry factor and a larger spectral variation of the extinction.

The different model size distributions are also compared, including the mode radius, the average radius and the effective radius, as well as the effective variance. With the purpose of simplification and homogeneization, it is suggested to keep the same Log-normal size distribution for all the SRA components; it is shown that this can be achieved without introducing too large changes in the radiative characteristics of the stratospheric aerosols.

After completion of this work, a workshop on "Aerosols and their Climatic Effects" was held in Williamsburg Va. USA, on March 28–30, 1983. In discussions the necessity of improving the SRA models has been underlined; the main recommendations were the choice of LND models for the stratospheric aerosols and the introduction of a specific Saharan model.

References

ABELE, J. and CLEMENT, D., 1980: Chebyshev approach to fit atmospheric aerosol size distributions. Beitr. Phys. Atmosph. 53, 469–485.

BIGG, E. K., 1976: Size distribution of stratospheric aerosols and their variations with altitude and time. J. Atmos. Sci. 33, 1080–1086.

DEEPAK, A. and BOX, G. P., 1979: Analytic modeling of aerosol size distributions. NASA contractor Report 159170 IFAORS Hampton VA 23666.

DEIRMENDJIAN, D., 1969: Electromagnetic scattering on spherical polydispersions. Elsevier, New York. 290 pp.

ELTERMAN, L., WEXLER, R. and CHANG, D. T., 1969: Features of tropospheric and stratospheric dust. Appl. Optics 8, 893–903.

GERBER, H. E., 1982: Absorption of light by atmospheric aerosol particles: review of instrumentation and measurements. In "Light absorption by aerosol particles" edit. by H. GERBER and E. HINDMAN. Spektrum Press Hampton VA., 21–53.

GRAS, J. L. and MICHAEL, C. G., 1979: Measurement of the stratospheric aerosol size distribution. J. Appl. Meteor. 18, 855–860.

GOROCH, A. K., FAIRALL, G. W. and DAVIDSON, K. L., 1982: Modeling wind speed dependence of marine aerosol distribution by a Gamma-function. J. Appl. Meteor. 21, 666–671.

HÄNEL, G., 1976: The properties of atmospheric aerosol particles as functions of the relative humidity at thermodynamic equilibrium with the surrounding moist air. Advances in Geophysics 19, 73–188, Academic Press, New York.

HANSEN, J. E. and HOVENIER, J. W., 1974: Interpretation of the polarization of Venus. J. Atmos. Sci. 31, 1137–1160.

JUNGE, C. E., 1953: Die Rolle der Aerosole und der gasförmigen Beimengungen der Luft im Spurenstoffhaushalt der Troposphäre. Tellus 5, 1–26.

JUNGE, C. E., 1963: Air chemistry and radioactivity. Academic Press, New York.

KURIYAN, J. G., 1974: Particulate sizes from polarization measurements. Proc. UCLA International Conference on Radiation and Remote Probing of the Atmosphere; August 1973; Western Periodical Company, 337–366.

McCLATCHEY, R. A., FENN, R. W., SELBY, J. E. A., VOLTZ, F. E. and GARING, S., 1971: Optical properties of the atmosphere. AFCRL 71-0279 Environmental Research Papers N° 354.

McCLATCHEY, R. A., BOLLE, H. J. and KONDRATIEV, K. Ya., 1980: Report of the IAMAP Radiation Commission Working Group on a Standard Radiation Atmosphere. WMO/IAMAP. (see also World Climate Research Programme WCP. 12).

McCORMICK, M. P., CHU, W. P., GRAMS, G. W., HAMILL, P., HERMAN, B. M., McMASTER, L. R., PEPIN, T. J., RUSSELL, P. B., STEELE, H. M. and SWISSLER, T. J., 1981: High latitude stratospheric aerosols measured by the SAM II satellite system in 1978 and 1979. Science 214, 328–331.

PALMER, K. F. and WILLIAMS, D., 1975: Optical constants of sulfuric acid: Application to the clouds of Venus. Appl. Optics 14, 208–219.

PATTERSON, E. M. and GILLETTE, D. A., 1977: Commonalities in measured size distributions for aerosols having a soil-derived component. J. Geophys. Res. 82, 2074–2082.

PINNICK, R. G., ROSEN, J. M. and HOFMANN, D. J., 1976: Stratospheric aerosol measurements III: Optical model calculations. J. Atmos. Sci. 33, 304–314.

POLLACK, J. B., TOON, O. B. and KHARE, B. N., 1973: Optical properties of some terrestrial rocks and glasses. Icarus 19, 372–389.

POLLACK, J. B. and CUZZI, J. N., 1980: Scattering by nonspherical particles of size comparable to a wavelength: a new semi-empirical theory and its application to tropospheric aerosols. J. Atmos. Sci. 37, 868–881.

RADIATION COMMISSION OF IAMAP, 1083: A preliminary cloudless standard atmosphere for radiation computation (to appear).

RUSSELL, P. B., SWISSLER, T. J., McCARMICK, M. P., CHU, W. P., LIVINGSTON, J. M. and PEPIN, T. J., 1981: Satellite and correlative measurements of the stratospheric aerosol 1: An optical model for data conversions. J. Atmos. Sci. **38**, 1279–1294.

SHETTLE, E. P. and FENN, R. W., 1979: Models for the aerosols of the lower atmosphere and the effects of humidity variations on their optical properties. AFGL TR 790214, Environmental Research Papers N° 676.

TANRE, D., HERMAN, M., DESCHAMPS, P. Y. and de LEFFE, A., 1979: Atmospheric modeling for space measurements of ground reflectances, including bidirectional properties. Appl. Optics 18, 3587–3594.

TOON, O. B. and POLLACK, J. B., 1976: The optical constants of several atmospheric aerosol species: ammonium sulfate, aluminium oxyde and sodium chloride. J. Geophys. Res. 81, 5733–5748.

TOON, O. B. and POLLACK, J. B., 1976: A global average model of atmospheric aerosols for radiative transfer calculations. J. Appl. Meteor. 15, 225–246.

TWOMEY, S., 1977: Atmospheric aerosols. Developments in atmospheric science 7, Elsevier Amsterdam, 302 pp.

RADIATIVE CHARACTERISTICS OF STRATOSPHERIC AEROSOLS FROM SAGE DATA

J. Lenoble, C. Brogniez, and P. Pruvost
Laboratoire d'Optique Atmosphérique, UA 713
Université des Sciences et Techniques de Lille
59655 Villeneuve d'Ascq Cedex, France

The four channel mission SAGE (Stratospheric Aerosol and Gas Experiment) provide aerosol extinction profiles at 1.0 µm and 0.45 µm (Chu and Mc Cormick, 1979). The 1.0 µm channel gives directly the aerosol extinction $\sigma_e(1.0)$ and has been widely used. The stratospheric aerosol enhancement due to the Mount St. Helens eruption was observed by SAGE from almost immediately after the eruption and followed until its dissipation (Kent, 1982).

The 0.45 µm data are of poorer quality, mainly because of the strong perturbation due to the Rayleigh molecular scattering ; moreover the relative contributions of NO_2 and aerosol extinction are of the same order. However the separtion can be achieved, and the results, expressed by a mean Angström coefficient between 0.45 µm and 1.0 µm defined by $\sigma_e(.45) = (0.45)^{-\alpha}\sigma_e(1.0))$, are quite meaningful, at least up to 25 km, i.e. when the NO_2 contribution is not too large (Lenoble and Pruvost, 1983).

We have used the SAGE profiles of July 1980 in the latitude band between 70°N and 50°N ; the 1.0 µm profiles reveal the presence of Mount St. Helens aerosols, with an optical depth larger than 3.10^{-3}, and a maximum extinction between 18-20 km (Kent,1982). The Angström coefficient profile typically exhibits a minimum at the maximum extinction level, pointing to large particles, followed by a rapid increase toward a maximum (small particles) in the region 21-23 km (Lenoble et al. 1984). This feature is more or less pronounced but the minimum of α often reaches 0.5 and the maximum 3.0. A few profiles are rather smooth, but the general behaviour is typical enough to reflect on the latitude average profiles. Figure 1 compares a volcanic profile of $\sigma_e(1.0)$ and α (fig. 1a) with an unperturbed case (fig. 1b). Figure 2 compares the latitude average profiles of α for the band 60°-70°N at approximately the same period of the year for 1979 and 1980. The regular increase of α with height in 1979 is found for a few latitudes and months ; more often α is almost constant around 1.6-1.7 within the unperturbed stratosphere ; a more detailed study remains to be done to improve the modelization of the unperturbed stratosphere.

The experimental value of α can be used to retrieve one parameter of an assumed size distribution. For a log-normal size distribution with an effective variance of 0.250 which seems a reasonnable choice, the logarithmic mode radius is found around 0.20 µm in the layer 18-20 km and around 0.06 µm in the layer 21-23 km for strong volcanic profiles ; for the unperturbed atmosphere the mode radius is between 0.10 µm and 0.14 µm. Of course an infinity of such "equivalent" size distributions can be built by changing either the variance or the mathematical formulation.

The equation is how such an "equivalent" size distribution, which fits the experimental value of α , does permit the retrieval of the other radiative characteristics, important for the studies of climatic impact (solar average optical depth, solar average asymmetry factor, infrared optical depth) or necessary for correlative experiments (backscattering to extinction ratio). We have addressed this problem by a simulation study using log-normal, modified gamma and bimodal log-normal size distributions and we present here the results concerning the ratio of the solar average extinction $\sigma_e^{\odot}$ to the extinction $\sigma_e(1.0)$ at 1.0 µm, and the solar average asymmetry factor $g_{\odot}$.

Four log-normal size distribution (LND) with effective variances of 0.1, 0.25, 0.528, 1.0 were used, with varying mode radius in order to vary α within a large range. It has been checked that a Modified Gamma size distribution (MGD) and a LND with the same effective variance and the same effective radius give similar results. Bimodal size distributions (BM) have been built by mixing two LND ; the concentration of the two componsents is varied in order to very α. One model (BM1) is made of a mixture of very small and very large particles (mode radius of 0.03 µm and 0.60 µm) and the other (BM2) of a mixture of average background particles (0.13 µm) with either the large or the small particle component.

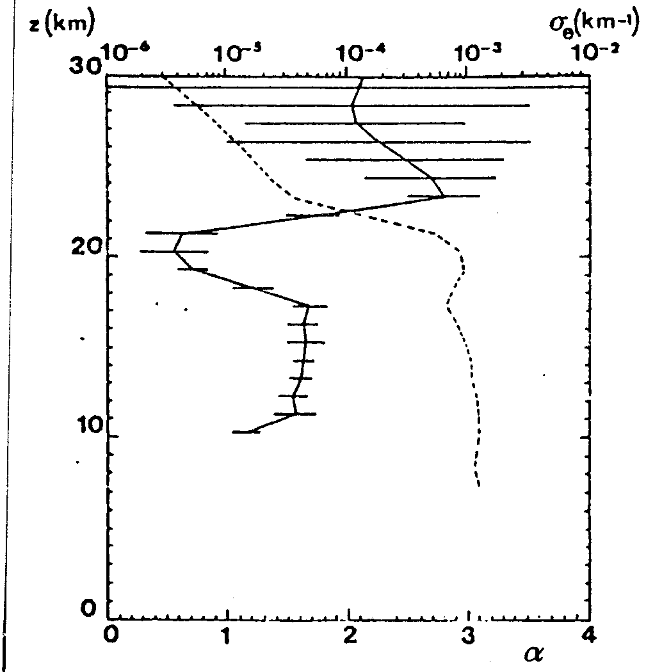

Figure 1. Aerosol extinction coefficient $\sigma_e(1.0)$ at 1.0 μm and Angström coefficient α.
a) – Volcanic case

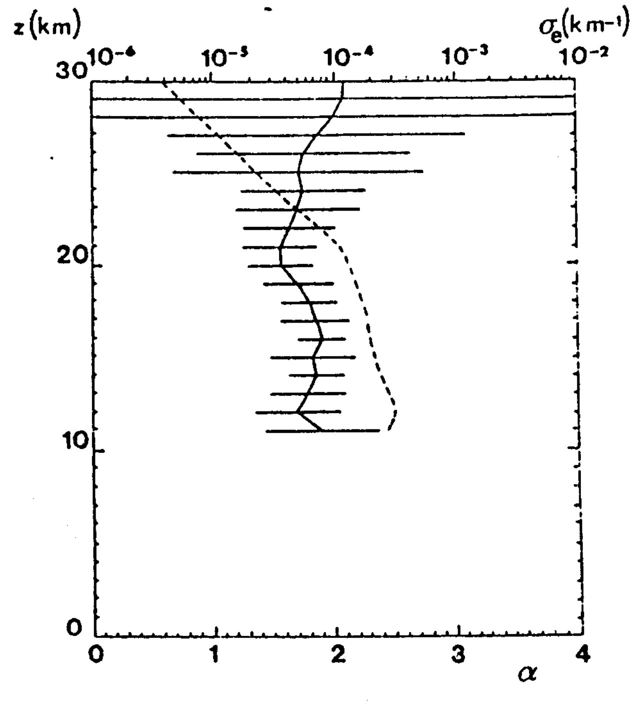

Figure 1. b) – Clear case

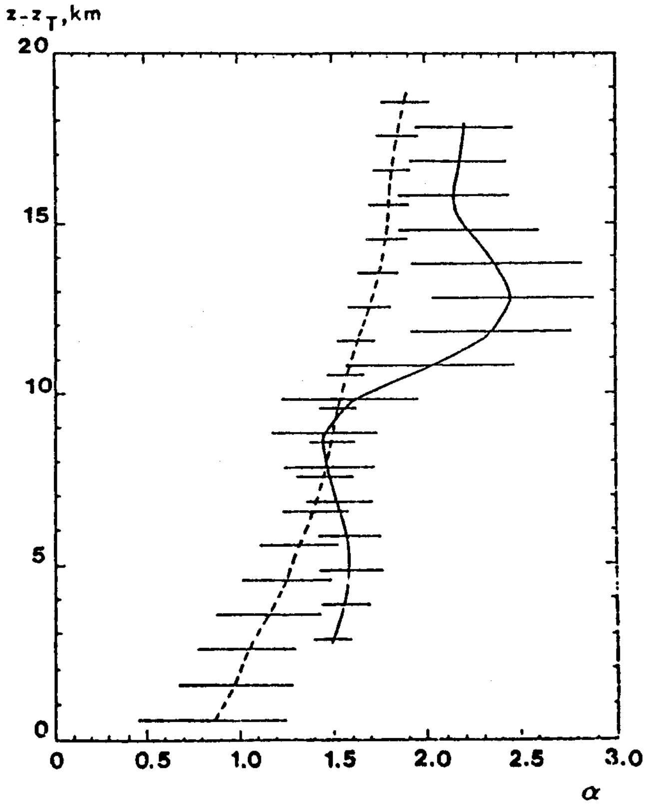

Figure 2. Angström coefficient profile averaged over 60-70°N.
------August 1979 ———July 1980

Figure 3 presents the variation of $\sigma_e^{\odot}/\sigma_e(1.0)$ versus α ; the points for all models including BM are on the same curve for α smaller than 3, i.e. for the values of α of practical interest. This means that the solar average extinction coefficient and therefore the solar average optical depth can be retrieved uniquely from the two SAGE aerosol channel data.

Unfortunately, the results are not so satisfactory for the other quantities. Figure 4 presents the solar average asymmetry factor $g_{\odot}$ versus α . If the aerosol size distribution is known to be monomodal, the knowledge of α leads to reasonable brackets for $g_{\odot}$; but if the size distribution is bimodal no information can be retrieved. There is some hope that the additional channels of SAGE II will give a two-parameter information about the size distribution and will allow a better determination of the radiative characteristics.

ACKNOWLEDGMENT

This work has been supported by the Centre National d'Etudes Spatiales under contract 83230.

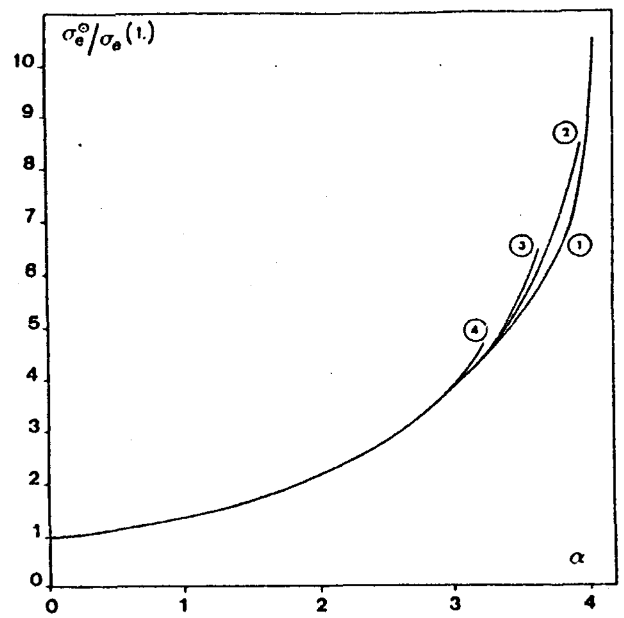

Figure 3. Ratio of solar average extinction to 1.0μm extinction versus α. LND: 1-v_{eff} = .1 ; 2-v_{eff} = .250 ; 3-v_{eff} = .528 ; 4-v_{eff} = 1. GMD and BM points are on the same curve for α < 3.

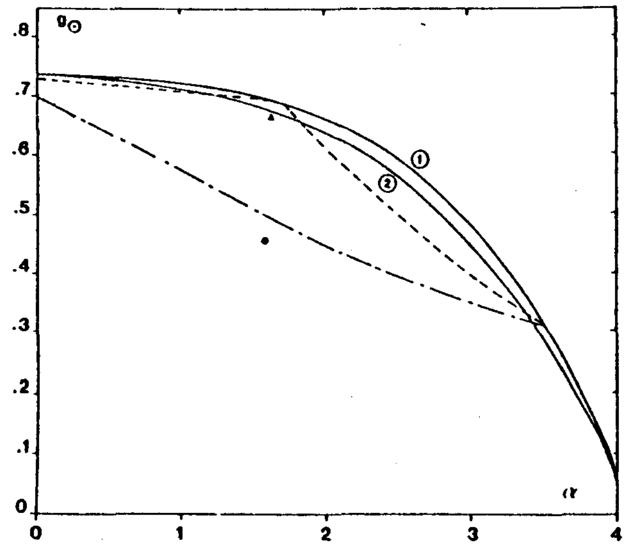

Figure 4. Solar average asymmetry factor versus α
1-LND, v_{eff} = .250 ;
2-LND, v_{eff} = .528 ;
—·— BM1 ; - - - - - - BM2.

REFERENCES

Chu, W.P., and M.P. Mc Cormick, 1979 : Inversion of stratospheric aerosol and gaseous constituents from spacecraft solar extinction data in the 0.38-1.0 μm wavelength region. Appl. Opt., 18, 1404-1413.

Kent, G.S., 1982 : SAGE measurements of Mount St. Helens volcanic aerosols, in "Atmospheric effects and potential climatic impact of the 1980 eruptions of Mount St. Helens". Proc. of a symposium held at Washington D.C. Nov. 18-19, 1980. NASA Conference Publications 2240, 109-115.

Lenoble, J., and P. Pruvost, 1983 : Inference of the aerosol Angström coefficient from SAGE short-wavelength data. J. Clim. Appl. Meteor., 22, 1717-1725.

Lenoble, J., P. Pruvost, and C. Brogniez, 1984 : SAGE observations of stratospheric aerosols from Mount St. Helens eruptions : a two wavelength analysis. To appear in J. Geophys. Res.

Lenoble, J., and C. Brogniez, 1984 : Information on stratospheric aerosol characteristics contained in SAGE satellite multiwavelength extinction measurements. Submitted to Appl. Opt.

JOURNAL OF GEOPHYSICAL RESEARCH, VOL. 89, NO. D7, PAGES 11,666–11,676, DECEMBER 20, 1984

SAGE Satellite Observations of Stratospheric Aerosols From Mount St. Helens Eruption: A Two-Wavelength Analysis

J. LENOBLE, P. PRUVOST, AND C. BROGNIEZ

Laboratoire d'Optique Atmosphérique, Université des Sciences et Techniques de Lille, France

The Angström coefficient profiles deduced from 93 SAGE Satellite observations in July 1980 between 50°N and 70°N have been used to study the variation of the aerosol size distribution in the Mount St. Helens aerosol layer. In most cases a layer of large particles corresponding to the maximum extinction at 18–20 km is topped by a layer of small particles. The study of profiles averaged over 10° latitude bands for May to November 1980 have confirmed the extent of this situation, which contrasts with a rather constant size distribution within the unperturbed stratosphere in 1979. Assuming an equivalent log-normal size distribution with an effective variance of 0.250, the logarithmic mode radius is found around 0.20 μm for the large-particle layer and around 0.06 μm for the top layer. The inferred mass density profile is strongly influenced by this structure.

1. INTRODUCTION

Volcanic eruptions generally produce a substantial increase of the stratospheric aerosol content, which may have important radiative and climatic effects. A period of low-background stratospheric aerosol levels was interrupted by the Mount St. Helens eruption on May 18, 1980, and was followed by a series of more or less important eruptions until the most important El Chichon eruption (April 1982). The stratospheric aerosol variations following these eruptions, especially Mount St. Helens and El Chichon, have been subject to extensive scientific studies, including in situ balloon and aircraft measurements, ground-based lidar, and satellite remote observations [*National Aeronautic and Space Administration*, 1980; *International Association of Meteorology and Atmospheric Physics*, 1983]. The satellite has the major advantage of giving a global picture of the volcanically perturbed stratosphere and of following its temporal variations; however, it does not allow such a detailed description as the in situ measurements.

NASA's SAM 2 (Stratospheric Aerosol Measurement 2) and SAGE (Stratospheric Aerosol and Gas Experiment) satellite experiments [*Chu and McCormick*, 1979; *McCormick et al.*, 1979] were especially designed for the monitoring of stratospheric aerosols between approximately 70°N and 70°S for SAGE and at higher latitudes for SAM 2. Unfortunately, only SAM 2 was working at the time of the El Chichon eruption [*McCormick et al.*, 1983], but the Mount St. Helens stratospheric aerosol enhancement was observed by SAGE from almost immediately after the eruption and was followed until its dissipation [*Kent*, 1982]. The results are presented as profiles of the extinction coefficient at 1.0 μm and maps of the stratospheric optical depth at the same wavelength; using aerosol models, values of the total mass of material are deduced. The SAGE data also contain profiles of the extinction coefficients at 0.45 μm—of somewhat poorer quality than the 1.0-μm profiles—but can be used to infer further information about the aerosol characteristics [*Lenoble and Pruvost*, 1983]. The ratio of extinction coefficients at 0.45 μm and 1.0 μm (or the related Angström coefficient) exhibits typical variations within the volcanic stratosphere, that are likely to be due to variations in the aerosol size distribution.

In section 2 we examine the Angström coefficient profiles computed from SAGE observations in July 1980 for high latitudes where a strong quasi-homogeneous volcanic layer exists. An "equivalent size distribution" with one adjustable parameter can be deduced and compared to in situ size distribution measurements [*Hofmann and Rosen*, 1982]. In section 3 the profiles averaged over 10° latitude bands are compared in 1980 and 1979, showing a typical difference on the global scale between the perturbed and the background stratosphere. In section 4 we discuss the applicability of this "equivalent size distribution" in deriving the mass of volcanic dust.

2. SAGE OBSERVATIONS JULY 1980

SAGE first observed locally enhanced stratospheric extinction profiles between 55°N and 25°N during the end of May 1980, soon after the Mount St. Helens May 18 eruption. The volcanic material then started its dispersion along more or less complex trajectories, and at the end of July it was spread longitudinally around the globe north of 30°N, with the highest concentrations north of 50°N. SAGE, starting its sweep movement southward from 70°N on July 21, 1980, observed enhanced extinction profiles at 1.0 μm almost everywhere between 70°N and 50°N; the corresponding stratospheric optical depth at 1.0 μm was evaluated and found always larger than 3.10^{-3} and often larger than 5.10^{-3} [*Kent*, 1982; see also *Newell and Deepak*, 1982, map Figure 4.3].

We have used 93 profiles of the extinction coefficients $\sigma_e(1.0)$ and $\sigma_e(0.45)$, at 1.0 μm and 0.45 μm, respectively, given on the SAGE July data tape. Even when the aerosol extinction does not follow exactly the Angström law $\sigma_e(\lambda) = \sigma_e(1.0)\lambda^{-\alpha}$, it is customary to introduce an average Angström coefficient α within a limited spectral interval. We have found more convenient to use the Angström coefficient computed from

$$\alpha = -\log(\sigma_e(0.45)/\sigma_e(1.0))/\log(0.45) \qquad (1)$$

than the extinction ratio; the $\sigma_e(1.0)$ profile has been smoothed over 3 km to make it consistent with the smoothed $\sigma_e(0.45)$ profile. The error bars on α are directly computed from the uncertainties on $\sigma_e(1.0)$ and $\sigma_e(0.45)$ given on the SAGE tape; these error bars are reasonably small between 11 and 25 km, and the variations of α appear much larger than the possible errors and quite significant. A detailed discussion of the accu-

Copyright 1984 by the American Geophysical Union.

Paper number 4D1108.
0148-0227/84/004D-1108$05.00

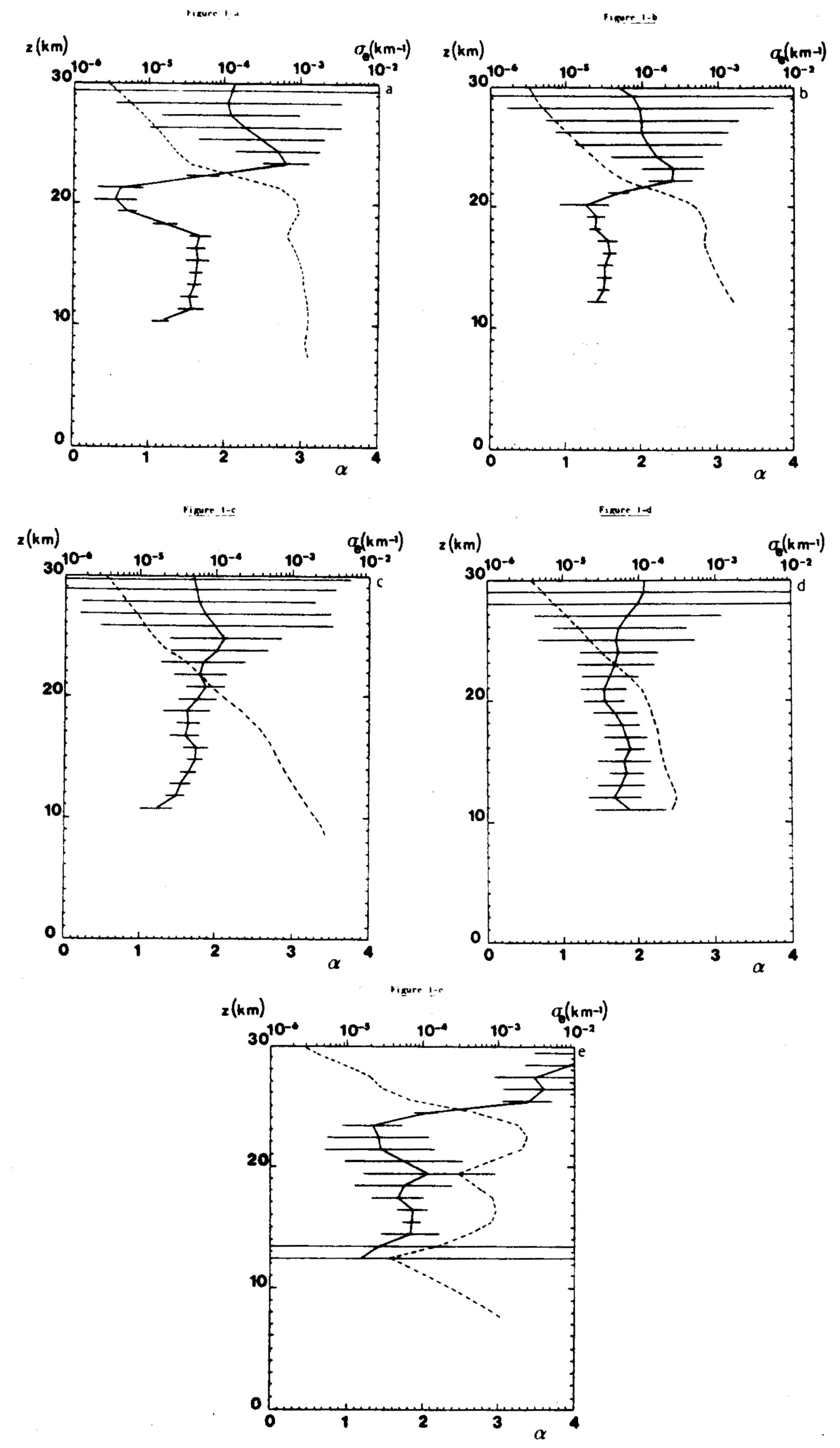

Fig. 1. Profiles of the extinction coefficient $\sigma_e(1.0)$ (dashed line) and of the Angström coefficient α (solid line): (*a*) July 28, 1980, 1843 GMT, 57.3°N, 22.8°E; (*b*) July 29, 1980, 1223 GMT, 55.4°N, 115.0°E; (*c*) July 27, 1980, 0056 GMT, 61.3°N, 296.9°E; (*d*) May 21, 1980, 2332 GMT, 54.3°N, 307.2°E; (*e*) May 24, 1980, 0435 GMT, 47.8°N, 225.2°E.

racy of α, including the perturbation caused by NO_2 extinction, can be found in *Lenoble and Pruvost* [1983]. The tropopause level is between 9 and 12 km for the observation latitudes, and as the α profiles generally exhibit either oscillations or a tendency to decrease downward in the first few kilometers above the tropopause—independently of any volcanic contribution—we will focus our attention on the layer between 15 and 25 km.

Figures 1*a* and 1*c* present typical extreme α profiles with the corresponding $\sigma_e(1.0)$ profiles. Profiles of type *a* are generally found in the areas where the optical depth δ is larger than 5.10^{-3} and are associated with extinction profiles showing a strong maximum around 18–20 km. A minimum of α corresponds to the maximum of $\sigma_e(1.0)$, pointing to a layer of relatively large particles at the level of maximum extinction. Above this layer the extinction coefficient decreases rapidly, whereas the Angström coefficient increases to a maximum around 22–23 km, corresponding to particles much smaller than those for the background stratosphere. At higher altitudes it seems that α decreases toward the background value of about 1.7, but the error bars become too large above 25 km to reach a clear conclusion.

The profiles of type *c* are generally found in areas with an optical depth between 3.10^{-3} and 4.10^{-3}; the extinction coefficient decreases rather regularly with increasing altitude but has values much higher than in nonvolcanic cases below 20

TABLE 1. SAGE Observations July 25 to July 31, 1980

Case Number	Latitude, N	Longitude, E	Optical Depth	α_{min}	α_{max}	$r_{m,max}$, µm	$r_{m,min}$, µm
1	65.0	262.0	$4.0\text{–}5.0 \times 10^{-3}$	1.11	2.63	0.18	0.065
2	64.9	237.5	$>5.0 \times 10^{-3}$	1.40	2.63	0.15	0.065
3	64.8	213.0	$>5.0 \times 10^{-3}$	1.09	2.78	0.18	0.060
4	64.6	188.5	$>5.0 \times 10^{-3}$	1.00	2.70	0.19	0.060
5	64.4	139.5	$>5.0 \times 10^{-3}$	1.11	2.86	0.18	0.055
6	64.3	115.0	$4.0\text{–}5.0 \times 10^{-3}$	1.46	2.20	0.14	0.090
7	64.1	90.5	$>5.0 \times 10^{-3}$	1.30	2.75	0.16	0.060
8	64.0	66.0	$4.0\text{–}5.0 \times 10^{-3}$	1.43	2.47	0.15	0.075
9	63.9	41.5	$>5.0 \times 10^{-3}$	0.50	2.53	0.25	0.070
10	63.7	17.0	$>5.0 \times 10^{-3}$	0.65	3.41	0.23	0.035
11	63.6	352.5	$4.0\text{–}5.0 \times 10^{-3}$	1.36	2.47	0.15	0.075
12	63.5	328.0	$3.0\text{–}4.0 \times 10^{-3}$	1.37	1.99	0.15	0.10
13	63.4	303.6	$3.0\text{–}4.0 \times 10^{-3}$	1.34	1.89	0.16	0.11
14	63.2	279.1	$4.0\text{–}5.0 \times 10^{-3}$	1.54	2.03	0.14	0.10
15	63.1	254.6	$>5.0 \times 10^{-3}$	1.41	2.21	0.15	0.090
16	63.0	230.2	$>5.0 \times 10^{-3}$	1.07	2.73	0.19	0.060
17	62.8	205.7	$>5.0 \times 10^{-3}$	0.77	3.47	0.22	0.030
18	62.7	181.3	$>5.0 \times 10^{-3}$	1.28	2.77	0.16	0.060
19	62.5	156.8	$>5.0 \times 10^{-3}$	1.06	2.62	0.19	0.065
20	62.4	132.4	$>5.0 \times 10^{-3}$	1.07	2.96	0.19	0.050
21	62.3	107.9	$4.0\text{–}5.0 \times 10^{-3}$	1.52	2.14	0.14	0.090
22	62.1	83.5	$>5.0 \times 10^{-3}$	1.55	2.48	0.14	0.075
23	62.0	59.0	$4.0\text{–}5.0 \times 10^{-3}$	1.38	2.30	0.15	0.080
24	61.8	34.6	$>5.0 \times 10^{-3}$	0.43	2.87	0.27	0.055
25	61.7	10.2	$>5.0 \times 10^{-3}$	0.87	3.12	0.21	0.045
26	61.6	345.7	$4.0\text{–}5.0 \times 10^{-3}$	1.03	2.79	0.19	0.060
27	61.4	321.3	$3.0\text{–}4.0 \times 10^{-3}$	1.08	1.96	0.19	0.10
28	61.3	296.9	$3.0\text{–}4.0 \times 10^{-3}$	1.59	2.11	0.13	0.090
29	61.1	272.5	$4.0\text{–}5.0 \times 10^{-3}$	0.95	2.48	0.20	0.075
30	61.0	248.0	$>5.0 \times 10^{-3}$	1.28	2.61	0.16	0.070
31	60.8	223.6	$>5.0 \times 10^{-3}$	1.14	2.83	0.18	0.060
32	60.7	199.2	$>5.0 \times 10^{-3}$	0.98	3.17	0.20	0.045
33	60.5	174.8	$>5.0 \times 10^{-3}$	1.30	2.18	0.16	0.090
34	60.4	150.4	$>5.0 \times 10^{-3}$	1.32	2.15	0.16	0.090
35	60.2	126.0	$>5.0 \times 10^{-3}$	1.02	2.60	0.19	0.070
36	60.1	101.6	$>5.0 \times 10^{-3}$	1.46	2.34	0.14	0.080
37	59.9	77.2	$4.0\text{–}5.0 \times 10^{-3}$	1.16	2.32	0.18	0.080
38	59.8	52.8	$4.0\text{–}5.0 \times 10^{-3}$	1.08	2.24	0.19	0.085
39	59.6	28.4	$>5.0 \times 10^{-3}$	0.20	3.00	0.31	0.050
40	59.5	4.0	$>5.0 \times 10^{-3}$	1.07	3.12	0.19	0.045
41	59.3	339.6	$>5.0 \times 10^{-3}$	0.89	2.80	0.21	0.060
42	59.2	315.3	$>5.0 \times 10^{-3}$	1.48	2.12	0.14	0.095
43	59.0	290.9	$>5.0 \times 10^{-3}$	1.44	1.96	0.15	0.10
44	58.9	266.5	$4.0\text{–}5.0 \times 10^{-3}$	1.30	2.63	0.16	0.065
45	58.7	242.1	$>5.0 \times 10^{-3}$	0.96	2.50	0.20	0.070
46	58.5	217.7	$>5.0 \times 10^{-3}$	0.90	2.53	0.21	0.070
47	58.4	193.4	$>5.0 \times 10^{-3}$	1.40	2.37	0.15	0.080
48	58.2	169.0	$>5.0 \times 10^{-3}$	1.39	1.99	0.15	0.10
49	58.1	144.6	$4.0\text{–}5.0 \times 10^{-3}$	1.54	2.39	0.14	0.080
50	57.9	120.3	$>5.0 \times 10^{-3}$	1.40	2.61	0.15	0.070
51	57.7	95.9	$4.0\text{–}5.0 \times 10^{-3}$	1.59	2.01	0.13	0.10
52	57.6	71.5	$4.0\text{–}5.0 \times 10^{-3}$	1.47	2.37	0.14	0.080
53	57.4	47.2	$4.0\text{–}5.0 \times 10^{-3}$	1.43	2.27	0.15	0.085
54	57.3	22.8	$>5.0 \times 10^{-3}$	0.56	2.81	0.25	0.060
55	57.1	358.4	$4.0\text{–}5.0 \times 10^{-3}$	1.39	2.34	0.15	0.080
56	56.9	334.1	$>5.0 \times 10^{-3}$	1.07	2.61	0.19	0.070
57	56.8	309.7	$4.0\text{–}5.0 \times 10^{-3}$	1.58	2.05	0.13	0.10
58	56.6	285.4	$>5.0 \times 10^{-3}$	1.32	2.42	0.16	0.075
59	56.4	261.0	$>5.0 \times 10^{-3}$	1.25	2.78	0.17	0.060

TABLE 1. (Continued)

Case Number	Latitude, N	Longitude, E	Optical Depth	α_{min}	α_{max}	$r_{m,max}$, μm	$r_{m,min}$, μm
60	56.3	236.7	$4.0–5.0 \times 10^{-3}$	1.62	2.44	0.13	0.075
61	56.1	212.4	$>5.0 \times 10^{-3}$	1.17	2.58	0.18	0.070
62	55.9	188.0	$>5.0 \times 10^{-3}$	1.48	2.08	0.14	0.095
63	55.7	163.7	$4.0–5.0 \times 10^{-3}$	1.36	2.13	0.15	0.095
64	55.6	139.3	$4.0–5.0 \times 10^{-3}$	1.06	2.34	0.19	0.080
65	55.4	115.0	$>5.0 \times 10^{-3}$	1.26	2.42	0.17	0.075
66	55.2	90.7	$4.0–5.0 \times 10^{-3}$	1.45	2.50	0.15	0.070
67	55.1	66.3	$4.0–5.0 \times 10^{-3}$	1.62	2.23	0.13	0.085
68	54.9	42.0	$4.0–5.0 \times 10^{-3}$	1.44	2.38	0.15	0.080
69	54.7	17.6	$4.0–5.0 \times 10^{-3}$	1.41	2.35	0.15	0.080
70	54.5	353.3	$4.0–5.0 \times 10^{-3}$	1.27	2.24	0.16	0.085
71	54.3	329.0	$>5.0 \times 10^{-3}$	1.45	2.46	0.15	0.075
72	54.2	304.7	$4.0–5.0 \times 10^{-3}$	1.29	2.01	0.16	0.10
73	54.0	280.3	$>5.0 \times 10^{-3}$	1.46	2.15	0.14	0.090
74	53.8	256.0	$>5.0 \times 10^{-3}$	1.54	2.61	0.14	0.070
75	53.5	207.4	$4.0–5.0 \times 10^{-3}$	1.34	1.96	0.15	0.10
76	53.3	183.1	$>5.0 \times 10^{-3}$	1.57	2.17	0.13	0.090
77	53.1	158.7	$4.0–5.0 \times 10^{-3}$	1.49	2.35	0.14	0.080
78	52.9	134.4	$4.0–5.0 \times 10^{-3}$	1.43	2.08	0.15	0.095
79	52.7	110.1	$>5.0 \times 10^{-3}$	1.25	2.57	0.17	0.070
80	52.5	85.8	$4.0–5.0 \times 10^{-3}$	1.51	2.07	0.14	0.095
81	52.4	61.5	$3.0–4.0 \times 10^{-3}$	1.31	2.17	0.16	0.090
82	52.2	37.2	$4.0–5.0 \times 10^{-3}$	1.41	2.27	0.15	0.085
83	52.0	12.9	$>5.0 \times 10^{-3}$	1.76	2.57	0.12	0.070
84	51.8	348.6	$3.0–4.0 \times 10^{-3}$	1.26	1.90	0.17	0.11
85	51.6	324.2	$4.0–5.0 \times 10^{-3}$	1.35	2.23	0.16	0.085
86	51.4	299.9	$3.0–4.0 \times 10^{-3}$	0.88	2.05	0.21	0.10
87	51.2	275.6	$4.0–5.0 \times 10^{-3}$	1.34	2.18	0.16	0.090
88	51.0	251.3	$4.0–5.0 \times 10^{-3}$	1.56	2.18	0.13	0.090
89	50.8	227.0	$4.0–5.0 \times 10^{-3}$	1.51	1.82	0.14	0.11
90	50.6	202.7	$>5.0 \times 10^{-3}$	1.39	2.19	0.15	0.090
91	50.4	178.4	$4.0–5.0 \times 10^{-3}$	0.90	2.47	0.21	0.075
92	50.3	154.1	$4.0–5.0 \times 10^{-3}$	1.44	2.14	0.15	0.090
93	50.1	129.8	$4.0–5.0 \times 10^{-3}$	1.52	2.10	0.14	0.095

The Angström coefficient is represented by α; r_m is the radius in a log normal distribution with $\sigma = 1.604$ ($r_{eff} = 0.250$).

km. The α profile is quite regular with values similar to the background values, and the volcanic material seems well mixed and homogeneous, in opposition to case *a*, where there is a sharp separation between a bottom layer of large particles and a top layer of small particles. The small oscillations observed on the extinction profiles of type *c* either can be erratic or can reveal very fine structures; they may seem to reflect slightly on the α profile, but the smoothing over 3 km and the uncertainties on α do not allow us to consider the small α oscillations as significant.

Various intermediate profiles between type *a* and type *c* are observed, more often in zones with intermediate values of the optical depth. Figure 1*b* shows an example of such an intermediate profile; a slight minimum of α is associated with the maximum of $\sigma_e(1.0)$ around 20 km, but the increase of α to a maximum value at about 22–23 km remains clear. No definite correlation has been found between the type of extinction and Angström coefficient profiles and either the tropopause height or the temperature profile.

For comparison, Figure 1*d* shows the profiles of $\sigma_e(1.0)$ and α for a clear case without volcanic material (δ between 1.10^{-3} and 2.10^{-3}). For 25 clear cases considered in the same zone in May 1980 we have always found α profiles to be nearly constant or to have small irregular oscillations between 1.5 and 2.1, with an average value around 1.75. On the May 1980 tape we have selected eight profiles in the vicinity of Mount St. Helens that show a strong volcanic contribution ($\delta > 3.10^{-3}$). The profile given on Figure 1*e* exhibits two strong extinction maxima around 16–18 km and 23 km. On the α profile, minimum values of α (large particles) correspond to these maximum of $\sigma_e(1.0)$, but the smoothing does not permit us to follow the detailed structure of the layer. The layer of small particles (fast decrease of $\sigma_e(1.0)$ and increase of α) is located above 23 km, i.e., higher than in July. Not all the May volcanic profiles display this particular structure, and they are, as expected, quite variable near the time of eruption. Many studies [*Newell and Deepak*, 1982] have been devoted to the dispersion of the volcanic material in the first days or weeks after the eruption, and SAGE observations are certainly more adapted and useful to study the quasi-stable global situation obtained after 2 months.

Table 1 presents the values of the maximum (α_{max}) and minimum (α_{min}) Angström coefficients for the 93 volcanic profiles of July 1980. The average of α_{max} is 2.42, and the average of α_{min} is 1.26.

The knowledge of the Angström coefficient α enables fixing one size distribution parameter for the aerosol. It has been shown by many authors [*Pinnick et al.*, 1976; *Gras and Laby*, 1981] that experimental observations of the stratospheric aerosol size distribution can be fitted by log-normal distributions. We have thus chosen a log-normal distribution

$$n(r) = \frac{1}{\sqrt{2\pi}\, r \ln \sigma} \exp\left(-\frac{\ln^2 r/r_m}{2 \ln^2 \sigma}\right) \qquad (2)$$

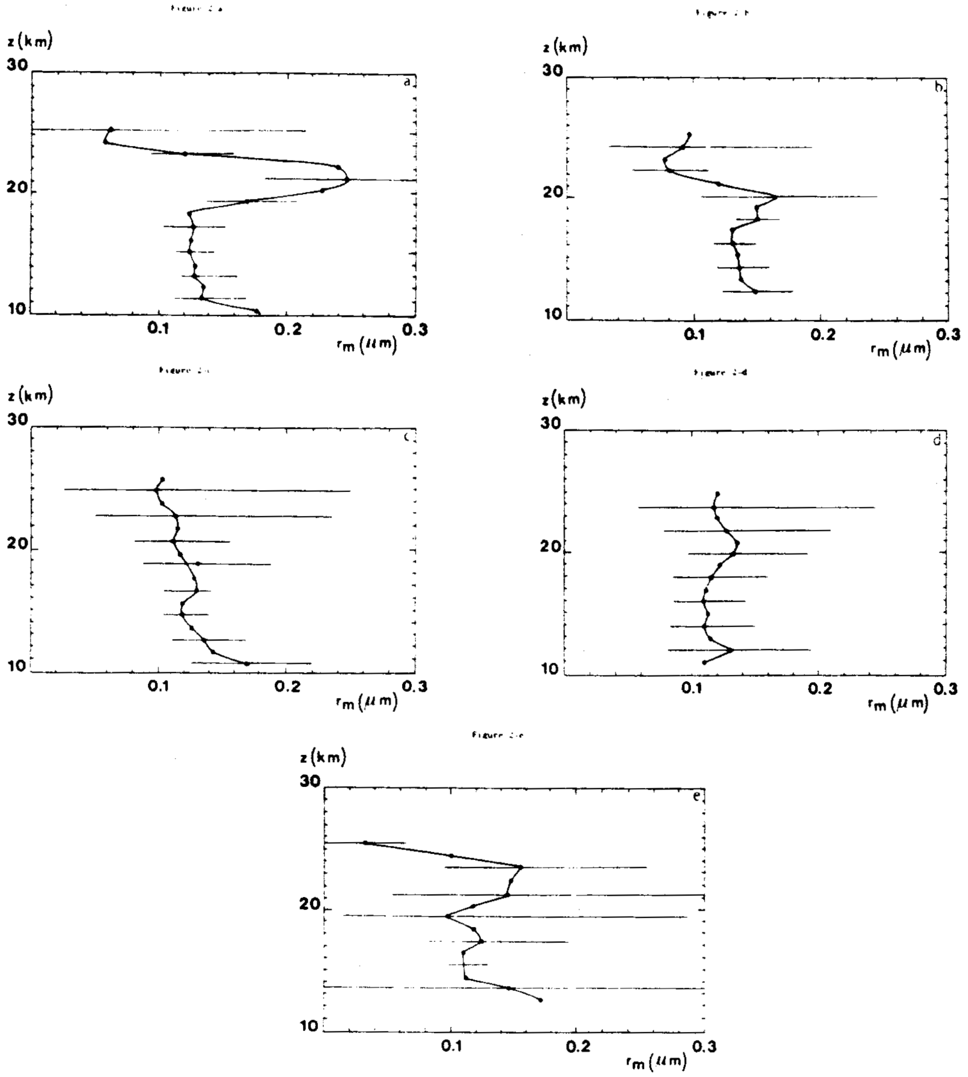

Fig. 2. Profiles of the mode radius r_m for an equivalent log-normal distribution with $v_{eff} = 0.250$ ($\sigma = 1.604$). Same cases as in Figure 1.

where $n(r)\,dr$ is the number of particles with a radius between r and $r + dr$ normalized to one particle per unit volume; r_m is a mode radius on a semilogarithmic scale, and σ defines the width of the distribution. They are related to the effective radius r_{eff} and effective variance v_{eff} [*Hansen and Hovenier*, 1974] by

$$v_{eff} = \exp(\ln^2 \sigma) - 1 \qquad r_{eff} = r_m \exp\left(\frac{5}{2}\ln^2 \sigma\right) \tag{3}$$

From the above mentioned observations, σ varies between 1.5 and 2.0. We have chosen here $\sigma = 1.604$, which gives $v_{eff} = 0.250$ [*Lenoble and Brogniez*, 1984], i.e., the value of v_{eff} assumed in the Standard Radiation Atmosphere models [*McClatchey et al.*, 1980]. The particles are assumed to be 75% H_2SO_4 droplets [*Rosen*, 1971], and the relation between α and r_m has been tabulated using Mie theory. For the background nonvolcanic case ($1.5 \leq \alpha \leq 2.1$ with $\bar{\alpha} = 1.75$) this leads to an average value of 0.12 μm for the mode radius r_m, with oscillations between 0.10 μm and 0.14 μm. For the volcanic profiles of type *a*, particles with mode radius of about 0.20 μm ($\alpha = 0.94$) or even larger are often found in the 20-km layer; in the top layer around 23 km, particles with $r_m \simeq 0.06$ μm ($\alpha \simeq 2.7$) are usually found. Figure 2 shows the profiles of r_m corresponding to the α profiles of Figure 1, with the error bars caused by the uncertainties on α. Table 1 gives the maximum $r_{m,max}$ and minimum $r_{m,min}$ mode radius corresponding to α_{max} and α_{min}, respectively.

The size distributions obtained by this procedure must be understood as "equivalent size distributions" in the sense that the equivalent and the real size distributions lead to the same ratio between the extinction coefficients at 0.45 and 1.0 μm. If we had chosen a log-normal distribution with a larger variance, the values of r_m would have been found to be smaller for a given α as a result of the predominant influences of the large particles in the size distributions; roughly, r_m would be divided by 2 when v_{eff} was increased from 0.25 to 0.53, which corresponds to an increase of σ from 1.6 to 1.92. However, this "equivalent size distribution" can be used with some caution to derive the mass density profile, as will be discussed in section 4.

The effective radius r_{eff} defined by (3) is much less sensitive than r_m to the assumption on v_{eff} for a given α; for the same change of v_{eff} from 0.25 to 0.53, r_{eff} is divided by 1.4 around $\alpha = 2$; the modification of r_{eff} then decreases towards smaller

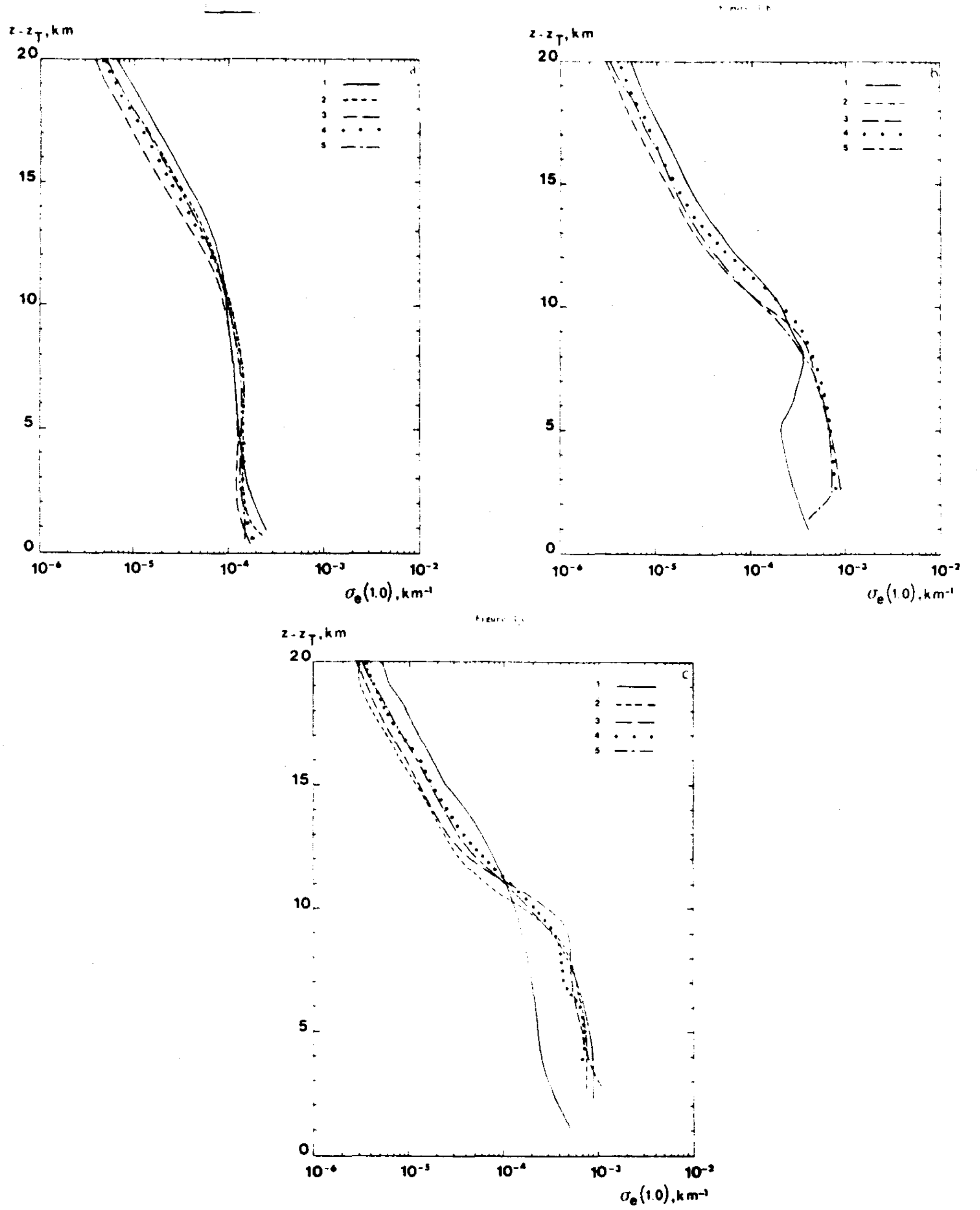

Fig. 3. Latitude average profiles of the extinction coefficient $\bar{\sigma}_e(1.0)$ at 1 μm above the tropopause height z_T; (*a*) 1979 profiles at 55°N and 65°N—(curve 1) April 29 to June 1; (curve 2) June 1 to August 7; (curve 3) August 7 to September 14; (curve 4) September 14 to October 21; (curve 5) October 21 to November 22. Curves 1, 2, and 3 present the averages of the 55°N and 65°N profiles, which are very close. Curves 4 and 5 are the 55°N profiles (no observations at 65°N). (*b*) 1980 profiles at 55°N—(curve 1) May 11 to June 23; (curve 2) June 23 to July 20; (curve 3) July 20 to August 28; (curve 4) August 28 to September 28; (curve 5) September 28 to October 31. The satellite movement starts north to south on May 11 and reverses for each period. (*c*) 1980 profiles at 65°N—same as for Figure 3*b*.

α to reach zero at $\alpha \simeq 0.6$. Therefore it can be expected that the utilization of our equivalent size distribution will allow the determination of some radiative characteristics of the aerosol, such as the asymmetry factor [*Lenoble and Pruvost*, 1983]; this problem of radiative characteristics will be discussed in detail in another paper.

The most extended direct measurements of the stratospheric aerosol size distributions after the Mount St. Helens eruption have been done by *Hofmann and Rosen* [1982], using various balloon-borne particle counters. Their measurements cover the period May 1980 to May 1981 and are made at Laramie (41°N). From the SAGE optical depth maps the July–August 1980 measurements should be in a zone with $\delta \simeq 3\text{–}4.10^{-3}$. From June until November 1980 their results consist of profiles of aerosol and condensation nuclei concentration N for the three classes of dimension $r \geq 0.25$ μm, $r \geq 0.15$ μm, and $r \geq 0.01$ μm. A quantitative comparison between these data and SAGE results is of course not possible, as the observations are not coincident in time and are not made at the same latitude; moreover, SAGE observations integrate atmospheric properties over a horizontal path of a few hundred kilometers, whereas balloon-borne instruments measure local profiles; however, some qualitative comparison can be tried.

From *Hofmann and Rosen* [1982] results the several identifiable layers observed during the first weeks merge slowly into a main layer at about 18 km; this quasi-static aerosol profile is attained in September at Laramie, but it is probably this main layer we observe on SAGE profiles in July at about 18–20 km. The size ratio $N(r \geq 0.15\ \mu m)/N(r \geq 0.25\ \mu m)$ is very variable, with some regions of relatively large particles and some of relatively small particles. Hofmann and Rosen also found an important enhancement of condensation nuclei (CN) both in the main layer and at higher levels (retrograde layer, 22–24 km). The CN levels are back to normal approximately 4–5 months after the eruption. Their Figure 15 shows the three profiles $N(r \geq 0.25\ \mu m)$, $N(r \geq 0.15\ \mu m)$, and $N(r \geq 0.01\ \mu m)$ for July 14, 1980, and it appears that the peak heights are inverse to the size, in agreement with our observation of smaller particles at about 23 km. However, the size ratio indicates unusually large particles at about 22 km, a result which can only be reconciled with SAGE observation of large α values at this level if we consider that the size ratio concerns only the particles in the size range 0.15–0.25 μm and larger than 0.25 μm. The α value can be strongly influenced by the presence of smaller particles (CN) also detected at this level by Hofmann and Rosen.

Fitting their results with a log-normal function, *Hofmann and Rosen* [1982] found $\sigma \simeq 1.6$–1.9 and $r_m \simeq 0.07$–$0.09\ \mu m$ between 16 and 20 km (Figure 19 and Figure 24 of their paper): from their Figure 24 it seems that σ regularly decreases and r_m increases when the layer is aging. This opposite variation cannot be detected by the only parameter α, which could even remain approximately constant. If we assume for July $\sigma \simeq 1.9$ from Hofmann and Rosen values, r_m is about 0.09 μm, close to their values in the large-particle layer (18–20 km). For August 1980, r_m decreases to about 0.015 μm at 22 km, probably due to a large quantity of CN. After November 1980, measurements of larger particles $N(r > 0.95\ \mu m)$, $N(r > 1.2\ \mu m)$, and $N(r > 1.8\ \mu m)$ were added; they revealed the existence of a second mode with $r_m \simeq 1.0\ \mu m$. It is not known if this mode existed earlier or how it might have evolved in time. How the presence of a small number of such large particles would influence our equivalent model remains to be checked, but it might explain why our values of r_m are larger than those of Hofmann and Rosen for the main layer.

Hofmann et al. [1983] have proposed to fit the January 15, 1981, data at 15 km by the bimodal distribution: $r_{m0} = 0.073\ \mu m$, $\sigma_0 = 1.76$, $N_0 = 28$ particles cm^{-3}; $r_{m1} = 1.0\ \mu m$, $\sigma_1 = 1.10$, $N_1 = 0.01$ particles cm^{-3}; this model leads to a value $\alpha = 1.62$ for the Angström coefficient, in reasonable agreement with the SAGE average value. Smaller values of α in the main layer can be fitted by increasing the concentration of the large particles in such a model. But values larger than $\alpha = 1.95$ cannot be obtained with $r_m = 0.073\ \mu m$ and $\sigma = 1.76$, and a smaller mode is necessary to fit the data in the 23-km layer.

3. SAGE AVERAGE PROFILES OVER LATITUDE BANDS

The individual volcanic profiles of the Angström coefficient used in the previous section clearly prove a typical variation of the particle sizes within the 15–25 km layer. In order to see if this variation is important on a global scale and persists during several months after the eruption, we have used profiles of the extinction coefficients $\bar{\sigma}_e(1.0)$ and $\bar{\sigma}_e(0.45)$ averaged over 10° latitude bands. These average profiles have been computed at NASA Langley Research Center for each sweep of the satellite and provided to us with the corresponding $\bar{\alpha}$ average profiles. For 1979 these profiles provide a good reference for modeling the background stratosphere, whereas the 1980 average profiles are, at least for the northern latitudes, perturbed by the volcanic eruptions.

To be understood clearly, the meaning of these average profiles requires some discussion. When the size distribution and the nature of the particles do not change, averaging an extinction coefficient simply results in averaging the number density of particles or the mass density of the material. But this is not the case when the size distribution changes, as indicated by the different variations of the extinction coefficients at 1.0 and 0.45 μm (leading to variations of α). From Mie theory the extinction coefficient at λ is defined as

$$\sigma_e(\lambda) = N \int_0^\infty \pi r^2 Q_{ext}(\lambda, r, m) n(r)\, dr \tag{4}$$

where Q_{ext} is the Mie extinction cross section, m the refractive index, and N the total number density. At each level we associate with the average $\bar{\alpha}$ an average size distribution $\bar{n}(r)$, defined by

$$\frac{\int_0^\infty r^2 Q_{ext}(0.45, r, m)\bar{n}(r)\, dr}{\int_0^\infty r^2 Q_{ext}(1.0, r, m)\bar{n}(r)\, dr} = \lambda^{-\bar{\alpha}} \tag{5}$$

and the average density number $\bar{N}$ derives from

$$\bar{\sigma}_e(1.0) = \bar{N} \int_0^\infty \pi r^2 Q_{ext}(1.0, r, m)\bar{n}(r)\, dr \tag{6}$$

Figure 3 shows the average extinction profiles at 1.0 μm for the latitude belts centered at 55°N and 65°N from May 1980 to the end of October 1980 and for the same period in 1979; no observations are available at these latitudes for November and December; all the profiles are presented from the average tropopause level, which is at about 9.5 or 10 km, as origin of the altitudes. As previously, we will focus our attention on the layer 15–25 km, i.e., between 5 and 15 km, above the tropopause. All the 1979 profiles are very similar. For 1980 a slight perturbation appears on the May 11 to June 23 profile and becomes more pronounced at 55°N as the Mount St. Helens dust has spread only slightly north. All the following 1980 profiles exhibit for both latitudes a strong enhancement below approximately 20–22 km if we assume an altitude around 10 km for the tropopause. Above this altitude the extinction is close to the background, and even a little smaller, due probably to the smaller size of the particles, as it will be discussed later.

Figure 4 presents the corresponding $\bar{\alpha}$ average profiles. The 1979 profiles are quite regular, slightly increasing toward high altitudes in summer and almost constant during the other months; most of the values range between 1.5 and 1.8. The perturbation appears small in May 1980; it reaches its maximum in June–July, where the shape of the average profile reflects the features observed on individual profiles in July 1980, with a minimum (large particles) around 19–20 km and a maximum (small particles) around 22–23 km. The variation is larger at 65°N ($\alpha_{max} \simeq 2.5$; $\alpha_{min} \simeq 1.45$) than at 55°N ($\alpha_{max} \simeq 2.2$, $\alpha_{min} \simeq 1.5$), corresponding to a higher value of σ_e (1.0) around 20 km at 65°N. At the end of September and beginning of October the oscillations of the α profile have diminished, pointing to a slow homogenization of the aerosol sizes, although the extinction remains quite high (see Figure 3); in October, α_{max} is about 2.0 and α_{min} about 1.5 for both latitudes.

Figure 5 compares the $\bar{\alpha}$ average profiles at 65°N for the end of July 1980 and the beginning of August 1979 with the standard deviations of the mean value. The standard devi-

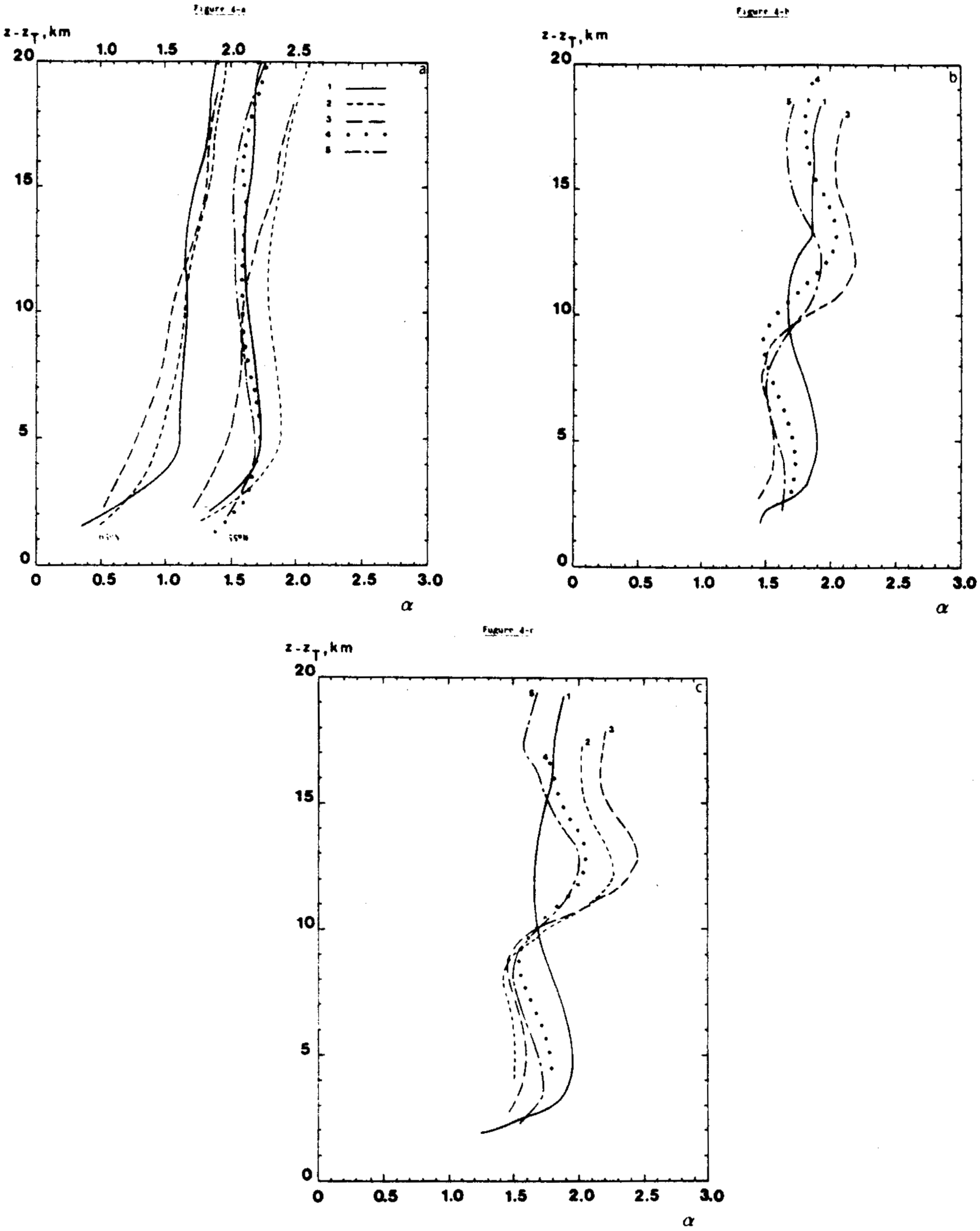

Fig. 4. Latitude average profiles of the Angström coefficient $\bar{\alpha}$: (*a*) 1979 profiles at 55°N and 65°N—same as Figure 3*a*, except that profiles at 55° and 65° are shown separately; the 3 curves on the left are for 65°N and correspond to the upper scale. (*b*) Same as Figure 3*b*. (*c*) Same as Figure 3*c*.

ations are larger for the volcanic case, as would be expected from the observation of the individual profiles (see section 2).

The observation of the average profiles confirms that the structure with a layer of relatively large particles around 19–20 km, topped by a layer of small particles at about 22–23 km, is important on a global scale during a few months after the eruption. In the 20 km layer the particle sizes are close to the extreme higher values found in the background stratosphere, whereas in the top layer they are definitely smaller, even in October, 5 months after the eruption. Translated in terms of an average size distribution $\bar{n}(r)$ as defined above, the extreme values of α lead to the mode radius values given in Table 2 for a log-normal distribution with $\sigma = 1.604$ ($v_{\rm eff} = 0.250$).

4. AEROSOL MASS DISTRIBUTION

If the normalized size distribution $n(r)$ is known, the number density N of the particles is obtained from the measured extinction coefficient $\sigma_e(1.0)$, using equation (4) written for $\lambda = 1.0$ μm; the integral on the right side of (4) is computed from the Mie theory for one particle per unit volume. The mass of material per unit volume derives from

$$M = N\rho \frac{4}{3}\pi \int_0^\infty r^3 n(r)\, dr \qquad (5)$$

where ρ is the material density taken as 1.75 for the 75% H_2SO_4 particles at 220 K.

As our only knowledge about the size distribution from

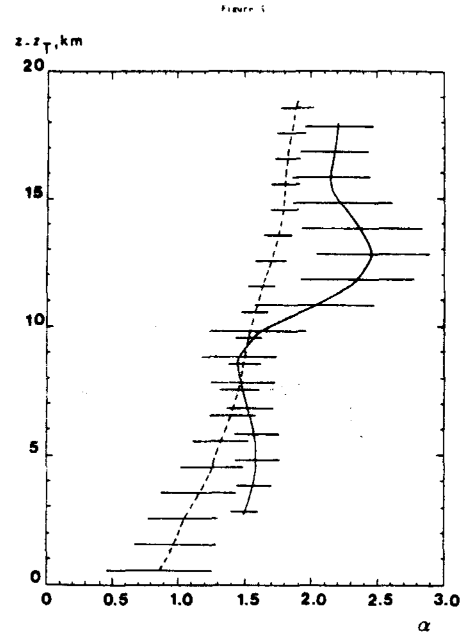

Fig. 5. Comparison of the latitude average profiles of the Angström coefficient α at 65°N for the periods July 20 to August 28, 1980 (solid line) and August 7 to September 14, 1979 (dashed line), with the standard deviations.

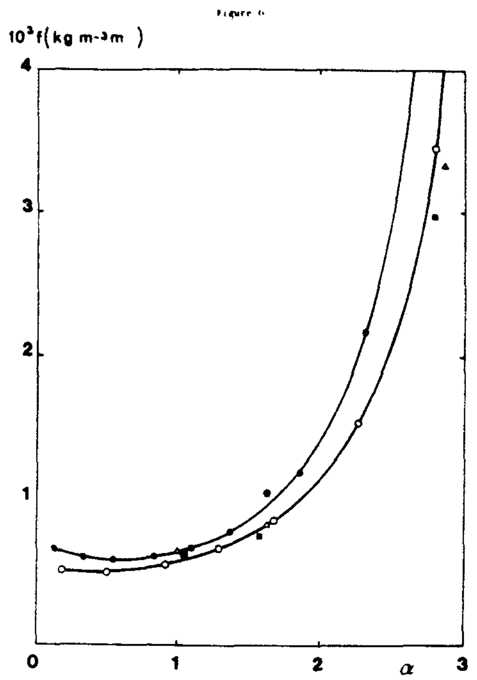

Fig. 6. Variation of the ratio f of mass density M to extinction $\sigma_e(1.0)$ versus the Angström coefficient α for log-normal distributions with $v_{eff} = 0.250$ (open circles) and $v_{eff} = 0.528$ (filled circles). The open triangles refer to gamma distributions and the filled squares to an increase of 2% for the refractive index. The star is for *Hofmann et al.* [1983] distribution.

SAGE data comes through the α value, we have computed the mass factor $f = M/\sigma_e(1.0)$ and the Angström coefficient α for various log-normal distributions. We have chosen two different variances $v_{eff} = 0.250$ ($\sigma = 1.604$) and $v_{eff} = 0.528$ ($\sigma = 1.918$) which encompass most of the directly observed values. For each variance the mode radius has been varied within limits chosen in order to have α varying between 0 and 3.5. Figure 6 shows the variations of the mass factor f versus α; therefore the mass can be obtained directly from the $\sigma_e(1.0)$ and α profiles associated with Figure 6, without trying a retrieval of the mode radius. It has been checked that modified gamma distributions with the same effective variance and the same effective radius give points on the same curves. The influence of a 2% change in the refractive index, which could be due to temperature or to concentration variations, has also been found negligible. For small particles the extinction cross section decreases much faster than the geometric section, leading to a fast increase of f toward large α values, whereas for large particles the extinction cross section increases like r^2, leading to an increase of f toward larger radius, as it appears on the curves for α approaching zero. As long as monomodal distributions are assumed, the two curves drawn on Figure 6 delimit reasonably well the domain of variation of f for α given. The behavior of bimodal distributions is, of course, much more complex, as we have five variables to consider, the two variances, the two mode radii, and the relative concentration; for the bimodal distribution observed by *Hofmann et al.* [1983] and defined in section 2 the point (f, α) is shown on Figure 6 very close to the monomodal curve for $v_{eff} = 0.528$.

Figure 7 shows the mass density profile for the case of Figure 1*a*. Two curves correspond to the assumptions $v_{eff} = 0.250$ or $v_{eff} = 0.528$, and the error bars on each curve are related to the uncertainties on α and to a smaller degree on $\sigma_e(1.0)$. The oscillation which appears in the top layer can be spurious, as the general slow decrease of M is due to a partial compensation of the rapid decrease of $\sigma_e(1.0)$ by the rapid increase of f; therefore the error bars become large, and individual points should be considered with caution. However, if the information contained in the α coefficient retrieved from SAGE data does not allow a very precise retrieval of the aerosol mass profile, it brings an important improvement; if we had neglected the variations of the aerosol sizes, using the same aerosol model within the whole layer, we would have obtained a mass density proportional to $\sigma_e(1.0)$ that is decreasing approximately by a factor 50 between 20 and 25 km, whereas the decrease is only by a factor 15. This is made

TABLE 2. Mode Radius r_m(μm) for Latitude Average Size Distributions at 55°N and 65°N After the Mount St. Helens Eruption

	June 23 to July 20		July 20 to August 28		August 28 to September 28		September 28 to October 31	
Layer, km	55°	65°	55°	65°	55°	65°	55°	65°
18–20		0.151	0.142	0.146	0.142	0.137	0.142	0.142
22–23		0.084	0.090	0.073	0.100	0.100	0.106	0.103

The distribution is assumed log normal with $\sigma = 1.604$ ($v_{eff} = 0.250$).

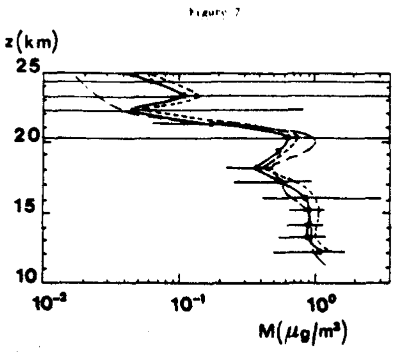

Fig. 7. Mass profile for the volcanic case of Figure 1*a* for $v_{eff} = 0.250$ (filled circles on solid line) and $v_{eff} = 0.528$ (short-dashed line) with exact α profile and for $v_{eff} = 0.250$ with $\bar{\alpha} = 1.7$ (long-dashed line).

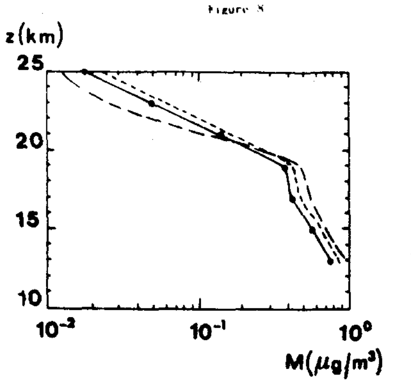

Fig. 8. Same as Figure 7 for the average profile at 65°N, July 20 to August 28, 1980.

clearer on Figure 7, where the mass profile obtained with a constant background value $\bar{\alpha} \simeq 1.7$ for the same case is presented for comparison. For the latitude average profiles the variations of α are smoothed, and the mass density profile can generally be deduced with an average mass factor; however, the influence of the variable size distribution with height remains apparent at 65°N in July, as shown on Figure 8.

Hofmann and Rosen [1982] present on their Figure 19 profiles of the aerosol mass derived from their balloon measurements of the size distribution made at Laramie (41°N). Their value in the main layer is around 0.3 μg m^{-3}, which compares with our value of 0.45 μg m^{-3} on Figure 8. The optical depth at 1.0 μm remains around 3.0–4.0×10^{-3} at 40°N from July to the end of 1980, whereas it is larger than 4.0×10^{-3} and often larger than 5.0×10^{-3} for the latitude band 60–70°N in July 1980; the ratio 1.5 between Hofmann and Rosen's mass density and our value corresponds reasonably to the ratio of the observed optical depths at the two latitudes. Lidar measurements and SAGE data worked out at NASA Langley Research Center [*Newell and Deepak*, 1982] lead to an average value of 0.3 μg m^{-3} over the northern hemisphere in the volcanic layer; this figure averages lower values at low latitudes and higher values at high latitudes, as we have found.

Our Figure 7 proves that much higher values (~0.8 μg m^{-3}) can be found locally for extreme volcanic cases. Table 3 gives for the extreme volcanic case of Figure 7 the total column mass above the tropopause (11.3 km) and in the layers 18.3–21.3 km and 21.3–25.3 km, with the different assumptions. Taking into account our knowledge of the variation of α with height leads to an estimation of the total column mass between 7.1×10^3 and 8.3×10^3 μg m^{-2}, choosing an average size distribution ($\bar{\alpha} \simeq 1.7$) overestimates the mass by approximately 15%. Most of the overestimation concerns the layer between 18–21 km (overestimation ~65%), whereas the mass between 21 and 25 km is strongly underestimated (by 25%). For local detailed studies this certainly has to be taken into account.

5. CONCLUSION

The volcanic extinction profiles at 1.0 and 0.45 μm observed at high northern latitudes in July 1980 have been used to retrieve the Angström coefficient α profiles. The observed α profiles vary between two extreme cases which can be interpreted in terms of particle size distribution as follows: Case 1—a layer of large particles at about 18–20 km, corresponding to the maximum extinction, is topped by a layer of small particles at about 22–23 km. Case 2—the whole layer between 15 and 25 km is well mixed with particles of approximately the same size as the background stratosphere. Case 1 is generally found when the volcanic loading is maximum, associated with optical depth around 5×10^{-3}. Its frequency is large enough to influence the latitude average profiles at 55°N and 65°N, which exhibits this structure of a layer of large particles topped by a layer of small particles at least until October 1980, with a slow homogenization starting after the maximum of July. This structure has to be considered in the theories of volcanic aerosol formation and could hopefully be explained.

It is impossible with the only parameter α to obtain quantitative information about the particles sizes. Only an "equivalent size distribution" with one free parameter can be derived from the measured value of α; choosing a log-normal model with an effective variance $v_{eff} = 0.250$ ($\sigma = 1.604$) leads to a logarithmic mode radius $r_m \simeq 0.20$ μm for the large particle layer, $r_m \simeq 0.06$ μm for the top layer, and $r_m \simeq 0.12$ μm for the background; with $v_{eff} = 0.528$ ($\sigma = 1.918$) the mode radii would be $r_m \simeq 0.09$ μm for large particles, $r_m \simeq 0.02$ μm for small particles, and $r_m \simeq 0.06$ μm for the background.

The mass density profile retrieved with this equivalent size

TABLE 3. Estimated Column Mass (mg m^{-2}) for the volcanic profile of Figure 1*a*, Assuming a Log-Normal Size Distribution with $v_{eff} = 0.250$ ($\sigma = 1.604$) and $v_{eff} = 0.528$ ($\sigma = 1.918$)

	Exact α Profile		$\bar{\alpha} = 1.7$	
Layer, km	$v_{eff} = 0.250$	$v_{eff} = 0.528$	$v_{eff} = 0.250$	$v_{eff} = 0.528$
11.3–25.3	7.5	8.28	8.33	9.88
18.3–21.3	1.42	1.65	2.35	2.78
21.3–25.3	0.32	0.40	0.24	0.29

In columns 2 and 3 the variation with altitude of the mode radius deduced from the α profile is taken into account. In columns 4 and 5 the size distribution is independant of altitude.

distribution is not too sensitive to the exact choice of the model within the limits considered of an effective variance between 0.250 and 0.528. For strong volcanic profiles, neglecting the variation of particle sizes with height would generally lead to a small error on the total column mass but to a large error on its distribution, overestimating the mass in the main layer 18–21 km by 65% and underestimating it in the top layer by 25%, where the fast decrease of extinction is not due entirely to the decrease of dust but, for a nonnegligible part, to the decrease of the particle sizes.

Acknowledgments. The authors are grateful to the Aerosol Research Branch of the NASA Langley Research Center for providing them with SAGE data. We are particularly grateful to G. S. Kent and U. O. Farrukh, who have kindly prepared the latitude average profiles. This work has been supported by the Centre National d'Etudes Spatiales under contract 83/230.

REFERENCES

Chu, W. P., and M. P. McCormick, Inversion of stratospheric aerosol and gaseous constituents from spacecraft solar extinction data in the 0.38–1.0 μm wavelength region, *Appl. Opt.*, *18*, 1404–1413, 1979.

Gras, J. L., and J. E. Laby, Southern hemisphere stratospheric aerosol measurements, 3, Size distribution 1974–1979, *J. Geophys. Res.*, *86*, 9767–9775, 1981.

Hansen, J. T., and J. W. Hovenier, Interpretation of the polarization of Venus, *J. Atmos. Sci.*, *31*, 1137–1160, 1974.

Hofmann, D. J., and J. M. Rosen, Balloon-borne observations of statospheric aerosol and condensation nuclei during the year following the Mount St. Helens eruption, *J. Geophys. Res.*, *87*, 11,039–11,061, 1982.

Hofmann, D. J., J. M. Rosen, R. Reiter, and H. Jäger, Lidar and balloon-borne particle counter comparisons following recent volcanic eruptions, *J. Geophys. Res.*, *88*, 3777–3782, 1983.

International Association of Meteorology and Atmospheric Physics, Symposium on Atmospheric Effects of the 1982 Eruptions of El Chichon Volcano, Hamburg, Fed. Repub. Germany, Aug. 19–20, 1983.

Kent, G. S., SAGE measurements of Mount St. Helens volcanic aerosols, Atmospheric Effects and Potential Climatic Impact of the 1980 Eruptions of Mount St. Helens, *NASA Conf. Publ. 2240*, pp. 109–115, 1982.

Lenoble, J., and C. Brogniez, A comparative review of radiation aerosol models, *Contr. Atmos. Phys.*, *57*, 1–20, 1984.

Lenoble, J., and P. Pruvost, Inference of the aerosol Angström coefficient from SAGE shortwavelength data, *J. Clim. Appl. Meteorol.*, *22*, 1717–1725, 1983.

McClatchey, R. E., H. J. Bolle, and K. Ya. Kondratiev, Report of the IAMAP Radiation Comission Working Group on a Standard Radiation Atmosphere, 33 pp., WMO/IAMAP, Geneva, 1980. (Available from Air Force Geophysics Laboratory, Hanscom AFB, MA 01731.)

McCormick, M. P., P. Hamill, T. J. Pepin, W. P. Chu, T. J. Swissler, and L. R. McMaster, Satellite studies of the stratospheric aerosol, *Bull. Am. Meteorol. Soc.*, *60*, 1038–1046, 1979.

McCormick, M. P., C. R. Trepte, and G. S. Kent, Spatial changes in the stratospheric aerosol associated with the north polar vortex, *Geophys. Res. Lett.*, *10*, 941–944, 1983.

National Aeronautic and Space Administration, Symposium on Atmospheric Effects and Potential Climatic Impact of the 1980 Eruptions of Mt. St. Helens, Wash., D.C., November 18–19, 1980.

Newell, R. E., and A. Deepak (Ed.), Mount St. Helens eruptions of 1980: Atmospheric effects and potential climatic impact, *NASA SP-458*, 119 pp., 1982.

Pinnick, R. G., J. M. Rosen, and D. J. Hofmann, Stratospheric aerosol measurements, 3, Optical model calculations, *J. Atmos. Sci.*, 33, 304–314, 1976.

Rosen, J. M., The boiling point of stratospheric aerosols, *J. Appl. Meteorol.*, *10*, 1044–1045, 1971.

J. Lenoble, P. Pruvost, and C. Brogniez, Laboratoire d'Optique Atmosphérique, ERA 466, Universite des Sciences et Techniques de Lille, 59655 Villeneuve d'Ascq Cedex, France.

(Received April 19, 1984;
revised July 11, 1984;
accepted August 9, 1984.)

Reprinted from Applied Optics, Vol. *24*, page 1054, April 1, 1985
Copyright © 1985 by the Optical Society of America and reprinted by permission of the copyright owner.

Information on stratospheric aerosol characteristics contained in the SAGE satellite multiwavelength extinction measurements

J. Lenoble and C. Brogniez

Aerosol models with monomodal and bimodal size distributions are used to simulate the retrieval of mass density, optical depth and asymmetry factor averaged over the solar spectrum, infrared optical depth and backscatter coefficient from the two-wavelength SAGE satellite extinction measurements. The solar optical depth is well retrieved. For the other parameters only brackets can be given for monomodal size distributions and the main difficulty appears with bimodal size distributions. The four-wavelength extinction measurements from the future SAGE II should lead to better retrieval.

I. Introduction

The best present global climatology of stratospheric aerosols is provided by the NASA satellite experiments SAM II (Stratospheric Aerosol Measurement II) and SAGE (Stratospheric Aerosol and Gas Experiment).[1] Whereas SAM II provides aerosol extinction profiles at 1.0 μm, SAGE is a four-channel instrument; the 1.0- and 0.6-μm channels give, respectively, good quality extinction profiles for aerosols and ozone. The short-wavelength channels at 0.45 and 0.385 μm are more difficult to handle as NO_2 and aerosols give similar contributions to both channels. However, the separation can be achieved and the SAGE products contain aerosol extinction profiles at 0.45 μm and NO_2 extinction profiles at 0.385 μm. Moreover up to 25 km the influence of NO_2 on the retrieval of aerosol extinction is small.[2]

From the 1.0-μm extinction profiles, the aerosol mass and main radiative characteristics can be inferred only by assuming an aerosol model with a given size distribution,[3] whereas measurements at a second wavelength can bring further information and help put constraints on the possible models. Some attempts have already been made to retrieve one parameter of the size distribution[4] or to relate directly the volume or mass distribution of the aerosol[5,6] or the asymmetry factor[2] to the ratio of extinction in channels 1.0 and 0.45 μm. But no systematic study of the information content of the 1.0- and 0.45-μm extinction ratio has been made so far. We will address this problem by studying the relationship between several important aerosol properties and the Angström coefficient [related to the extinction ratio by Eq. (1) below], for a large range of aerosol size distributions, either monomodal or bimodal.

The main aerosol characteristics to be considered in addition to their size and mass are the radiative characteristics which either control their climatic impact or have to be used for comparison of different correlative measurements. The characteristics we chose are defined in Sec. II, where the problem is presented in more detail. Section III describes the method and the aerosol models. Section IV gives the results for aerosols with a monomodal size distribution and Sec. V for the bimodal size distributions. In Sec. VI we discuss these results and suggest the improvement which could be gained by the use of more wavelengths as in SAGE II.

II. Deriving Aerosol Characteristics from SAGE Observation

The SAGE aerosol data consist of vertical profiles of the aerosol extinction coefficient $\sigma_e(\lambda)$ for $\lambda = 1.0$ μm and $\lambda = 0.45$ μm. It is convenient to introduce an average Angström coefficient between 0.45 and 1.0 μm by

$$\alpha = -\log[\sigma_e(0.45)/\sigma_e(1.0)]/\log(0.45). \qquad (1)$$

From SAGE measurements, the average value of α is ~1.6–1.7 for the background stratospheric aerosol and varies between ~0.5 and 3.0 for volcanic profiles.[6] For very large particles α may exhibit negative values and

---

The authors are with Universite des Sciences et Techniques de Lille, Laboratoire d'Optique Atmospherique, ERA 466, 59655 Villeneuve d'Ascq CEDEX, France.

Received 26 May 1984.
0003-6935/85/071054-10$02.00/0.
© 1985 Optical Society of America.

the Rayleigh limit for very small particles is close to 4 with a small correction because of the spectral variation of the refractive index (4.05 for sulfuric acid). If the particles are spherical, as it seems reasonable to assume from polarization measurements,[7] the extinction coefficient at wavelength λ is defined by the Mie theory as

$$\sigma_e(\lambda) = N \int_0^\infty \pi r^2 Q_{\text{ext}}(\lambda,r,m) n(r) dr, \tag{2}$$

where Q_{ext} is the Mie extinction cross section, m is the refractive index, $n(r)$ is the size distribution normalized to 1 particle per unit volume, and N is the total number density. The ratio of extinction at two wavelengths (or the Angström coefficient) depends on the type of aerosols only through m and $n(r)$. Stratospheric aerosols are known to consist mainly of a sulfuric acid solution in water, which allows us to fix the refractive index within narrow limits, the variations being due to the variations of temperature and dilution and to small quantities of other soluble materials such as ammonium sulfate. In what follows we will assume the stratospheric aerosols are 75% H_2SO_4 (Ref. 8) and check the influence of small variations of the refractive index. The possible presence of strongly absorbing impurities is a more tricky problem, which we have not tackled because of the total lack of information on this point.

Assuming a size distribution with one adjustable parameter, the measured value of α leads to a unique determination of this parameter and therefore to an equivalent size distribution $n_e(r)$; the meaning of equivalent is restricted to mean that an aerosol with the size distribution $n_e(r)$ gives the same ratio $\sigma_e(0.45)/\sigma_e(1.0)$ as the actual aerosol with the unknown size distribution $n(r)$. Generally at least two parameters are necessary to define a monomodal size distribution, and several parameters are necessary for multimodal size distributions. In such cases, all parameters except one have to be assumed; the one parameter left is determined uniquely from the known value of α. The total number density N of the aerosols is then derived by Eq. (2) written for $n_e(r)$ from the measured extinction coefficient $\sigma_e(1.0)$ at 1.0 μm. How this equivalent size distribution permits one to obtain values for the other aerosol characteristics, reasonably close to the real values, is the problem we want to address here.

Among the aerosol characteristics we want to retrieve are the volume of aerosol per unit volume of air

$$V = N \frac{4\pi}{3} \int_0^\infty r^3 n(r) dr, \tag{3}$$

and the aerosol mass density

$$M = \rho V, \tag{4}$$

where ρ is the density of the aerosol material.

The optical depth $\delta(1.0)$ at 1.0 μm is directly obtained by integration over altitude of the measured vertical profile of $\sigma_e(1.0)$. For the climatic impact of the aerosols, the optical depth has to be known for the whole solar spectrum, or at least by its average value $\delta_\odot$ weighted by the sun spectral intensity $S(\lambda)$. In addition to the average solar optical depth, the major parameters to be known are the single scattering albedo $\bar{\omega}_\odot$ and the asymmetry factor $g_\odot$ of the phase function, also averaged over the solar spectrum, and the optical depth $\delta(10)$ in the atmospheric infrared window around 10 μm. All these radiative characteristics can be derived from Mie theory as soon as the refractive index and the size distribution are assumed known. The average solar and infrared optical depths are obtained by integration over altitude of the corresponding extinction coefficients $\sigma_e^\odot$ and $\sigma_e(10)$ with $\sigma_e(\lambda)$ given by Eq. (2) and

$$\sigma_e^\odot = \int_0^\infty \sigma_e(\lambda) S(\lambda) d\lambda \Big/ \int_0^\infty S(\lambda) d\lambda. \tag{5}$$

The average asymmetry factor is defined by

$$g_\odot = \int_0^\infty g(\lambda) \sigma_S(\lambda) S(\lambda) d\lambda \Big/ \int_0^\infty \sigma_S(\lambda) S(\lambda) d\lambda, \tag{6}$$

with

$$g(\lambda) = \int_0^\infty g(\lambda,r,m) \pi r^2 Q_{\text{scatt}}(\lambda,r,m) n(r) dr \Big/ \int_0^\infty \pi r^2 Q_{\text{scatt}}(\lambda,r,m) n(r) dr; \tag{7}$$

$g(\lambda,r,m)$ is given by Mie theory for individual particles; Q_{scatt} is the Mie scattering efficiency factor, which is equal to Q_{ext} for nonabsorbing particles; the scattering coefficient $\sigma_S(\lambda)$ is derived from Q_{scatt} by an equation similar to Eq. (2).

The asymmetry factor and the spectral variation of the optical depth depend slightly on the refractive index and more strongly on the size distribution; therefore, the information gained from the Angström coefficient [equivalent size distribution $n_e(r)$], with a reasonable assumption about the refractive index, can be expected to improve the retrieval of $\delta_\odot/\delta(1.0)$, $\delta(10)/\delta(1.0)$, and $g_\odot$.

Unfortunately the single scattering albedo $\bar{\omega}$ is strongly dependent on the imaginary part of the refractive index, which is close to zero for pure sulfuric acid, leading to $\bar{\omega}_\odot \simeq 1$ in the solar spectrum for any size distribution. It is very sensitive to small quantities of highly absorbing particles or to absorbing impurities within the sulfuric droplets; direct measurements of $\bar{\omega}$ lead to values between 0.98 and 0.995.[9,10] It remains a major problem to improve our knowledge of the value of $\bar{\omega}$ or of the aerosol absorption, but no information can be obtained from multiwavelength extinction measurements and the retrieval of $\bar{\omega}$ is not further considered in this paper.

Besides the satellite extinction measurements, one of the most powerful tools for observing the stratospheric aerosol is lidar, either ground-based or airborne. Lidar systems give values of the aerosol backscatter coefficient defined[11] as

$$B(\lambda) = \frac{1}{4\pi} \int_0^\infty \pi r^2 p(\lambda,r,m;180°) Q_{\text{scatt}}(\lambda,r,m) n(r) dr, \tag{8}$$

$$B(\lambda) = \frac{1}{4\pi} \sigma_S(\lambda) p(\lambda;180°) \tag{9}$$

Table I. Aerosol Models: Lognormal Size Distributions

Log-normal size distributions $n(r) = \frac{1}{\sqrt{2\pi}\, r \ln\sigma} \exp\left[-\frac{\ln^2 r/r_m}{2\ln^2\sigma}\right]$.

The mode radius r_m, listed in columns 2 to 5, have been chosen in order to have the same effective radius r_{eff} (column 1) for all four variances

	r_m (μm)			
r_{eff} (μm)	v_{eff}=0.1, σ=1.362	v_{eff}=.25, σ=1.604	v_{eff}=.528, σ=1.918	v_{eff}=1, σ=2.299
0.025	0.0197	0.0143	0.0088	0.0044
0.05	0.0394	0.0286	0.0173	0.0088
0.1	0.0788	0.0572	0.0346	0.0177
0.15	0.1182	0.0859	0.0520	0.0265
0.222	0.1751	0.1272	0.0770	0.0393
0.281	0.2214	0.1609	0.0974	0.0497
0.35	0.2758	0.2004	0.1213	0.0619
0.45	0.3546	0.2576	0.1559	0.0795
0.55	0.4334	0.3148	0.1906	0.0972
0.7	0.5516	0.4007	0.2425	0.1237
1	0.7880	0.5724	0.3465	0.1768

at the lidar wavelength λ; $p(\lambda,r,m;180°)$ and $p(\lambda,180°)$ are the phase function values in the backward direction, respectively, for individual particles and for the size distribution $n(r)$. The comparison of lidar backscatter and extinction measurements involves knowledge of the ratio $B(\lambda)/\sigma_e(1.0)$, which again depends on the aerosol size distribution and refractive index. The equivalent size distribution derived from the measurement of the Angström coefficient can be expected to give information on the backscatter-to-extinction ratio; and the retrieval of this quantity is considered in what follows.

III. Method and Aerosol Models

Our approach consists of computing by Mie theory the radiative characteristics (extinction coefficient, asymmetry factor, backscatter coefficient) for a large variety of stratospheric aerosol models at ten wavelengths in the solar spectrum and at 10 μm in the infrared window. Averaging of the extinction coefficient and of the asymmetry factor over the solar spectrum has been performed.

The aerosols are assumed to be spherical particles of 75% H_2SO_4 with the refractive index listed in the SRA (Standard Radiation Atmosphere) report.[12] These values correspond to a temperature of 300 K, which is obviously not a reasonable choice for the stratosphere. However, since we have found that correcting the refractive indices to their values at 220 K introduces only very small modifications to the results (see discussion in Sec. IV), we have decided to keep the SRA values in order to use previously computed values and to save computer time.

Our main selection of aerosol models consists of log-normal size distributions (LNDs),

$$n(r) = \frac{1}{\sqrt{2\pi}\ln\sigma\, r}\exp\left(-\frac{\ln^2 r/r_m}{2\ln^2\sigma}\right); \qquad (10)$$

the two parameters σ and r_m can be conveniently replaced by

$$v_{\rm eff} = \exp(\ln^2\sigma) - 1, \qquad (11)$$

$$r_{\rm eff} = r_m \exp\left(\frac{5}{2}\ln^2\sigma\right), \qquad (12)$$

where $v_{\rm eff}$ and $r_{\rm eff}$ are, respectively, the effective variance and the effective radius defined by Hansen and Hovenier.[13] We have chosen four values of the effective variance $v_{\rm eff}$ (or of σ) from a very wide ($v_{\rm eff} = 1.0$) to a very narrow ($v_{\rm eff} = 0.1$) size distribution. In fact, most of the observed size distributions at the stratosphere level lie between $v_{\rm eff} = 0.250$ and $v_{\rm eff} = 0.528$, which correspond, respectively, to the background and to the volcanic stratospheric models in the SRA.[14] The effective radius $r_{\rm eff}$ (or the mode radius r_m) is varied in order to vary the Angström coefficient α between 0 and a value larger than 3 for each variance (Table I). Only a few modified gamma size distributions (MGDs),

$$n(r) = Cr^a \exp(-br^\gamma), \qquad (13)$$

have been considered, as they have been found to give results very close to the LNDs with the same $v_{\rm eff}$ and $r_{\rm eff}$. Table II summarizes the models chosen.

Various bimodal size distributions have been built by mixing two LNDs. There are now five unknown parameters: $\sigma_1,\sigma_2,r_{m1},r_{m2}$ (where the subscript i refers to the component i) and the relative concentration of the two components. We chose to fix $\sigma_1,\sigma_2,r_{m1},r_{m2}$, as explained below and shown in Table III, and we varied the volume concentrations C_1 and $C_2 = 1 - C_1$ of the

Table II. Aerosol Models: Modified Gamma Size Distributions; $n(r) = Cr^{a} \exp(-br^{\gamma})$

Model	r_{eff} (μm)	v_{eff}	a	b(μm$^{-\gamma}$)	γ
MGD1	0.05	0.250	1	80	1
MGD2	0.1	0.250	1	40	1
MGD3	0.222	0.250	1	18	1
MGD4	0.281	0.528	1	16	0.5
MGD5	1.0	0.1	7	10	1

Table III. Aerosol Models: Bimodal Size Distributions

Model	σ_1	r_{m1}(μm)	σ_2	r_{m2}(μm)	C_1	C_2
B1	1.604	.0286	1.604	.5724	variable	
B2	1.604	.0286	1.604	.1272	variable	
B3	1.604	.1272	1.604	.5724	variable	
HRH	1.76	0.073	1.10	1.0	0.815	0.185
HRC	1.604	0.02	1.604	0.7	0.9	0.1

two components within each mixture to vary the Angström coefficient within a large range. Finally we included one bimodal size distribution (HRH) observed with dustsondes by Hofmann *et al.*[15] after the Mount St. Helens eruption. For El Chichon aerosols, Hofmann and Rosen[16] found a large particle mode with $r_m = 0.7$ μm and a small particle mode with $r_m = 0.02$ μm; we built a model referred to as HRC, assuming the same $v_{eff} = 0.250$ for both modes, and a relative concentration leading to an average value of α. These two models are also defined in Table III.

IV. Results for Monomodal Size Distributions

A. Lognormal Size Distributions

The LNDs contain two adjustable parameters σ and r_m or v_{eff} and r_{eff}.

From the measured value of α we can define only one of these parameters and it seems reasonable to fix the width of the distribution (by σ or v_{eff}) and to adjust the mode radius r_m (or the effective radius r_{eff}). Figure 1 shows, for the four assumed variances, the variation of r_{eff} vs α. From a measured value of α, a value of r_{eff} [and of r_m by Eq. (12)] is retrieved for each value of v_{eff} (or of σ), leading to a family of equivalent size distributions $n_e(r)$. For each value of v_{eff} we can either express any aerosol characteristic A as a function of the effective radius r_{eff} (derived from α), or more directly express A in terms of α. If the relation between A and α is not dependent, or only slightly dependent, on the choice of v_{eff}, we can conclude that a measure of α leads to a reasonable retrieval of A. The information provided by α is more useful the faster A varies with α.

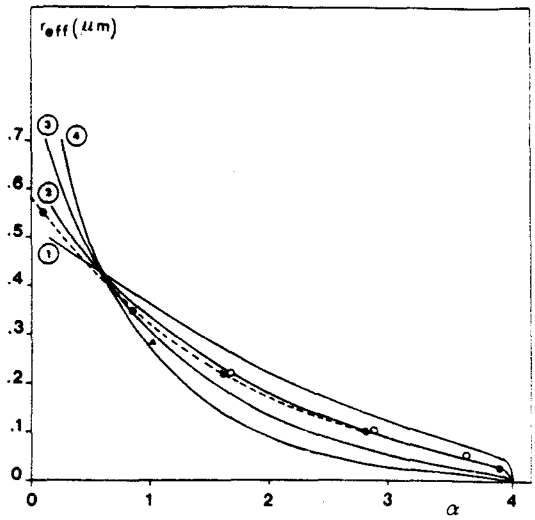

Fig. 1. Effective radius r_{eff} vs Angstrom coefficient α. Solid curves are for LNDs, with refractive index of 75% H_2SO_4 at 300 K: (1) $v_{eff} = 0.1$; (2) $v_{eff} = 0.250$; (3) $v_{eff} = 0.528$; (4) $v_{eff} = 1.0$. Dotted line with solid circles is for a LND with refractive index of 75% H_2SO_4 at 220 K, $v_{eff} = 0.250$. Open circles ($v_{eff} = 0.250$) and solid triangles ($v_{eff} = 0.528$) are for MGDs.

Figures 2–6 present the results for the aerosol parameters reviewed in Sec. III. The curves represent either A or $A/\sigma_e(1.0)$ vs α for the four selected values of v_{eff}; if A does not depend on the total number of particles, its retrieval is directly sought from the curves (A–α); if A depends on the total number of particles, the curves represent $A/\sigma_e(1.0)$ and the retrieved value has to be multiplied by the SAGE profile of $\sigma_e(1.0)$ in order to retrieve the A profile.

Figure 2 is for the mass factor $f = M/\sigma_e(1.0)$; when α increases (small particles), f exhibits a fast increase because $\sigma_e(1.0)$ decreases very rapidly (as r^6 in the Rayleigh domain). On the other hand, for large particles $\sigma_e(1.0)$ varies as r^2 whereas M varies as r^3 and f again increases, as seen for α close to zero on the curves in Fig. 2. When v_{eff} increases the contribution of large particles becomes more important leading to a slight shift of the curves toward a large rf for a given value of α; this behavior is to be compared with the behavior of bimodal distributions (see Sec. V). As mentioned above, the SAGE profiles give values of α between 0.5 and 3.0, which correspond to variations of f of approximately an order of magnitude. The uncertainty in the determination of f due to the assumption on v_{eff} is quite large especially for large values of α; however if we limit ourselves to the range $0.250 < v_{eff} < 0.528$, which corresponds to most of the observations in the stratosphere, the information retrieved for f is within ±15% for α smaller than 2 and within ±50% for large α. This uncertainty has to be compared to the range of variation of f which increases by a factor of 10 when α increases from 0.5 to 3; Table IV gives the retrieved values for $\alpha = 0.5$ and 3.0 and for the background value $\alpha = 1.7$.

Figure 3 exhibits the extinction coefficient averaged over the solar spectrum. The four curves are indistinguishable for α smaller than 3; for larger values of α, the influence of the large particles in the size distribution

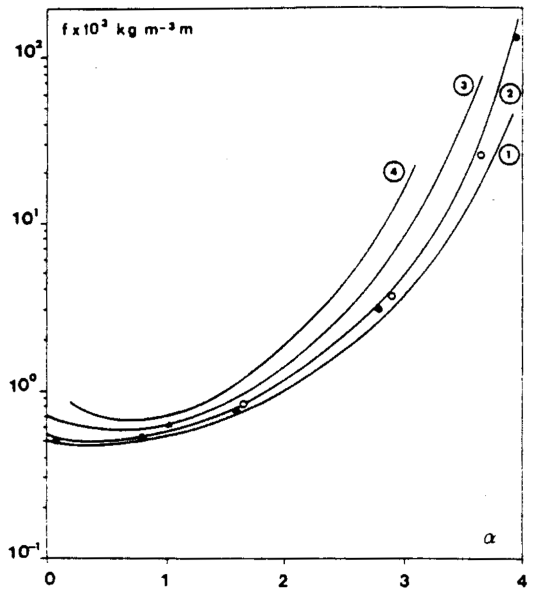

Fig. 2. Mass factor $f = M/\sigma_e(1.0)$ vs Angström coefficient α; M is the mass per unit volume and $\sigma_e(1.0)$ is the extinction coefficient at 1.0 μm. The rest of the information is the same as in Fig. 1; the dotted line was not drawn as it is almost indiscernible from solid line (2).

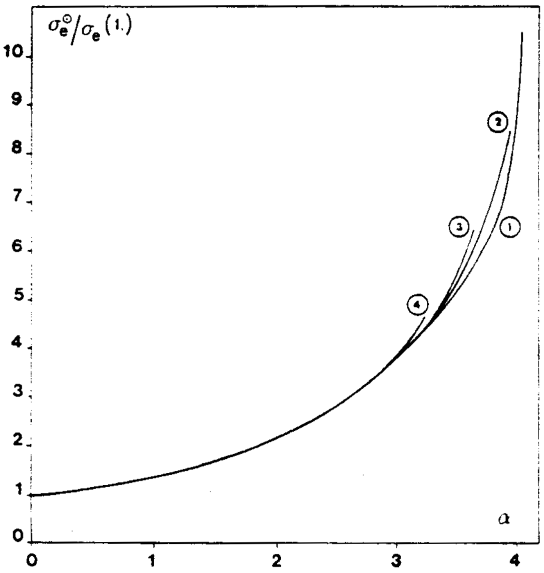

Fig. 3. Ratio of the solar average extinction coefficient $\sigma_e^{\odot}$ to the extinction $\sigma_e(1.0)$ at 1.0 μm vs Angström coefficient α. All the curves (including bimodal size distributions) are indiscernible up to $\alpha \simeq 3$. For α larger than 3, the numbers have the same meaning as in Fig. 1.

is indicated by values of $\sigma_e^{\odot}/\sigma_e(1.0)$ which increase with v_{eff} for the same α. Within the useful range $0.5 \leqslant \alpha \leqslant 3.0$, $\sigma_e^{\odot}/\sigma_e(1.0)$ is retrieved uniquely and therefore the SAGE extinction profiles at 1.0 μm can be transformed into solar average extinction profiles which are more important for the climatic impact.

Figure 4 shows the solar average asymmetry factor $g_{\odot}$ which is independent of the total number of particles: $g_{\odot}$ increases from 0 to a limit at 0.73 from very small to large particles. The influence of v_{eff} on the retrieval of

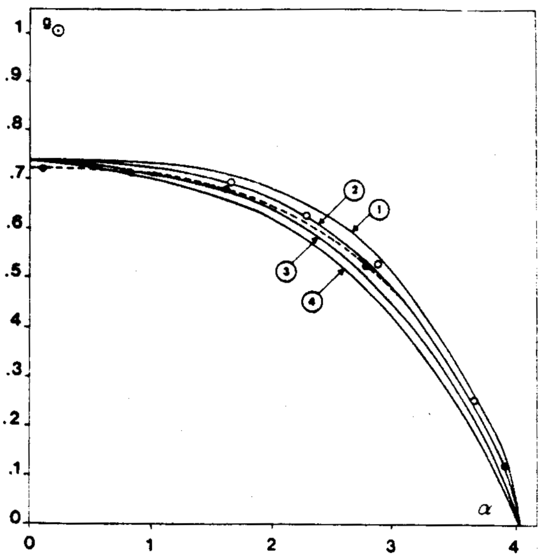

Fig. 4. Asymmetry factor averaged over the solar spectrum $g_{\odot}$ vs Angström coefficient α. The rest of the information is the same as in Fig. 1.

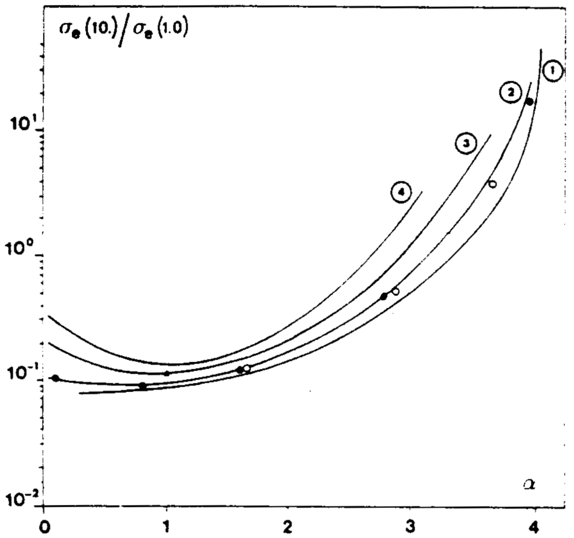

Fig. 5. Ratio of the extinction coefficient $\sigma_e(10)$ at 10 μm to the extinction coefficient $\sigma_e(1.0)$ at 1.0 μm vs Angström coefficient α. The rest of the information is the same as in Fig. 1 [dotted line is indiscernible from solid line (2)].

$g_{\odot}$ is to decrease $g_{\odot}$ when v_{eff} increases for a given α (see Table IV).

Figure 5 illustrates the infrared extinction at 10 μm. Since the H_2SO_4 particles are strongly absorbing at 10 μm, $\sigma_e(10)$ is mainly due to the absorption; the single scattering albedo $\bar{\omega}(10)$ is ~0.3 for the larger particles considered, around 0.01–0.02 for the models corresponding to the background stratospheric aerosols with $\alpha \simeq 1.7$, and ~10^{-4} for the small particle models. The ratio $\sigma_e(10)/\sigma_e(1.0)$ increases as r^{-3} in the Rayleigh domain and shows again a slight increase for large particles (α close to zero). The values for α = 0.5, 1.7, and 3.0 and the two v_{eff} are shown in Table IV.

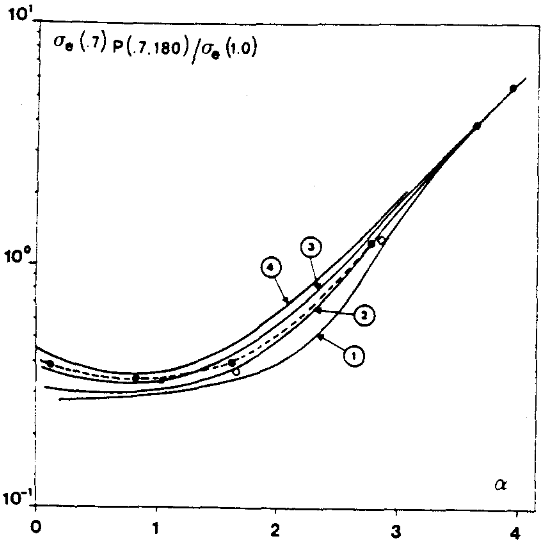

Fig. 6. Lidar factor $\sigma_e(0.7)p(0.7;180)/\sigma_e(1.0) = 4\pi B(0.7)/\sigma_e(1.0)$ vs Angström coefficient α; $B(0.7)$ is the backscatter coefficient at 0.7 μm and $\sigma_e(1.0)$ is the extinction coefficient at 1.0 μm. The rest of the information is the same as in Fig. 1.

Finally Fig. 6 shows the lidar factor $4\pi B(0.7)/\sigma_e(1.0)$. We chose wavelength $\lambda = 0.7$ μm as representative of the ruby laser (0.694 μm). The Rayleigh limit is $3/2\lambda^4$. When the particle size increases, the phase function $p(\lambda;180°)$ decreases rapidly at first, exhibits oscillations, and then increases for large particles; the multiplying factor $\sigma_e(0.7)/\sigma_e(1.0)$ decreases toward small α. The retrieved values for $\alpha = 0.5$, 1.7, and 3.0 are given in Table IV.

B. Modified Gamma Size Distributions

The five MGDs have been chosen to cover a large range of α from a slightly negative value (very large particles) to 3.5 (very small particles) and the optical parameters are compared to their values for LNDs with the same r_{eff} and v_{eff}. Table V shows the differences in percent between LND and MGD values of $\sigma_e(\lambda)/\sigma_e(0.55)$, g and $p(\lambda;180°)$. They are generally of the order of a few percent, sometimes smaller than 1%. The only differences larger than 10% appear for g in the infrared for the small particle models; they are not important as scattering is almost negligible at these

Table IV. Aerosol Parameters Retrieved from α for LND Size Distributions with Two Variances $v_{\text{eff}} = 0.250$ and 0.528

	$\alpha = 0.5$		$\alpha = 1.7$		$\alpha = 3.0$	
	$v_{eff} = 0.250$	$v_{eff} = 0.528$	$v_{eff} = 0.250$	$v_{eff} = 0.528$	$v_{eff} = 0.250$	$v_{eff} = 0.528$
$10^3\ M/\sigma_e(1.0)$ ($kg\ m^{-3}/m^{-1}$)	0.52	0.60	0.85	1.00	5.0	8.5
$\sigma_e^{\Theta}/\sigma_e(1.0)$	1.1	1.1	1.85	1.85	3.85	3.85
g^{Θ}	0.735	0.73	0.69	0.67	0.485	0.45
$\sigma_e(10.)/\sigma_e(1.0)$	0.09	0.12	0.13	0.15	0.8	1.2
$4\pi B(0.7)/\sigma_e(1.0)$	3.8	4.1	4.9	5.7	20.1	22.6

Table V. Comparison of LND and MGD Models with Same v_{eff} and r_{eff}

	MGD 1			MGD 2			MGD 3			MGD 4			MGD 5		
λ (μm)	σ_e	g	p(180°)	σ_e	g	p(180°)	σ_e	g	p(180°)	σ_e	g	p(180°)	σ_e	g	p(180°)
.385	-3.4	4.0	-1.0	-1.0	-1.5	5.1	3.7	0.1	-3.0	3.1	0.5	-5.3	1.6	0.2	-0.2
.45	-1.9	8.2	-5.3	-0.8	-1.3	6.2	1.7	-0.5	-1.3	1.8	0.2	-4.1	1.1	-0.8	0.6
.525	-0.5	13.1	-8.6	-0.3	-0.7	6.1	0.4	-0.9	-0.1	0.5	-0.1	-3.0	0.2	-0.7	1.3
.55	0	14.7	-9.3	0	-0.4	5.8	0	-1.0	0.3	0	-0.2	-2.5	0	-0.9	1.3
.7	2.7	22.4	-11	1.6	2.4	1.3	-1.2	-1.4	2.6	-2.4	-0.7	-3.4	1.2	-0.7	0.5
.85	5.1	27.5	-10	3.2	6.7	-3.9	-1.4	-1.4	4.8	-4.1	-1.1	1.6	2.9	0.4	-1.0
1	7.0	31	-8.6	4.5	12	-7.7	-1.1	-1.2	6.1	-5.3	-1.5	3.3	3.5	0.6	-1.4
1.6	9.1	36	-4.3	9.3	26	-10	1.6	3.3	0.2	-6.2	-1.3	5.2	1.4	-0.1	-0.3
2.2	1.3	37	-2.4	10.2	31	-7.3	4.0	12.0	-7.8	-4.5	0.6	2.3	0.8	-0.3	-0.2
3.6	-2.8	37	-0.9	3.0	35	-3.2	2.6	24	-8.8	-2.1	5.9	4.2	1.2	-0.7	-1.5
10	-2.8	38	-0.1	2.9	36	-0.5	2.7	39	-3.1	-0.4	26	-10	1.1	4.0	-2.2

The table gives LND values-MGD values/LND values in percent for the different MGD models. σ_e is normalized at 1 for $\lambda = 0.55$ μm.

Table VI. Influence of the Refractive Index

	r_{eff}=0.025 μm			r_{eff} = 0.1 μm			r_{eff} = 0.222 μm			r_{eff} = 0.35 μm			r_{eff} = 0.55 μm			r_{eff} = 1 μm		
λ(μm)	σ_e	g	p(180°)	σ_e	g	p(180°)	σ_e	g	p(180°)	σ_e	g	p(180°)	σ_e	g	p(180°)	σ_e	g	p(180°)
.385	-0.4	-1.6	0.7	1.3	1.1	-3.0	3.2	2.2	-24	3.1	2.8	-38	1.0	2.4	-37	-0.8	1.0	-13
.45	-0.1	-1.6	0.5	0.7	0.8	-1.2	1.7	1.9	-17	1.8	2.5	-31	0.8	2.6	-36	-0.5	1.2	-13
.525	-0.1	-1.6	0.4	0.1	0.5	-0.1	0.4	1.7	-12	0.4	2.3	-26	0.3	2.7	-36	-0.1	1.6	-19
.55	0	-1.7	0.3	0	0.4	0.1	0	1.7	-11	0	2.2	-25	0	2.7	-36	0	1.7	-19
.7	0.2	-1.6	0.2	0.4	0.2	0.9	-1.8	1.3	-5.7	-2.3	1.9	-17	-1.8	2.5	-31	0.3	2.4	-30
.85	0.3	-1.5	0.1	0.6	-0.6	1.0	-2.9	1.0	-2.8	-4.0	1.7	-11	-3.6	2.3	-25	0	2.7	-34
1	0.3	-1.4	0.1	0.7	-1.0	1.0	-3.7	0.7	-1.2	-5.4	1.4	-7.4	-5.3	2.0	-19	-0.8	2.7	-34
1.6	5.4	-1.2	0	0	-1.9	0.6	-4.4	0.3	0.8	-7.8	0.6	-1.0	-9.4	1.2	-0.6	-5.2	1.9	-19
2.2	8.8	-1.1	0	2.3	-2.8	0.5	-3.9	0.8	0.8	-8.3	0	0.4	-11	0.7	-1.9	-8.5	1.3	-9.1
3.6	6.0	-1.1	0	6.0	-4.5	0.4	1.3	-1.1	0.4	-3.6	-0.6	0.6	-8.1	0	0.6	-8.1	0.6	0.2
10	16	-2.8	0	6.0	-8.2	0.1	1.9	-3.1	0.2	-2.6	-2.5	0.5	-7.6	-1.1	0.6	-9.3	1.1	-0.6

The table gives the variation in percent for $\sigma_e, g, p(180°)$ when changing the refractive index of 75% H_2SO_4 from its value at 300 K to its value at 220 K for six LND models with v_{eff} = 0.250. σ_e is normalized at 1 for λ = 0.55 μm. Similar results arise from changing the concentration from 60% to 80%.

wavelengths and they reflect only slightly on $g_{\odot}$. The points corresponding to MGD models have been plotted in Figs. 1, 2 and 4–6; they have been omitted from Fig. 3 since they are exactly on the curve for LNDs.

It is clear that the difference between a LND and a MGD model is completely negligible for our purpose of retrieving the aerosol characteristics from α measurements, especially if we consider the uncertainty in v_{eff}.

C. Influence of the Refractive Index

To check if we could use the preliminary computed values at 300 K we recomputed the optical parameters with the refractive index of 75% H_2SO_4 at 220 K for six of the LND models with v_{eff} = 0.250. This study of the influence of variations of the refractive index has a more general interest, as such variations can occur not only because of temperature changes but also because of concentration variations or of presence of other constituents mixed with the H_2SO_4 particles. For example, if the sulfuric acid fraction varies from 60% to 80%, the real refractive index varies from 1.43 to 1.45,[17] which is similar to the variation we have when changing the temperature from 300 to 220 K. The corresponding points are plotted in Figs. 1, 2 and 4–6. They have been omitted from Fig. 3 since they are exactly on the curve for LNDs; the differences in percent between values with the refractive index at 300 and 220 K are given in Table VI. The only noticeable difference is for the lidar factor when the particles are large. In this case the retrieval may have a systematic error due to the uncertainty in the refractive index (influence of temperature, dilution, impurities).

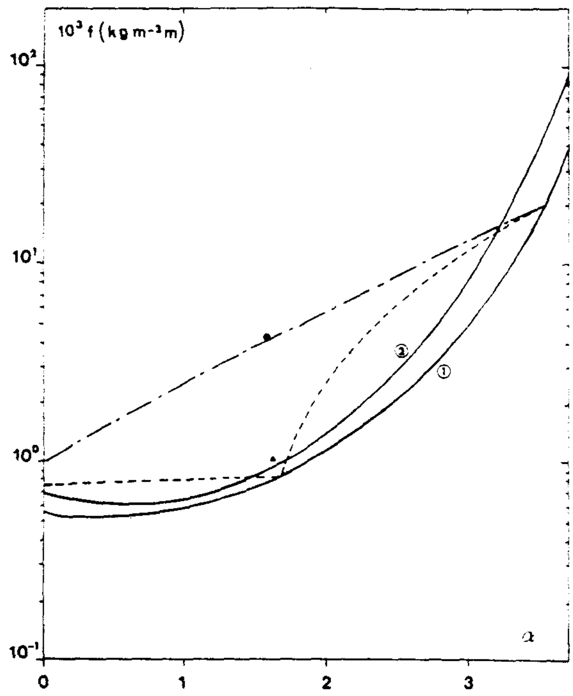

Fig. 7. Mass factor $f = M/\sigma_e(1.0)$ vs Angström coefficient α; M is the mass per unit volume and $\sigma_e(1.0)$ the extinction coefficient at 1.0 μm. Comparison of bimodal and monomodal size distributions. Solid lines are for monomodal LNDs: (1) v_{eff} = 0.250; (2) v_{eff} = 0.528. Dotted line is for bimodal size distribution $B2$ on the right and $B3$ on the left. The dash–dot line is for bimodal size distribution $B1$. The solid circle is for the HRC model and the solid triangle for the HRH model (see Table III).

V. Results for Bimodal Size Distribution

Figure 7 presents the variation of the mass factor $f = M/\sigma_e(1.0)$ vs α for the bimodal size distributions. For comparison the curves for monomodal LND with v_{eff} = 0.250 and 0.528 have been repeated in the figure. The dash–dot curve corresponds to the model $B1$, which is a mixture of very large and very small particles. It appears that the behavior of f as a function of α is completely different depending on whether it is due to

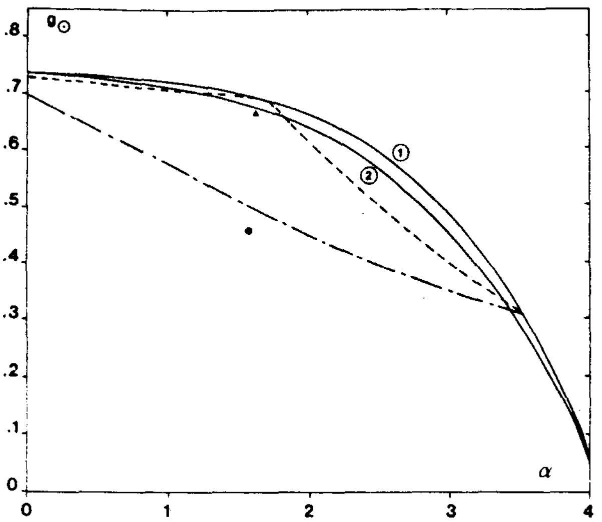

Fig. 8. Asymmetry factor averaged over the solar spectrum $g_{\odot}$ vs Angström coefficient; comparison of bimodal and monomodal size distributions. The rest of the information is the same as in Fig. 7.

a variation of the mode radius in a monomodal size distribution or to a variation of the relative concentration of the two modes within a bimodal size distribution. When a few large particles are added to a population of small particles, $\sigma_e(1.0)$, which was close to zero, begins to increase very fast, rapidly decreasing α, whereas the other parameters vary only slowly. This is the reason f remains larger for bimodal than for monomodal distribution when the decrease of α begins. On both sides the limiting point of the bimodal curve is the point corresponding to one of its LND components. The dotted curve corresponds to the case of a background aerosol model ($v_{\text{eff}} = 0.250$; $r_{\text{eff}} = 0.222$; $\alpha = 1.68$) with the addition either of small particles to increase α (model $B2$) or of large particles to decrease α (model $B3$). The curve is, of course, closer to the monomodal curve. The HRH model[15] for Mount St. Helens gives a point very close to the monomodal curve $v_{\text{eff}} = 0.528$, whereas the HRC El Chichon model,[16] which contains a mode of very small particles, gives a point close to our $B1$ model.

For the solar average asymmetry factor (Fig. 8), the ratio of extinction at 10 and 1.0 μm (Fig. 9) and the lidar factor (Fig. 10), the difference of behavior for monomodal and bimodal size distributions, are similar to what has been explained previously for the mass factor. This leads to the conclusion that all these aerosol parameters can be retrieved with reasonable accuracy from the Angström coefficient, i.e., from a two-wavelength extinction measurement, only if the size distribution is known to be approximately monomodal. For bimodal size distributions the problem seems hopeless, unless a reasonable guess can be made about the radius and the variance of each mode.

For the extinction coefficient averaged over the solar spectrum, the curves for bimodal size distributions have not been drawn, as they are completely indistinguishable from the unique curve of Fig. 3. Therefore this parameter $\sigma_e^{\odot}$ can be retrieved from the measure of α with reasonable accuracy, whatever the exact size distribution.

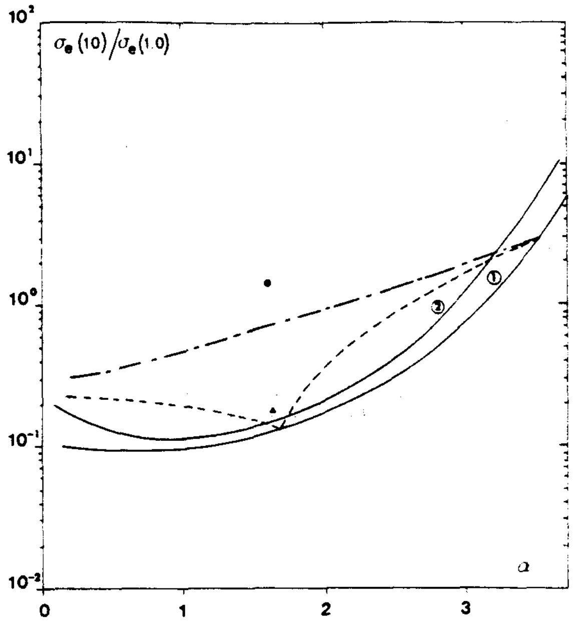

Fig. 9. Ratio of the extinction coefficient $\sigma_e(10)$ at 10 μm to the extinction coefficient $\sigma_e(1.0)$ at 1.0 μm vs Angström coefficient α. Comparison of bimodal and monomodal size distributions. The rest of the information is the same as in Fig. 7.

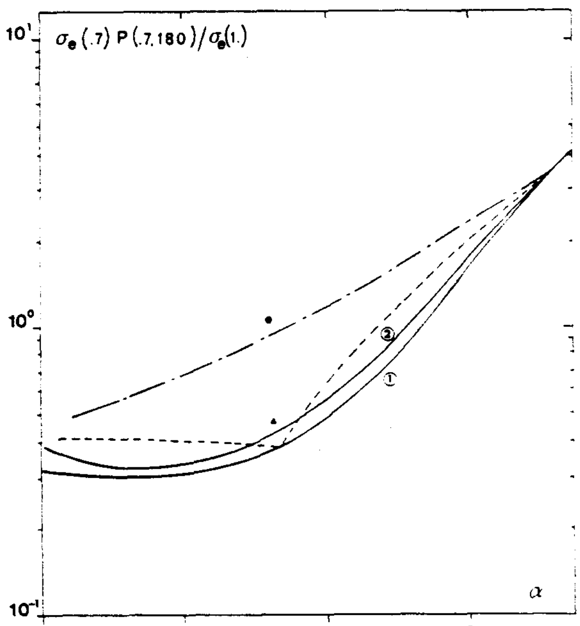

Fig. 10. Lidar factor $\sigma_e(0.7)p(0.7;180)/\sigma_e(1.0) = 4\pi B(0.7)/\sigma_e(1.0)$ vs Angström coefficient α; $B(0.7)$ is the backscatter coefficient at 0.7 μm and $\sigma_e(1.0)$ the extinction coefficient at 1.0 μm. Comparison of bimodal and monomodal size distributions. The rest of the information is the same as in Fig. 7.

VI. SAGE II Multiwavelength Extinction Measurements

As we have seen above, the SAGE aerosol extinction measurements at two wavelengths, 0.45 and 1.0 μm,

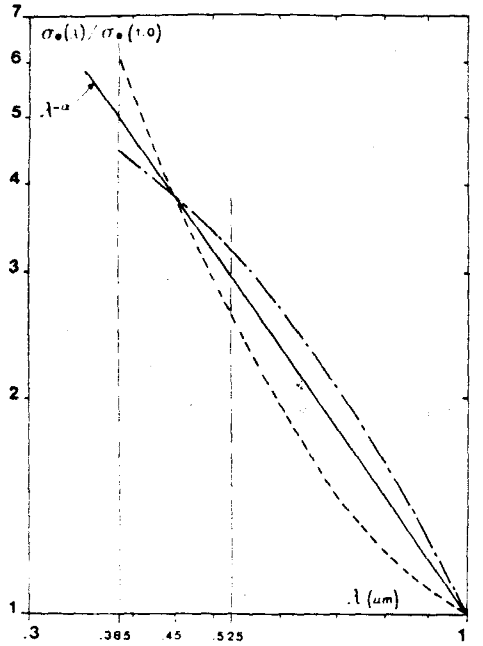

Fig. 11. Spectral variation of the extinction coefficient for monomodal (dash–dot line; $v_{\text{eff}} = 0.250$) and bimodal (dashed line; $B1$) size distributions, with the same ratio $\sigma_e(0.45)/\sigma_e(1.0)$ corresponding to $\alpha = 1.68$. The solid line is for Angström's law.

allow the determination of the extinction profile and of the optical depth averaged over the solar spectrum, but the other radiative parameters and the aerosol mass can be retrieved only if some further information about the size distribution modes is known. This information can be expected from multiwavelength extinction measurements, if the spectral variation of extinction is significantly different for a monomodal and a bimodal size distribution. Figure 11 compares this spectral variation for a LND with $v_{\text{eff}} = 0.250$ and a model $B1$; the parameter in both models (mode radius or concentration) has been adjusted to give the same ratio $\sigma_e(0.45)/\sigma_e(1.0)$ or the same $\alpha = 1.68$ (background value). The two curves have opposite curvatures, being on each side of the Angström straight line $\sigma_e(\lambda) = \sigma_e(1.0) \cdot \lambda^{-\alpha}$. A similar result is found for all values of α.

Assuming a standard profile for NO_2 below 25 km, where its contribution is small, it is possible to deduce from SAGE data an aerosol extinction profile at 0.385 μm. For most of the nonvolcanic cases we have considered, the ratio $\sigma_e(0.385)/\sigma_e(1.0)$ is smaller than expected from the Angström law, pointing to monomodal size distributions.[2] For volcanic cases, the same is true at low levels where background and large particles are found, whereas at altitudes of 21–23 km, where small particles (large α) are found, the ratio $\sigma_e(0.385)/\sigma_e(1.0)$ appears larger than $(0.385)^{-\alpha}$, suggesting a bimodal size distribution, which could be due to the formation of small particles in addition to the background aerosol. These remarks are very tentative and must, of course, be supported by a more thorough study.

The future SAGE II instrument with seven channels[18] is expected to give aerosol extinction at four wavelengths, 0.385, 0.45, 0.525, and 1.0 μm. This would not allow the determination of all the parameters needed in a multimodal or even a bimodal size distribution. However from Fig. 11, there is clearly some hope that the additional information contained in channels 0.385 and 0.525 μm can help to decide between monomodal and bimodal size distributions, and to improve the retrieval of aerosol characteristics. How this information can be used most effectively, considering the expected accuracy of measurements, will be the subject of future work.

VII. Conclusion

The SAGE data contain aerosol extinction profiles at 1.0 and 0.45 μm. Using the ratio of extinction $\sigma_e(0.45)/\sigma_e(1.0)$ to gain information on the size distribution and then the extinction $\sigma_e(1.0)$ at 1 μm to infer the number density should allow the retrieval of the aerosol mass and of most aerosol radiative parameters, with the only exception of the single scattering albedo which is strongly dependent on the imaginary refractive index (or absorption) of the aerosol material.

Here we have simulated the variations of the main aerosol parameters in terms of the extinction ratio, or more exactly in terms of the Angström coefficient defined by Eq. (1), for a large range of aerosol models with monomodal and bimodal size distribution.

The most positive conclusion is that the optical depth averaged over the solar spectrum, which is the main climatic parameter, can be retrieved uniquely from the SAGE two-channel extinction measurements.

For the other parameters considered, which include the mass density, the solar average asymmetry factor, the 10-μm extinction and backscattering coefficients, the knowledge of α only allows one to fix their values within brackets due to the uncertainty of the width of the size distribution. If we admit that this width is defined by v_{eff} between 0.250 and 0.528, the information obtained is not too bad (see Table IV), especially if we consider the large range of variation of the aerosol parameters when α varies between 0.5 and 3.0, as observed on volcanic profiles. However, this conclusion remains true only for monomodal or near monomodal size distributions. For bimodal size distributions, especially if we assume that the variations of α are due to the variations of concentration within a mixture containing large and very small particles, the parameters retrieved from the α value would be very different.

The only approach to reduce this uncertainty is the addition of more wavelengths in the extinction data, which is what SAGE II is designed to do. The two additional aerosol channels at 0.385 and 0.525 μm may help to solve the problem.

We are grateful to D. Tanré who provides us with the Mie codes. This work has been supported by the Centre National d'Etudes Spatiales under contract 83/230.

References

1. M. P. McCormick, P. Hamill, T. J. Pepin, W. P. Chu, T. J. Swissler, and L. R. McMaster, "Satellite Studies of the Stratospheric Aerosol," Bull. Am. Meteorol. Soc. **60**, 1038 (1979).

2. J. Lenoble and P. Pruvost, "Inference of the Aerosol Angström Coefficient from SAGE Short Wavelength Data," J. Clim. Appl. Meteorol. **22,** 1717 (1983).
3. P. B. Russell, F. J. Swissler, M. P. McCormick, W. P. Chu, J. M. Livingston, and T. J. Pepin, "Satellite and Correlative Measurements of the Stratospheric Aerosol: I—An Optical Model for Data Conversions," J. Atmos. Sci. **38,** 1279 (1981).
4. G. K. Yue and A. Deepak, "Retrieval of Stratospheric Aerosol Size Distribution from Atmospheric Extinction of Solar Radiation at Two Wavelengths," Appl. Opt. **22,** 1639 (1983).
5. J. M. Livingston and P. B. Russell, Informal Progress Report, SAGE II Science Team Meeting, 27-29 Feb. 1984.
6. J. Lenoble, P. Pruvost, and C. Brogniez, "Observations of Stratospheric Aerosols from Mount St. Helens Eruption: Size and Mass Determination," J. Geophys. Res. **00,** 0000 (1984).
7. M. Herman, Universitides Sciences et Technignes de Lille, private communication (1984).
8. J. M. Rosen, "The Boiling Point of Stratospheric Aerosols," J. Appl. Meteorol. **10,** 1044 (1971).
9. J. A. Ogren, R. J. Charlson, L. F. Radke, and S. K. Domonkov, "Absorption of Visible Radiation by Aerosols in the Volcanic Plume of Mount St. Helens," Science **211,** 834 (1981).
10. J. J. DeLuisi, B. G. Mendonca, E. G. Dutton, M. A. Box, and B. M. Herman, "Radiative Properties of the Stratospheric Dust Cloud from the May 18, 1980 Eruption of Mount St. Helens," J. Geophys. Res. **88,** 5290 (1983).
11. J. D. Spinhirne, J. A. Reagan, and B. M. Herman, "Vertical Distribution of Aerosol Extinction Cross-Section and Inference of Aerosol Imaginary Index in the Troposphere by Lidar Technique," J. Appl. Meteorol. **19,** 426 (1980).
12. Radiation Commission of IAMAP, A Preliminary Cloudless Standard Atmosphere for Radiation Computation, Boulder. Section 2 on Aerosol Models published as Appendix A in World Climate Research Programme 1983, WCP 55 (1982).
13. J. E. Hansen and J. W. Hovenier, "Interpretation of the Polarization of Venus," J. Atmos. Sci. **31,** 1137 (1974).
14. J. Lenoble and C. Brogniez, "A Comparative Review of Radiation Aerosol Models," Contrib. Atmos. Phys. **57,** 1 (1984).
15. D. J. Hofmann, J. M. Rosen, R. Reiter, and H. Jager, "Lidar and Balloon-Borne Particle Counter Comparisons Following Recent Volcanic Eruptions," J. Geophys. Res. **88,** 3777 (1983).
16. D. J. Hofmann and J. M. Rosen, "Stratospheric Sulfuric Acid Fraction and Mass Estimate for the 1982 Volcanic Eruption of El Chichon," Geophys. Res. Lett. **10,** 313 (1983).
17. H. M. Steele and P. Hamill, "Effects of Temperature and Humidity on the Growth of Sulphuric Acid Water Droplets in the Stratosphere," J. Aerosol Sci. **12,** 517 (1981).
18. N. H. Zaun, L. E. Mauldin, and M. P. McCormick, "Design and Performance of the Stratospheric Aerosol and Gas Experiment II (SAGE II) Instrument," Proc. Soc. Photo-Opt. Instrum. Eng. **430** (1983).

SIZE DISTRIBUTION OF STRATOSPHERIC AEROSOLS FROM SAGE II MULTIWAVELENGTH EXTINCTIONS

C. Brogniez and J. Lenoble
Laboratoire d'Optique Atmosphérique
Université des Sciences et Techniques de Lille Flandres Artois
59655 Villeneuve d'Ascq Cedex, France

ABSTRACT

Measurements of aerosol extinction profiles in the stratosphere in four channels are used to retrieve two parameters of the particle size distribution. Good agreement between these two parameters and those deduced from balloon data has been found.

1. INTRODUCTION

The Stratospheric Aerosol and Gas Experiment I (SAGE I) has provided aerosol extinction profiles in two channels at 1.00 µm and 0.45 µm during two and a half years. The ratio of the two channel extinctions allows the retrieval of one parameter of the particle size distribution, i.e., a mode radius r_m or an effective radius r_{eff} (Yue and Deepak, 1983; Lenoble and Brogniez, 1985). Alternatively, most of the aerosol radiative characteristics can be retrieved from this two-channel ratio, unless the distribution is bimodal (Lenoble and Brogniez, 1985). Variations of the aerosol size with latitude, season, and altitude have been studied (Yue and Deepak, 1984; Brogniez and Lenoble, 1987) for the unperturbed atmosphere of 1979, and the influence of the Mount St. Helens eruption on the aerosol size has been demonstrated from SAGE I data (Lenoble et al., 1984).

Since October 1984, SAGE II provides profiles of the aerosol extinction $\sigma(\lambda)$ in four channels: 1.02 µm, 0.525 µm, 0.45 µm, and 0.385 µm. Therefore, at least, the same information can be retrieved from SAGE II as from SAGE I, using the 1.02 µm and 0.45 µm channels. The quality from SAGE II is probably a little better, due to a smaller error on the extinction, especially at 0.45 µm, where the two narrow-band channels allow a better separation of NO_2 and aerosol contributions.

The issue addressed here concerns what further information about the size distribution can be obtained using four channels instead of two. We do not seek an operational algorithm to retrieve a size distribution from SAGE II aerosol channels, but rather try to clarify what can be expected from the physical considerations of the data with their error bars and from comparison with aerosol models. We will limit ourselves to seeking two parameters of a monomodal size distribution; this proves difficult enough to show that the search for three parameters is absolutely unrealistic. Various combinations of the four channels (in sets of two) can be tried to achieve this goal.

AEROSOLS AND CLIMATE
Peter V. Hobbs and M. Patrick McCormick (Eds.)

Copyright © 1988 A. DEEPAK Publishing
All rights of reproduction in any form reserved

ISBN 0-937194-11-5

Another approach consists of using an analytical fit that smoothes the spectral distribution of extinction $\sigma(\lambda)$ given by the four channels. If the size distribution happens to be bimodal, there would be too many parameters to expect their retrieval from SAGE II data; however, we will see that qualitative information about the bimodality can probably be achieved.

2. SPECTRAL VARIATION OF EXTINCTION FROM SAGE II DATA

Figure 1 shows, for example, the spectral variation $\sigma(\lambda)$ observed by SAGE II (28 November 1984 at 1645 GMT) at various altitudes between 16.5 km and 24.5 km, in relative value $(\sigma(\lambda)/\sigma(1.02))$. The dots correspond to the measured values at the three wavelengths 0.525 µm, 0.45 µm, and 0.385 µm; the curves represent a rms best fit, using the analytical expression

$$\ln \sigma(\lambda) = \ln \sigma(1.02) - a\ln(\lambda/1.02) - b(\ln(\lambda/1.02))^2 \qquad (1)$$

For comparison Fig. 2 represents the spectral variation of the extinction for aerosol models with a lognormal size distribution (LND), expressed by

$$n(r) = \frac{1}{\sqrt{2\pi}r\ \ln\sigma} \exp\{-\frac{\ln^2 r/r_m}{2\ln^2\sigma}\} \qquad (2)$$

where r_m and σ are the mode radius and the variance. An alternative convenient choice of parameters (Hansen and Hovenier, 1974) are the effective radius and effective variance defined by

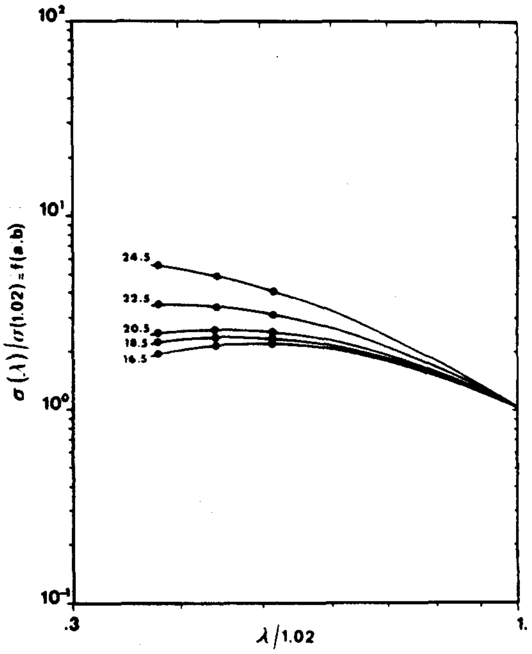

FIGURE 1. Spectral variation of the extinction coefficient $\sigma(\lambda)/\sigma(1.02)$. The dots are the measured values from SAGE II on 28 November 1984, 1645 GMT. The curves represent a rms best fit.

$$r_{eff} = r_m \exp(2.5 \ln^2 \sigma) \qquad (3)$$

$$v_{eff} = \exp(\ln^2\sigma) - 1 \qquad (4)$$

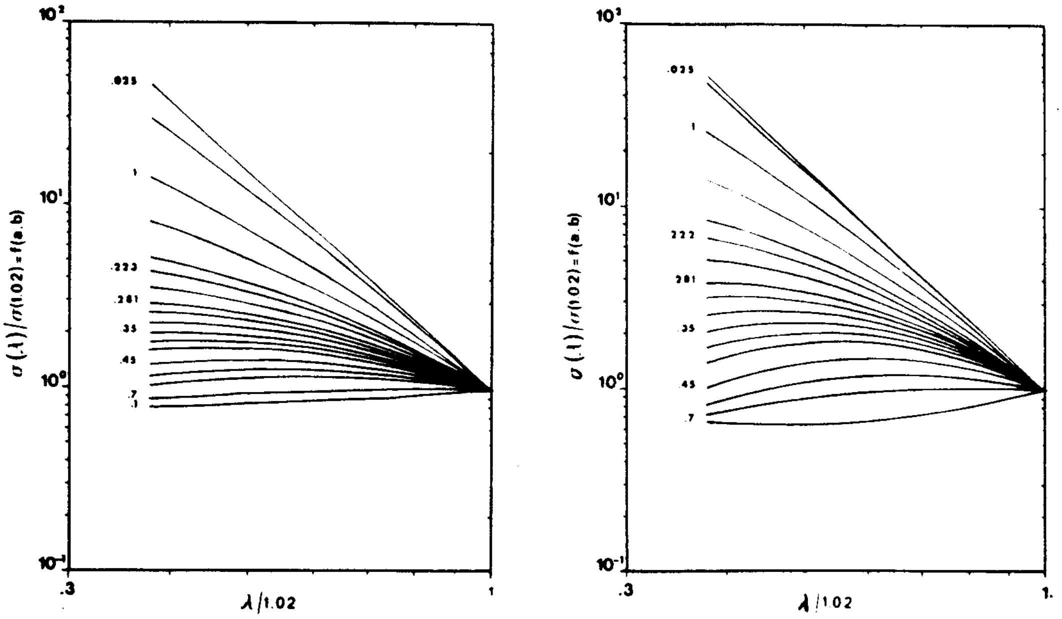

FIGURE 2. Spectral variation of the extinction coefficient $\sigma(\lambda)/\sigma(1.02)$ fitted by a rms for several aerosol models with a LND size distribution (a/ v_{eff} = .25, b/ v_{eff} = .05). The values on the curves are r_{eff} in μm.

Figure 2a is for v_{eff} = .25 (σ = 1.60) and Fig. 2b for v_{eff} = .05(σ= 1.25); the set of curves corresponds to different values of r_{eff}. A qualitative comparison between Figs. 1 and 2 shows that the aerosols observed by SAGE II have an effective variance generally close to .05 (curvature of the curves) and an effective radius decreasing with altitude from about 0.40 μm to 0.25 μm.

A more quantitative comparison between SAGE II data and the aerosol models is possible using the expansion (1), which fits almost perfectly the spectral variation of the extinction for the LND models. Figure 3 is a diagram (a-b) for the LND models with various r_{eff} and v_{eff}. The values of a and b for size distributions with two LND modes have also been drawn; they correspond to very small or even negative values of b (inversion of the curvature of the spectral curves from monomodal to bimodal size distributions already noted (Lenoble and Brogniez, 1985)). The points corresponding to three successive SAGE II observations in October 1985 (12 at 0502 GMT and 0639 GMT, 13 at 0651 GMT) for altitudes between 16.5 and 24.5 km are plotted on the (a-b) diagram of Fig. 3. The error rectangles are reported for two points. The points for the same altitude cluster reasonably and the shift with altitude confirms the qualitative observations of the size distribution variation. The values of r_{eff}

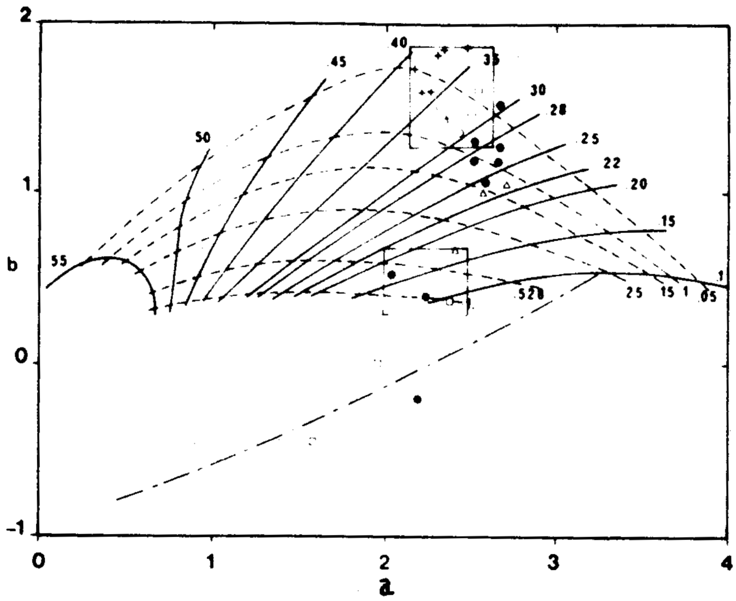

FIGURE 3. Diagram (a-b), where a and b are the coefficients of the rms fit (Eq. (1) in the text), for LND models. Full lines are for constant r_{eff} (in µm), dashed lines are for constant v_{eff}, and dot-dashed line is for bimodal size distributions (v_{eff} = .1, r_{eff} = 1 µm; v_{eff} = .25, r_{eff} = .1 µm). The points are deduced from SAGE II observations on 12 October, 1985 (0502 GMT and 0639 GMT) and on 13 October, 1985 (0651 GMT) at different altitudes :

+	16.5-17.5 km	o	18.5-19.5 km	●	20.5-21.5 km
Δ	22.5 km	*	23.5 km	▫	24.5 km

and v_{eff} for a LND model "equivalent" to the aerosol by SAGE II, from the point of view of spectral extinction between 1.02 µm and .385 µm, can be read in Figure 3. The results are summarized in Table 1.

Up to 21 km the variance is surprisingly small; above, it increases and the possible presence of two modes cannot be rejected. However, the SAGE II data are of poor quality above 23 km, especially at short wavelengths.

TABLE 1. Value of v_{eff} and r_{eff} in m retrieved from the (a-b) diagram for 12 October, 1985 (0639 GMT)

Z, km	16.5	17.5	18.5	19.5	20.5	21.5	22.5	23.5
v_{eff}	<.05	.05	.07	.05	.05	.10	.40	bimo-
r_{eff}, µm	.375	.35	.325	.325	.30	.25	.18	dal?

3. USE OF SAGE II CHANNEL RATIOS

Another, somewhat more direct approach to the size distribution study, is the utilization of various SAGE II channel extinction ratios

$$R_{\lambda_1\lambda_2} = \sigma(\lambda_1)/\sigma(\lambda_2) \qquad (5)$$

or of the related average Angström coefficient for the spectral intervals $(\lambda_1\lambda_2)$, defined as

$$\alpha_{\lambda_1\lambda_2} = -\ln R_{\lambda_1\lambda_2}/\ln(\lambda_1/\lambda_2) \qquad (6)$$

Figure 4 shows the diagram $(\alpha_{.45/1.02}-\alpha_{.385/1.02})$ for the LND models; all the points are very close to the diagonal and the same behavior is observed for the other combinations using the ratios of two short wavelengths (.385 µm, .45 µm or .525 µm) to the channel 1.02µm. This forbids the retrieval of r_{eff} and v_{eff} from the SAGE II data.

Figure 5 is the diagram $(\alpha_{.45/1.02}-\alpha_{.385/.525})$ that looks much more promising for an analysis of SAGE II data, although the ratio of two short wavelength channels $(\sigma(.385)/\sigma(.525))$ has a larger error than the ratios of a short wavelength to 1.02 µm channel. In Fig. 5 is also drawn the curve for two LND mode size distributions and the points for SAGE II observations in October 1985 (same data as in Fig. 3); the error rectangles are given, as examples for two points. The retrieved values of r_{eff} and v_{eff} agree almost exactly with the values retrieved from the previous analysis on the (a-b) diagram (Fig. 3), and the uncertainties are of the same order.

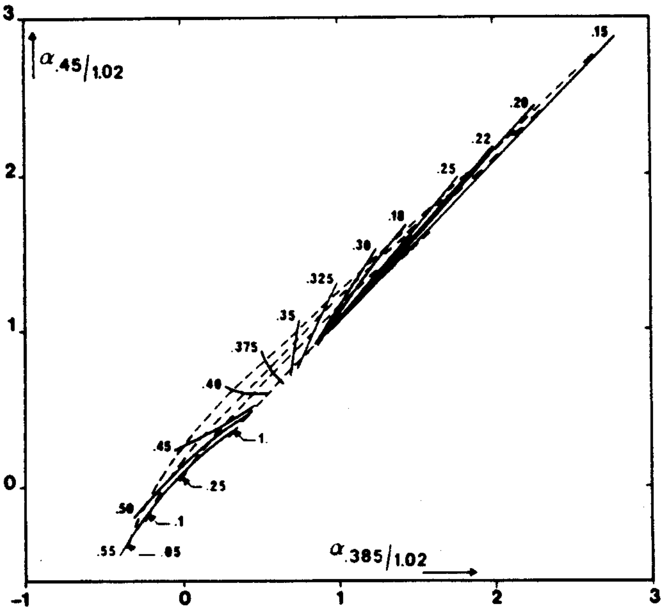

FIGURE 4. Diagram $(\alpha_{.45/1.02}-\alpha_{.385/1.02})$ for LND models. Full lines are for constant r_{eff} (in µm) and dashed lines are for constant v_{eff}.

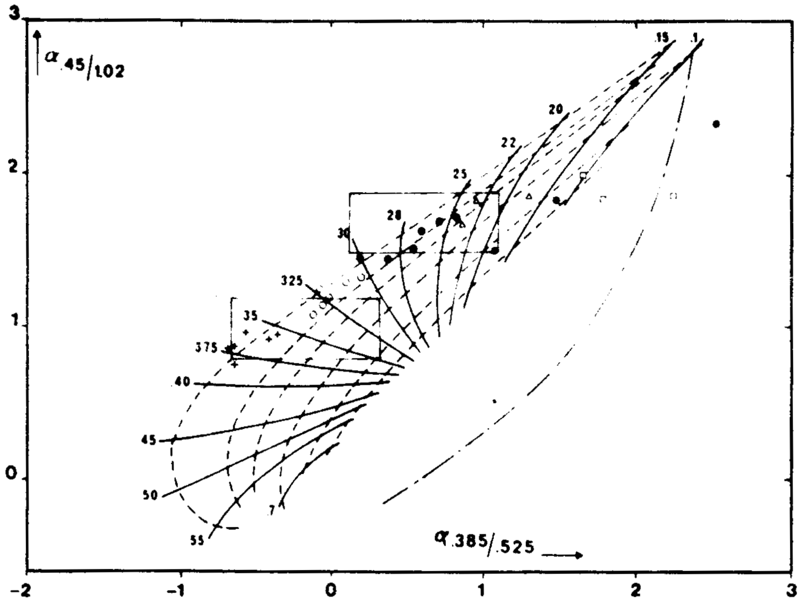

FIGURE 5. Diagram ($\alpha_{.45/1.02}-\alpha_{.385/.525}$) for LND models. Full lines are for constant r_{eff} (in µm), dashed lines are for constant v_{eff}, dot-dashed line is for bimodal size distributions, and the points are for SAGE II observations as defined in Fig. 3.

4. COMPARISON WITH BALLOON DATA

The aerosol size distribution was deduced from balloonborne infrared polarimetry measurements on 12 October, 1985, during an European SAGE II validation experiment (Herman et al, 1986). The profiles of r_{eff} and v_{eff}, shown in Fig. 6, compare reasonably with the values given in Table 1; a more detailed error analysis remains to be done.

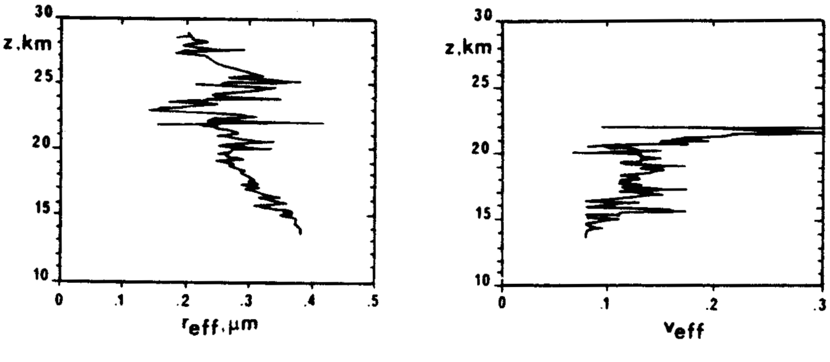

FIGURE 6. Profiles r_{eff} (in µm) and v_{eff} deduced from balloon experiment on 12 October, 1985.

5. CONCLUSION

The present analysis, although preliminary, proves that the SAGE II four-channel extinction should allow the retrieval of two parameters of a monomodal aerosol size distribution, although the error bars on the retrieved values are rather large, especially for the variance. Furthermore, it appears that the presence of a bimodal size distribution could be deduced, unless the relative contribution of one mode is too small.

ACKNOWLEDGMENTS

The SAGE II data were kindly provided to us by the NASA Langley Research Center. This study has been supported by the Centre National d'Etudes Spatiales (Contrat CNES 1259).

REFERENCES

Brogniez, C.,and J. Lenoble, 1987: Modeling of the Stratospheric Background Aerosols from Zonally Average SAGE Profiles, J. Geophys. Res., 92, D3, 3051-3060.

Hansen, J.E.,and J.W. Hovenier, 1974: Interpretation of the Polarization of Venus, J. Atm. Sci., 31, 1137-1160.

Herman, M., J.Y. Balois, L. Gonzalez, P. Lecomte, J. Lenoble, R. Santer and C. Verwaerde, 1986: Stratospheric Aerosol Observations from Balloonborne Polarimetric Experiment, App. Opt., 25, 3573-3584.

Lenoble, J., P. Pruvost and C. Brogniez, 1984: SAGE Satellite Observations of Stratospheric Aerosols from Mount St. Helens Eruption: A two Wavelength Analysis, J. Geophys. Res., 89, 11666-11667.

Lenoble, J., and C. Brogniez, 1985: Information on Stratosphere Aerosol Characteristics Contained in the SAGE Satellite Multiwavelength Extinction Measurements, App. Opt., 24, 1054-1063.

Yue, G.K., and A. Deepak, 1983: Retrieval of Stratospheric Aerosol Size Distribution from Atmospheric Extinction of Solar Radiation at Two Wavelengths, App. Opt. 22, 1639-1645.

Yue, G.K., and A. Deepak, 1984: Latitudinal and Altitudinal Variation of Size Distribution of Stratospheric Aerosols Inferred From SAGE Aerosol Extinction Coefficient Measurements at Two Wavelengths, Geophys. Res. Letts., 11, 999-1002.

JOURNAL OF GEOPHYSICAL RESEARCH, VOL. 94, NO. D6, PAGES 8339–8351, JUNE 20, 1989

SAGE II Inversion Algorithm

W. P. CHU AND M. P. MCCORMICK

Atmospheric Sciences Division, NASA Langley Research Center, Hampton, Virginia

J. LENOBLE, C. BROGNIEZ, AND P. PRUVOST

Laboratoire d'Optique Atmospherique, Universite des Sciences et Technique de Lille
Villeneuve d'Ascq, France

This paper provides a detailed description of the current operational SAGE II multichannel data inversion algorithm implemented at NASA Langley Research Center, Hampton, Virginia. This algorithm is compared to an independently developed inversion algorithm from the Laboratory of Atmospheric Optics, University of Lille, Lille, France. Inverted aerosol and ozone profiles from these two algorithms are shown to be similar within their respective uncertainties.

INTRODUCTION

Routine monitoring of the stratosphere utilizing the solar occultation approach started with the Stratospheric Aerosol Measurement (SAM) II instrument, which was launched in 1978 on the Nimbus 7 satellite. SAM II is a single spectral channel instrument built specifically for monitoring stratospheric aerosol extinction properties in the 1.0-μm wavelength region [*McCormick et al.*, 1979]. Inversion of the SAM II data has been relatively simple because it is a single-channel instrument. In February 1979 a four-channel instrument, the Stratospheric Aerosol and Gas Experiment (SAGE), was launched and operated for almost 3 years. The four spectral channels on the SAGE instrument were centered in the 1.0-, 0.6-, 0.45-, and 0.385-μm wavelength regions. The inversion problem for the SAGE data is more difficult owing to the additional channels with overlapping contributions from the various stratospheric species [*Chu and McCormick*, 1979]. The next version of the SAGE instrument, SAGE II, was launched in October of 1984 on the Earth Radiation Budget Satellite (ERBS). A detailed description of the SAGE II instrument has been given elsewhere [*Mauldin et al.*, 1985]. The SAGE II instrument is a seven-channel Sun photometer, with spectral passbands centered at 1.02, 0.94, 0.6, 0.525, 0.453, 0.448, and 0.385 μm. In addition to the measurements of water vapor at 0.94 μm, ozone (O_3) at 0.6 μm, and nitrogen dioxide (NO_2) from the differential channels at 0.453 and 0.448 μm, SAGE II data can provide aerosol extinction data at four of the seven spectral channel locations.

The inversion algorithm for the seven-channel SAGE II instrument has evolved from the earlier SAM II algorithm through the more complex SAGE I algorithm [*Chu and McCormick*, 1979], with various modification adapting to the SAGE II seven-channel measured data. This paper is intended to provide a detailed description of the operational algorithm that is being used at NASA Langley Research Cener (LaRC), Hampton, Virginia, to process the SAGE II data for archival purposes. The aerosol and O_3 retrievals will be discussed in detail in this paper. The retrieval of NO_2 and water vapor will be deferred for discussion in future publications. This paper also describes the comparison of these inversion results to those obtained from an inversion algorithm independently developed at the Laboratory of Atmospheric Optics, University of Lille, Lille, France. The purpose for the comparison between the results from these two different algorithms is to ensure that the archived products are freed from errors produced by the algorithm itself. Moreover, it will illustrate that similar results can be obtained from the same SAGE II data using different inversion algorithms. Comparison of the inversion results to correlative measurements will not be discussed in this paper. These comparisons are discussed in several companion articles [*Osborn et al.*, this issue; *Cunnold et al.*, this issue; *Ackerman et al.*, this issue].

Since the instrument configuration, operation, and data acquisition schemes for the SAGE I and SAGE II instruments are almost identical [*Mauldin et al.*, 1985], this paper will not repeat the details concerning the operation and data acquisition of the SAGE II instrument. Interested readers could consult an earlier article, which contained most of this information [*Chu and McCormick*, 1979].

SAGE II MEASUREMENTS AND DATA PROCESSING

The irradiance H_λ measured by the SAGE II instrument at a given time t is given by

$$H_\lambda = \int_{\Delta\lambda}\int_{\Delta\omega} W_\lambda(\theta, \phi)F_\lambda(\theta, \phi, t)T_\lambda(\theta)\, d\Omega\, d\lambda \qquad (1)$$

where W is the radiometer's field of view function, ϕ is the azimuthal angle; Ω is the solid angle, T is the transmittance of the atmosphere as a function of view angle θ, which is a unique function of the tangent height h_t; and F is the extraterrestrial solar radiance for wavelength λ. The mean transmittance of the atmosphere over the spectral bandwidth and instrument field of view is calculated by ratioing the irradiance measured within the atmosphere to that measured outside the atmosphere. The transmittance function in terms of the ray tangent height h_t, according to the Bouguer law, is given by

$$T_\lambda(h_t) = \exp\left[-\delta_\lambda(h_t)\right] = \exp\left[-\int \sigma_\lambda(h)\, d\rho_\lambda(h)\right] \qquad (2)$$

Copyright 1989 by the American Geophysical Union.

Paper 89JD00113.
0148-0227/89/89JD-00113$05.00

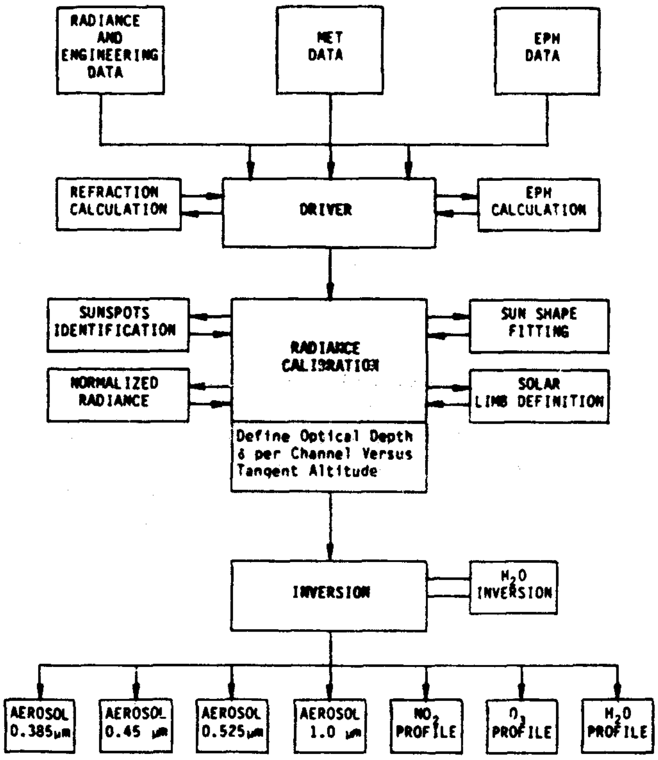

Fig. 1. Block diagram for the SAGE II data processing algorithm implemented at LaRC.

where $\delta_\lambda(h_t)$ is the total slant path optical depth at wavelength λ with ray tangent height h_t; σ_λ is the total extinction coefficient of the atmosphere as a function of altitude h and wavelength λ; an ρ is the geometric path length corrected for refraction.

The total extinction at each tangent altitude is a linear combination of the extinctions of each of the species, as given by

$$\sigma_\lambda = \sigma^{\mathrm{Ray}}(\lambda) + \sigma^{\mathrm{O_3}}(\lambda) + \sigma^{\mathrm{NO_2}}(\lambda) + \sigma^{\mathrm{aero}}(\lambda) \tag{3}$$

where $\sigma^{\mathrm{Ray}}(\lambda)$ is the extinction coefficient for Rayleigh scattering, and $\sigma^{\mathrm{O_3}}(\lambda)$, $\sigma^{\mathrm{NO_2}}(\lambda)$, and $\sigma^{\mathrm{aero}}(\lambda)$ are the extinction coefficients for O_3, NO_2, and aerosol at wavelength λ, respectively. For O_3 and NO_2 the extinction coefficients are determined by the product of the species number density and their absorption cross section at the given wavelength. The aerosol extinction coefficient is a function of aerosol size distribution, shape, and index of refraction. For homogeneous, spherical particles, one has

$$\sigma^{\mathrm{aero}}(\lambda) = \int_0^\infty Q(n, r, \lambda)N(r)\, dr \tag{4}$$

where $N(r)$ is the size distribution function, and $Q(n, r, \lambda)$ is the extinction cross section for a particle with refractive index n and radius r, as computed from Mie theory.

The approach used for the processing of the SAGE II data is to reduce the solar radiance measurements at the seven spectral channels into transmittance functions of the atmosphere at the seven wavelength regions and to invert the transmittance data as described by (2), (3), and (4) in order to determine the vertical extinction profiles for each of the species. The actual flow of the SAGE II processing begins with the acquisition at LaRC of three data tapes: (1) the instrument raw radiance data, collected by the Goddard Space Flight Center (GSFC) and transferred to LaRC in the form of "experimenter tapes"; (2) a MET tape received from the National Weather Service (NWS) of the National Oceanic and Atmospheric Administration (NOAA) containing the meteorological data associated with each SAGE II measurement event; and (3) satellite ephemeris data tapes, also prepared by GSFC. The information contained in these three tapes are first merged at LaRC to produce an archival product, the "Merdat" tape. The Merdat tapes contain all of the information required to perform the SAGE II data reduction. The SAGE II radiance data are then processed through the data reduction algorithm to produce aerosol extinction profiles at the four wavelengths centred at 1.02, 0.525, 0.453, and 0.385 μm and to produce vertical O_3, NO_2, and water vapor concentration profiles. The inverted results for each of the species plus all of the auxiliary information, such as the coincident temperature profiles provided by NWS, are being archived at National Space Sciences Data Center (NSSDC) at GSFC.

LARC SAGE II DATA REDUCTION ALGORITHMS

Figure 1 shows the functional blocks diagram of the SAGE II data reduction algorithms implemented at LaRC for processing of SAGE II raw radiance data. The algorithms consists of three main subsections and are denoted as the driver, radiance calibration, and inversion programs, respectively.

Driver Program

The driver program performs data screening and calculations using the meteorological data and the ephemeris data from the Merdat tapes. The effects of atmospheric refraction are calculated for each measurement event using the NWS temperature versus altitude profile, according to the procedure described by *Chu* [1983]. Tables relating the angles of refraction and air masses to the line of sight tangent height levels are generated from these calculations for subsequent use. The measurement geometry relating the positions of the spacecraft, the Sun, and the Earth at specific times is determined from the solar and spacecraft ephemeris data [*Buglia*, 1988]. The SAGE II solar scan data from approximately 120-km tangent altitude down to the lowest altitude level are selected, together with the other computational results, for use in subsequent analysis.

Radiance Calibration Program

The radiance calibration program is used to perform calibration of the Sun scan data in order to produce slant path atmospheric transmission profiles for the seven SAGE II wavelength regions. The procedure has been described by *Chu and McCormick* [1979] for the SAGE I data processing procedure.The only difference between this portion of the SAGE I and the SAGE II algorithms is that the procedures for determination of the tangent altitude locations for each of the measured radiance data points are different. For the SAGE II measurements the tangent altitudes are determined solely from the spacecraft/Sun/Earth ephemeris data, while the SAGE I procedure uses a fitting scheme between the measured Rayleigh vertical profile and the NWS data for the reference height determination.

TABLE 1. Comparison of LaRC and LOA Values for a_i and b_i

	Wavelength, μm						
	λ_1	λ_2	λ_3	λ_4	λ_5	λ_6	λ_7
	1.02	0.94	0.6	0.525	0.453	0.448	0.385
a_i (LaRC)	0.	0.005	1.0	0.439	0.0338	0.0299	0.
a_i (LOA)	0.	···	1.0	0.435	0.0332	0.0257	0.
b_i (LaRC)	0.	0.	0.055	0.348	0.847	1.0	1.14
b_i (LOA)	0.	0.	0.0	0.367	0.837	1.0	1.14

O_3 cross section at 0.6 μm = 5.067 10^{-21} cm^2 [*Penney*, 1979]; NO_2 cross section at 0.448 μm = 5.46 10^{-19} cm^2 [*Goldman et al.* [1978].

In brief, the purpose of the radiance calibration program is to reconstruct the SAGE II measurement geometry from the measured solar radiance versus time data, together with the time variation of the SAGE II scan mirror motion. The instrument viewing directions during the course of time for the measurement event, expressed in terms of tangent altitudes for the ray path, and the corresponding vertical positions on the solar limb curve are computed from the spacecraft and solar ephemeris data for each of the SAGE II measurement points. After the location information for each of the SAGE II data points is determined, a sequence of Sun scans above the atmosphere are selected for use as the calibrated solar limb curves for each of the seven spectral channels. The solar-calibrated limb curves express the unattenuated solar radiance values at each of the seven wavelength channels as a function of vertical solar limb position. They are used for normalizing measurements obtained from Sun scans transversing the atmosphere to form the atmospheric transmittance values at the seven spectral channels. The procedure is repeated until all of the atmospheric measurements are normalized. The transmittance values are then averaged over 1-km layers, over a vertical height range of 70 km. The averaging procedure is applied to the slant path optical depth values, and the standard errors for the mean optical depth values are determined for used as an estimate for the measurement uncertainties. For the calculation of the standard errors, consecutive measurements with an overlapping field of view are assumed to be correlated.

Inversion Program

The inversion program is the most important part of the SAGE II processing algorithm. It performs the conversion of the measured slant path atmospheric transmission data from the seven wavelength channels into optical parameters describing the vertical distribution of the four atmospheric constituents (aerosol, O_3, NO_2, and water vapor). The conversion process required three consecutive operations on the input data, as described below.

Removal of Rayleigh component. The Rayleigh scattering contribution is present in all the seven-channel SAGE II measurements, with the Rayleigh components varying approximately as the inverse fourth power of the wavelength. The SAGE II channels with wavelengths of less than 0.5 μm are therefore more heavily dominated by the Rayleigh component. The atmospheric vertical density profiles are calculated from the the temperature versus geometric altitude data supplied by NWS. The updated correction of the temperature values at pressure altitude levels higher than 10 mbar has been included [*Gelman et al.*, 1986]. Since the temperature versus altitude data are given at the standard 18 fixed pressure levels up to 0.4 mbar, linear interpolation of the temperature is assumed to be valid for heights within the given pressure levels. The temperature versus altitude profiles are also extended to 0.01 mbar by adding two temperature data points, based on climatological mean values from the U.S. Standard Atmosphere Supplement (1966). The vertical profiles of air density are then calculated using the hydrostatic equation. The Rayleigh extinction cross section values at the seven wavelengths are computed using the latest estimate of the depolarization ratio values, as given by *Young* [1980], and the simplified dispersion formula, as described by *Edlen* [1953]. A 70-level path length matrix including the atmospheric refraction effect is also calculated. The corresponding Rayleigh slant path optical depth values for the seven wavelengths can then be computed and subtracted from the seven measured optical depth profiles. Finally, by excluding the water vapor channel at 0.94 μm, the following six reduced equations would represent the SAGE II measurements at each of the 70 height levels.

$$\delta(\lambda_1) = \delta^{\text{aero}}(\lambda_1) \tag{5}$$

$$\delta(\lambda_3) = \delta^{\text{aero}}(\lambda_3) + \delta^{O_3}(\lambda_3) + b_3\delta^{NO_2}(\lambda_6) \tag{6}$$

$$\delta(\lambda_4) = \delta^{\text{aero}}(\lambda_4) + a_4\delta^{O_3}(\lambda_3) + b_4\delta^{NO_2}(\lambda_6) \tag{7}$$

$$\delta(\lambda_5) = \delta^{\text{aero}}(\lambda_5) + \delta_5\delta^{O_3}(\lambda_3) + b_5\delta^{NO_2}(\lambda_6) \tag{8}$$

$$\delta(\lambda_6) = \delta^{\text{aero}}(\lambda_6)\delta + a_6\delta^{O_3}(\lambda_3) + b_6\delta^{NO_2}(\lambda_6) \tag{9}$$

$$\delta(\lambda_7) = \delta^{\text{aero}}(\lambda_7) + b_7\delta^{NO_2}(\lambda_6) \tag{10}$$

where $\delta(\lambda)$ is the slant path optical depth at wavelength λ, with the Rayleigh contribution removed; and λ_i, a_i, and b_i, as tabulated in Table 1, are the center wavelengths of the seven channels and the ratio of the O_3 and NO_2 cross sections at the seven wavelength channels, respectively. The NO_2 cross section values are obtained from the unpublished measurements by Graham and Johnston, as used by *Goldman et al.* [1978], and the O_3 absorption cross section values at the Chappuis band are obtained from Penney's measurements [*Penney*, 1979]. All ratios of cross section values are computed from the convolution of the absorption spectra with the measured SAGE II instrument spectral response functions.

Separation of species. Equations (5)–(10) completely describe the SAGE II measurements, showing the overlapping contributions from aerosols, O_3, and NO_2. The set of equations can be reduced further by taking the difference between (9) and (8):

$$\delta_D[(\lambda_6) - (\lambda_5)] = \delta^{\text{aero}}(\lambda_6) - \delta^{\text{aero}}(\lambda_5) + (a_6 - a_5)\delta^{O_3}(\lambda_3) + (b_6 - b_5)\delta^{NO_2}(\lambda_6) \tag{11}$$

Equation (11) can provide a good estimate of the NO_2 contribution by using $\delta^{O_3}(\lambda_3) \approx \delta(\lambda_3)$ and by assuming that the difference in aerosol contributions from the two closely spaced spectral channels is negligible. After removing the estimated NO_2 contributions in the other three channels, we are left with the following four equations:

$$\delta'(\lambda_3) = \delta^{\text{aero}}(\lambda_3) + a_3\delta^{O_3}(\lambda_3) \tag{12}$$

$$\delta'(\lambda_4) = \delta^{\text{aero}}(\lambda_4) + a_4\delta^{O_3}(\lambda_3) \tag{13}$$

$$\delta'(\lambda_5) = \delta^{\text{aero}}(\lambda_5) + a_5\delta^{O_3}(\lambda_3) \tag{14}$$

$$\delta'(\lambda_7) = \delta^{\text{aero}}(\lambda_7) \tag{15}$$

Where the $\delta'(\lambda)$ denotes the SAGE II measured slant path optical depth values with the Rayleigh and NO_2 components removed. Equations (5) and (12)–(15) constitute the five basic equations which are used to solve for the vertical profiles of O_3 density and the aerosol extinction values at the corresponding wavelength locations. A close inspection of these equations reveals that there are six unknowns in these five equations, consisting of five unknowns for aerosol and one unknown for O_3. In order for the retrieval process to produce unique solutions from these equations, either the total number of unknowns has to be reduced, or an extra equation describing the relationship between the unknowns has to be included. The approach being adapted for the routine processing of SAGE II data at Langley Research Center is to include an additional equation relating the behavior of the aerosol optical depth values at different wavelengths. The detailed procedure is described in the next paragraph.

Equation (4) can be used to represent the aerosol optical depth $\delta^{\text{aero}}(\lambda)$ by replacing the aerosol number density with the integrated aerosol density along the ray tangent slant path. Using numerical quadrature with unity weights, the integral is replaced with a numerical sum of the products of the aerosol extinction cross section, with the slant-path–integrated aerosol size distribution $N(r)$ at a finite number of mean radii r_j, $j = 1, 2, \cdots, m$, as follows:

$$\delta_i^{\text{aero}} = \sum_{j=1}^{m} Q_{ij}N_j \qquad i = 1, \cdots, 4 \tag{16}$$

Equation (16) can be put into matrix form, with $\mathbf{x}^T = (N_1, N_2, \cdots, N_m)$ and $(\delta^{\text{aero}})^T = (\delta_1^{\text{aero}}, \delta_2^{\text{aero}}, \cdots, \delta_n^{\text{aero}})$, and the matrix element $(\mathbf{K})_{ij} = (Q_{ij})$:

$$\begin{bmatrix} \delta_1^{\text{aero}} \\ \delta_2^{\text{aero}} \\ \vdots \\ \delta_n^{\text{aero}} \end{bmatrix} = \begin{bmatrix} Q_{11} & Q_{12} & \cdots & Q_{1n} \\ Q_{21} & Q_{22} & \cdots & Q_{2n} \\ \vdots & \vdots & \vdots\vdots & \vdots \\ Q_{m1} & Q_{m2} & \cdots & Q_{mn} \end{bmatrix} \begin{bmatrix} N_1 \\ N_2 \\ \vdots \\ N_m \end{bmatrix} \tag{17}$$

This matrix equation can be inverted with Twomey's linear constraint method [*Twomey*, 1963] to produce the solution

$$\mathbf{x} = \mathbf{K}^T(\mathbf{K}\mathbf{K}^T + \Gamma)^{-1}\delta^{\text{aero}} \tag{18}$$

where the diagonal matrix Γ consists of elements which are proportional to the estimated noise level at each of the wavelength channels. The aerosol optical depth at 0.6 μm (δ_3^{aero}) can then be expressed as a linear combination of the aerosol optical depth values at the other four wavelengths, with the linear coefficients α_i given by

$$\delta_3^{\text{aero}} = \mathbf{K}_3\mathbf{x} = \mathbf{K}_3\mathbf{K}^T(\mathbf{K}\mathbf{K}^T + \Gamma)^{-1}\delta_i^{\text{aero}} = \sum_{i=1}^{4} \alpha_i\delta_i^{\text{aero}} \tag{19}$$

The aerosol extinction cross sections are calculated with the anomalies diffraction approximation, assuming that the aerosol refractive index is 1.43.

Thus (19) constitutes the additional equation required to provide a unique solution for solving the set of equations consisting of (5) and (12)–(15). Since the SAGE II measurements consist of only a very limited number of wavelength channels, there are only four measured aerosol optical depth values that can be used in (19). Therefore the linear constraint method would necessarily produce solutions that are compatible with the aerosol size distribution being very smooth and its shape being very unstructured. It is well known that the background stratospheric aerosol size distribution can be described by the lognormal distribution [*Pinnick et al.*, 1976], which is very smooth in shape. Therefore the use of (19) is justified, at least for the background stratospheric aerosol condition.

The complete procedure, beginning from estimating the NO_2 contributions (as described by equation (11)), to the separation of aerosol and O_3 optical depth, is then repeated in one more iteration, using the updated values for O_3 and aerosol. This additional iteration is primarily used to stabilize the NO_2 retrieval and does not appreciably perturb the O_3 and aerosol retrievals. The retrievals of O_3 and aerosols are not sensitive to the initial estimates on the NO_2 distribution, since the NO_2 contributions in the various spectral channels are relatively small.

Vertical profile inversion. The inversion from slant path optical depth data for each of the species to vertical extinction profiles for aerosol at the different wavelength channels, and for O_3 at 0.6 μm, is performed with the standard Twomey modification of Chahine nonlinear inversion algorithm [*Twomey*, 1975]. The algorithm is iterative, and the updating procedure is as follows:

$$\sigma_j^{n+1} = \sigma_j^n[1 + (r_i - 1)P_{ij}/P_{ii}] \tag{20}$$

where $r_i = \delta_i^m/\Sigma_j P_{ij}\sigma_j^n$, P_{ij} is the path length element (i, j), and σ_j^n is the extinction value at j for the n iteration. For an N-level profile, one iteration consists of N j loops for each i level until all N i levels are updated. The iteration stops when the difference between the computed signal $\delta_i^{\text{comp}} = \Sigma_j P_{ij}\sigma_j^n$ and the measured signal δ_i^{meas} is less than the estimated error on $\delta_i^{\text{meas}}(\lambda)$ for all levels i. Furthermore, a 5-km altitude smoothing is incorporated for extinction levels at ≤ 0.00002 km^{-1} for all vertical profile retrievals. The smoothing is done between each iteration by computing a running mean average on the log of the retrieval extinction values from the top down and ending at the extinction level of 0.00002 km^{-1}. Notice that the P matrix is a triangular matrix, which implies that the inversion problem is well posed [*Chu*, 1985]. The reason for using (20) to solve for the vertical profiles is to accommodate the 5-km vertical smoothing on the retrieved profiles.

Error Estimate for the SAGE II Inverted Profiles

The error estimate for the inverted extinction profiles of aerosol and ozone can be derived from the procedure described by *Russell et al.* [1981]. Only the random compo-

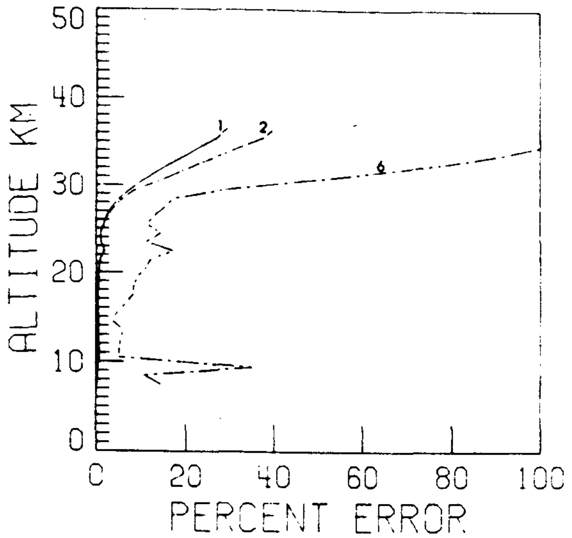

Fig. 2. Height dependence of expected uncertainty for the SAGE II 1.02-μm aerosol extinction, showing contribution by various sources. Sources of uncertainty are as follows: (1) altitude uncertainty, (2) Rayleigh uncertainty, (3) ozone uncertainty, (4) nitrogen dioxide uncertainty, (5) aerosol uncertainty, and (6) measurement uncertainty.

nent of the error estimate is computed and tabulated for the SAGE II inverted products. In general, there are four error sources that contribute to the total uncertainties of the retrieved vertical profiles. They are (1) the measurements errors, (2) the uncertainty in the calculated Rayleigh profiles caused by the uncertainty in the temperature profiles, (3) the uncertainty in the reference altitude, and (4) the uncertainties associated with the removal of other species which have overlapping contributions in the spectral wavelength channel. The total error of the inverted extinction at each height level is then given by the root-mean-square of these four errors, assuming that they are uncorrelated. The measurement errors in this case are given by the estimated uncertainties from the transmission program in calculating the standard errors of the mean optical depth values at each tangent height level. The Rayleigh errors are calculated from the temperature errors given by the NWS data associated with each temperature profile. The magnitude of the temperature errors generally is within the range from 2°C at sea level to about 12°C at 0.4-mbar pressure level. The reference altitude error is the uncertainty in assigning the corrected geometric altitude for each measurement position in order to subtract the Rayleigh components in all of the SAGE II channels. This error is estimated to be about 200 m (1σ) from the spacecraft ephemeris calculations for each SAGE II sunrise or sunset measurement event. The errors contributed by the other species arise from the uncertainties in removing contributions from different species in the particular spectral channel. The total estimated error for the inverted extinction at each height level is given by

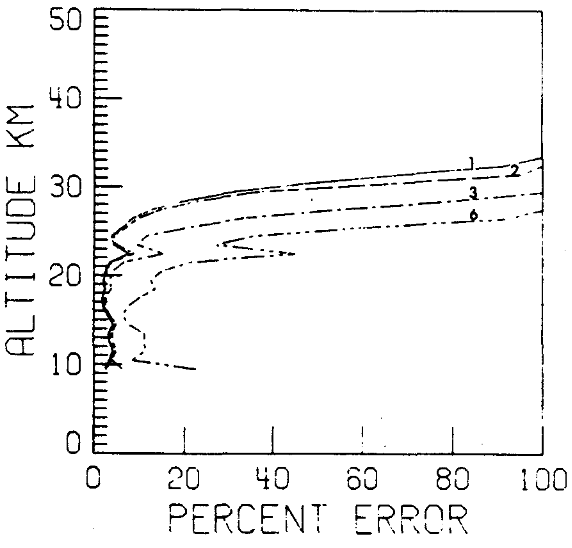

Fig. 3. Similar to Figure 3, except for height dependence of expected uncertainty for the SAGE II 0.525-μm aerosol extinction, showing contributions by various sources. (See Figure 2 caption for identification of sources.)

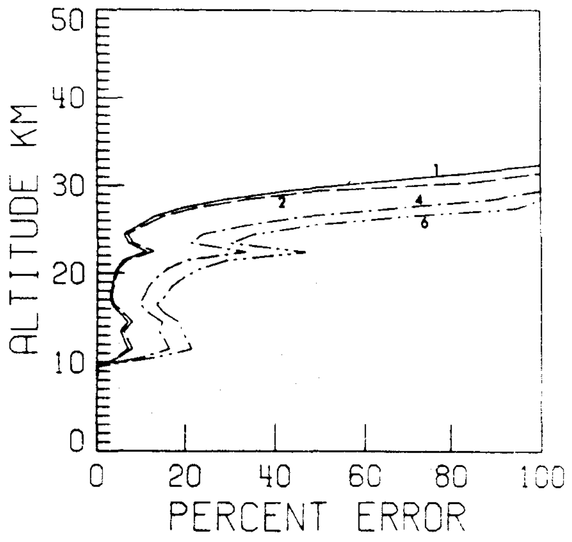

Fig. 4. Similar to Figure 3, except for height dependence of expected uncertainty for the SAGE II 0.453-μm aerosol extinction, showing contributions by various sources. (See Figure 2 caption for identification of sources.)

$$(\Delta\sigma)^2 = \Delta_1^2 + \Delta_2^2 + \Delta_3^2 + \Delta_4^2 \tag{21}$$

where the first term on the left-hand side of (21) is the measurement error, the second is the Rayleigh error, the third is the altitude error, and the fourth is the error from other species;

$$\Delta_1^2 = \sum (P_{ij}^{-1}\Delta\delta_j)^2$$

is the optical depth error; and the temperature error is

$$\Delta_2 = (\partial\sigma^{\text{Ray}}/\partial T)\Delta T$$

The altitude error is

$$\Delta_3 = (\partial\sigma^{\text{Ray}}/\partial Z)\Delta Z$$

and, for n species,

$$\Delta_4^2 = \sum (P_{ij}^{-1}\alpha_n\Delta\delta_{jn})^2$$

where P_{ij}^{-1} is the (i, j) element of the inverse of the path length matrix P, σ^{Ray} is the Rayleigh extinction, T and Z are the temperature and altitude, respectively, $\Delta\delta_j$ is the estimated measurement error for the optical depth values at tangent height level j, and α_n is the a_n or b_n coefficients in Table 1.

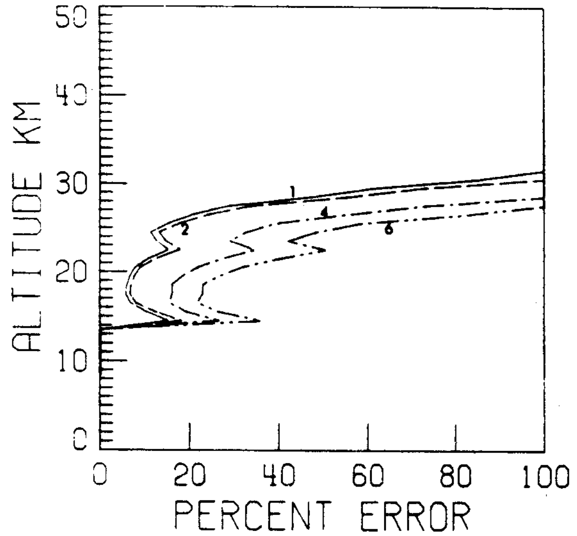

Fig. 5. Similar to Figure 3, except for height dependence of expected uncertainty for the SAGE II 0.385-μm aerosol extinction, showing contributions by various sources. (See Figure 2 caption for identification of sources.)

Figures 2–6, illustrate the typical height dependence of the expected uncertainties for the SAGE II four wavelength aerosol extinction profiles at 1.02, 0.525, 0.453, and 0.385 μm, and the O_3 vertical profile, respectively. The estimated measurement errors are taken from a typical mid-altitude measurement event in 1985. The relative size and height dependence of these four sources of uncertainty and how they contribute to the total uncertainty are computed and displayed. The measurement errors are shown to be the dominating source of uncertainty for the retrieval O_3 profiles and, similarly, for the aerosol profiles at the two long wavelength channels. The partitioning of the error sources for the two short wavelength aerosol extinction profiles is more complex. As illustrated in Figures 2–6, O_3 profiles can be retrieved from the SAGE II measurements with uncertainties up to 10% between cloud top height and about 60 km altitude. The aerosol extinction profiles at 1.02 μm can similarly be retrieved with uncertainties up to 10% between cloud top height and about 25 km altitude, depending on the shape of the aerosol vertical distribution. For the aerosol extinction profiles at shorter wavelengths, the uncertainties would increase because of the stronger Rayleigh influence in these wavelength regions. The total uncertainties are about 30% at 0.385 μm for the aerosol extinction profiles for an altitude range limited to between 15- and about 22-km height.

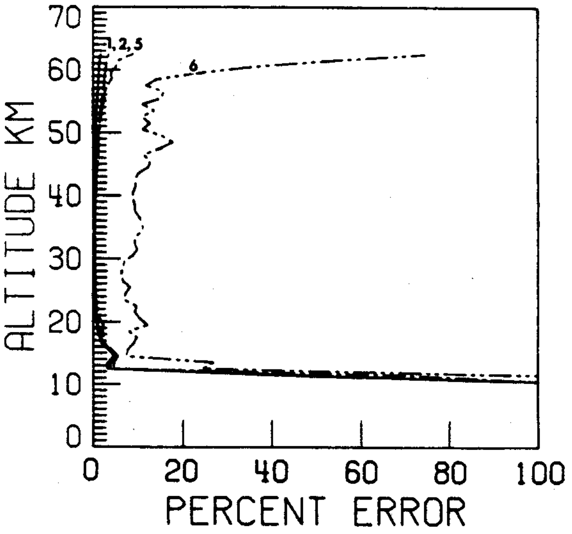

Fig. 6. Similar to Figure 3, except for height dependence of expected uncertainty for the SAGE II ozone, showing contributions by various sources. (See Figure 2 caption for identification of sources.)

LOA INVERSION ALGORITHM

For the SAGE II European Correlative Program [*Lenoble*, this issue], an inversion algorithm for the SAGE II data was independently developed at the Laboratoire d'Optique Atmospherique (LOA) of the University of Lille, France. This inversion procedure utilizes the slant path optical depth profile data generated from the radiance calibration program mentioned previously for the six spectral channels centered at 1.02, 0.6, 0.525, 0.453, 0.448, and 0.385 μm and uses the corresponding meteorological data provided by NWS to correct for the Rayleigh contribution.

There are three reasons for separately developing the LOA inversion scheme. They are (1) to get a better insight into the physical process of SAGE II measurements, (2) to understand how the retrieval of one species can be perturbed by the presence of other species in the same spectral region, and (3) to provide the user community with an alternative inversion algorithm to check the archival data when necessary. The LOA algorithm is not intended to be used as an operational tool. Therefore a conservative approach has been taken to evaluation of the uncertainties and to estimation of the altitude range where the inversion is of good quality for each channel and species and the altitude range where the data must be used with caution.

The flow chart for the LOA inversion scheme is summarized in Figure 7. The Rayleigh transmission are computed for each channel, using the atmospheric density data derived from the meteorological data. The density profiles are calculated by linear interpolation of the temperature values between the standard levels, assuming the validity of the hydrostatic equation and the ideal gas equation of state. The elements of the path length matrix P_{ij} are computed with a geometrical method, with 1-km layers which are subdivided into 0.025-km sublayers. The depolarization ratio for Rayleigh scattering is taken as 1.0254. The Rayleigh-corrected optical depth profiles for the six channels at the wavelength λ = 1.02, 0.6, 0.525, 0.453, 0.448, and 0.385 μm and the Rayleigh-corrected optical depth difference for $\delta(\lambda_6) - \delta(\lambda_5)$ are inverted, using a simple Chahine inversion procedure [*Chahine*, 1972]

$$\sigma_i^{(n)} = \sigma_i^{(n-1)}\delta_j/\sum \sigma_i^{(n-1)}P_{ij} \tag{22}$$

where n is the iteration order; the inversion is stopped after 10 iterations, which is generally more than sufficient to produce convergence. The error in the extinction coefficient is evaluated as

$$\Delta\sigma_i = [(\Delta\sigma_i^{\text{meas}})^2 + (\Delta\sigma_i^{\text{Ray}})^2]^{1/2} \tag{23}$$

where the error due to the slant path optical depth error $\Delta\sigma_i^{\text{meas}}$ is

$$\Delta\sigma_i^{\text{meas}} = \Delta\delta_i^{\text{meas}}/P_{ii} \tag{24}$$

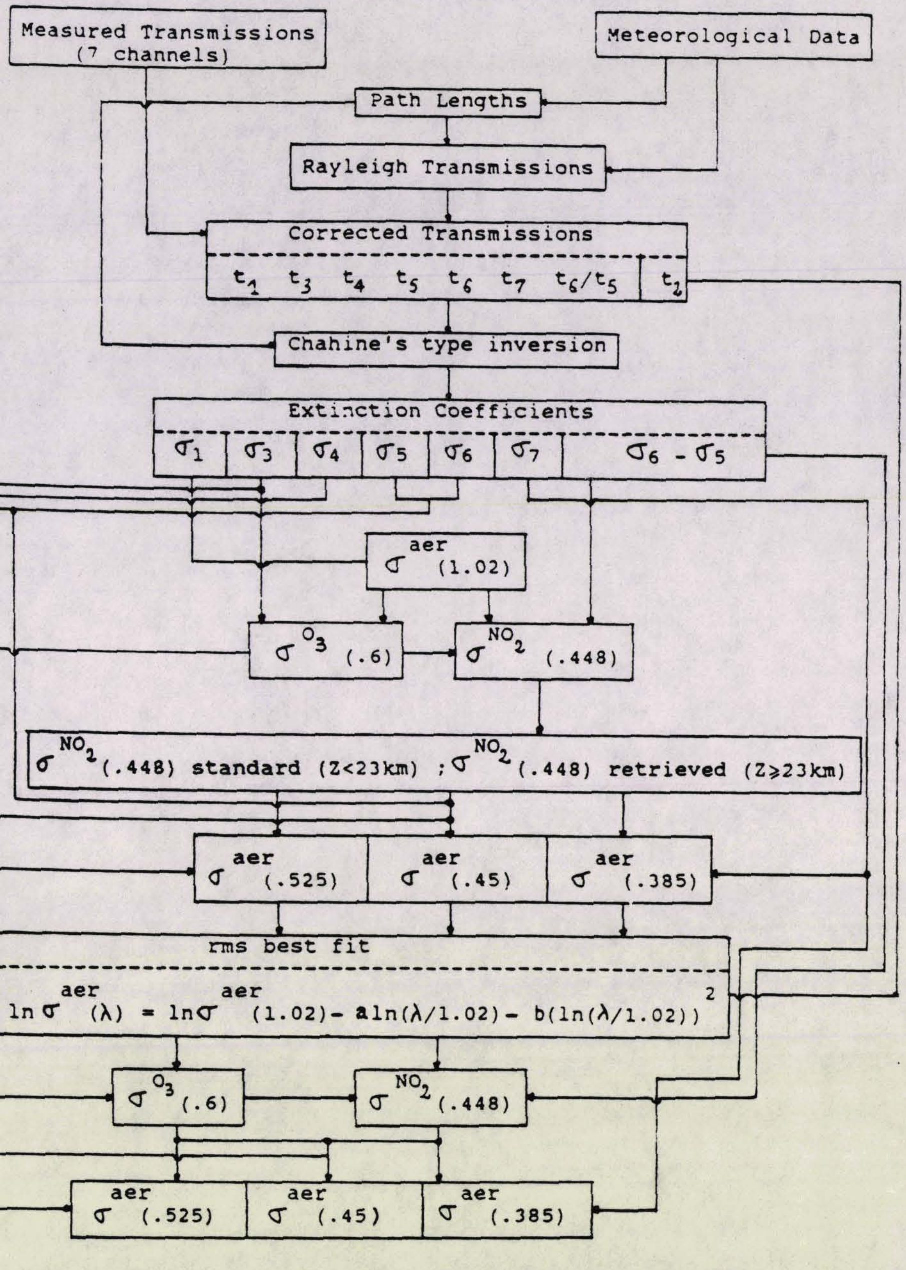

Fig. 7. Block diagram of the SAGE II inversion algorithm developed at LOA.

since the major contribution to the slant path optical depth is due to the first layer above z_i, and

$$\Delta\sigma_i^{\mathrm{Ray}} \simeq 0.05\sigma_i^{\mathrm{Ray}} \tag{25}$$

based on the assumption of an error of 1.5% in the atmospheric density and an error of 0.25 km in the altitude [*Lenoble and Pruvost*, 1983].

The steps used for the separation of species in this inversion algorithm proceed as follows:

1. The inversion of the 1.02 μm data produces the aerosol extinction coefficient at 1.02 μm directly. When the transmission value is very close to unity at high altitudes where the aerosol content is low, the retrieved values become erratic. Therefore it is necessary to stabilize the 1.02-μm aerosol retrieval at this altitude region in order to perform the aerosol correction for the other channels. This is accomplished by extrapolating the profile $\sigma^{\mathrm{aero}}(\lambda_1)$ exponentially from the height level where the retrieval is well behaved to a standard extinction value of 10^{-7} km^{-1} at 45 km, which is the upper limit of this inversion.

2. The aerosol contribution at the 0.6-μm channel data is removed by extrapolating $\sigma^{\mathrm{aero}}(\lambda_1)$ to different wavelengths, using the Angstrom law as described in (26):

$$\sigma^{\mathrm{aero}}(\lambda) = \sigma^{\mathrm{aero}}(\lambda_1)\lambda^{-\alpha} \tag{26}$$

where the value of α varies from 0.65 below 15 km to 1.7 above 20 km altitude. This permits one to obtain an initial estimate of the ozone extinction $\sigma^{O_3}(\lambda_3)$ at 0.6 μm. The aerosol correction is large below 20 km, and therefore the initial estimate of $\sigma^{O_3}(\lambda_3)$ is poor at this height. Above 20 km altitude the aerosol correction diminishes rapidly, and the initial estimate of $\sigma^{O_3}(\lambda_3)$ is quite accurate.

3. Find the difference between the 0.453- and the 0.448-μm channel data and remove the O_3 extinction contribu-

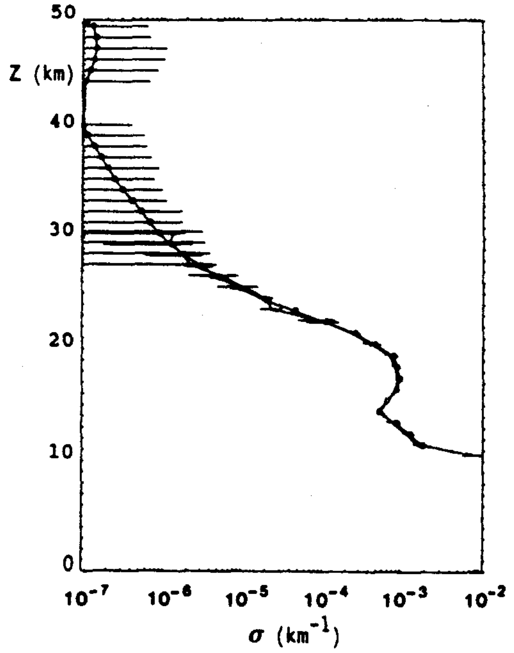

Fig. 8. Comparison of aerosol extinction profiles at 1.02 μm, retrieved by LaRC (solid curve with circles) and by LOA (solid curve) for measurement event on April 21, 1985, at 1854 UT.

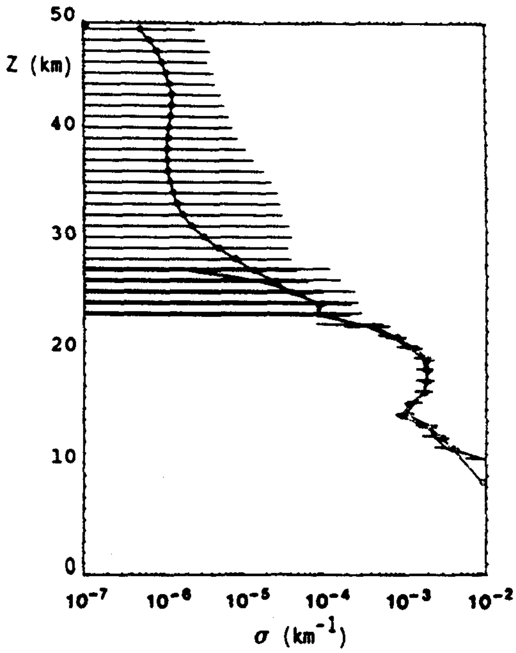

Fig. 10. Same as Figure 8, except for aerosol profiles at 0.453 μm.

tions, using the initial estimate of $\sigma^{O_3}(\lambda_3)$ and the O_3 cross section ratios, as tabulated in Table 1 for the LOA inversion code. Similarly, the aerosol extinction contributions are removed, using the profile $\sigma^{aer}(\lambda_1)$, and extrapolated to the corresponding wavelength regions with the Angstrom law, as described in the preceeding paragraph. This leads to an initial estimate for the NO_2 extinction difference $\sigma^{NO_2}(\lambda_6)-\sigma^{NO_2}(\lambda_5)$ and an initial estimate for the extinction $\sigma^{NO_2}(\lambda_6)$. The O_3 correction should be quite accurate, since its contribution becomes important only at high altitudes, i.e., when the initial estimate of $\sigma^{O_3}(\lambda_3)$ is good. The aerosol correction is small above 23 km but becomes large and model-dependent at lower altitudes; therefore the initial estimate of $\sigma^{NO_2}(\lambda_6)$ is very inaccurate at low altitudes.

4. The three-channel data at 0.525, 0.453, and 0.385 μm can therefore be used to estimate the aerosol contribution by removing the O_3 and NO_2 contributions, using the initial estimates of $\sigma^{O_3}(\lambda_3)$ and $\sigma^{NO_2}(\lambda_6)$ as derived earlier. The NO_2 profiles below 23 km altitude are obtained from extrapolating along a standard profile [*Lenoble and Pruvost*, 1983]. This procedure provides the initial estimates of the aerosol extinction profiles $\sigma^{aero}(\lambda_4)$, $\sigma^{aero}(\lambda_5)$, and $\sigma^{aero}(\lambda_7)$. Fortu-

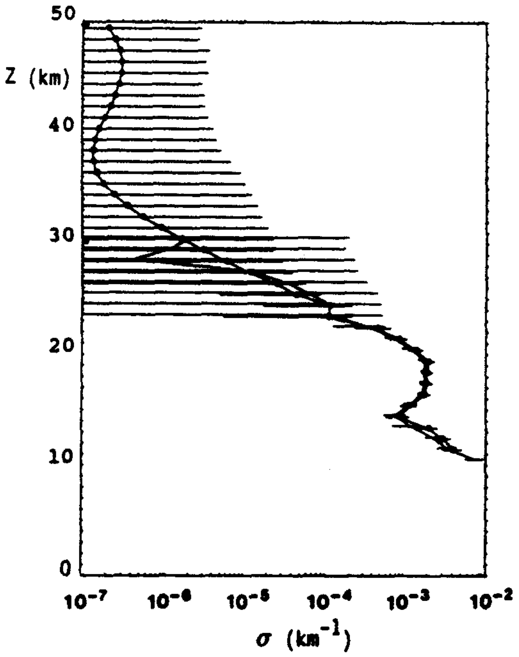

Fig. 9. Same as Figure 8, except for aerosol profiles at 0.525 μm.

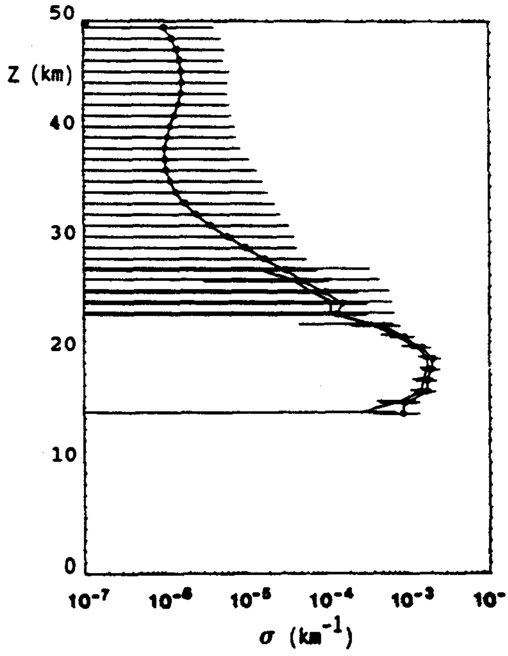

Fig. 11. Same as Figure 8, except for aerosol profiles at 0.385 μm.

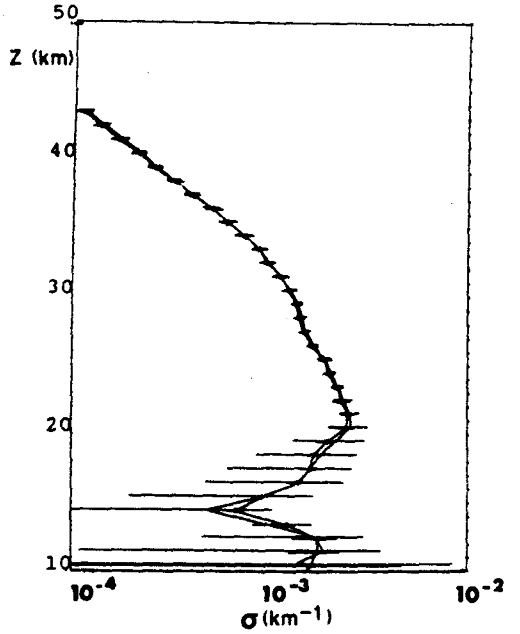

Fig. 12. Same as Figure 8, except for ozone extinction profile at 0.60 μm.

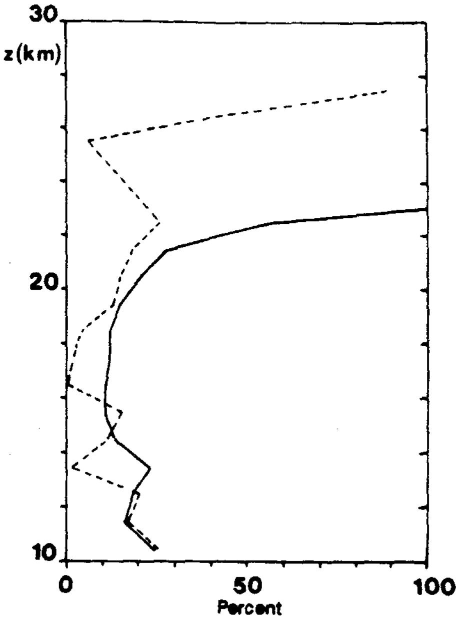

Fig. 14. Same as Figure 13, but applying to results from Figure 9.

nately, the O_3 and NO_2 corrections become large only at high altitudes, where their initial estimates are reasonably accurate.

5. The spectral variation of the aerosol extinction $\sigma^{aero}(\lambda)$ is smoothed and interpolated, using the best least squares fit

$$\ln \sigma^{aero}(\lambda) = \ln \sigma^{aero}(1.0) - a \ln \lambda - b(\ln \lambda)^2 \qquad (27)$$

to the three initial values $\sigma^{aero}(\lambda_4)$, $\sigma^{aero}(\lambda_5)$, and $\sigma^{aero}(\lambda_7)$. The value retrieval at 1.02 μm has been kept at a fixed point. It is expected to be most accurate because it is derived from direct retrieval, with small contribution from the Rayleigh scattering.

6. An iteration is then performed using $\sigma^{aero}(\lambda)$ from (27) to correct the 0.6-μm data and to retrieve the final value of the ozone extinction $\sigma^{O_3}(\lambda_3)$ and to correct the difference between the channels at 0.453 and 0.448 μm and to retrieve the final value of the NO_2 $\sigma^{NO_2}(\lambda_6)$.

7. Finally, the improved values $\sigma^{O_3}(\lambda_3)$ and $\sigma^{NO_2}(\lambda_6)$ are used in data from channels at 0.525, 0.453, and 0.385 μm to retrieve the improved values of the aerosol extinctions $\sigma^{aero}(\lambda_4)$, $\sigma^{aero}(\lambda_5)$, and $\sigma^{aero}(\lambda_7)$. In general, the changes introduced by this iteration are negligble.

The error in the extinction coefficients of each species at each wavelength is due to the error $\Delta\delta_\lambda$ for each channel and

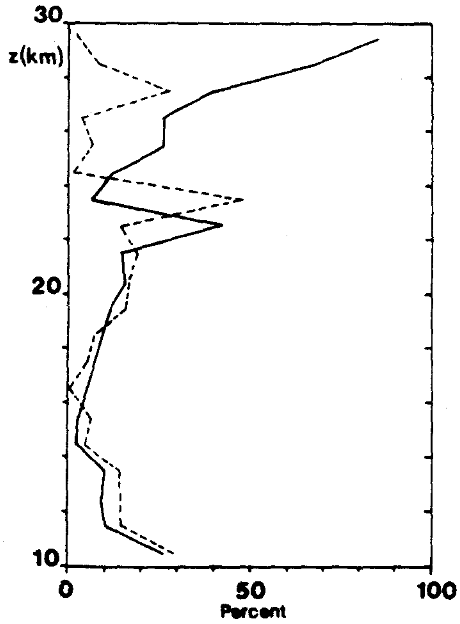

Fig. 13. Differences in percents for the results in Figure 8 (dotted line) compared to the estimated uncertainties from equation (22) (solid curve).

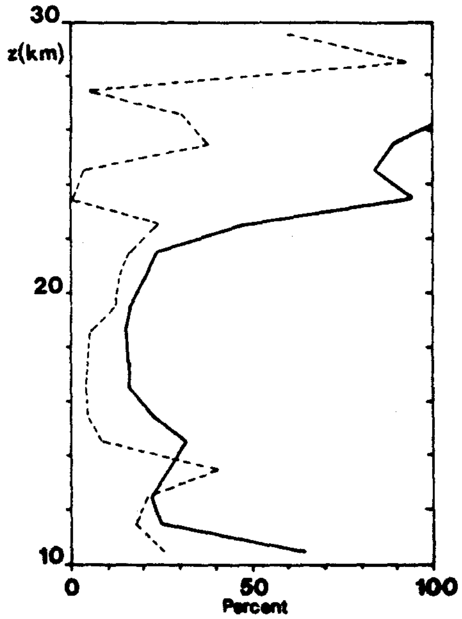

Fig. 15. Same as Figure 13, but applying to results from Figure 10.

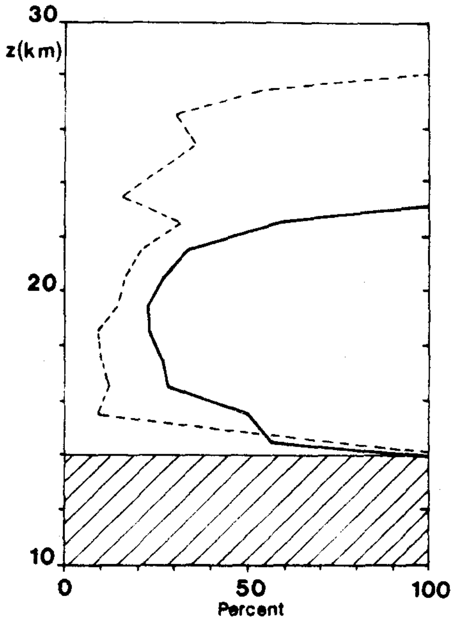

Fig. 16. Same as Figure 13, but applying to results from Figure 11.

to the error in the correction term due to the other species. These errors have been considered as independent.

COMPARISON OF LOA AND LARC INVERSION ALGORITHMS

The two inversion algorithms have been developed independently at LOA and at LaRC. They follow the same general scheme, which is naturally imposed by the mathematical formalism of the inverse problem. However, there are significant differences between the two algorithms:

1. The path length P_{ij} is computed at LOA by a geometrical method using discrete layers of 0.025 km. The results have been directly compared with those obtained at LaRC using the ray trace procedure [*Chu*, 1983]. The agreement is almost perfect, except in the first 2 or 3 km near the ground.
2. The inversion at LOA is done with the Chahine's method [*Chahine*, 1972], whereas the LaRC scheme uses Twomey's modification of Chahine's algorithm [*Twomey*, 1975]. The comparison of the results for the aerosol extinction at 1.02 μm, since it is equal to total extinction in the 1.02-μm channel data, is in fact a direct comparison of the two inversion algorithms.
3. A more fundamental difference is that the LOA algorithm first inverts the optical depths for each channel and then makes the species separation in the extinction coefficients, whereas the opposite is done by the LaRC algorithm, which starts with the separation of species in the optical depth and then inverts for each species.
4. The aerosol spectral extinction versus wavelength behavior is approximated by (27) in the LOA algorithm, instead of the Mie kernel interpolation scheme, illustrated by (19), used by the LaRC algorithm.
5. The spectroscopic values of O_3 and NO_2 over the wavelength range are slightly different in the two inversion algorithms. This is to reflect the uncertainties associated with these spectroscopic data and also provides a sensitivity check on the retrieval of O_3 and aerosol to these spectroscopic parameters.

The results of the two inversion procedures have been compared for several days, including sunset and sunrise measurements during the European comparison program. The conclusions are always qualitatively the same, and the results for April 21, 1985, (event at 1854 UT, latitude 50.18°N, longitude 1.27°E) will be presented here.

Figures 8–11 present the comparison of the aerosol extinction profiles at 1.02 0.525, 0.453, and 0.385 μm, respectively, retrieved by the LOA (solid curves) and LaRC (solid curves with circles) algorithms. The LOA inversion has been stopped at 30 km for 1.02 μm and between 25 and 30 km for the other channels, i.e., when the error estimates become exceedingly great. The results from the two inversion algorithms always agree within the error bars. For the 1.02-μm aerosol data the LOA profile above 25 km shows oscillations around the LaRC profile. These small oscillations disappear and the agreement with the LaRC profile is improved when a vertical smoothing over 3 km altitude (as has been done in the LaRC algorithm) is introduced here for extinction values smaller than 10^{-5} km^{-1}. Figure 12 compares the two retrieved O_3 extinction profiles at 0.6 μm. The agreement is almost perfect above 20 km, and it remains within the error bars down to 12 km.

Figures 13–17 present the percent differences between LOA- and LaRC-retrieved values (dotted curves) and the error in percent given on the LaRC values (solid curves). They present a better view of the comparison illustrated in Figures 8–12. The details of the curves are different for the different events, and the peaks which appear at some levels are due to random errors. But generally, the differences between the two retrievals are smaller than or of the same order as the expected uncertainties. Surprisingly, for the three aerosol short-wavelength channels the agreement be-

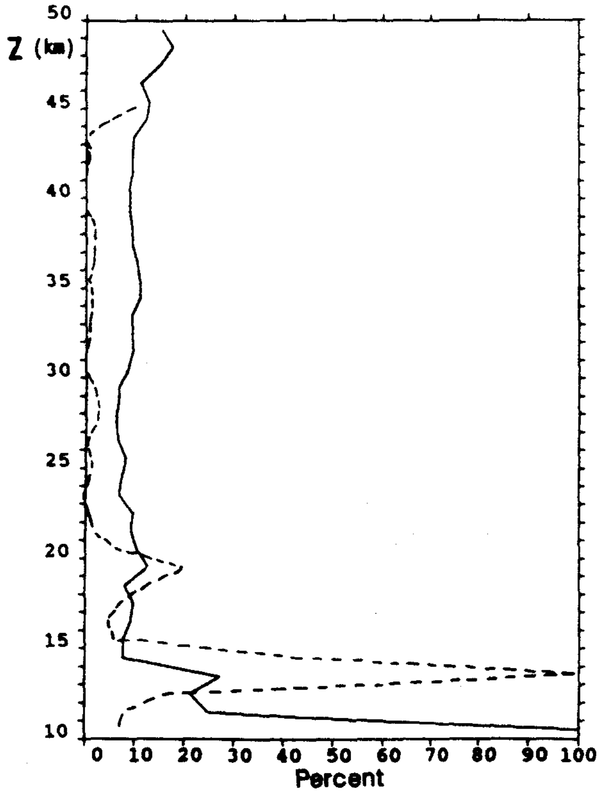

Fig. 17. Same as Figure 13, but applying to results from Figure 12.

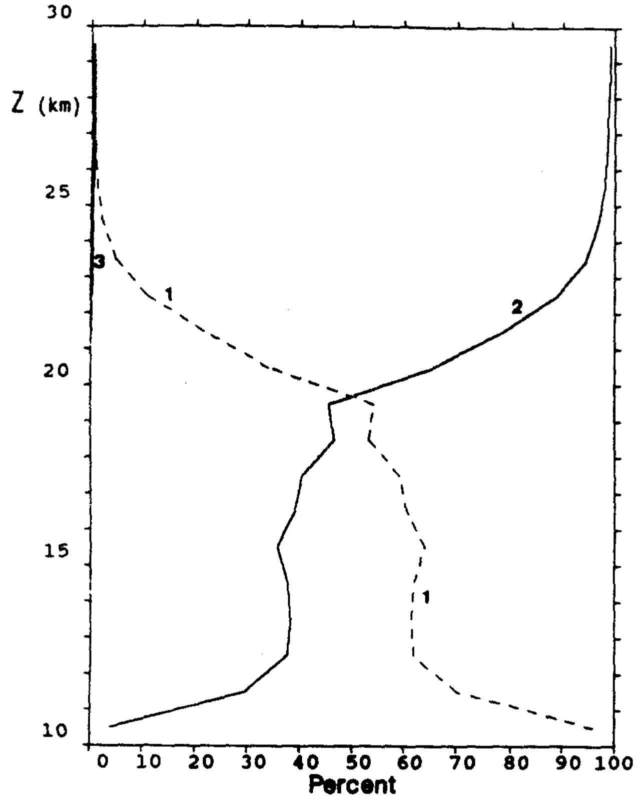

Fig. 18. Relative contributions in percent of aerosol (curve 1), ozone (curve 2), and nitrogen dioxide (curve 3) to the total extinction at 0.60 μm.

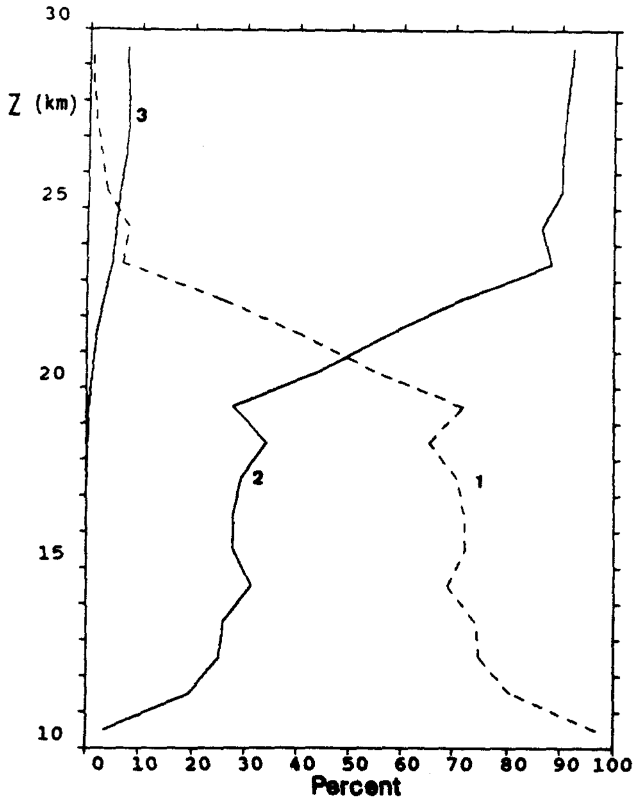

Fig. 19. Same as Figure 18, except at 0.525 μm.

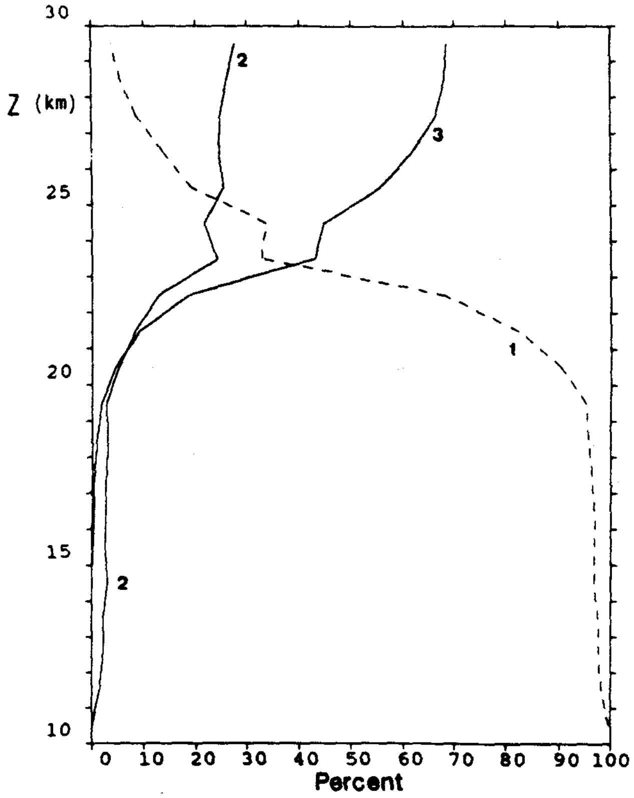

Fig. 20. Same as Figure 18, except at 0.453 μm.

tween the two retrievals remains good at levels where the errors are very large. However, this may be due to the similarities between the two inversion procedures and does not prove that the errors are overestimated.

DISCUSSION

Figures 18–21 show the percentage of relative contribution of the three species, aerosol, O_3, and NO_2, to the SAGE II channels at 0.6, 0.525, 0.453, and 0.385 μm for the same measurement event on April 21, 1985. The other two channels are not shown because the 1.02-μm channel contains only aerosol extinction, while the 0.448-μm channel is very similar to the 0.453-μm channel, with a little more NO_2 extinction contribution. Comparisons with Figures 13–17 confirm the expected results that a species is well retrieved as long as its contribution in a wavelength channel is not too small. The O_3 profile is easily retrieved above 20 km, as it is the major contributor to the 0.6-μm channel data. Below 20 km altitude the aerosol contribution introduces an increasing perturbation. At the 0.525-μm channel the O_3 contribution becomes equal to the aerosol contribution around 20 km. Since the O_3 is well retrieved from the 0.6-μm channel, the correction is rather accurate and the aerosol extinction can be retrieved higher. For altitudes above 25 km, the aerosol contribution becomes about 3%, while the O_3 contribution reaches 90% and the NO_2 contribution reaches 7%. Therefore the aerosol in this region can not be retrieved with confidence. In the 0.453- and 0.448-μm channels there are ozone contributions which reach 30% at high altitudes but could be accurately corrected. For both of these channels and the channel at 0.385 μm, the NO_2 and aerosol contributions become approximately equal between 22 and 24 km

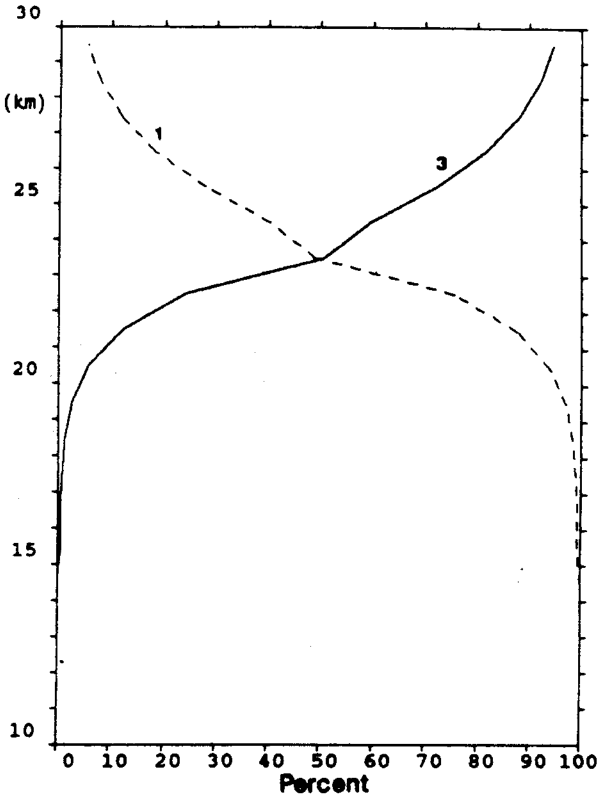

Fig. 21. Same as Figure 18, except at 0.385 μm.

altitudes. The aerosol contribution increases very rapidly at low altitudes, whereas the NO_2 contribution increases equally fast at the higher altitudes. This behavior is reflected clearly in the error bars, which are large for the three short-wavelength aerosol extinctions above 24 km.

These remarks generally can be applied to most of the SAGE II measurements. However, there are variations that are caused either by the temporal or spatial changes of the atmospheric state, or by some sudden perturbation. For example, the profiles presented here correspond to mid-latitudes with a tropopause at about 10 km. As the aerosol profiles are related to the tropopause height, their contribution will remain important higher at low latitudes. Similarly, after a strong volcanic eruption the aerosol contribution will increase in all channels, and the aerosol extinction will be retrieved more easily and at higher altitudes.

SUMMARY

Two inversion algorithms independently developed at LaRC and at LOA for the inversion of SAGE II data have been described and discussed. The LaRC algorithm is being used for the operational processing of the SAGE II data, while the LOA algorithm is being used for validating the operational algorithm. Both algorithms have demonstrated that SAGE II data can provide O_3 profiles with an uncertainties of about 10% from cloud top height to about 60 km altitude and aerosol extinction profiles with an uncertainties of about 10% at the longest wavelength channel to an uncertainties of about 30% at the shortest wavelength channel over the Junge layer region.

Inverted aerosol extinction profiles at 1.02, 0.525, 0.453, and 0.385 μm and the O_3 profiles have been compared using these two inversion algorithms. The agreement is always within the error estimates. Very often the differences between the two retrievals are much smaller than the estimated uncertainties, i.e., for the short-wavelength aerosol extinction the agreement between the two retrieval values is around 10–20% up to 26 km, whereas the relative error reaches 100% around 23 km. Although there are both significant similarities and significant differences in these two algorithms, a major disagreement between the two retrievals would have been disturbing. However, their agreement does not necessarily prove that the retrieved values are absolutely accurate. For example, both algorithms could be susceptible to certain systematic errors and could produce identical retrievals which are biased identically from the true value.

Considering both the estimated retrieval uncertainties and the differences between the two retrieved values against the relative contribution of each species in each channel leads us to the conclusion that the retrieval of the extinction profiles of a species in a given wavelength channel is reasonably good only when its contribution to the total extinction becomes larger than a few percent. This condition would restrict the lower altitude limits at about 10 km for the ozone retrieval and an upper altitude limit of about 25–27 km for the aerosol extinction profiles at 0.525, 0.453, and 0.385 μm at the European latitudes during the time period in 1984–1985. The upper altitude limit for the aerosol extinction profile at 1.02 μm is due to the rapid decrease of extinction level leading to transmission values close to unity, which typically occurs at about 30 km height at mid-latitude. The range of good quality of the retrieved values will be slightly different for different latitudes, seasons, and atmospheric states.

REFERENCES

Ackerman, M., et al., European validation of SAGE II aerosol profiles, *J. Geophys. Res.*, this issue.

Buglia, J. J., Compilation of methods in orbital mechanics and solar geometry, *NASA Ref. Publ., NASA RP 1204*, 1988.

Chahine, M. T., A general relaxation method for inverse solution of the full radiative transfer equation, *J. Atmos. Sci.*, *29*, 741—747, 1972.

Chu, W., Calculation of atmospheric refraction for space craft remote sensing applications, *Appl. Opt.*, *22*, 721—726, 1983.

Chu, W. P., Convergence of Chahine's nonlinear relaxation inversion method used for limb viewing remote sensing, *Appl. Opt.*, *24*, 445–447, 1985.

Chu, W., and M. P. McCormick, Inversion of stratospheric aerosol and gaseous constituents from spacecraft solar extinction data in the 0.38–1.0 μm wavelength region, *Appl. Opt.*, *18*, 1404–1414, 1979.

Cunnold, D., W. P. Chu, R. A. Barnes, M. P. McCormick, and R. E. Veiga, Validation of SAGE II ozone measurements, *J. Geophys. Res.*, this issue.

Edlen, B., The dispersion of standard air, *J. Opt. Soc. Am.*, *43*, 339–345, 1953.

Gelman, M. E., A. J. Miller, K. W. Johnson, and R. M. Nagatani, Detection of long term trends in global stratospheric temperature from NMC analyses derived from NOAA satellite data, *Adv. Space Res.*, *6*, 17–26, 1986.

Goldman, A., F. G. Fernald, W. J. Williams, and D. G. Murcray, Vertical distribution of NO_2 in the stratosphere as determined from balloon measurements of solar spectra in the 4500 A region, *Geophys. Res. Lett.*, *5*, 257–260, 1978.

Lenoble, J., Presentation of the European correlative experiment program for SAGE II, *J. Geophys. Res.*, this issue.

Lenoble, J., and P. Pruvost, Inference of the aerosol angstrom coefficient from SAGE short-wavelength data, *J. Clim. Appl. Meteorol.*, *22*, 1717–1725, 1983.

Mauldin, L. E., III, N. H. Zaun, M. P. McCormick, J. H. Guy, and W. R. Vaughn, Stratospheric Aerosol and Gas Experiment II instrument: A functional description, *Opt. Eng.*, *24*, 307–312, 1985.

McCormick, M. P., P. Hamill, T. J. Pepin, W. P. Chu, T. J. Swissler, and L. R. McMaster, Satellite studies of the stratospheric aerosol, *Bull. Am. Meteorol. Soc.*, *60*, 1038–1046, 1979.

Osborn, M. T., J. M. Rosen, M. P. McCormick, P. H. Wang, J. M. Livingston, and T. J. Swissler, SAGE II aerosol validation: Profile measurements, *J. Geophys. Res.*, this issue.

Penney, C. M., Study of temperature dependence of the Chappuis band absorption of ozone, *NASA Contract. Rep., NASA CR 158977*, 1979. (Available as *NTIS X79-10050* from Natl. Tech. Inf. Serv., Springfield, Va.)

Pinnick, R. G., J. M. Rosen, and D. J. Hofmann, Stratospheric aerosol measurements, III, Optical model calculations, *J. Atmos. Sci.*, *33*, 304–314, 1976.

Russell, P. B., et al., Satellite and correlative measurements of the stratospheric aerosol, II, Comparison of measurements made by SAM II, dustsondes, and an airborne Lidar, *J. Atmos. Sci.*, *38*, 1295–1312, 1981.

Twomey, S., On the numerical solution of Fredholm integral equation of the first kind by the inversion of the linear system produced by quadrature, *J. Assoc. Comput. Mach.*, *10*, 97–101, 1963.

Twomey, S., Comparison of constrained linear inversion and an iterative nonlinear algorithm applied to the indirect estimation of particle size distributions, *J. Comput. Phys.*, *18*, 188–198, 1975.

Young, A. T., Revised depolarization corrections for atmospheric extinction, *Appl. Opt.*, *19*, 3427–3430, 1980.

C. Brogniez, J. Lenoble, and P. Pruvost, Laboratoire d'Optique Atmospherique, Universite des Sciences et Techniques de Lille, 59655 Villeneuve d'Ascq Cedex, France.

W. P. Chu and M. P. McCormick, Atmospheric Sciences Division, NASA Langley Research Center, Hampton, VA 23665.

(Received April 4, 1988;
revised November 29, 1988;
accepted November 29, 1988.)

2 Intervalidation des expériences SAGE II et RADIBAL

Des validations de l'expérience SAGE II ont été entreprises :

-aux USA au moyen d'expériences utilisant des compteurs de particules ainsi que l'enregistrement des profils de rapport de rétrodiffusion obtenus avec un lidar.

-en Europe avec également des mesures lidar (P. Gobbi, H. Jäger et G. Mégie), et une methode originale d'étude des aérosols stratosphériques. Cette méthode consiste en la mesure de l'intensité et de la polarisation du rayonnement solaire diffusé par les particules à l'aide d'un instrument embarqué à bord d'un ballon stratosphérique (expérience RADIBAL, dirigée par M. Herman et R. Santer). Cette expérience a été validée parallèlement par comparaison à des mesures sol effectuées par C. Devaux, à des mesures au limbe de M. Ackerman et à des mesures d'occultation de l'expérience SAM II (9).

En ce qui concerne les profils d'extinction dans un intervalle d'altitudes d'environ 16 à 25 km, les comparaisons effectuées lors des coïncidences de 1984 et 1985 se sont révélées encourageantes compte tenu des incertitudes affectant les trois méthodes. Néanmoins ces comparaisons ont montré certains désaccords concernant notamment les variations du rayon effectif avec l'altitude. J'ai poursuivi ce travail pour des coïncidences ayant eu lieu fin 1985 et 1986 en collaboration avec S. Diallo dans le cadre de sa thèse. La dernière comparaison pour laquelle nous avons également disposé de mesures lidar (procurées par H. Jäger de Garmisch-Partenkirchen, RFA) s'est montrée encore une fois particulièrement satisfaisante pour ce qui est des profils d'extinction. En ce qui concerne le rayon des particules l'accord entre les résultats RADIBAL et SAGE II est tout à fait correct dans la couche principale, c'est à dire de 15 km à environ 21 km. Aux niveaux plus élevés les dimensions des aérosols déduites des mesures SAGE II décroissent tandis que celles dérivées de l'expérience RADIBAL demeurent sensiblement constantes (7)(8).

L'exploitation des vols ballon a été suspendue à la suite du départ de S. Diallo et j'ai entrepris en 1990 l'analyse de nouvelles mesures de polarisation effectuées en 1987 et 1989. Pour ces deux vols je disposais de mesures SAGE II avec en complément pour 1987 des tirs lidar réalisés par H. Jäger à Garmisch-Partenkirchen. J'ai fait cette fois une étude très précise du bilan d'erreur sur toutes les expériences. Comme précédemment les résultats sont concordants en ce qui concerne les coefficient d'extinction. Les dimensions des aérosols obtenues par les deux expériences sont aussi très voisines dans la couche principale; au dessus de cette couche des différences notables apparaîssent. Ce travail est actuellement soumis pour publication à J. Geophys. Res. (10).

CHARACTERIZATION OF THE STRATOSPHERIC AEROSOLS FROM POLARIZATION MEASUREMENTS COMPARISON WITH SAGE II OBSERVATIONS

Boubacar S. Diallo, Colette Brogniez, Maurice Herman,
Richard Santer, and Jacqueline Lenoble
Laboratoire d'Optique Atmosphérique
Université des Sciences et Techniques de Lille
59655 Villeneuve d'Ascq Cedex, France

ABSTRACT

A balloon-borne polarimetric experiment (RADIBAL) was developed in 1983 for the purpose of monitoring the stratospheric aerosols from limb scannings of the radiance and polarization of the scattered sunlight. From December 1983, the experiment was launched ten times. Three flights were conducted, within a European correlative experiment program, in conjunction with passages of SAGE II. The aerosol characteristics, as derived from the SAGE II and RADIBAL experiments, are compared.

1. DESCRIPTION OF THE EXPERIMENTS

The RADIBAL experiment is designed to retrieve the aerosol scattering properties-phase function $p(\theta)$ and polarization ratio for single scattering $P(\theta)$- at near infrared wavelengths: 850 and 1650 nm (Herman et al. (1987)). For this purpose, a narrow field of view polarimeter is fixed on a stratospheric platform, and by rotating the platform, the radiance and polarization of the scattered sunlight are measured in an horizontal plane in different directions. The balloon sounding allows observation of the aerosol scattering features for altitudes ranging from about 15 to 30 km. Flights are conducted near sunrise or sunset, with solar elevations ranging from 0° to about 30° to 35° during the sounding.

In order to retrieve the aerosol characteristics, the signals have to be corrected from (*i*) the known molecular contribution, (*ii*) some amount of multiply scattered light and (*iii*) scattering from the diffuse upward tropospheric radiation field. Molecular and multiple scattering contributions are small terms. Multiple scattering is estimated from Monte Carlo calculations for standard stratospheric models. The correction of the tropospheric contribution is based also on signal modeling, as a function of the troposphere reflectance. It is important only for large solar elevations; say $h_s > 10°$.

From the corrected signals, the aerosol slant optical thickness τ_a, and the single scattering functions, $p(\theta)$ and $P(\theta)$ are derived for the two observation wavelengths. As a final step, inversion of $p(\theta)$ and $P(\theta)$ allows estimation of the aerosol size distribution function, $n(r)$ (Santer et al. (1988)). By assuming a log-normal distribution:

$$n(r) = \frac{N_0}{\sqrt{2\pi}\sigma r} \exp - \left(\frac{Log \frac{r}{\bar{r}}}{\sqrt{2}\sigma} \right)^2 \tag{1}$$

the inversion provides vertical profiles of the distribution parameters, $\bar{r}(z)$ and $\sigma(z)$.

The SAGE II experiment is designed for the monitoring of NO_2, O_3 and stratospheric aerosols, from transmission measurements of the solar beam through the stratosphere at six wavelengths: 385, 448, 453, 525, 600 and 1020 nm (Mauldin et al. (1985)). The measurements are first corrected from the known molecular contribution. At 1020 nm the resulting total slant optical thickness is just the aerosol slant optical thickness, since this channel is free from gaseous absorption (Brogniez and Lenoble (1987)). By using the Chahine scheme, the transmission profiles are inverted to yield vertical profiles of the total extinction coefficients. These profiles in turn, are processed to derive the NO_2 and O_3 concentration profiles and the aerosol extinction coefficients profiles, $\sigma^a_\lambda(z)$ at four wavelengths (1020, 525, 453, 385 nm). The quality of the aerosol data is lesser at the short wavelengths than at 1020 nm, because of the influence of NO_2, O_3 and of a larger molecular correction. Finally, the information about the aerosol size distribution may be obtained from the spectral behaviour of $\sigma^a_\lambda(z)$ (Lenoble and Brogniez (1985)), in the form of the vertical profiles of the parameters, $\bar{r}(z)$ and $\sigma(z)$, of the assumed log-normal size distribution.

Copyright © 1989 A. DEEPAK Publishing
All rights reserved

2. RESULTS

Three comparison flights were launched from the CNES balloon Center of Aire sur l'Adour, South-West of France (43.4° N; 0.15° W). Table 1 gives the dates of the flights and the mean distances between the vertical stratospheric columns sounded by SAGE II and RADIBAL.

TABLE 1: LOCALISATION OF SAGE II AND RADIBAL

Dates	RADIBAL	SAGE	Distance
11 – 28 – 84	0.15°W 43.4° N	16.76°E 45.18° N	1357 km
10 – 12 – 85	0.15°W 43.4° N	7.10°W 41.25°N	619 km
04 – 21 – 86	0.15°W 43.4° N	2.90°W 48.34°N	589 km

We first compare in Figure 1 the aerosol slant optical thickness $\tau_a(z)$ at 1020 nm. From SAGE II, except for molecular correction, $\tau_a(z)$ is directly derived from the data and the resulting profile is quite accurate. For RADIBAL, interpolation at 1020 nm from measurements at 850 nm and 1650 nm is based on the retrieved model, with a negligible error; the error bars onballoon data in figures correspond to the errors in the absolute calibration. Systematic discrepancies larger than the calibration error are observed in some occasions but, on account of the distances between the two soundings, such differences are not surprising. In the same conditions, similar departures are observed between results derived from SAGE II, lidar soundings and limb photometry experiments. There is a general good consistency between the profiles retrieved from SAGE II and the balloon data, and a very good agreement was achieved on April 21 1986.

The comparison between the aerosol size characteristics is more delicate. In order to validate the SAGE II aerosol data at the shorter wavelength channels, we first compare on Figures(2) the ratios

$$R_\lambda(z) = \frac{\sigma^a_\lambda(z)}{\sigma^a_{1020nm}(z)} \tag{2}$$

for λ =385, 453 and 525 nm respectively. $R_\lambda(z)$ is derived from the SAGE II data as explained previously. For RADIBAL, $R_\lambda(z)$ is calculated according to the scattering properties of the retrieved aerosol model. The general trends in $R_\lambda(z)$ are in agreement. The error bars on the RADIBAL data correspond to the uncertainty in the aerosol model resulting from errors in calibration and in estimates for multiple scattering, molecular contribution and tropospheric light contamination. Theuncertainty ΔR on SAGE II data is shown on the curves for the third flight, where the two extreme curves present respectively $R + \Delta R$ and $R - \Delta R$. It is quite large, especially at higher altitudes, so that, within this error, the two experiments are certainly consistent.

We compare finally estimates of the aerosol size distribution parameters. Rather than $\bar{r}(z)$ and $\sigma(z)$, we compare the resulting effective parameters $r_{eff}(z)$ and $v_{eff}(z)$ of the distributions i.e:

$$r_{eff} = \bar{r}e^{2.5\sigma^2} \tag{3}$$

and

$$v_{eff} = e^{\sigma^2} - 1 \tag{4}$$

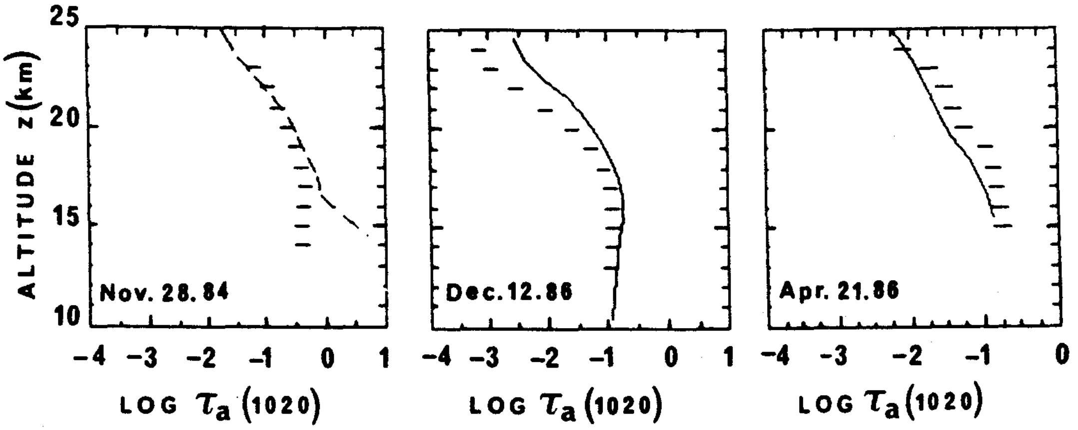

Fig. 1: aerosol slant optical thickness $\tau_a(z)$ at 1020 nm. Full lines: SAGE II results. Dots with error bars: RADIBAL results.

which are known to be more representative of the aerosol scattering properties. Comparisons are shown on Figure 3. At least for lower altitudes where the estimates of SAGE II are reasonably accurate, the derived effective radius are in a good agreement. The decrease with altitude of the particle mean dimension is a general feature which is retrieved by the two experiments. Consistency between the retrieved effective variances is no more than qualitative; this is not too important, however, since the aerosol radiative properties depend mainly on r_{eff} and to a lesser extent only on v_{eff}.

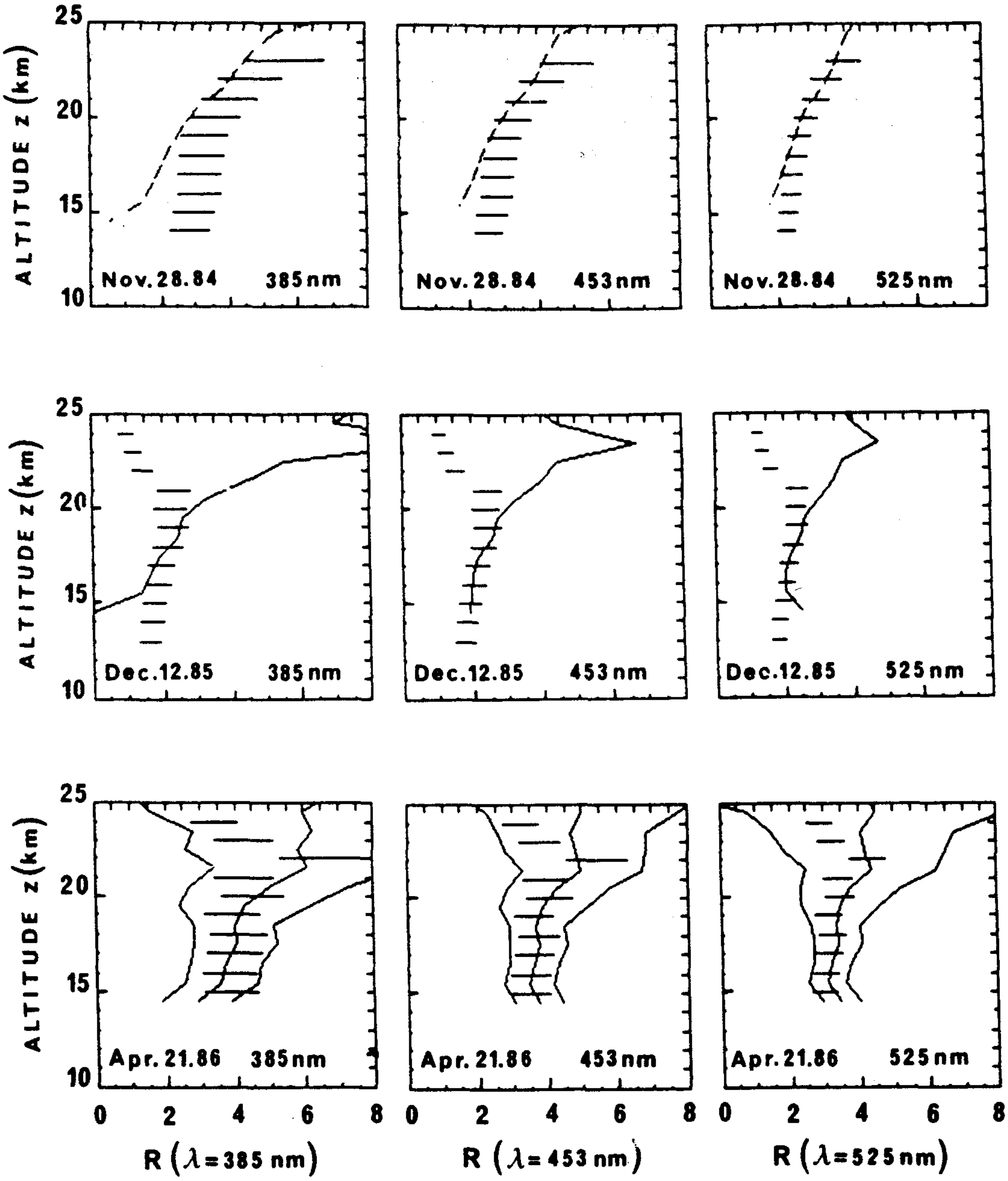

Fig. 2: $R_\lambda(z)$ profiles at 385, 453 and 525 nm. Full lines: SAGE II results. Dots with error bars: RADIBAL results. For the third flight, the SAGE II estimated accuracy is indicated by the extreme profiles.

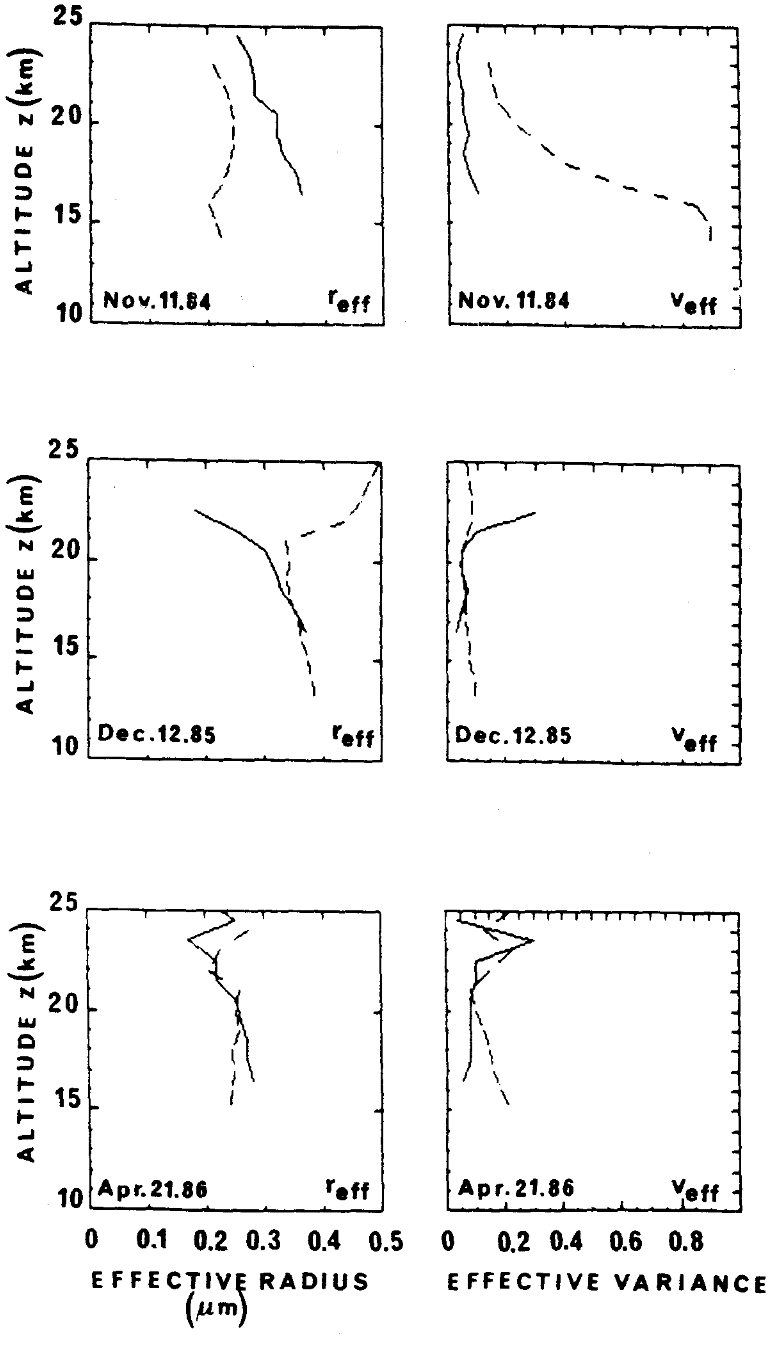

Fig. 3: Effective values profiles $r_{eff}(z)$ and $v_{eff}(z)$. Full lines :SAGE II results. Dashed lines: RADIBAL results.

3. CONCLUSION

Because of the high sensitivity of polarization to the aerosol properties especially at near infrared wavelengths, RADIBAL observations are clearly more efficient than the SAGE II data for aerosol characteristics retrieval. The fits in Figures therefore provide a correct validation of the SAGE II aerosol data. According to the observed fits, the errors in $R_\lambda(z)$ as estimated from the SAGE II measurements should be somewhat overestimated and the aerosol data quality of SAGE II are probably better than indicated.

ACKNOWLEDGMENTS

We acknowledge J. Y. Balois, L. Gonzalez, P. Lecomte and C.Verwaerde for technical assistance. This work was supported by the Centre National d'Etudes Spatiales and by the Centre National de la Recherche Scientifique, ATP Atmosphère Moyenne.

REFERENCES

Brogniez C. and J. Lenoble, 1987: Modeling of the stratospheric background aerosols from SAGE zonally averaged profiles. J. Geophys. Res., 92, 3051-3060.

Herman M., J.Y.Balois, L. Gonzalez, P .Lecomte, J.Lenoble, R. Santer and C. Verwaerde, 1986: Stratospheric aerosol observations from a balloon-borne polarimetric experiment. Appl. Optics, 25, 3573-3584.

Lenoble J., and C. Brogniez, 1985: Information on stratospheric aerosol characteristics contained in SAGE multi-wavelength extinction measurements. Appl. Optics, 24, 1054-1063.

Mauldin L.E., N.H. Zaun, M.P. Mc Cormick, J.H. Guy and W.R. Waughn, 1985. Stratospheric Aerosol and Gas Experiment II instrument: a functional description. Optical Engineering, 24, 307-312.

Santer R., M. Herman, D. Tanre and J. Lenoble, 1988: Characterization of the stratospheric aerosol from polarization measurements. To appear in J. Geophys. Res.

JOURNAL OF GEOPHYSICAL RESEARCH, VOL. 94, NO. D6, PAGES 8399–8411, JUNE 20, 1989

European Validation of SAGE II Aerosol Profiles

M. Ackerman,[1,2] C. Brogniez,[3] B. S. Diallo,[3] G. Fiocco,[4] P. Gobbi,[5]
M. Herman,[3] M. Jäger,[6] J. Lenoble,[3] C. Lippens,[2] G. Mégie,[7]
J. Pelon,[7] R. Reiter,[6,8] and R. Santer[3]

A SAGE II validation program has been performed in Europe using ground-based lidars and balloon-borne polarimetric and photographic experiments. Between the tropopause height and about 23 km, good agreement is found between the SAGE II 1.02-μm extinction profiles and the lidar profiles, using for the conversion of backscattering into extinction an aerosol model consistent with the SAGE II spectral extinction. The extinction profiles deduced from the limb photographs at 0.44 and 0.375 μm present a good agreement with the SAGE II profiles at 0.453 and 0.385 μm, respectively. The size distribution retrieved from the near-infrared polarimetric observations leads to a spectral variation of the extinction in good agreement with SAGE II data in the same altitude range. Above 23–25 km the observations are scarce and the data of poorer quality because of the low aerosol content. The 1.02-μm extinction profiles seem to agree with the ruby lidar and the limb photograph profiles. But any conclusion concerning the short-wavelength profiles and the size distribution at these high altitudes would be risky.

1. Introduction

SAGE II provides aerosol extinction profiles at 1.02, 0.525, 0.453, and 0.385 μm. The 1.02-μm channel is free from any other contribution except the Rayleigh correction, which is not too large for most of the altitude range. The results are retrieved without difficulties almost down to the ground level in cloud-free cases. The upper limit of retrieval is due to the low aerosol concentration, which leads to transmissions very close to 1 above some altitudes (around 30 km at middle latitudes), for the present state of the atmosphere; smoothing procedures allow retrieval at higher altitudes, but with increasing error bars. The three short-wavelength channels are contaminated by ozone and nitrogen dioxide absorption; the separation of these contributions has been discussed by *Chu et al.* [this issue]. The upper limit of a reasonable quality retrieved profile is probably a little below 30 km for the three channels, because of the increasing contribution of O_3 and NO_2 with altitude. Moreover, the Rayleigh correction increases toward the short wavelengths, leading to an increasing error in the retrieved extinctions and limiting the retrieval to altitudes above 8, 10, and 14 km for the 0.525-, 0.453-, and 0.385-μm aerosol extinction profiles, respectively.

The aerosol extinction depends on their total number density and on their size distribution, as well as on their shape and refractive index; they are generally assumed to be spherical droplets of an aqueous sulfuric acid solution. This means that there is no direct, simple validation experiment for the aerosol data as there is for the gas data, where only one parameter (the gas concentration) has to be measured. The most direct approach is to measure in situ the absolute size distribution $n(r)$ of the particles (including the total number $N = \int_0^\infty n(r)\,dr$ per unit volume) and to compute by Mie theory the extinction profiles to be compared to the SAGE II extinction profiles. This can be achieved by various instruments, such as wire impactors, quartz crystal microbalance (QCM) multifilters, and optical counters [*Russell et al.*, 1981, 1984; *Oberbeck et al.*, 1986; *Osborn et al.*, this issue]; however, all instruments have limitations in the range of sizes detected. Another approach consists of using other scattering measurements that should be consistent with the SAGE II extinction profiles. The best known example of this procedure is the lidar backscattering profile. The backscattering data have to be converted into extinction profiles, using a model of the aerosol size distribution and the Mie theory; for consistency, the same model must reproduce the spectral variation of the extinction deduced from the four SAGE II aerosol channels.

During the correlative experiments made in Europe [*Lenoble*, this issue], ground-based lidars were used at four different stations; the results are presented in section 2. Two other scattering techniques have been simultaneously used from balloon platforms: photographs of the Earth's limb and infrared polarimetric measurements. These are presented with some details in sections 3 and 4, respectively. Analysis and comparisons of the results are discussed in section 5.

2. Lidar

Nd: Yag lasers operating at 0.532 μm have been used at the Observatoire de Haute Provence (OHP), Frascatti, and Florence, and a ruby laser operating at 0.694 μm has been used at Garmisch-Partenkirchen. All of the lidar profiles are corrected for extinction; the three lidars are calibrated assuming $R_{\min} = 1$ in the altitude range 30–40 km. The ruby laser allows retrieval of the profiles up to altitudes higher than the Nd: Yag laser, because of the smaller contribution of Rayleigh scattering at the larger wavelength. The data provided by the experimenters are the backscattering ratio

---

[1] Authors are listed in alphabetical order.

[2] Institut d'Aéronomie Spatiale de Belgique, Brussels, Belgium.

[3] Laboratoire d'Optique Atmosphérique, Université des Sciences et Techniques de Lille, Villeneuve d'Ascq, France.

[4] Instituto di Fisica "Guglielmo Marconi", Universita Degli Studi Roma, Rome, Italy.

[5] Instituto di Fisica dell'Atmosphere, Consiglio Nazionale della Ricerche, Frascati, Italy.

[6] Institut für Atmosphärische Umweltforschung, Garmisch-Partenkirchen, Federal Republic of Germany.

[7] Service d'Aéronomie du Centre National de la Recherche Scientifique, Verrières-le-Buisson, France.

[8] Now at Consulting Bureau, Garmisch-Partenkirchen, Federal Republic Germany.

Copyright 1989 by the American Geophysical Union.

Paper number 89JD00242.
0148-0227/89/89JD-00242$05.00

$R = (b^{aer} + b^{mol})/b^{mol}$, versus the altitude; b^{aer} is the aerosol and b^{mol} the molecule backscattering coefficient.

The aerosol backscattering is deduced from R and b^{mol} (computed for a standard atmosphere). The aerosol extinction coefficient is related to the backscattering coefficient by

$$\sigma^{aer}(\lambda) = 4\pi b^{aer}(\lambda)/p^{aer}(\lambda, 180°) \tag{1}$$

where $p^{aer}(\lambda, 180°)$ is the aerosol phase function (normalized at 4π). The exact phase function, which depends on the characteristics and size distribution of the aerosols, is unknown. Therefore it is replaced by the phase function computed for an "aerosol model." The same model is used to transform $\sigma^{aer}(\lambda)$ into $\sigma^{aer}(1.02)$ for comparison with the SAGE II profiles at 1.02 μm. The following transformation equations are used:

$$b^{aer}(\lambda) = (R - 1)b^{mol}(\lambda) \tag{2}$$

$$\sigma^{aer}(\lambda) = 4\pi b^{aer}(\lambda)/[p^{aer}(\lambda, 180°)]^{model} \tag{3}$$

$$\sigma^{aer}(1.02) = \sigma^{aer}(\lambda)[\sigma^{aer}(1.02)/\sigma^{aer}(\lambda)]^{model} \tag{4}$$

or combining (2), (3), and (4),

$$\sigma^{aer}(1.02) = 4\pi(R - 1)b^{mol}(\lambda)/K(\lambda) \tag{5}$$

where

$$K(\lambda) = [\sigma^{aer}(\lambda)p^{aer}(\lambda, 180°)/\sigma^{aer}(1.02)]^{model} \tag{6}$$

We have chosen to compare the lidar data with the SAGE II profiles at 1.02 μm, because they are of better quality and are retrieved at higher altitudes than the SAGE II profiles at 0.525 μm, which are closer to the lidar wavelengths. Similarly, the statistical error ΔR due to signal fluctuations is transformed into an error $\Delta\sigma^{aer}(1.02)$. The conversion of backscattering at λ into extinction at 1.02 μm has been made with various models, and it has proved insensitive to the detailed shape of the size distribution, the main parameter being the effective radius r_{eff} and the effective variance v_{eff}, defined by

$$r_{eff} = \int_0^\infty r^3 n(r)\, dr \Big/ \int_0^\infty r^2 n(r)\, dr \tag{7}$$

$$v_{eff} = \int_0^\infty (r - r_{eff})^2 r^2 n(r)\, dr / r_{eff}^2 \int_0^\infty r^2 n(r)\, dr \tag{8}$$

The simplest choice for modeling is a lognormal size distribution (LND):

$$n(r) = (N/\sqrt{2\pi} \ln s) \exp\left[-\frac{\ln^2 r/r_m}{2 \ln^2 s}\right] \tag{9}$$

The r_{eff} and v_{eff} are related to the mean radius r_m and the variance s by [*Lenoble and Brogniez*, 1984]

$$r_{eff} = r_m \exp(2.5 \ln^2 s) \tag{10}$$

$$v_{eff} = \exp(\ln^2 s) - 1 \tag{11}$$

Figure 1 presents the conversion factor ($K(\lambda) = \sigma^{aer}(\lambda)$ $p^{aer}(\lambda, 180°)/\sigma^{aer}(1.02)$ versus r_{eff} for LND models (75% H_2SO_4 droplets at 220 K), with $v_{eff} = 0.25$ ($s = 1.60$), for the two lidars. It varies slowly for r_{eff} larger than 0.20 μm and is almost constant for r_{eff} larger than 0.30 μm; but it increases very rapidly for smaller particles. Similar curves can be drawn for other values of v_{eff}. However, the influence of v_{eff} becomes large only for particles smaller than 0.20 μm; it is almost negligible for $r_{eff} \approx 0.30$ μm, as K increases with v_{eff} for $r_{eff} > 0.30$ μm and decreases for $r_{eff} < 0.30$ μm. For example, the curves corresponding to $v_{eff} = 0.1$ and $v_{eff} = 0.58$ at $\lambda = 0.532$ μm are shown in Figure 1.

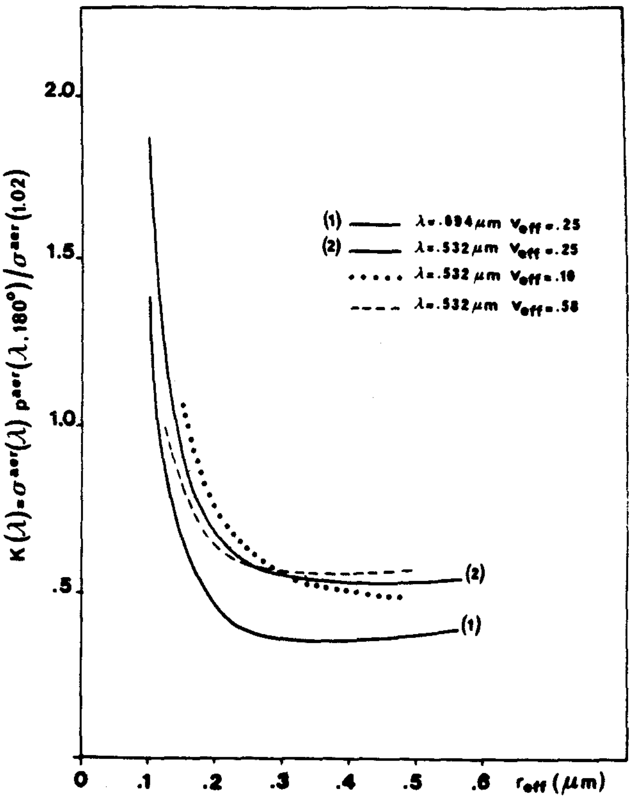

Fig. 1. Lidar conversion factor $K(\lambda)$ versus the effective radius r_{eff} for aerosol LND models; particles are 75% H_2SO_4 at 220 K.

The results of the lidar/SAGE II profile comparisons will be presented, using for the conversion of backscattering into extinction the model (or models) with $v_{eff} = 0.25$, which gives the best agreement between the two profiles. The choice will be checked for consistency with the SAGE II spectral extinction and/or with the in situ observations in section 5.

The four periods of observations were November 10–13, 1984, November 27–30, 1984, April 21–23, 1985, and October 12–14, 1985; the locations of the SAGE II events and of the ground stations are presented by *Lenoble* [this issue].

2.1. *November 10–13, 1984*

During the period from November 10 through 13, 1984, the aerosol layer was very unstable on the local scale, as shown by the in situ balloon observations, and on the scale of the observation zone, as proved by the important differences between the six SAGE II profiles. The lidar profiles obtained at OHP and at Garmisch-Partenkirchen on November 11 are also quite different, as are the profiles obtained at OHP on November 11 and November 13. However, on November 13 the situation seems to stabilize and the two SAGE II profiles at 8.49°W (1703 UT) and 15.8°E (1527 UT) are very similar; this allows a comparison with the OHP lidar profile obtained at the same latitude and 6°E, from 1705 to 1817 UT (Figure

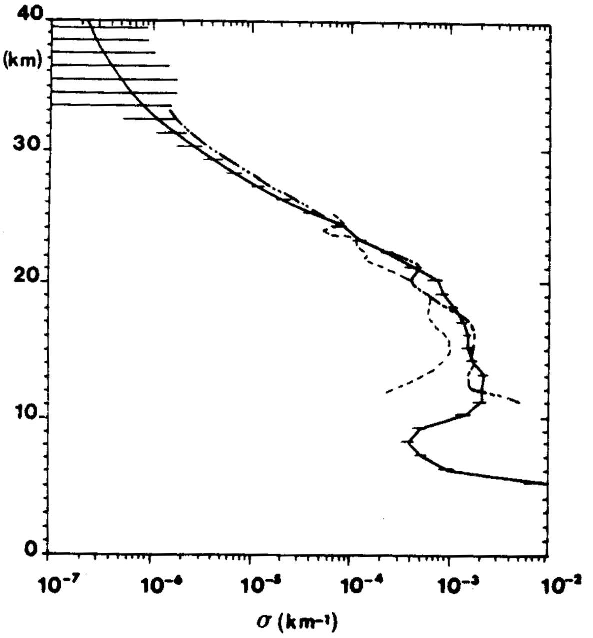

Fig. 2. Comparison of aerosol extinction profiles at 1.02 μm from SAGE II and retrieved from lidar backscattering with a LND model v_{eff} = 0.25 (see text) on November 13, 1984: solid curve, SAGE II, 1703 UT, 44.62°N, 8.49°W; dash-double-dotted curve; SAGE II, 1527 UT, 44.50°N, 15.81°E (error bars omitted); dashed curve, OHP lidar, 1705–1817 UT, 44°N, 6°E (aerosol model: r_{eff} = 0.35 μm).

2). The agreement is very good above 18 km and certainly within the error limits of the lidar profile; below 18 km the differences are probably due to the variability of the aerosol layer. The conversion from backscattering into extinction has been made with a LND model, r_{eff} = 0.35 μm, for all altitudes. But as mentioned earlier, the conversion is not very sensitive to the effective radius in this size range and any model with r_{eff} between 0.20 and 0.50 μm would lead to a similar agreement.

2.2. *November 26–30, 1984*

For the period November 26–30, 1984, the situation was more stable. From the eight SAGE II profiles, only the western profiles of November 28 and 29 seem to correspond to a different air mass with more aerosols above 25 km; the other six profiles (eastern profiles for the whole period and western profiles for November 26 and 27) are very similar. The several lidar profiles obtained during this period (OHP, November 27–29; Frascatti, November 28–30; Garmisch-Partenkirchen, November 27) confirm a good stability for the aerosol layer over the zone and the period. This provides conditions much better than during the middle of November for a comparison program. Figures 3, 4, and 5 present the results of these comparisons. For November 27 (Figure 3), two lidar profiles are available: one from OHP up to 25 km and one from Garmisch-Partenkirchen up to 30 km. To obtain agreement with SAGE II, the conversion from backscattering into extinction has to be made using models with a particle size decreasing with altitude z; we have used r_{eff} = 0.25 μm for $z < 21$ km, r_{eff} = 0.10 μm for 21 km $< z <$ 25 km, and r_{eff} = 0.05 μm for $z > 25$ km; a gradual change of r_{eff} with altitude is more likely than an abrupt one, but should appear around 20–22 km and 25–26 km. Above 28 km, even smaller particles would give better agreement than the model with r_{eff} = 0.05 μm, but the accuracy of both the SAGE II and the lidar profiles is probably not good enough at these altitudes to give a definite conclusion. The error bars on the Garmisch-Partenkirchen lidar profile have been given every 2 km; they are somewhat larger for the OHP lidar profile.

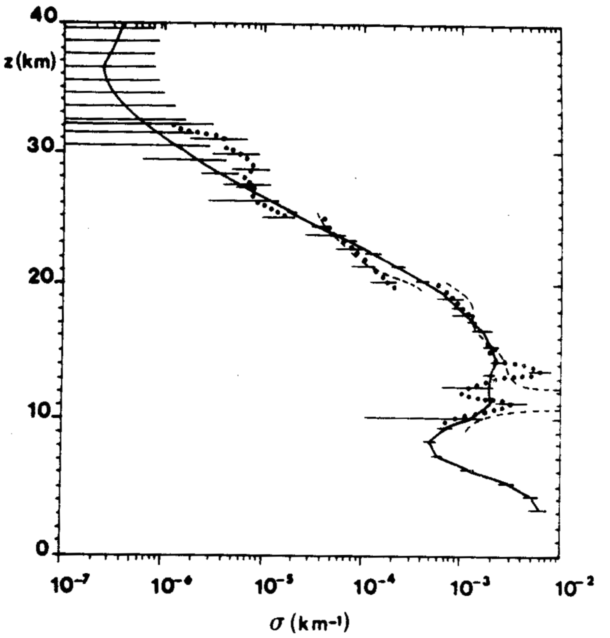

Fig. 3. Same as Figure 2 except on November 27, 1984: solid curve, SAGE II, 1457 UT, 46.53°N, 18.63°E; dashed curve, lidar OHP, 1720 UT, 44°N, 6°E; dotted curve, Garmisch-Partenkirchen lidar, 47.5°N, 11°E (aerosol model: r_{eff} = 0.25 μm, $z < 21$ km; r_{eff} = 0.10 μm, 21 km $< z <$ 25 km; r_{eff} = 0.05 μm, $z > 25$ km).

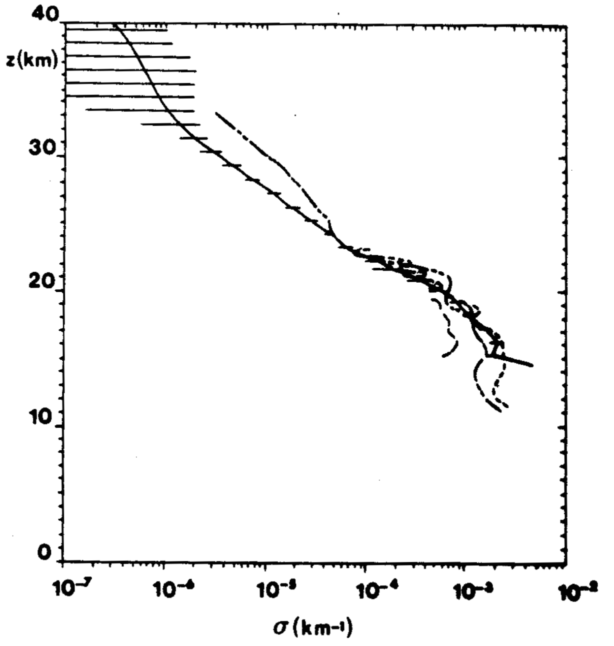

Fig. 4. Same as Figure 2, except on November 28, 1984: solid curve, SAGE II, 1509 UT, 45.18°N, 16.76°E; dash-double-dotted curve, SAGE II, 1645 UT, 45.07°N, 7.36°W (error bars omitted); dashed curve, OHP lidar, 1657–1830 UT, 44°N, 6°E; long-dashed curve, Frascatti lidar, 1800 UT, 42°N, 13°E (aerosol model: r_{eff} = 0.25 μm).

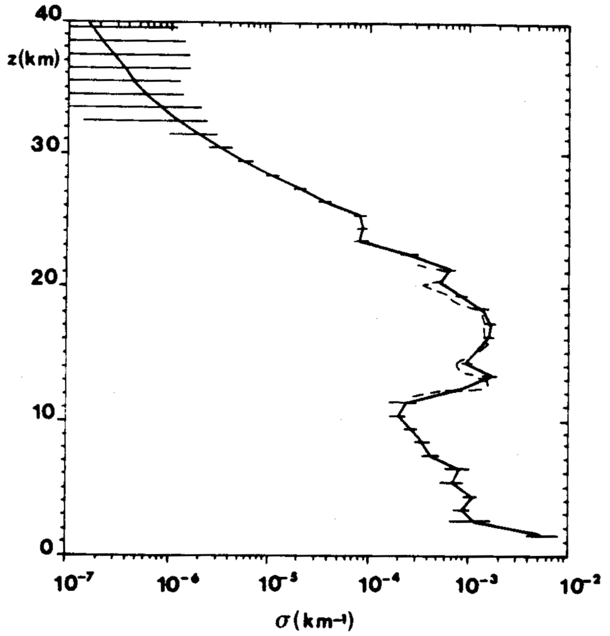

Fig. 5. Same as Figure 2, except on November 30, 1984: solid curve, SAGE II 1533 UT, 41.40°N, 13.61°E; long-dashed curve, Frascatti lidar, 1936 UT, 42°N, 13°E (aerosol model: $r_{eff} = 0.35$ μm).

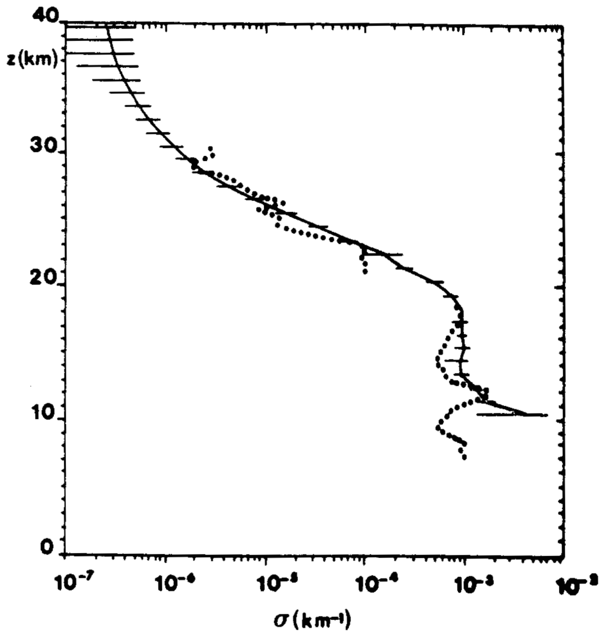

Fig. 6. Same as Figure 2, except on April 21, 1985: solid curve, SAGE II, average of five profiles (April 21–23 between 50.14° and 43.80°N and 7.20°W and 21.29°E) with standard deviations; dotted curve, Garmisch-Partenkirchen lidar, April 21, 47.5°N; 11°E (aerosol model: $r_{eff} = 0.35$ μm, $z < 21$ km; $r_{eff} = 0.10$ μm, $z > 21$ km).

The two lidar profiles agree with each other reasonably well, as well as with the SAGE II profile above 15 km; below this level they exhibit oscillations, probably due to local conditions. For November 28 (Figure 4) the conversion has been made with $r_{eff} = 0.25$ μm up to 23 km, which is the upper limit of the lidar profiles (OHP and Frascatti). The agreement between the OHP lidar and the SAGE II profiles is very good; the Frascatti lidar leads to somewhat smaller extinctions below 20 km. November 30 (Figure 5) corresponds to the closest coincidence, as the SAGE II tangent point is about 90 km from Frascatti. The conversion has been made with $r_{eff} = 0.35$ μm, and the agreement between the Frascatti lidar and the SAGE II profiles is almost perfect in the altitude range of the lidar profile (12–22 km).

2.3. *April 1985*

In April 1985 the five SAGE II aerosol profiles available over the zone are almost identical, pointing to very stable conditions for the aerosol layer. Unfortunately, weather conditions did not permit lidar observations, except at Garmisch-Partenkirchen on April 21. As the SAGE II tangent points were not very close to Garmisch-Partenkirchen on April 21, and considering the homogeneity mentioned earlier, we have chosen to make the comparison with the average SAGE II profile for the considered zone and period. The result of this comparison is presented in Figure 6. The bars on the SAGE II average profile in Figure 6 are the standard deviations; they are of the same order as the error bars on individual profiles. No error bars have been given for the lidar profile, but the errors can be expected to be of the same order as in Figure 3. The conversion of backscattering into extinction had to be made with $r_{eff} = 0.35$ μm below 21 km and $r_{eff} = 0.10$ μm above that level in order to find the best agreement between the two profiles; the change of particle size seems rather abrupt between 20–22 km. The agreement is within the error bars.

2.4. *October 1985*

In October 1985 the six SAGE II profiles are rather similar, but not as similar as in April. Lidar profiles were obtained at OHP for 4 successive days, and they show a good stability of the aerosol layer at this station. Figure 7

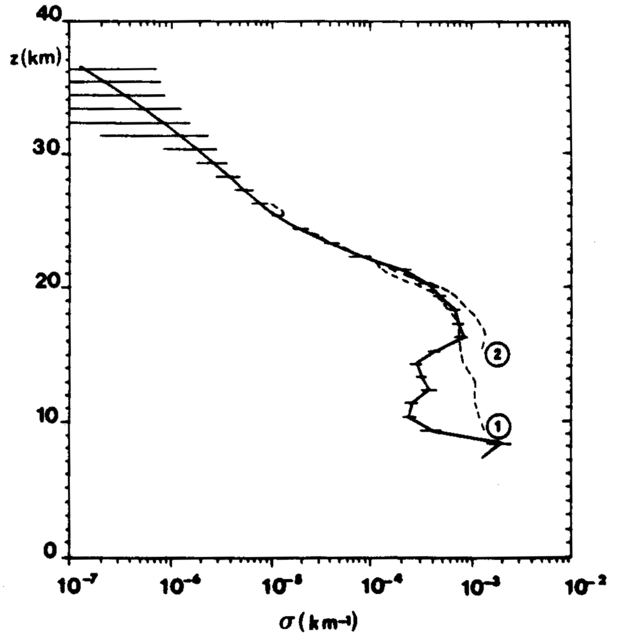

Fig. 7. Same as Figure 2, except on October 12, 1985: solid curve, SAGE II, 0502 UT, 41.03°N, 17.03°E; dashed curve, OHP lidar, 1900–1920 UT, 44°N, 6°E (1, aerosol model $r_{eff} = 0.17$ μm; 2, aerosol model deduced from polarization measurements).

compares the OHP lidar profile for the evening of October 12 with the SAGE II morning profile on October 12, approximately 10° east of OHP. The SAGE II profile at about 14° west of OHP is very similar above 16 km and so are the two profiles for the morning of October 13, however, with values slightly higher above 21 km for the eastern profile. Below 16 km the four profiles are quite different, and no comparison can be sought. A good agreement above 16 km is found by using an aerosol model with $r_{eff} = 0.17$ μm for the conversion of the lidar profile.

In conclusion, the extinction profiles retrieved from lidar profiles seem in reasonably good agreement (generally within the error bars) with the SAGE II extinction profiles at 1.02 μm, provided r_{eff} is chosen suitably. The best validation is obtained on November 30, 1984, where there is a close coincidence in time and location between the SAGE II and the Frascatti lidar profiles (Figure 5). The periods of stability of the aerosol layer allow rather good validations with noncoincident observations; this is the case for April 21–24, 1985 (Figure 5). The conversion of backscattering lidar profiles into extinction profiles has to be done with variable models, the particle sizes being generally smaller at high altitudes. The consistency of the choice of the model with the other observations will be discussed in section 5.

3. BALLOON LIMB PHOTOGRAPHS

Photographs of the limb radiance were made from balloons at Aire sur l'Adour by the Institut d'Aéronomie Spatiale de Belgique (IASB); the photographs were made for low Sun elevation, at various solar azimuths for two wavelengths (0.84 and 0.44 μm) during the first flight and for three wavelengths (0.84, 0.44, and 0.375 μm) during the second flight [*Ackerman et al.*, 1981]. The extinction is deduced from the radiance measured at 30° scattering angle, and the Rayleigh extinction is subtracted to obtain the aerosol extinction. Only direct solar radiation falling on the atmosphere is considered, since the solar elevation is low and since it has been checked that the effects of illumination by clouds or lower atmospheric layers are negligible. Only single scattering is taken into account, which is reasonable, since only observations at low extinction are used. Most of the uncertainties originate from film calibration (±20%). A value equal to 3 is used for the phase function at 30°. The uncertainty is here equal to ±15% for a range of asymmetry parameters from 0.4 to 0.7. Two flights took place, on November 10, 1984, and April 22, 1985. They were simultaneous to flights of the polarimetric instrument described in section 4.

3.1. *November 10, 1984*

On November 10, 1984, the photographs confirm the aerosol layer inhomogeneity mentioned previously (section 2). To the south of the balloon position, well-marked vertical structures were observed [*Ackerman et al.*, 1985]. Toward the north a much smoother vertical profile was observed. The SAGE II tangent point on November 10 is rather far to the southeast, over the Mediterranean Sea, and the SAGE II profiles on November 11, closer to the balloon launch site, are completely different than the November 10 profiles. We have therefore chosen to compare the balloon profiles with the two SAGE II profiles of November 10 and 11 in Figures 8 and 9. Figure 8 compares the balloon profile at 0.44 μm with the two SAGE II profiles at 0.453 μm; we have not introduced a correction for the small wavelength difference. Figure 9 concerns the comparison at 1.02 μm; the balloon profiles at 0.84 μm have been converted to 1.02 μm, using two aerosol models with $r_{eff} = 0.28$ μm and $r_{eff} = 0.05$ μm, respectively, but the conversion is not very sensitive to the model. At 1.02 μm the balloon profile on November 10 and

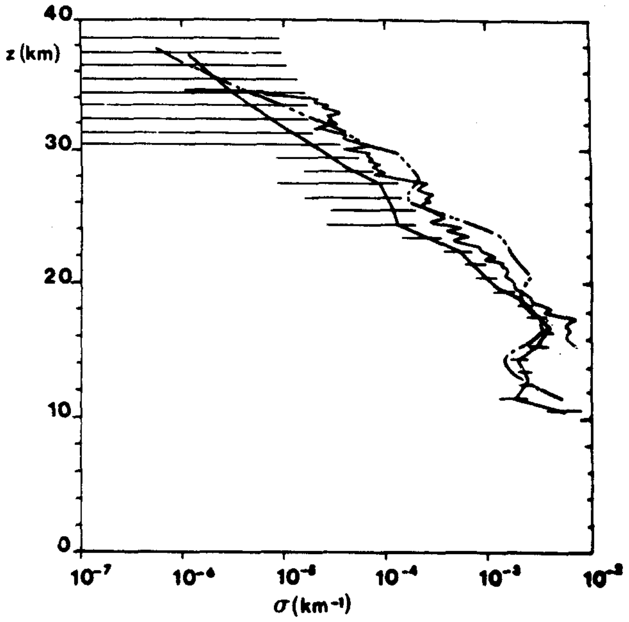

Fig. 8. Comparison of aerosol extinction profiles from SAGE II on November 10, 1984, at 1627 UT, 37.80°N, 5.27°E; (dash-double-dotted curve) and SAGE on November 11, 1984, at 1639 UT, 40.50°N, 0.56°E (solid curve) and from balloon limb photographies on November 10, 1984, at sunset, launch site 44°N, 0° (thin solid curve); SAGE II $\lambda = 0.453$ μm; balloon $\lambda = 0.44$ μm.

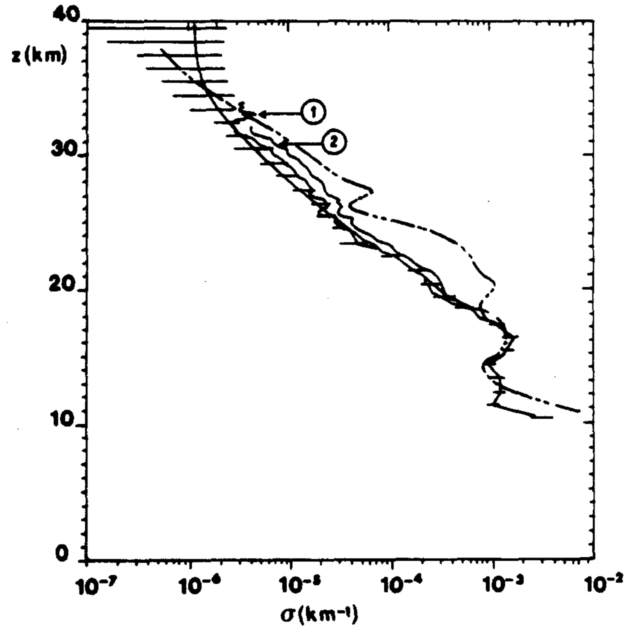

Fig. 9. Same as Figure 8, except $\lambda = 1.02$ μm. Balloon data are converted from 0.84 to 1.02 μm with LND aerosol models, $v_{eff} = 0.10$; 1, $r_{eff} = 0.05$ μm; 2, $r_{eff} = 0.28$ μm.

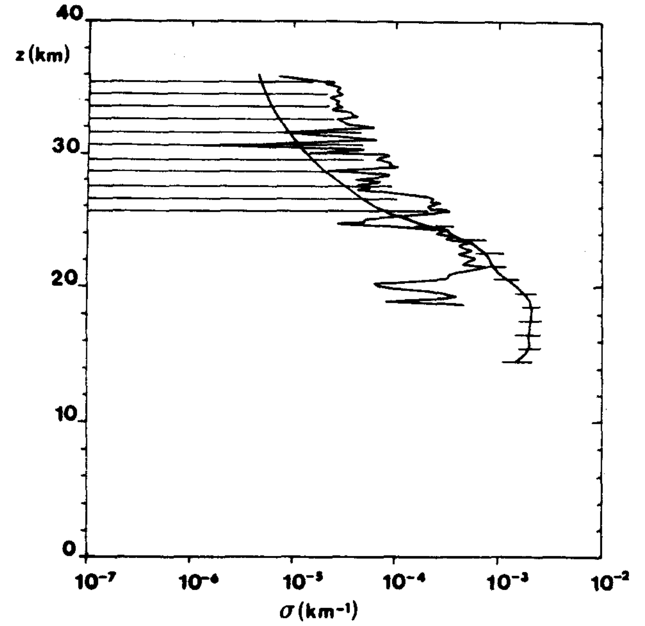

Fig. 10. Comparison of aerosol extinction profiles from SAGE II on April 22, 1985, at 1906 UT, 47.17°N, 2.90°W (solid curve) and from balloon limb photographies on April 22, 1985, at sunset, launch site 44°N, 0° (thin solid curve); SAGE II $\lambda = 0.385$ μm; balloon $\lambda = 0.375$ μm.

the SAGE II profile on November 11 are in very close agreement, whereas the SAGE II profile on November 10 is quite different. At 0.44/0.453 μm, the balloon profile is between the two SAGE II profiles, with a general shape more similar to the SAGE II profile of November 11.

3.2. *April 22, 1985*

On April 22, 1985, the conditions were very stable, and the air mass observed at 30° from the Sun and for a tangent height of 20 km was very close to the SAGE II tangent point [*Ackerman et al.*, 1987]. Figure 10 compares the balloon and the SAGE II extinction profiles at 0.375 and 0.385 μm, respectively; Figure 11 gives the same comparison for 0.440 and 0.453 μm; the error due to the small difference in wavelength is in both cases smaller than 5%, and we have not found necessary to introduce a correction. Figure 12 presents the comparison of the balloon and the SAGE II extinction profiles at 0.84 μm. The SAGE II profile at 1.02 μm has been converted to 0.84 μm, using a LND model($v_{\text{eff}} = 0.25$) with an effective radius of 0.10 μm above 22 km and 0.35 μm below 22 km, i.e., the model which gives the best agreement between lidar and SAGE II profiles (section 2, Figure 6); however, the conversion between 1.02 and 0.84 μm is not very sensitive to the choice of the model, as mentioned above. The balloon profiles exhibit oscillations which are smoothed on the SAGE II profiles. Above 21 km the general agreement is very good up to 26–28 km for the 0.44/0.453-μm and the 0.375/0.385-μm profiles, and up to 32 km for the 0.84-μm profile. Below 20 km the balloon profiles deduced from scattering could be of poorer quality. However, in this case the photographically measured extinction becomes significant and hence reliable. The value of aerosol extinction (total extinction minus Rayleigh and O_3 extinction) deduced from the balloon data agrees well with SAGE II results at 18 km altitude (Figure 12). Above 26 km the error bars on SAGE II profiles become very large for the short-wavelength channels and the oscillations of the balloon profiles increase toward high altitudes and short wavelengths. However, the balloon extinctions for 0.44 μm and 0.375 μm are systematically higher than the SAGE II extinctions above 26 km, which would point to smaller particles observed by the balloon.

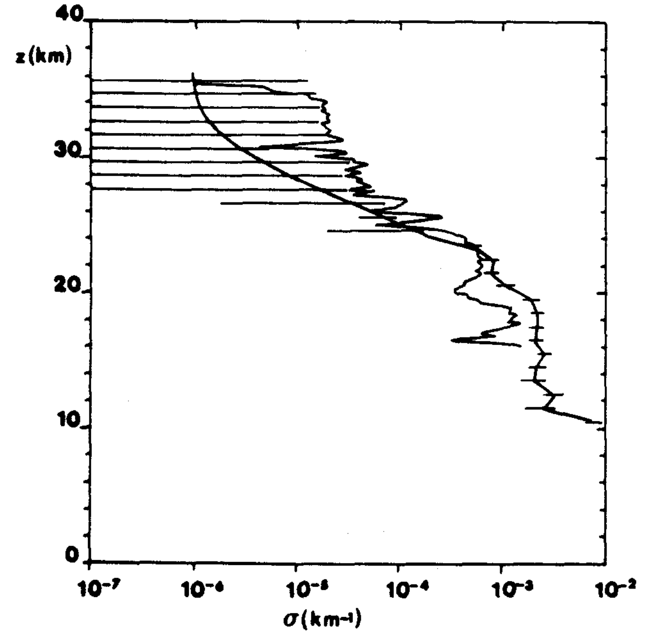

Fig. 11. Same as Figure 10, except SAGE II $\lambda = 0.453$ μm; balloon $\lambda = 0.44$ μm.

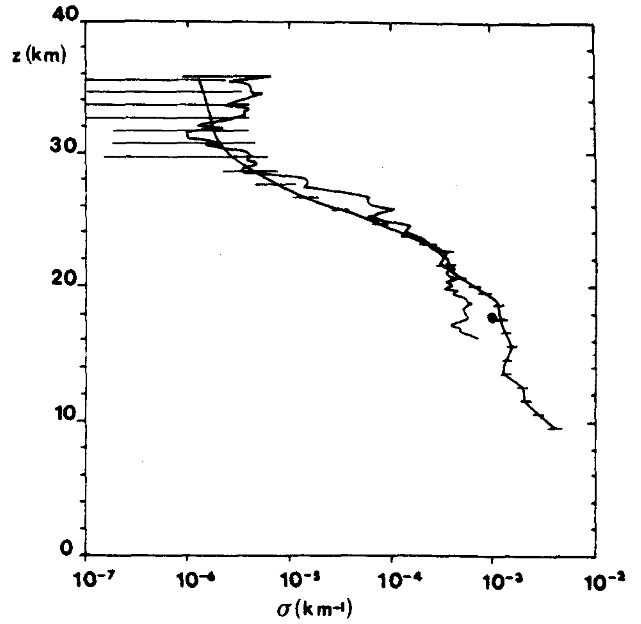

Fig. 12. Same as Figure 10, except $\lambda = 0.84$ μm. SAGE II data are converted from 1.02 to 0.84 μm with LND aerosol models, $v_{\text{eff}} = 0.25$; $r_{\text{eff}} = 0.35$ μm, $z < 22$ km; $r_{\text{eff}} = 0.10$ μm, $z > 22$ km. Solid circle is from balloon extinction.

The balloon limb photographs on April 22, 1985, provide an almost direct comparison with SAGE II profiles, for a close coincidence, and in a stable situation. The agreement for the three wavelengths is very good between 21 and 26 km.

4. BALLOON POLARIMETRIC OBSERVATIONS

The instrument [*Herman et al.*, 1986] is a narrow field of view polarimeter operating at two wavelengths in the near-infrared, 0.85 and 1.65 μm. The scanning is performed in an horizontal plane by rotation of the gondola. Measurements of the radiance L and of the degree of polarization P at the two wavelengths can be made during the ascent and the descent or at the ceiling level; the best conditions are sunset or sunrise, when the Sun is close to the horizon, allowing the scattering angle θ to vary between 0° and 180°. The data are first corrected for multiple scattering and for the reflection by the ground or by the clouds, in the case when the Sun is above the horizon; the radiance is more conveniently expressed as a reflectance $\rho = \pi L/E$, where E is the solar irradiance. The inversion procedure uses first the polarization $P(\theta_0)$ at 1.65 μm ($\theta_0 = 100°$), assuming that the molecular contribution is negligible; this defines a family of LND size distributions (r_m versus s); the reflectance $\rho(\theta_0)$ are used to retrieve the tangent optical depths for the two wavelengths; finally, the polarization $P(\theta_0)$ at 0.85 μm is used to select a model amongst the family found previously. It is checked that the reflectance $\rho(\theta)$ and polarization $P(\theta)$ computed with this model agree with the measured values for the two wavelengths and all the scattering angles.

Four flights took place, one for each period during the SAGE II European correlative program. All of the flights were launched from the Centre National d'Etudes Spatiales (CNES) Center at Aire sur l'Adour in the southwest of France. The four flights are briefly described here, and the results will be presented in section 5.2.

4.1. *November 10, 1984*

On November 10, 1984 (sunset flight) the aerosol layer was very inhomogeneous and unstable around the balloon. The data recorded between 14 and 30 km, with a gap due to transmission problems between 19 and 23 km, are therefore of poor quality. The polarization diagrams can be inverted only around 16–19 km.

4.2. *November 28, 1984*

On November 28, 1984 (sunrise flight) the conditions were better. Unfortunately, the balloon did not fly above 24 km, but good quality data were recorded between 14 and 24 km.

4.3. *April 22, 1985*

During the flight of April 22, 1985 (sunset), the instrument broke down at ceiling level. Data were recorded only during the ascent between 15 and 22 km and 27 and 30 km, when the gondola was not very stable and the Sun was still rather high above the horizon.

4.4. *October 12, 1985*

The flight of October 12, 1985, took place during sunset in good stable conditions, and data were recorded from 16 to 33 km. However, above 22 km the aerosol content was low, and the results are of better quality at low altitudes.

5. ANALYSIS OF THE RESULTS: VALIDATION OF THE THREE SHORT WAVELENGTH CHANNELS

The aerosol extinction coefficient is retrieved from SAGE II data at four wavelengths 1.02, 0.525, 0.453, and 0.385 μm, leading to a spectral extinction curve $\sigma^{aer}(\lambda)$ which could "in principle" be inverted to give the size distribution $n(r)$. The lidar backscattering profiles have been converted into extinction profiles at 1.02 μm using the aerosol model with $v_{\mathrm{eff}} = 0.25$, which gives the best agreement with SAGE II profiles. Of course, varying v_{eff}, within a reasonable range, leads to a family of size distributions characterized by (v_{eff}, r_{eff}), which give the same conversion factor from lidar into extinction profiles. The model used for lidar conversion must be consistent with the model fitting the SAGE II spectral extinction $\sigma^{aer}(\lambda)$. The balloon polarization measurements lead to a retrieval of the size distribution $n(r)$, which best fit the polarization and the reflectance diagrams at 0.85 and 1.65 μm. This has also to be consistent with the SAGE II spectral extinction and with the lidar conversion factor. Finally, the balloon limb photographs provide profiles to be compared to the SAGE II short-wavelength extinction profiles (see Figures 8, 10, and 11).

Inverting the SAGE II spectral extinction $\sigma^{aer}(\lambda)$ is a rather delicate problem, and various approaches have been tried in order to retrieve two parameters of the size distribution, i.e., the effective radius r_{eff} and the effective variance v_{eff}, or the mean radius r_m and the variance s. The discussion of this inversion problem is beyond the scope of the present work and will be left for a future contribution. We limit ourselves here to deducing the effective radius r_{eff} [*Lenoble and Brogniez*, 1985] for an arbitrary fixed variance ($v_{\mathrm{eff}} = 0.25$) from the ratio $\sigma^{aer}(0.453)/\sigma^{aer}(1.02)$, or more conveniently, from the related mean Angstrom coefficient α for the spectral interval 0.453/1.02 μm, defined by

$$\sigma^{aer}(\lambda) = \sigma^{aer}(1.02)\lambda^{-\alpha} \tag{12}$$

Preliminary tests with a two-parameter retrieval procedure suggest that the effective variance is generally smaller than 0.25 at the low levels below 22 km [*Brogniez and Lenoble*, 1989].

5.1. *Consistency of Lidar Conversion Factor With SAGE II Spectral Extinction*

November 10–13, 1984. For this period a stable situation is found only on November 13, when a lidar comparison was possible (Figure 2). If we look at the Angström coefficient α for the wavelength interval (0.453/1.02 μm) from the SAGE II profiles on November 13, it varies approximately from 0.6 to 1.8 when the altitude increases from 15 to 25 km, pointing to a decrease of the particle effective radius from about 0.40 to 0.20 μm with altitude; the variation of $\sigma^{aer}(\lambda)$ between 0.525 and 0.385 μm suggests, at least for the low altitudes, a rather small effective variance, around 0.1 or a little larger than 0.1. As mentioned earlier, the conversion factor from lidar backscattering into extinction is not very sensitive to the model for particles with r_{eff} larger than 0.20 μm, and the agreement found between the lidar and the SAGE II profiles in Figure 2 would remain had we used the aerosol models derived from the SAGE II spectral extinction instead of the model $r_{\mathrm{eff}} = 0.35$ μm, $v_{\mathrm{eff}} = 0.25$.

November 26–30, 1984. For this period the comparison between SAGE II and lidar profiles on November 27 (Figure 3) requires an aerosol model with $r_{\mathrm{eff}} \simeq 0.25$ μm for $z < 21$ km, $r_{\mathrm{eff}} \simeq 0.10$ μm for 21 km $< z <$ 26 km, and $r_{\mathrm{eff}} \simeq 0.05$ μm for $z >$ 26 km. For the low altitudes, the SAGE II spectral extinction suggests r_{eff} between 0.35 and 0.24 μm (α between

0.8 and 1.5), which is consistent with the model (r_{eff} = 0.25 μm) chosen for the lidar conversion, considering the small sensitivity of the conversion factor in this size range. However, at higher altitudes, α increases from about 1.3 to 1.9, which means a decrease of r_{eff} from about 0.25 to 0.18 μm. Small particles, as chosen for the lidar conversion factor, would give α around 3; this is absolutely inconsistent with the SAGE II extinction values in the short-wavelength channels, which are much too low.

On November 28, as mentioned previously, the two SAGE II profiles are different above 25 km but quite close between 16 and 25 km, with a small extinction peak around 21 km for the western profile that does not appear on the eastern profile (Figure 4); in the peak the particles are slightly larger ($\alpha \simeq 1.2$ for the western profile, instead of 1.4 at the same level in the eastern profile). The two lidar profiles (Frascatti and OHP) are rather different, and the OHP profile agrees better with the SAGE II profiles. From SAGE II extinction profiles, α increases from 0.65 to 1.8 between 14 and 24 km, which means r_{eff} decreasing from 0.40 to 0.20 μm; this is again consistent with the choice r_{eff} = 0.35 μm for the lidar conversion factor.

On November 30 (Figure 5) we have the closest coincidence between a lidar and a SAGE II observation. The conversion factor for an aerosol model with r_{eff} = 0.35 μm gives a very good agreement between 13 and 22 km (upper limit of the lidar profile). In this altitude range the SAGE II Angström coefficient varies from 0.6 to 1.4, which corresponds to particles with r_{eff} decreasing slightly from about 0.40 to 0.25 μm. This is again perfectly consistent with the choice of r_{eff} = 0.35 μm for the conversion of lidar data.

April 1985. In April 1985 the aerosol layer over Europe during the observation period was very homogeneous and stable. The comparison between the SAGE II average profile and the Garmisch-Partenkirchen profile on April 21 was made using for the conversion factor r_{eff} = 0.35 μm below 22 km and r_{eff} = 0.10 μm above that level. The SAGE II spectral extinction gives r_{eff} decreasing from about 0.35 μm at 13 km, to 0.25 μm at 22 km, and then to 0.17 μm at 30 km ($\alpha \simeq 0.9$, $\alpha \simeq 1.4$, and $\alpha \simeq 2.0$, respectively). This is consistent with the choice r_{eff} = 0.35 μm for the lidar conversion factor below 22 km, but not at higher altitudes, where the SAGE II spectral extinction leads to particles much larger than the particles which are found necessary in order to obtain a good agreement between the lidar and the SAGE II profile. Again, we find the same difficulty as on November 27: the aerosol model derived from SAGE II spectral extinction would lead to a poor agreement with the lidar profile at high altitudes, whereas agreement is obtained by assuming much smaller particles than those given by SAGE II short-wavelength channels. The balloon limb photographs (section 3) on April 22 give extinction coefficients larger than SAGE II above 25 km for the short wavelengths (Figure 10 and 11), pointing to particles smaller than those retrieved from SAGE II. But it is difficult with the rapid oscillations of the balloon profiles to deduce the spectral variation $\sigma^{aer}(\lambda)$ at a given level and to make a quantitative comparison with SAGE II size distribution.

October 12, 1985. On this day the comparison between the SAGE II profile and the OHP lidar was made with r_{eff} = 0.17 μm, between 16 and 25 km, whereas the SAGE II spectral extinction leads to r_{eff} decreasing from 0.34 to 0.21 μm with altitude (α between 0.9 and 1.7). It is the only case where we find some inconsistency between the best choice for the lidar conversion factor and the best fit to $\sigma^{aer}(\lambda)$ at low altitudes. In Figure 7 we have also drawn the extinction profile deduced from the lidar profile using the aerosol model, which fits both the polarization measurements (see discussion in section 5.2) and the SAGE II spectral extinction. The agreement with the SAGE II profile is definitely not as good as that obtained with the model v_{eff} = 0.25, r_{eff} = 0.17 μm, but the disagreement appears only below 20 km and remains rather small: it might be attributed to small local or temporal variation of the aerosol, as the observations are not exactly coincident either in location, or in time. These results are summarized in Table 1.

TABLE 1. Comparison of Aerosol Effective Radius r_{eff} Used for Lidar/Sage II Best Fit at 1.02 μm and Retrieved From SAGE II Extinction Ratio $\sigma^{aer}(0.45)/\sigma^{aer}(1.02)$

Date	Altitude, km	r_{eff} (lidar), μm	r_{eff} (SAGE II), μm
November 13, 1984	12–25	0.35	0.40–0.20
November 27, 1984	12–21	0.25	0.35–0.24
	21–26	0.10	0.24–0.18
	26–30	0.05	0.18
November 28, 1984	12–23	0.35	0.40–0.20
November 30, 1984	13–32	0.35	0.40–0.25
April 21, 1985	10–22	0.35	0.35–0.25
	22–30	0.10	0.25–0.17
October 12, 1985	16–25	0.17	0.34–0.21

5.2. *Balloon Polarimetric Observations and Size Distribution*

The balloon polarimetric observations provide radiance and polarization diagrams at 0.85 and 1.65 μm, and their inversion leads to the retrieval of two parameters of the size distribution, assumed to be lognormal. However, it must be kept in mind that the actual aerosol size distribution may not be close to lognormal and may not even be monomodal. The retrieved size distribution must be understood as one of the many size distributions which give a good fit to the radiance and to the polarization of the diffuse radiation in the near-infrared. The inversion of the SAGE II spectral extinction between 0.385 and 1.02 μm is subject to the same remark as the inversion of the polarimetric data; the retrieved size distribution is one of many which give a good fit to the extinction coefficient in the visible range. Therefore using the balloon polarimetric data to validate the SAGE II short-wavelength channels is a rather delicate task, and the results must be considered with caution.

November 10, 1984. For the flight of November 10, 1984, Figure 13 compares the tangent optical depth at 1.02 μm observed from SAGE II on November 10 and 11 with the tangent optical depth observed by the balloon instrument. As noted previously, the SAGE II event tangent point is closer to the balloon launch site on November 11 than on November 10. The balloon data exhibit strong oscillations and have been averaged over 1 km. The balloon optical depth values at 0.85 μm have been converted into values at 1.02 μm, using an aerosol effective radius of 0.28 μm below 20 km and of 0.10 μm above 22 km; the influence of the model choice is, however, small. The balloon tangent optical depth profile given by the polarimeter is closer to the SAGE II profile on November 10, whereas the extinction profile

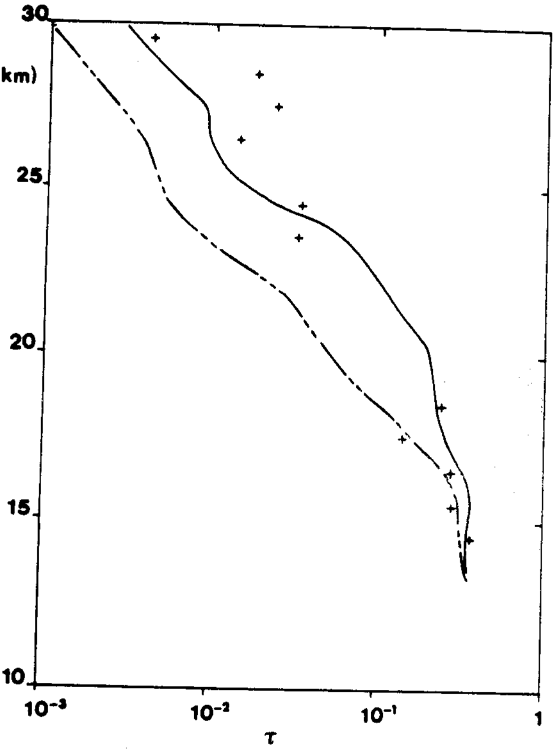

Fig. 13. Comparison of the tangent optical depth at 1.02 μm, measured by SAGE II on November 10, 1984, at 1627 UT, 37.80°N, 5.27°E (solid curve) and on November 11, 1984, 1639 UT, 40.50°N, 56°E (dash-double-dotted curve), and measured by the balloon polarimeter on November 10, 1984, sunset, launch site 44°N, 0° (crosses). The conversion of the balloon data from 0.85 to 1.02 μm has been done with r_{eff} = 0.28 μm below 20 km and r_{eff} = 0.10 μm above 22 km.

deduced from the balloon limb photographs on the same day was closer to the SAGE II profile on November 11. This is not too surprising in a very unstable situation, as the two balloons were not operating exactly at the same place and at the same time. The complete inversion of the polarization data has been performed only for the altitude range 16–19.5 km; the retrieved size distribution has an effective radius $r_{eff} \simeq 0.35$ μm and an effective variance $v_{eff} \simeq 0.17$ between 16 and 17 km; between 17.5 and 19.5 km the effective radius is slightly smaller; $r_{eff} \simeq 0.29$ μm with $v_{eff} \simeq 0.14$. This is in excellent agreement with the size distribution retrieved from the SAGE II extinction ratio $\sigma^{aer}(0.45)/\sigma^{aer}(1.02)$, which gives, for November 11, r_{eff} decreasing from 0.32 to 0.23 μm, if we assume $v_{eff} = 0.25$, and from 0.36 to 0.27 μm for v_{eff} = 0.10, between 15 and 20 km. For November 10, SAGE II data give, for the same altitude range of 15–20 km, an almost constant effective radius r_{eff} = 0.30 μm, if we assume v_{eff} = 0.25, and r_{eff} = 0.33 μm with v_{eff} = 0.10.

November 28, 1984. This flight took place in more stable conditions. The tangent optical depth measured by the balloon above 20 km is larger, by about a factor of 2, than the optical depth measured by SAGE II, whereas at the lower levels (13–17 km) the two values agree reasonably well. No explanation has been found for this disagreement, which may just be due to local conditions. The polarization data lead to a size distribution with an effective radius that is almost constant around 0.22 μm, and an effective variance decreasing from 0.80 to 0.18 between 15 and 22 km. The SAGE II extinction ratio $\sigma^{aer}(0.45)/\sigma^{aer}(1.02)$ leads to an effective radius decreasing from 0.38 to 0.22 μm, assuming v_{eff} = 0.25, for the same altitude range. The large variance found by the balloon at low levels seems to confirm the presence of particles different from those observed by SAGE II.

April 22, 1985. Unfortunately, on April 22, 1985, no inversion of the polarization diagram was possible owing to the instability of the data. However, at a few levels a relative stabilization appeared, and the diagram can be used for direct comparisons. Figure 14 shows the polarization diagram for the two wavelengths (0.85 and 1.65 μm) and three altitude levels (15, 18.2, and 21.5 km); the dots are the experimental data and present a rather large dispersion. The solid lines show the polarization computed with models derived from a best fit to the SAGE II spectral extinction(v_{eff} = 0.17; r_{eff} = 0.37 μm at 15 km, and r_{eff} = 0.29 μm at 18.2 km and 21.5 km). The comparison is satisfying. Unfortunately, no such comparison was possible at higher levels.

October 12, 1985. The flight of October 12, 1985, provides another good comparison to SAGE II data. Figure 15 presents the vertical profiles of r_{eff} and v_{eff} retrieved from the polarization data. Above 22 km the effective variance increases rapidly and stabilizes around 0.9, whereas the effective radius presents very large oscillations; these results at high altitudes are certainly dubious, because the aerosol content becomes very low above 22 km and the signal-to-noise ratio becomes bad. However, the large value retrieved for v_{eff} could suggest that the size distribution becomes bimodal at high altitudes; therefore the retrieval procedure, which assumes a monomodal distribution, leads to erratic results. Figure 16 demonstrates, for 17.5 km, the good quality of the inversion. Figure 17 shows the tangent optical depth at 1.02 μm deduced from the measured optical depth at 0.85 μm, using LND models which incorporate, at each altitude, the effective radius and the effective variance retrieved from the polarization data and averaged over 1 km; it is compared with the SAGE II tangent optical depth at 1.02 μm on the morning of October 12, 1985, 7° west of the launch site. The similarity above 16 km between the four SAGE II profiles over the zone on October 12 and 13 justify the comparison, despite the not very close coincidence in time and location. Figure 18 compares the extinction ratios for the three short wavelengths $\sigma^{aer}(0.525)/\sigma^{aer}(1.02)$, $\sigma^{aer}(0.45)/\sigma^{aer}(1.02)$, $\sigma^{aer}(0.385)/\sigma^{aer}(1.02)$ measured by SAGE II and computed at each level with the size distribution retrieved from the polarization data and averaged over 1 km. As a result of the low aerosol content, the extinction ratios derived from the polarization data are somewhat inaccurate. However, the agreement is good.

6. CONCLUSIONS

Although the SAGE II 1.02-μm channel allows retrieval of the extinction profile at very low levels, only the profiles a few kilometers above the tropopause (12–15 km) and higher have been considered; at lower altitudes the variability is such that only almost coincident observations would be necessary to validate SAGE II profiles.

From the data and the discussions presented in the previous sections, we must consider separately two altitude ranges. For safety, we will refer them as below 23 km and above 25 km, it being understood that the cutoff between the two ranges is somewhat variable, depending on the events and on the kind of observations.

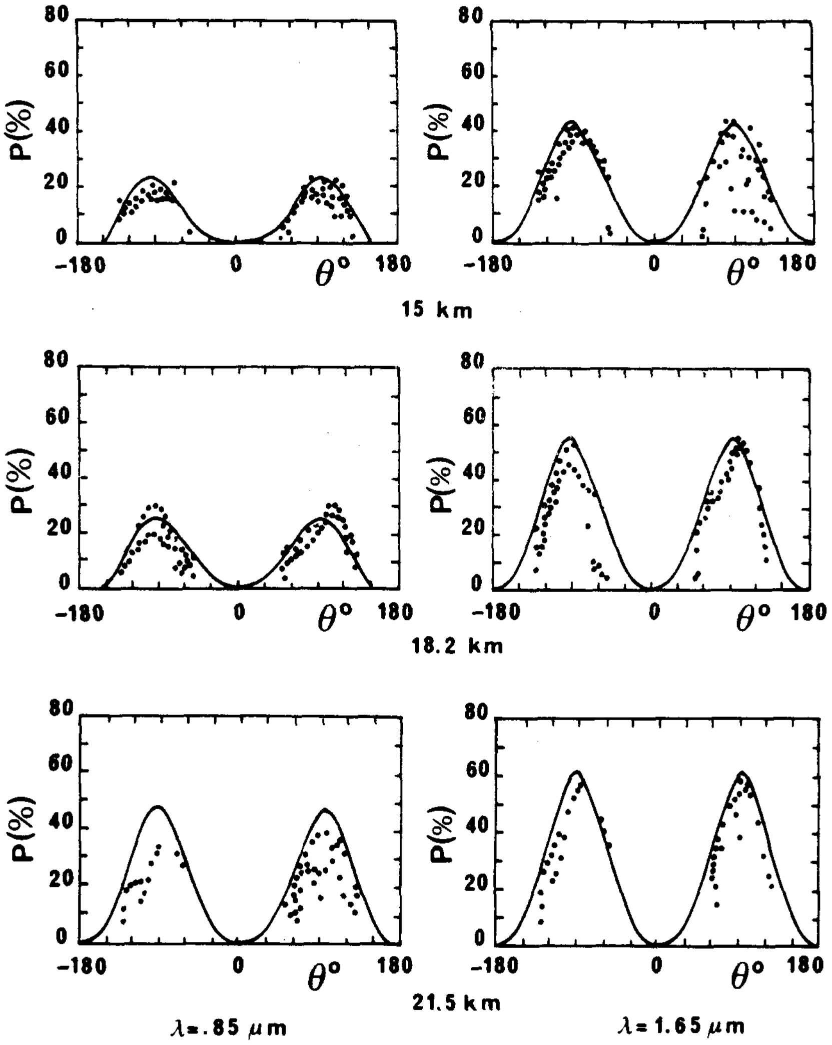

Fig. 14. Comparison on April 22, 1985, between the degree of polarization measured by the balloon polarimeter (dots) and computed using an aerosol model that fits the SAGE II spectral extinction (solid curve). The degree of polarization is given in percent versus the scattering angle. The left side curves are for 0.85 μm and the right side curves for 1.65 μm; the top panel is at 15 km, the middle panel at 18.2 km, and the bottom panel at 21.5 km.

6.1. *Altitude Range Below 23 km*

Below 23 km, we have at our disposal a large series of data, including lidar profiles (both ruby and Nd: Yag), limb photographs, and polarization diagrams. The main conclusions are as follows:

1. The SAGE II extinction profiles at 1.02 μm agree within the error bars with the several extinction profiles deduced from the lidar backscattering profiles using a conversion factor, consistent with the SAGE II spectral variation of the extinction coefficient (Figures 2–7 and Table 1). These comparisons comprise one case (November 30, 1984) of very close coincidence in time (4 hours) and in location (100 km) between the lidar and the SAGE II observations, and several cases with a very stable and homogeneous aerosol layer, as proved by the comparisons between various SAGE II and lidar profiles over Europe for the experiment period. However, the consistency of the chosen backscatter into extinction conversion factor with the aerosol size distribution, retrieved from the four-wavelength SAGE II extinction, does not really validate the SAGE II four channels because the conversion factor is almost insensitive to the aerosol model as long as the effective radius is larger than 0.20 μm, which is the case in this altitude range.

2. The SAGE II extinction profile at 1.02 μm also agrees with the limb photographs profile at 0.84 μm, the conversion between 1.02 and 0.84 μm being only very slightly sensitive to the aerosol model; the agreement is particularly good on April 22, 1985 (Figure 12) when the conditions are quite stable and the coincidence very close.

3. The SAGE II tangent optical depth profiles at 1.02 μm generally agree within the error bars with the optical depth profiles obtained by the balloon-borne polarimetric instrument.

4. The SAGE II extinction profiles at 0.453 and 0.385 μm have been compared directly to the extinction profiles at about the same wavelengths deduced from the limb photographs. April 22, 1985 (Figures 10 and 11) corresponds to a close coincidence (sunset, less than 100 km between the two observations). Despite the oscillations revealed by the high resolution of the photographs, the general agreement between the balloon and the SAGE II profiles is a good validation of the two channels 0.453 and 0.385 μm, for the altitude range 21–25 km.

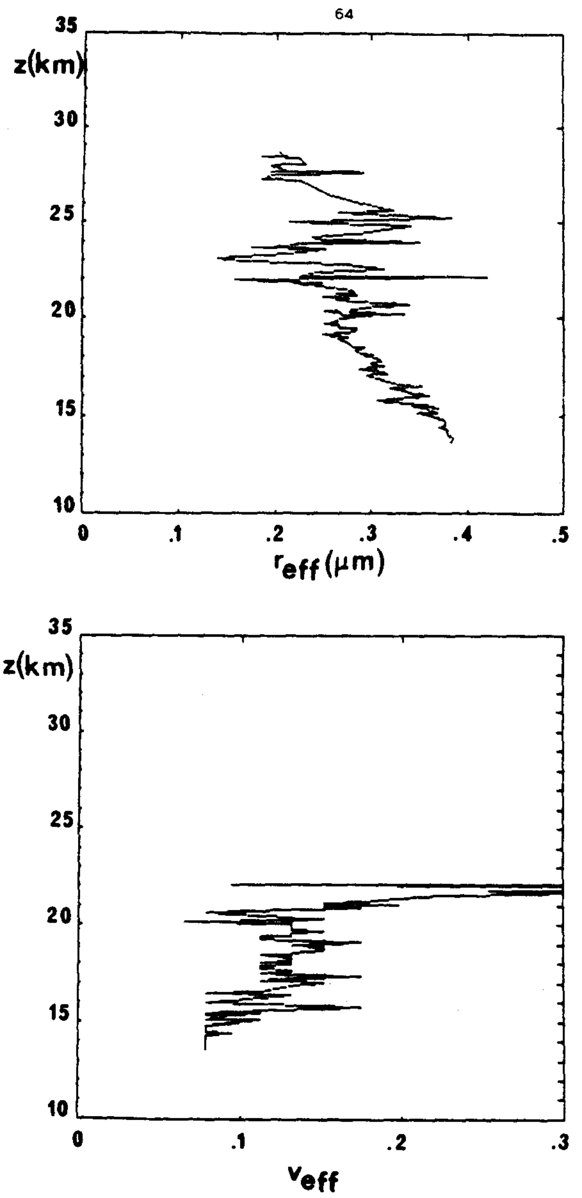

Fig. 15. (Top) Vertical profiles of the effective radius and (bottom) of the effective variance of the aerosol size distribution retrieved from the balloon polarimetric data on October 12, 1985.

5. The size distributions derived from the balloon polarization measurements and from SAGE II spectral extinction generally agree; the extinction ratio profiles $\sigma^{aer}(\lambda)/\sigma^{aer}(1.02)$ at 0.525, 0.453, and 0.385 μm, computed with the size distribution retrieved from the polarization measurements on October 12, 1985, agree well within the error bars with the corresponding SAGE II profiles (Figure 18). This is again a satisfying validation of the SAGE II short wavelength channels.

6.2. *Altitude Range Above 25 km*

Above 25 km, the situation is not as good. Most instruments failed in observing the low content of aerosols at these altitudes, and only a few data remain available: ruby lidar profiles on November 27, 1984, and April 21, 1985, and limb photograph profiles on April 22, 1985. Even these available data are not of the same quality as at lower levels. On the other hand, whereas the SAGE II profile at 1.02 μm remains

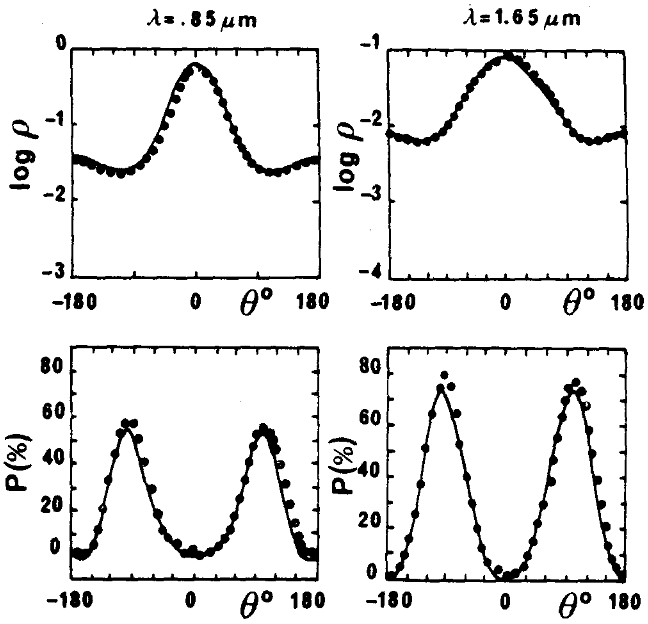

Fig. 16. Test of the inversion of the balloon polarimetric data on October 12, 1985. The dots are the measured values, which are to be compared with the curves computed with the retrieved aerosol model. (Top) Reflectance at 0.85 μm (left) and 1.65 μm (right). (Bottom) Degree of polarization in percent at 0.85 μm (left) and 1.65 μm (right) versus the scattering angle.

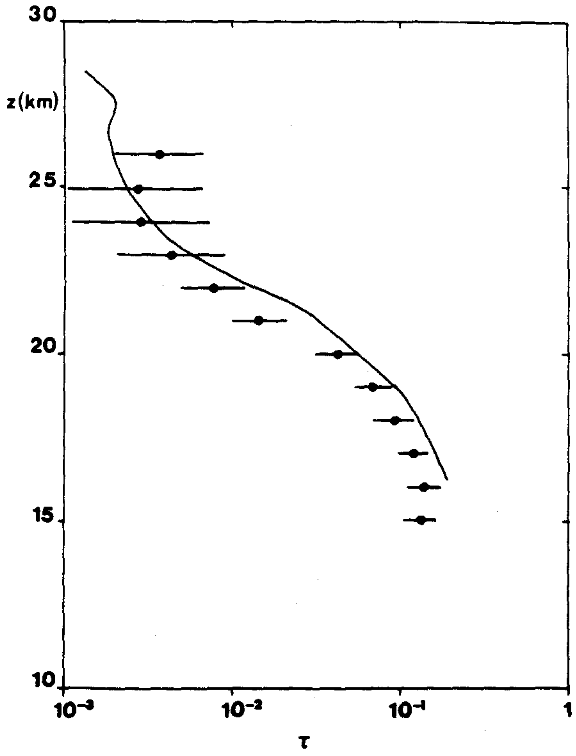

Fig. 17. Comparison of the tangent optical depth at 1.02 μm, measured by SAGE II on October 12, 1985, at 0639 UT, 41.25°N, −7.10°E (solid curve) and by the balloon polarimeter on October 12, 1985, at sunset, launch site 44°N, 0° (solid circles). The conversion of the balloon data from 0.85 to 1.02 μm has been made with the aerosol model retrieved from the polarization data.

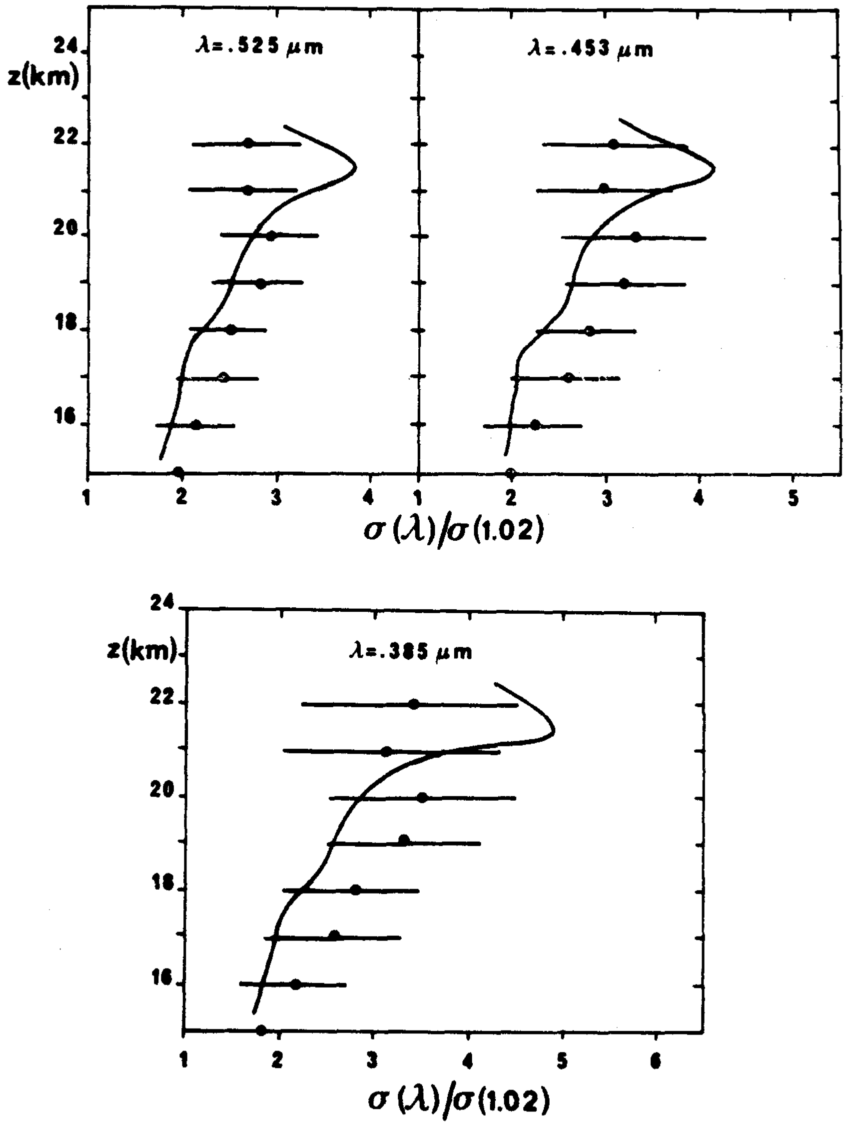

Fig. 18. Comparison of the aerosol extinction ratio $\sigma^{aer}(\lambda)/\sigma^{aer}(1.02)$ measured by SAGE II on October 12, 1985, at 0639 UT, 41.25°N, 7.10°E (solid curve) and computed using the aerosol model retrieved from the balloon polarization data on October 12, 1985, at sunset, launch site 44°N, 0° (solid circles); (Top) Curve on left, $\lambda = 0.525$ μm, curve on right, $\lambda = 0.453$ μm. (Bottom) curve shows $\lambda = 0.385$ μm.

rather good up to 30 km, the three short-wavelength profiles have increasingly large error bars above 25 km. The main conclusions for the high altitude range are the following:

1. The extinction profiles at 1.02 μm deduced from the lidar backscattering profiles can be put into agreement with the SAGE II profiles (Figures 3 and 6), using for the conversion of backscattering into extinction an aerosol model with very small particles ($r_{eff} \simeq 0.10$ μm to 0.05 μm). This choice is inconsistent with the size distribution derived from the SAGE II spectral variation of extinction, which leads to $r_{eff} \simeq 0.18$ μm. In this size range the conversion factor of backscattering into extinction is very sensitive to the aerosol model, and choosing $r_{eff} = 0.18$ μm would destroy the agreement of the SAGE II and the lidar profiles in Figures 3 and 6.

2. The limb photography profile at 0.84 μm agrees perfectly well (Figure 12) with the 1.02-μm SAGE II profile converted at 0.84 μm (conversion not very sensitive to the model choice).

3. The limb photography profiles at the short wavelengths show extinction significantly larger than SAGE II (Figures 10 and 11). This suggests particles with r_{eff} smaller than 0.18 μm, but the very large oscillations of the profiles do not allow a retrieval of r_{eff}.

Whereas a good validation of SAGE II aerosol extinction profiles is obtained below 23 km, it seems difficult to draw a clear conclusion from the few observations above 25 km. It is likely that the SAGE II 1.02-μm profile, which has small error bars, remains good. But the three SAGE II short-wavelength channels, as well as the ruby lidar profile and the limb photographs, have very large uncertainties at these high levels; it is hard to decide what must be better believed.

A very tentative guess to explain at least a part of the contradiction at high altitudes is that the size distribution becomes bimodal; for a fixed value of the ratio $\sigma^{aer}(0.45)/\sigma^{aer}(1.02)$, it has been shown [*Lenoble and Brogniez*, 1985] that the lidar conversion factor generally increases when a second mode is added to a size distribution. Qualitatively, this could reconciliate the SAGE II spectral extinction with the choice of the conversion factor necessary to have agreement between the lidar and the SAGE II 1.02-μm profile. This could also explain the bad quality of the polarization data inversion and the rapid increase of v_{eff} above 23 km.

Acknowledgments. The authors are grateful to the organizations that have provided financial support for their participation in this program. The success of the balloon flights is due to the efficient help of the staff of The CNES center at Aire sur l'Adour. The SAGE II data were kindly provided by the NASA Langley Research Center.

REFERENCES

Ackerman, M., C. Lippens, and C. Muller, Stratospheric aerosol properties from Earth limb photography, *Nature*, *292*, 587–591, 1981.

Ackerman, M., C. Lippens, and D. De Muer, Wave signature in stratospheric aerosols, *Geophys. Res. Lett.*, *12*, 445–447, 1985.

Ackerman, M., W. Chu, C. Lippens, and D. De Muer, SAGE II aerosol extinction and scattering data from balloon borne photography, *Adv. Space Res.*, *7*, 243–249, 1987.

Brogniez, C., and J. Lenoble, Size distribution of stratospheric aerosols from SAGE II multiwavelength extinction, in *Aerosols and Climate*, edited by P. V. Hobbs and M. P. McCormick, pp. 305–312, A. Deepak Publishing, Hampton, Va., 1989.

Chu, W. P., M. P. McCormick, J. Lenoble, C. Brogniez, and P. Pruvost, SAGE II inversion algorithm, *J. Geophys. Res.*, this issue.

Herman, M., J. Y. Balois, L. Gonzalez, P. Lecomte, J. Lenoble, R. Santer, and C. Verwaerde, Stratospheric aerosol observations from a balloon-borne polarimetric experiment, *Appl. Opt.*, *25*, 3573–3584, 1986.

Hofmann, D. J., J. M. Rosen, R. Reiter, and H. Jäger, Lidar- and balloon-borne particle counter comparisons following recent volcanic eruptions, *J. Geophys. Res.*, *88*, 3777–3782, 1983.

Lenoble, J., Presentation of the European correlative experiment program for SAGE II, *J. Geophys. Res.*, this issue.

Lenoble, J., and C. Brogniez, A comparative review of radiation aerosol models, *Contrib. Atmos. Phys.*, *57*, 1–20, 1984.

Lenoble, J., and C. Brogniez, Information on stratospheric aerosol characteristics contained in the SAGE satellite multiwavelength extinction measurements, *Appl. Opt.*, *24*, 1054–1063, 1985.

Oberbeck, V. R., J. Livingston, R. Pueschel, K. Snetsinger, G. Ferry, W. Fong, and S. Verma, Aerosol sampling for the August 7th, and 9th, 1985 SAGE II validation experiment, paper presented at Sixth Conference on Atmospheric Radiation, Am. Meteoral. Soc., Williamburg, Va., May 12–16, 1986.

Osborn, M. T., J. N. Rosen, M. P. McCormick, P. Wang, J. M. Livingstone, and T. J. Swissler, SAGE II aerosol correlative observations: Profile measurements, *J. Geophys. Res.*, this issue.

Russell, P. B., et al., Satellite and correlative measurements of the stratospheric aerosol, II, Comparison of measurements made by SAM II, dustsondes, and an airborne lidar, *J. Atmos. Sci.*, *38*, 1295–1312, 1981.

Russell, P. B., M. P. McCormick, T. J. Swissler, J. M. Rosen, D. J. Hofmann, and L. R. McMaster, Satellite and correlative measurements of the stratospheric aerosol, III, Comparison of measurements by SAM II, SAGE, dustsondes, filters, impactors and lidar, *J. Atmos. Sci.*, *41*, 1791–1800, 1984.

M. Ackerman and C. Lippens, Institut d'Aéronomie Spatiale de Belgique, 3 Avenue Circulaire, B1180 Brussels, Belgium.

C. Brogniez, B. S. Diallo, M. Herman, J. Lenoble and R. Santer, Laboratoire d'Optique Atmosphérique, Université des Sciences et Techniques de Lille, 59655 Villeneuve d'Ascq cedex, France.

G. Fiocco, Instituto di Fisica "Guglielmo Marconi," Universita Degli Studi Roma, Piezzale Aldo Moro 2, 1-00185 Rome, Italy.

P. Gobbi, Instituto di Fisica dell'Atmosphere, Consiglio Nazionale delle Ricerche, CP 27, 00044 Frascati, Italy.

M. Jäger, Institut für Atmosphärische Umweltforschung. Kreuzeckbahnstrasse 19, D 8100 Garmisch-Partenkirchen, Federal Republic of Germany.

G. Megie and J. Pelon, Service d' Aéronomie du Centre National de la Recherche Scientifique, B.P. 3, 91371 Verrières-le-Buisson, France.

R. Reiter, Consulting Bureau, Fritz Müllerstrasse 54, D 8100 Garmisch-Partenkirchen, Federal Republic of Germany.

(Received April 4, 1988;
revised February 3, 1989;
accepted February 3, 1989.)

CORRELATIVE MEASUREMENTS OF THE STRATOSPHERIC AEROSOLS

Santer, R.,, C. Brogniez, M. Herman, S. Diallo, M. Ackerman, M.P. Mc Cormick

(1) Laboratoire d'Optique Atmosphérique, Université des Sciences et Technologies de Lille,
59655 Villeneuve d'Ascq cedex, France.
(2) Institut d'Aéronomie Spatiale de Belgique, Brussels, Belgium.
(3) Atmospheric Sciences Division, NASA Langley Research Center, Hampton, Virginia, USA.

ABSTRACT

Joint experiments were organized or available during stratospheric flights of a photo-polarimeter, referred as RADIBAL. In May 1984, RADIBAL flown simultaneously with an other balloon-borne experiment conducted by the "Institut d'Aéronomie Spatiale de Belgique" which provides multi-wavelength vertical profiles of the aerosol scattering coefficient. At this time, the El Chichon layer was observable quite directly from mountain sites. A ground-based station set up at Pic du Midi allowed an extensive description of the aerosol optical properties. The IASB and the Pic du Midi observations are compatible with the aerosol properties derived from the RADIBAL measurement analysis. The ability of RADIBAL to retrieve the vertical profile of the aerosol extinction coefficient was also proved during a winter arctic campaign by comparison to SAM II data and to airborne lidar data. As a result, RADIBAL appears to be a good candidate for in situ validations of the SAGE II experiment and its derived products.

I - INTRODUCTION

After the El Chichon eruption, during the spring 1982, special attention was paid to the stratospheric aerosol observations. Taking advantage of the CNES facilities to launch stratospheric balloon, we developped, at the University of Lille, a photo-polarimeter, referred as RADIBAL, devoted to be set up on a gondolla. A first flight in December 1983 was carefully analysed in two articles (Herman et al, 1987; Santer et al, 1988). This first flight corresponded to constant level measurements. Since that time, this experiment has probed the stratospheric layer on a routine basis twice a year, both during ascent and descent of the balloon. Our first goal is to adapt our previous inversion scheme to the balloon trajectory.

On the other hand, in different circumstances, we had opportunities to fly simultaneously with other experiments. First, in May 1984 a ground-based station was set up at "l'Observatoire du Pic du Midi". From this 3000 m elevation site and with a stratosphere highly polluted by El Chichon, the stratospheric layer was quite directly accessible. During the same campaign, photographies at limb were performed as reported by Ackerman et al (1986). The intercomparison of the different techniques describing the stratospheric aerosol will be achieved.

The participation of RADIBAL to the CHEOPS (CHEmistry Of the Polar Stratosphere) experiment in January 1988 allowed to compare our measurements to SAM 2 data and to the NASA lidar data which simultaneously flown onboard a DC8.

II - THE PHOTOMETRIC EXPERIMENT - RADIBAL

II-1 - Principle of the experiment, expression of the signal

A detailed description of the instrument is given in Herman et al (1987) and is briefly recalled here. Every minute, the instrument measures the radiance and the degree of polarization of the sky light in horizontal directions at three wavelengths : 850 nm, 1350 nm and 1650 nm. The photo-polarimeter is horizontally set up on the gondolla of a stratospheric balloon which is rotated at a uniform rate of 1 r.p.m. At sunset or at sunrise, the radiometer scans the full range of scattering angles between 0 and 180 degrees.The horizontal stability of the gondolla is controlled by an inclinometer while its azimut is measured by a two axis magnetometer. The solar angles are computed from the location of the balloon recorded every 20 seconds.

We now propose a simple formulation of the signal. The radiance is converted into reflectance ρ expressed in the primary approximation versus the scattering angle Θ by :

$$\rho(\Theta) = \frac{t(h_s,\Theta)}{4}(\delta_a^s\ p_a + \delta_R^s\ p_R + (\delta_a^s + \delta_R^s)\ 2\rho_G \sin h_s) \qquad (1)$$

The subscripts a and R stand respectively for aerosols and Rayleigh. δ^s is the slant optical thickness. Primary scattering from the direct solar beam is proportionnal to the phase function p. The last term corresponds to primary scattering from light reflected by the Earth-troposphere system that is described by its reflectance ρ_G. This term depends upon the solar elevation h_S . The relevant isotropic contamination is proportionnal to the total optical thickness. The transmission term describes both the attenuation of the direct solar beam to reach an elementary scattering element within the field of view (F.O.V.) of the instrument and the attenuation of the diffuse light. In equation (1), we suppose the aerosols constant in nature with the altitude and uniformly mixed with the molecules. This last hypothesis allows us to factorize the transmission term which averagely describes the attenuation of the solar beam and of the diffuse light. Santer et al (1988) shown that this formulation is still quite valid if the mixture between Rayleigh and aerosols is no longer constant.

The polarization ratio

$$P = \frac{\delta_a^s p_a P_a + \delta_R^s p_R P_R}{\delta_a^s p_a + \delta_R^s p_R + (\delta_a^s + \delta_R^s)\ 2\rho_G \sin h_s} \qquad (2)$$

depends upon the degree of polarization of the aerosol P_a and of the molecules P_R. In equation (2), the transmission term, which affects in the same way the total reflectance and the polarized reflectance, is simplified and the tropospheric contamination is supposed to be unpolarized.

Equations (1) and (2) correspond to the primary scattering approximation. Santer et al (1988), using a Monte Carlo code to include the multiple scatterings, proved the validity of this approximation.

II-2 - Computation of the signal

At a given level z, we characterize the aerosols by their size distribution n(r), their refractive index and their abundance.

The size distribution is described by a log-normal law

$$n(r) = \frac{1}{r\sqrt{2\pi}\,\sigma} \exp\left(-\frac{\ln^2 r/r_m}{2\sigma^2}\right) \qquad (3)$$

with two flexible parameters : the mean radius r_m and the variance σ.

In standard conditions (i.e. except for Polar Stratospheric Clouds (PSC)), the aerosols will be considered as hydrated sulfuric aerosol particles and the relevant value of the refractive index will be chosen. The aerosol abundance is proportionnal to the scattering coefficient σ_a integrated here with the altitude, in respect to the geometry of the experiment, to get the slant optical thickness $\delta_a{}^s$. Finally, at a given altitude z, the aerosols are described by r_m, σ and $\delta_a{}^s$.

The two other contributors to the signal are the Rayleigh scattering, which is computed from the measurement of the barometric pressure at the balloon level, and the scattering of the diffuse tropospheric light. The determination of the tropospheric reflectance ρ_G requires a special attention. We first need to point out that the influence of this term is reduced by working around the sunset or the sunrise. A method to get ρ_G, is described in Santer et al (1988). The balloon is maintained at the same altitude long enough to observe the effects of the ground contribution when the solar elevation varies, the aerosols being identical one can derive ρ_G through :

$$\frac{1}{P} = \frac{1}{P^o}\{1 + C\,\rho_G \sin h_s\} \qquad (4)$$

where P^o is the polarization ratio for $h_s = 0$ and C is a constant.

This strategy was conducted for sunrise flights with an over-night ascent and a constant ceiling after the sunrise, providing the required h_s variations, before the descent, for which the gondolla is quite stable, could start. For sunset flights, we tried to maintain the altitude of the balloon at the end of the descent to wait for the sunset. Unfortunately it appears technically difficult to stabilize the balloon. An alternative is to take advantage of available measurements during both the ascent and the descent at the same altitude (i.e. with the same aerosols) for different solar elevations. Since the gondolla is much more stable during the descent, we will invert the signal for a set of ground reflectance values. Then we assume that the aerosols are identical during the ascent at the same altitude and we compare the measurements to the computation achieved with the invert model. The fit provides the suitable values of the ground reflectances at the two wavelengths.

II-3 - The inversion scheme

Four basic steps are involved in the inversion.

i) - The aerosol slant optical thickness $\delta_a{}^s$ is derived from the calibrated reflectance measurement at λ = 1650 nm and for Θ = 30°. This angle is selected because the phase function for that angle is quite independent upon the nature of the aerosols. Moreover, the Rayleigh scattering and the tropospheric light influences are small in the forward direction. The wavelength λ = 1650 nm is selected to reduce the molecular scattering and because the aerosol slant optical thickness is much weaker at this wavelength, so that the $\delta_a{}^s$ retrieval from the reflectance is more accurate. Effectively if we only consider the aerosol contribution, we can express the reflectance as

$$\rho(30°, h_S = 0°) = \frac{\delta_a^s . e^{-\delta_a^s}}{4} p_a \tag{5}$$

at sunrise, or as

$$\rho(30°, h_S > 5°) = (1 - e^{-\delta_a^s}) \frac{p_a}{4} \tag{6}$$

when the sun is high enough above the horizon (i.e. h_s > 5°). In these two cases, optical thicknesses of the order of one raises problem. Such values can be found in lower altitudes at λ = 850 nm. Conversely, at λ = 1650 nm, the sensitivity of ρ to $\delta_a{}^s$ is suitable with decreasing optical thicknesses when the wavelength increases.

ii) - We now consider the degree of polarization at Θ = 90° and λ = 1650 nm. The value of Θ = 90° corresponds to the maximum of polarization. The behavior of P versus the particle size is quite simple : starting from the Rayleigh regime and decreasing when the particle size increases. For a set of σ, the retrieval of the measurement is done via equation (2) using a dichotomy method on r_m. Since at λ = 1650 nm the Rayleigh scattering contribution is weak, the computation of the degree of polarization via equation (2) is not critically sensitive to $\delta_a{}^s$. A standard value of p_a in the $\delta_a{}^s$ retrieval, already provides a good guess for equation (2). The two first steps are iterated one time. The final results is a serie of values of (r_m, $\delta_a{}^{1650}$) for a selected set of σ.

iii) - For each solution, the degree of polarization at $\Theta = 90°$ for $\lambda = 850$ nm, is computed by using equation (2), and is compared to the corresponding measurement. When σ decreases, the wavelength dependence of the phase matrix is more important, so the computed polarization ratio P_a increases continuously with decreasing σ and the measurement retrieval provides an unique solution.

iiii) - Finally, for a complete scan, we compare the measurements at 850 nm and 1650 nm both for the reflectance and for the degree of polarization to the respective computations using equations (1) or (2). This procedure is achieved mainly to confirm the aerosol retrieval when the layer homogeneity is sufficient.

II-4 - Example of results

We apply our inversion scheme to the May 13, 1984 flight launched from the CNES balloon center at Aire sur l'Adour (43.°4N - 0.°15E). Figure 1 gives the main characteristics of this flight versus the UT time. The vertical profile corresponds to a rapid ascent with instability of the gondolla as indicated by the inclinometer data. The balloon was stabilized during one hour at 22 km altitude. Then the descent was stopped at 15 km and an attempt to stabilize the balloon was done to wait the sunset but the balloon slightly went up. The balloon reached three times the altitude 17 km. The depolarization by the tropospheric light corresponded to $\rho_G = 0.30$ at 850 nm and to 0.27 at 1650 nm.

As an example the retrieved diagrams obtained after inversion with $r_m = 0.22\ \mu m$ and $\sigma = 0.36$ (i.e. $r_{eff} = 0.30\ \mu m$ and $v_{eff} = 0.14$) are compared with the measurements in Figure 2 for z = 18 km. The reflectances measured at 1650 nm are more than 10 times larger than the reflectances corresponding to the molecular scattering and the restitution of the signal is quite perfect. At 1650 nm, a slight dissymetry appears in the backward region. The restitution of the polarization is also satisfying. At 850 nm, the neutral point around $\Theta = 140°$ is a characterisation of the sulfuric refractive index. Figure 3 reports the vertical distribution of the retrieved aerosol slant optical thicknesses at the two wavelengths. Between 14 km and 18 km, measurements correspond both to the descent (crosses) and to the small ascent (stars) at the end of the flight. The same altitudes are probed at different solar elevations, corresponding to different effects of the tropospheric light, and the good agreement between the two data sets indicates that ρ_G was correctly estimated. The ratio between the optical thicknesses at the two wavelengths is quite independent on the altitude, with an Angstrom coefficient around two.

The retrieved vertical profile follows almost an exponential law

$$\delta_a^s(z) = \delta_a^s(z_0)\, e^{-(z-z_0)/H_a} \qquad (7)$$

where $H_a \approx 3.7$ km.

In this case, the extinction coefficient is related to the slant optical thickness by

$$\sigma_a = \frac{\delta_a^s}{\sqrt{\frac{\pi R H_a}{2}}} \approx \frac{\delta_a^s}{200} \qquad (8)$$

where R is the Earth radius. A typical value of σ_a (850 nm) at 15 km is then 5.10^{-3} km^{-1}. Finally Figures 4 give the vertical profile of the effective radius and of the effective variance as defined by Hansen and Travis (1974). The characteristics of the particles are quite stable in altitude with $r_{eff} \approx 0.32$ µm for $v_{eff} \approx 0.15$; one can observe only a slight decrease of these parameters when the altitude is increasing.

III - VALIDATION OF THE RESULTS

We will verify, through comparisons, the ability for RADIBAL inverted models to describe correctly the aerosol layer, by means of the extinction coefficient profiles, and the optical properties of the medium, such as the phase function or the spectral dependence of the extinction coefficient. The preliminary critical point is to ensure that the joint experiments probe as close as possible the same air-mass or air-masses proved to be indentical. We met this opportunity two times. First during May 1984, with ground-based and balloon experiments, then during January 1988, with satellite and airborne experiments.

III - 1 - The May 1984 campaign

III-1-1 - The ground-based measurements

"L'observatoire du Pic du Midi" is located in the Pyrennées , at 3000 m elevation, 100 km south from Aire sur l'Adour. For the first flight of RADIBAL, in December 1983, the measurements indicated a vertical aerosol optical thickness of 0.10 at 850 nm for the stratospheric layer. We could then expect a significant contribution of the stratosphere in ground-based measurements, so a ground-based station with passive optical measurements was set up from May 4 to May 13, 1984.

a) - Optical thickness measurements

Two sun radiometers were used. The first one, using a silicium detector, has five bands in the range 450 nm- 860 nm while the second uses a cooled Pbs detector with the same bands plus the three atmospheric windows in the middle infrared at 1050 nm, 1650 m and 2200 nm. The two radiometers were calibrated using the Langley-Bouguer technique, the measurements provided then the aerosol vertical optical thicknesses. The Rayleigh optical thicknesses are derived from the barometric pressure measurements and the ozone optical thicknesses in the Chapuis band are computed from the climatologic ozone contents.

Figure 5 is a plot of the vertical aerosol optical thickness versus time at λ = 525 nm for the four dates available. The aerosol optical thickness is varying from 0.12 to .20. Since the stratospheric layer is usually quite stable with time, these variations are certainly due to the variable contribution of the troposphere. Figure 6 reports the spectral variations of the optical thicknesses observed at 10 am for the four dates. The main feature is the null spectral dependence in the visible. In the middle infrared the optical thicknesses decrease sharply; nevertheless, we need to be carefull in a quantitative use of these data. First, in regards with the small values of δ_a^v , of the order of the calibration error. Second, the measurements may be slightly affected at 1650 nm and 2200 nm by the water vapor absorption which was not corrected, assuming a negligible water vapor content above the Pic du Midi.

b) - Aureola measurements

The aureola is measured at 850 nm in the almucantar region. After pointing the sun, the 1° F.O.V. radiometer is rotated in azimut. Table 1 reports the data and the time of the measurements plus the air-mass and the aerosol vertical optical thickness at 850 nm on May 1984. All the measurements are normalized assuming a standard value of five for the phase function at Θ = 30°. The iterative scheme developped by Weinman et al (1975) was applied to correct the multiple scatterings. In these conditions, figure 7 is a plot of the measurements listed in table 1. The lower curve corresponds to the first set and all the curves are translated to each othors by a constant. All the measurements are quite identical except the 12 th and 13 th which present a sharper forward peak correlated to an increase of the optical thickness. Additional large tropospheric aerosols are very probably involved in the increase of the forward scattering.

c) - Polarization measurements

A twin photopolarimeter of the stratospheric instrument was scanning in the principal plane. Limited results are reported in figure 8. The slight decrease of the maximum of the polarization with time corresponds to the depolarization by the ground since this effect is known to be proportionnal to $\sin(h_s)$(equation 2).

d) - Inversion of the measurements

Different strategies can be conducted in the analysis of the ground based measurements. Devaux et al. (1987) suggest to combine an inversion method of the optical thicknesses as proposed by King et al. (1978) with an inversion method of the aureola as suggested by Santer and Herman (1983). When dealing with tropospheric aerosols, the deduced aerosol size distribution is quite insensitive to the particle refractive index. The polarization measurements are then used to determine this refractive index.

The goal here is to check the RADIBAL performances. The analysis is then based on the polarization measurements with a scheme quite identical to that of the balloon experiment. We also combine the degrees of polarization at Θ = 90° for the two wavelengths to derive the two flexible parameters of the log-normal size distribution. Simply, the computation of the signal suits the experimental conditions. A successive orders of scattering code is used to include the multiple scatterings. Moreover, the measured aerosol vertical optical thicknesses are used as inputs.

The inversion scheme was applied to the set of measurements obtained on May 13 at 5.20 am. The measured optical thickness is δ_a^v (850 nm) = 0.072. We first assumed that the signal had a stratospheric origin and the refractive index of the particles was then supposed to be 1.45. We got then r_m = 0.33 µm and σ = 0.35 (i.e. r_{eff} = 0.45 µm and v_{eff} =0.13). Then with this model, we simulated the various measurements. The measurements are compared with the computations (dashed lines) in figure 9. The measured polarization is quite correctly retrieved at the two wavelengths (Figures 9a-b). In the forward scattering, the model underestimates the aureola measurements in the first 10 degrees (Figure 9c). For the vertical optical thicknesses, the model predicts an unobserved decrease in the visible toward the blue. In the infrared, due to large uncertainties in the measurements, the comparison is unrealisable (Figure 9d).

A second inversion was made in an attempt to correct from the tropospheric contribution. We already pointed out that the variations of the observed optical thicknesses may originate from the troposphere. According to the WMO, a standard continental model with δ_a(550 nm) = 0.02 occupies the troposphere above the limit layer. We then corrected the signal from this tropospheric contamination The inversion of the polarization gives slightly smaller particles, with r_m = 0.32 µm and σ = 0.34 (i.e.with r\S\do5(eff) =0.43 µm and v_{eff} = 0.12). The ground-based measurements were simulated again with this two-layer model. The results are reported in Figure 9 (full lines). We can observe that the aureola measurements are now correctly retrieved and in the same way, that the flat spectral behavior of the optical thicknesses in the visible range is correctly fitted.

e) - Comparison with the RADIBAL results

We already saw (equations 7 and 8) how to convert approximately the slant optical thicknesses measured by RADIBAL into extinction coefficients all along the RADIBAL vertical profile, i.e. above 15 km. From radio-sondages we know that the tropopause was located at 8 km. If we suppose that the aerosol vertical distribution is exponential with the scale height equal to 3.7 km derived from figure 3, we get δ_a^v (850 nm) = 0.057, that is quite consistent with the ground-based measurement, i.e. 0.059 obtained when removing the tropospheric background (Figure 6).

In term of size distribution, we averaged the r_{eff} and v_{eff} profiles, weighted by the slant optical thickness, over the ballon vertical profile and get $r_m = 0.25\ \mu m$ and $\sigma = 0.36$ (i.e. $r_{eff} = 0.34\ \mu m$ and $v_{eff} = 0.14$). From the ground-based measurements, as seen previously, we derived larger particles with $r_m = 0.32\ \mu m$ and $\sigma = 0.34$ (i.e. $r_{eff} = 0.43\ \mu m$ and $v_{eff} = 0.12$). To interprete this discrepancy we can point out that the layer probed by RADIBAL only represents 40% of the stratospheric layer, and that a general trend of the particle size is to increase towards lower altitudes. On the other hand, from the ground-based measurements, we only introduced the troposphere background. Figure 5 where the measured optical thicknesses were drawn, indicated that May 13 was the turbidest day. If the tropospheric contamination is more important than supposed, then the ground-based measurements should provide smaller particles for the stratosphere.

III-1-2 - The limb experiment

A companion balloon equipped by IASB (Institut d'Aéronomie Spatiale de Belgique) was flown during the same period.

In the IASB experiment, images of the solar disk are taken from the gondolla of a stratospheric ballon stabilized above the stratospheric layer at 30 km height. Three Asselblat cameras are used, equipped with three filters at 440 nm, 650 nm and 840 nm. A first image of the sun is taken when the sun is high above the horizon. This reference image corresponds to a transmission equal to one. Then we have a serie of pictures after the sunset. For each image, the sun is viewed below the horizon at different tangent altitudes. The film sensitivity is measured using calibrated transmission plates and an absolute calibration is realized on the moon when it is high above the horizon. The film is digitalized and the result is a series of transmission factor for sun-to-balloon paths at different tangent altitudes below the gondolla.

An onion peal method is then applied to derive the vertical profile of the extinction coefficient (Ackerman et al, 1981). The results, reported on the Figure 10 after removing the Rayleigh contribution, indicate an inhomogeneous structure above the Junge layer. The blue and red vertical profiles are quite identical and we retrieve the null spectral dependence of the aerosols optical thicknesses measured from "Le Pic du Midi".

The extinction coefficients at 850 nm are converted into slant optical thicknesses with :

$$\delta_a^s(z) = \sqrt{\frac{R}{2}} \int_z^\infty \frac{\sigma_a(z')}{\sqrt{z'-z}} dz' \qquad (9)$$

The results, plotted on figure 11, compare favorably to the RADIBAL measurements.

III - 2 - The January 1988 campaign

RADIBAL was flown from Kiruna (Sweden) during the CHEOPS experiment on 01/28/88. On this day a set of data was acquired by SAM II at an approximate latitude of 70°N in the range of longitude (3°W - 30°E). Moreover, the rubis lidar of NASA airborne was flown on this day. These two data sets will be compared with the RADIBAL results.

III -2-1 - SAM II data

SAM II measures the extinction of the solar irradiance at $\lambda = 1020$ nm for the slant path at a tangent altitude z. After removing the residual Rayleigh optical thickness, the aerosol slant optical thicknesses are inverted to provide a vertical profile of the aerosol extinction coefficient. The nine recorded aerosol vertical profiles showed a quite stable aerosol layer. On a map of Scandinavia, Figure 12, we reported the two SAM events which bounded the RADIBAL trajectory. The SAM profile obtained at 7:56 GMT for a tangent point at (69.9°N, 28.3°E) is included in the error bars of the second profile obtained at 9:36 GMT for (69.9°N, 13.8°E) (Figure 13). This winter was mild and no PSC were recorded. Moreover, the air-masses were confined and isolated in the vortex. We had then a very stable and homogeneous situation.

The comparison with RADIBAL is done in Figure 14. The RADIBAL measurements confirmed the spatial homogeneity up to 22 km altitude where the Junge layer is vanishing. Along the profile probed (between 200 hp and 35 hp), the hydrated sulfuric acid aerosols are quite stable with and effective radius of $r_{eff} = 0.33 \pm 0.02$ µm for an effective variance of $v_{eff} = 0.10 \pm 0.02$.
The RADIBAL slant optical thicknesses at 1020 nm are computed using the spectral dependence of the inverted model deduced from the 1650 nm slant

optical thickness measurements. The two full-line curves correspond to the extreme SAM data obtained when taking into account the error bars. The agreement between the two experiments is very good.

III-2- 2 - Lidar measurements

During CHEOPS, PSC observations were performed by a rubis lidar ($\lambda = 532$ nm) set up on the NASA aircraft. Description of the apparatus is reported in Osborn et al. (1989) A joint flight with the RADIBAL experiment was planed on January 28th, 1988. Table 2 gives the conditions of the lidar measurements and Figure 15 reports the backscattering ratio derived from the lidar data:

$$R = \frac{\sigma_a p_a + 1.5\,\sigma_R}{1.5\sigma_R} \qquad (10)$$

where p_a is the aerosol phase function in backscattering. R is normalized at an altitude of 24 km assuming that the aerosol abundance is quite null at this altitude. R is a function of the altitude; σ_R is proportionnal to the barometric pressure and depends upon the temperature. Radio sondages are used to derive the P-T vertical profile and R can then be converted into an aerosol backscattering coefficient

$$b_a = \frac{\sigma_a p_a}{4\pi} \qquad (11)$$

To compare with RADIBAL, we need to integrate the lidar data over the slant path, we compute then a slant backscattering coefficient B_a for the lidar measurements as :

$$B_a^L(z) = \sqrt{\frac{R}{2}} \int_0^{\infty} \frac{b_a(z')}{\sqrt{z' - z}}\, dz' \qquad (12)$$

Using the log-normal distribution deduced from the RADIBAL measurements, the aerosol phase function p_a at $\Theta = 180°$ is computed at 532 nm. In the same way, using the spectral dependence of the model, the aerosol slant optical thickness is deduced at 532 nm from the 1650 nm measurements. The result is a slant backscattering coefficient

$$B_a(z) = \frac{\delta_a^S(z)\, p_a}{4\pi} \qquad (13)$$

The comparison is reported in Figure 16. In the main layer, the agreement is achieved within 20%. The discrepancies at the lower altitudes result from RADIBAL unaccuracies. These points correspond to sun position below the horizon and the atmospheric transmittances are difficult to estimate. Above the layer the behaviors of the two data sets are identical. The slight shift between the two kinds of measurements is certainly a related problem in altitude-pressure conversion.

IV - CONCLUSIONS

We first adapted the RADIBAL inversion scheme to suit the descending flight and we applied this strategy to the May 13, 1984 and to the January 28, 1988 measurements.

The analysis of the RADIBAL measurements is quite coherent with those based on polarization measurements done at "Le Pic du Midi". That indicates that the modelization of the signal in the spherical atmosphere of RADIBAL fits a more simple approach in a plane-parallele atmosphere at Le Pic du Midi. Moreover, the availability of complementary measurements on the ground-based station, such as multispectral extinction measurements or aureola measurements, offered an opportunity to verify the ability of the RADIBAL inverted model to retrieve the main optical properties of the medium.

The last section has shown the comparison of various measurements of the extinction coefficient, such as limb photographies, occultation measurements and lidar measurements, with RADIBAL predictions when the spatio-temporal coïncidence is suitable. The good agreements prove RADIBAL to be a good candidate to validate SAGE-II products and a further work will deal with this problem.

Acknowledgments. We acknowledge C. Devaux and P. Lecomte for data collection at "Le Pic du Midi", and the CNES for technical assistance during the balloon experiments. This work has been supported by the "Comité Atmosphère Moyenne".

=	Date	Hour	m	δ_a^V	P(2°)
1	04/05	8h10	1.7	0.048	26.5
2	04/05	13h18	1.18	0.068	35.9
3	07/05	5h21	8	0.055	21.5
4	07/05	6h27	3	0.055	25.5
5	09/05	9h50	1.2	0.063	29
6	09/05	14h35	1.4	0.048	29
7	09/05	15h06	1.6	0.048	26.2
8	09/05	15h44	1.7	0.044	26.5
9	09/05	16h24	2.5	0.043	25.7
10	10/05	6h39	2.4	0.043	24.5
11	10/05	7h14	2.1	0.053	27
12	10/05	8h21	1.5	0.073	34.5
13	10/05	9h13	1.7	0.078	35
14	13/05	7h00	2.25	0.068	20
15	13/05	7h41	1.75	0.063	21.6
16	13/05	8h32	1.51	0.058	22.2
17	13/05	9h11	1.35	0.058	23
18	13/05	9h51	1.2	0.063	23

Table 1 - Aureola measurements. One have reported the date and the hour of the starting measurements , the viewed air-mass, the aerosol vertical optical thickness and the phase function at 2°.

Shot =	1	2	3	4	5	6
Start-time	14h34	14h45	14h59	15h12	15h22	15h30
end-time	14h42	14h57	15h09	15h21	15h28	15h39
latitude N	67.7	67.7	68.2	68.1	67.9	67.8
	- 67.7	68.3	68.1	67.9	67.8	68.0
longitude	21.3	23.0	21.6	21.5	22.8	22.7
E	22.6	21.6	21.2	22.7	22.9	21.5

Table 2 - Conditions of the lidar measurements. Start-time and end-time are in GMT. Range in latitudes and longitudes during the shot.

REFERENCES

Ackerman, M., C. Lippens and C. Muller, "Stratospheric aerosol prospectives from Earth limb photography". Nature, 292, 587-591, 1981.

Devaux, C., M. Herman, R. Santer and D. Tanré, "On the complementarity of solar transmission and aureola measurements to derivce the aerosol size distribution : application to desert aerosol characteristic retrievals". Proceedings of the International Radiation Symposium, Lenoble and Geleyn editors. A. Deepak Publishing, 557-560, 1989.

Herman, M., J.Y. Balois, L. Gonzalez, P. Lecomte, J. Lenoble, R. Santer and C. Verwaerde, "Stratospheric aerosol observations from a balloon-borne polarimetric experiment". Appl. Opt. 25, 3573-3584, 1986.

King, M.D., D.M. Byrne, B.M. Herman and J.A. Reagan, "Aerosol size distributions obtained by inversion of spectral optical depth measurements". J. Atmos. Sc., 35,2153-2167, 1978.

Osborn, M.T., J.M. Rosen, M.P. McCormick, Pi-Huan Wang, J.M. Livingston and T.J. Swissler, "SAGE II aerosol correlative observations : profile measurements". J. Geophys. Res.,94,D6, 8353-8366, 1989.

Santer, R. and M. Herman, "Particle size distributions from forward scattered light using the Chahine inversion scheme". Appl. Opt., 22, 15, 2294-2301, 1983.

Santer, R., M. Herman, D. Tanré and J. Lenoble, "Characterization of the stratospheric aerosol polarization measurements". J. Geophys. Res. 93, 14209-14221, 1988.

Weinman, J.A., J.T. Twitty, S.R. Browing and B.M. Herman, " Derivation of phase functions from multiply scattered sunlight transmitted through a hazy atmosphere". J. Atmos. Sc., 32, 577-583,1975.

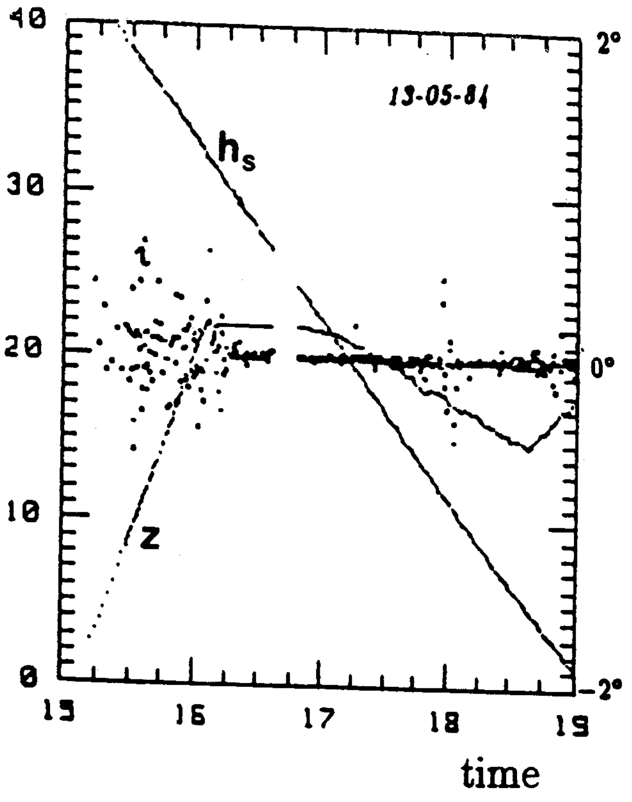

Figure 1 - Main characteristics of the May 13, 1984 flight. Balloon altitude (z in km), solar elevation (h_S in degree, left scale) and platform inclinaison (in degree, right scale) are plotted versus UT time.

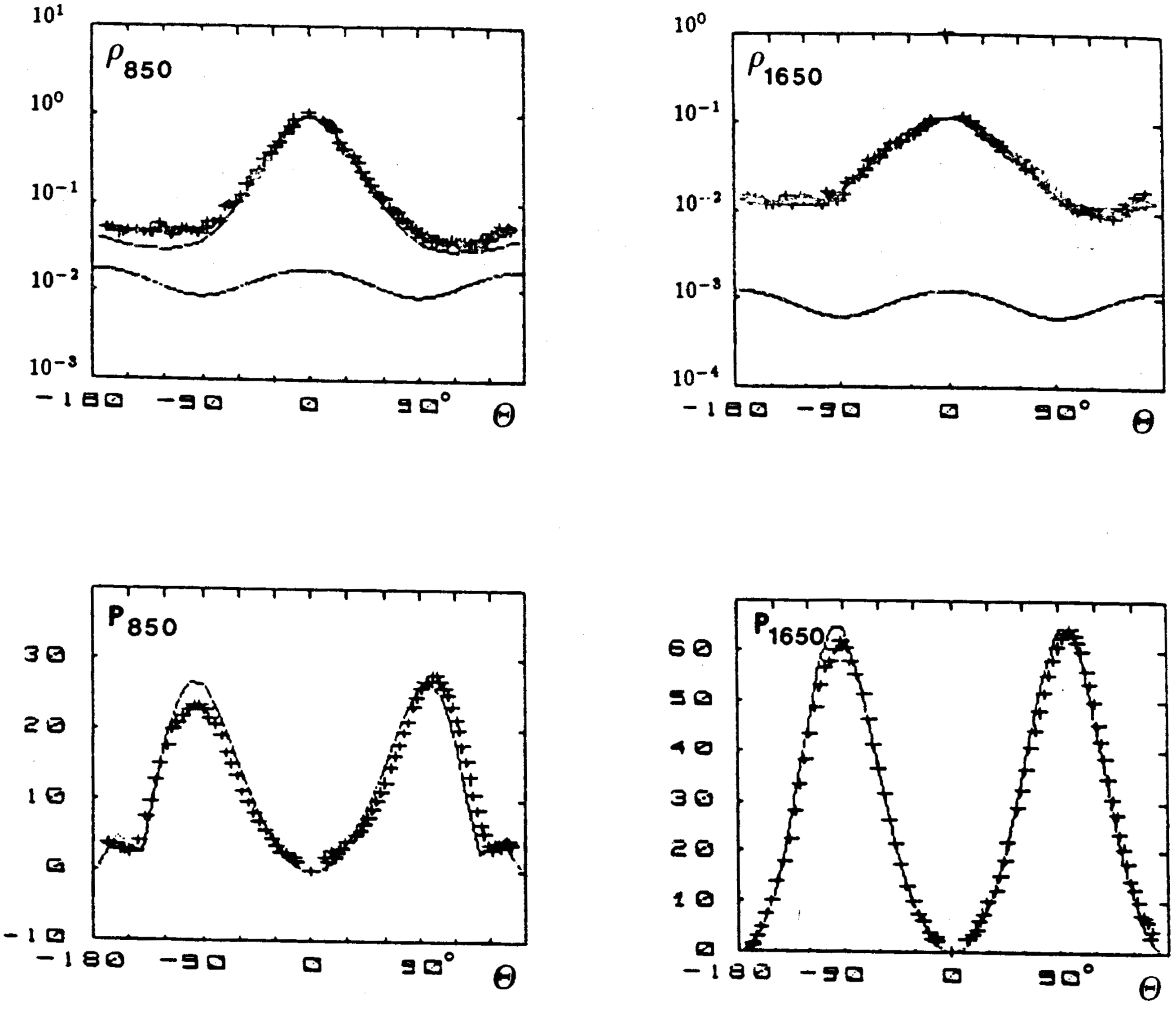

Figure 2 - Restitution of a sequence of measurements taken on May 13, 1984 at z = 18 km during the descent with the inverted model deduced from the polarization measurements at Θ = 90° (r_m = 0.22 µm for σ = 0.36). The measurements (plusses) are plotted versus the scattering angle (negative values correspond to the half space containing the North). For the two wavelengths, we plotted the reflectance (in log scale) and the degree of polarization (in percent). The computed signals are in full line and for the reflectances we added (lower curves) the intrinsec molecular reflectance.

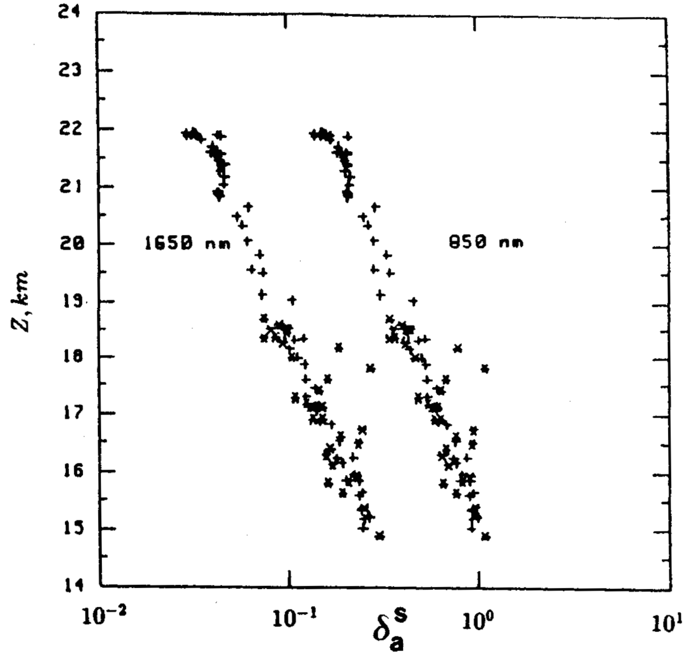

Figure 3 - Vertical profiles at the two wavelengths of the aerosol slant optical thicknesses on May 13, 1984. Crosses stand for the descent whole stars stand for the ascent.

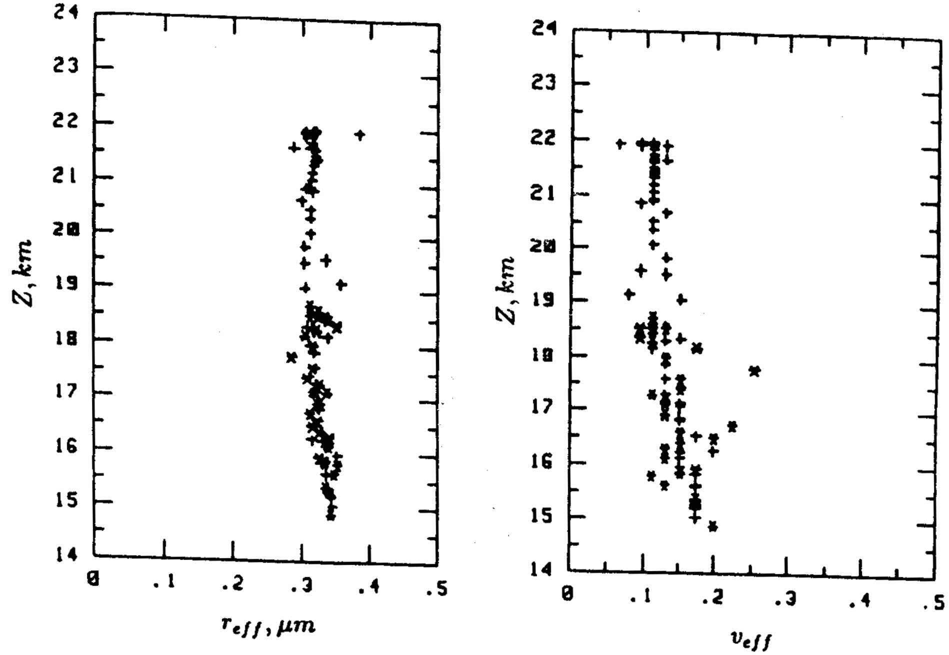

Figure 4 - Effective radius and effective variance of the aerosols versus altitude on May 13, 1984.

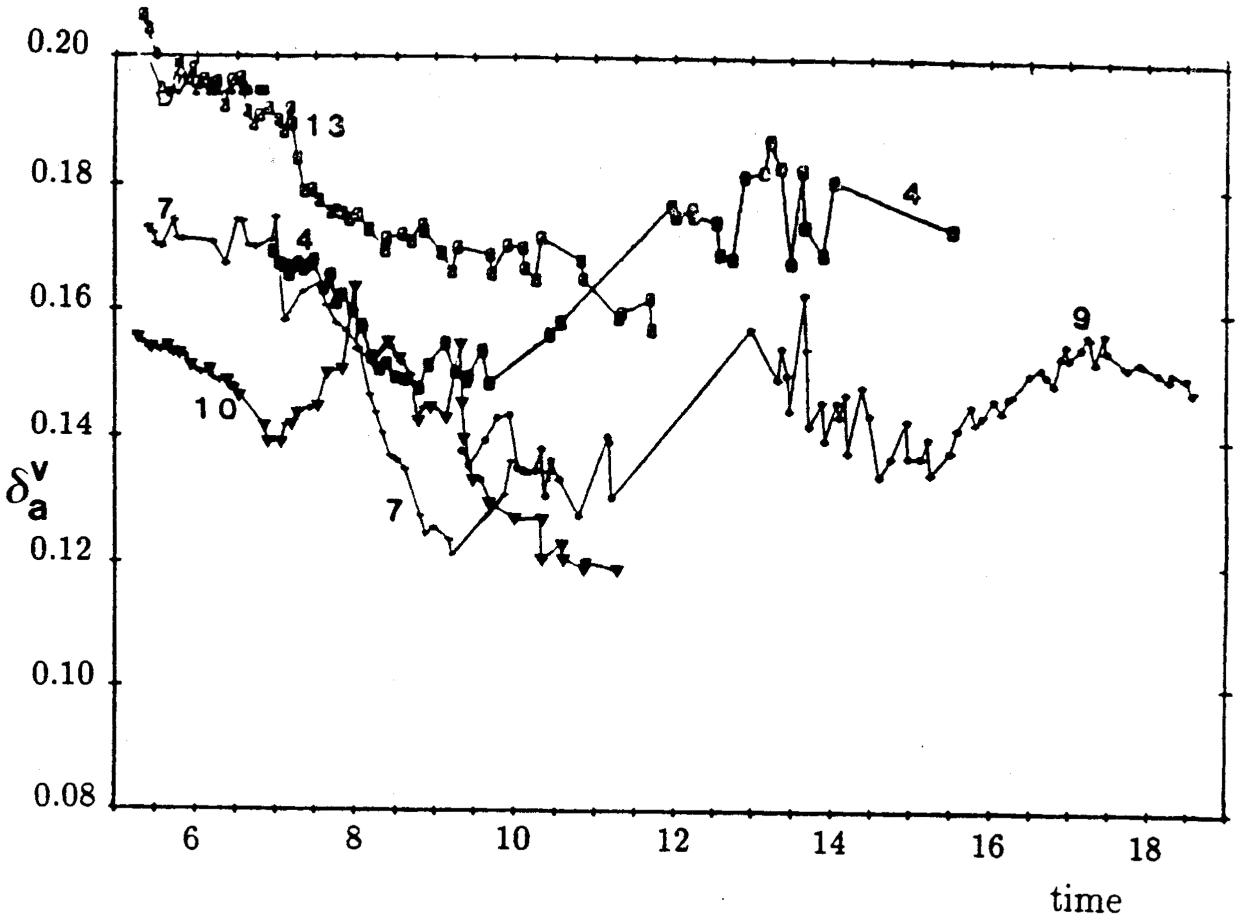

Figure 5 - Aerosol vertical optical thicknesses, measured at λ = 525 nm, from "L'Observatoire du Pic du Midi" in May 1984 versus UT time. The day number is labelled on each curve.

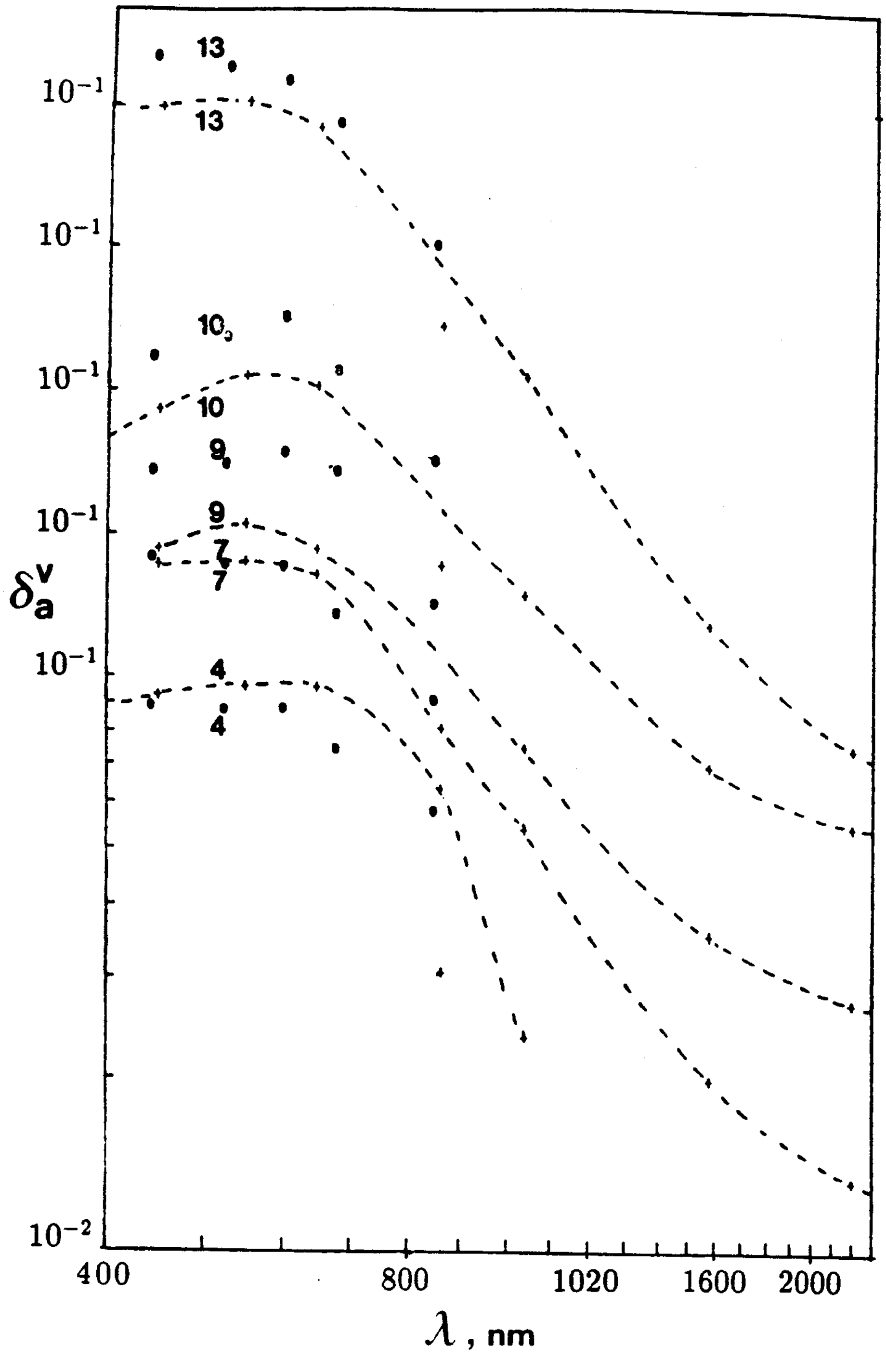

Figure 6 - Aerosol vertical optical thicknesses at the same dates as Figure 5, versus wavelength at 10 am. The vertical scale is given for May 4 and the curves are uniformly translated for each day. Dots correspond to the Si detector while black circles stand for the Pbs detector.

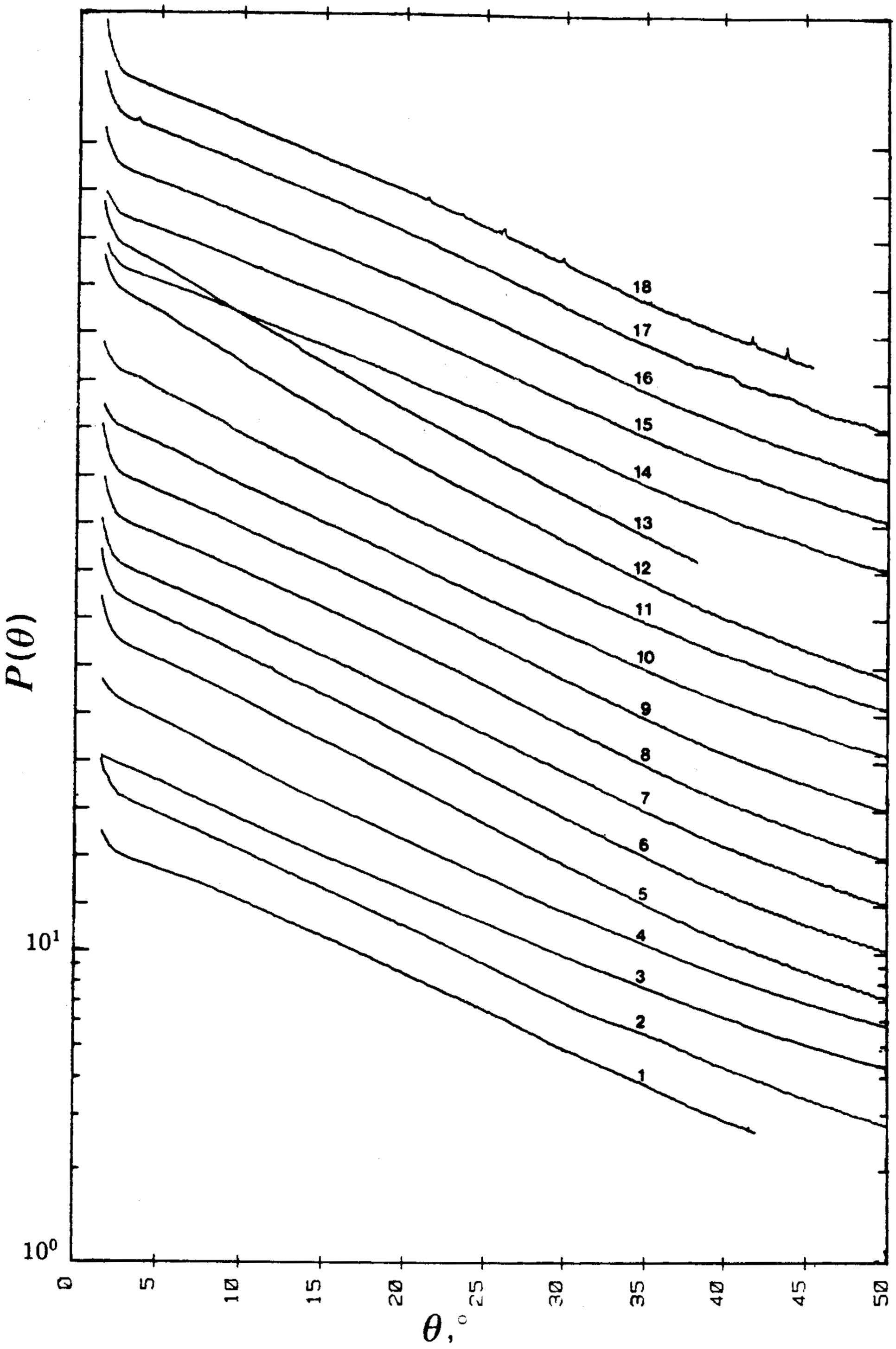

Figure 7 - Aerosol phase functions deduced of the aureola measurements listed on Table 1. The vertical log-scale is given for the first measurements. All sets are uniformly translated from each to other.

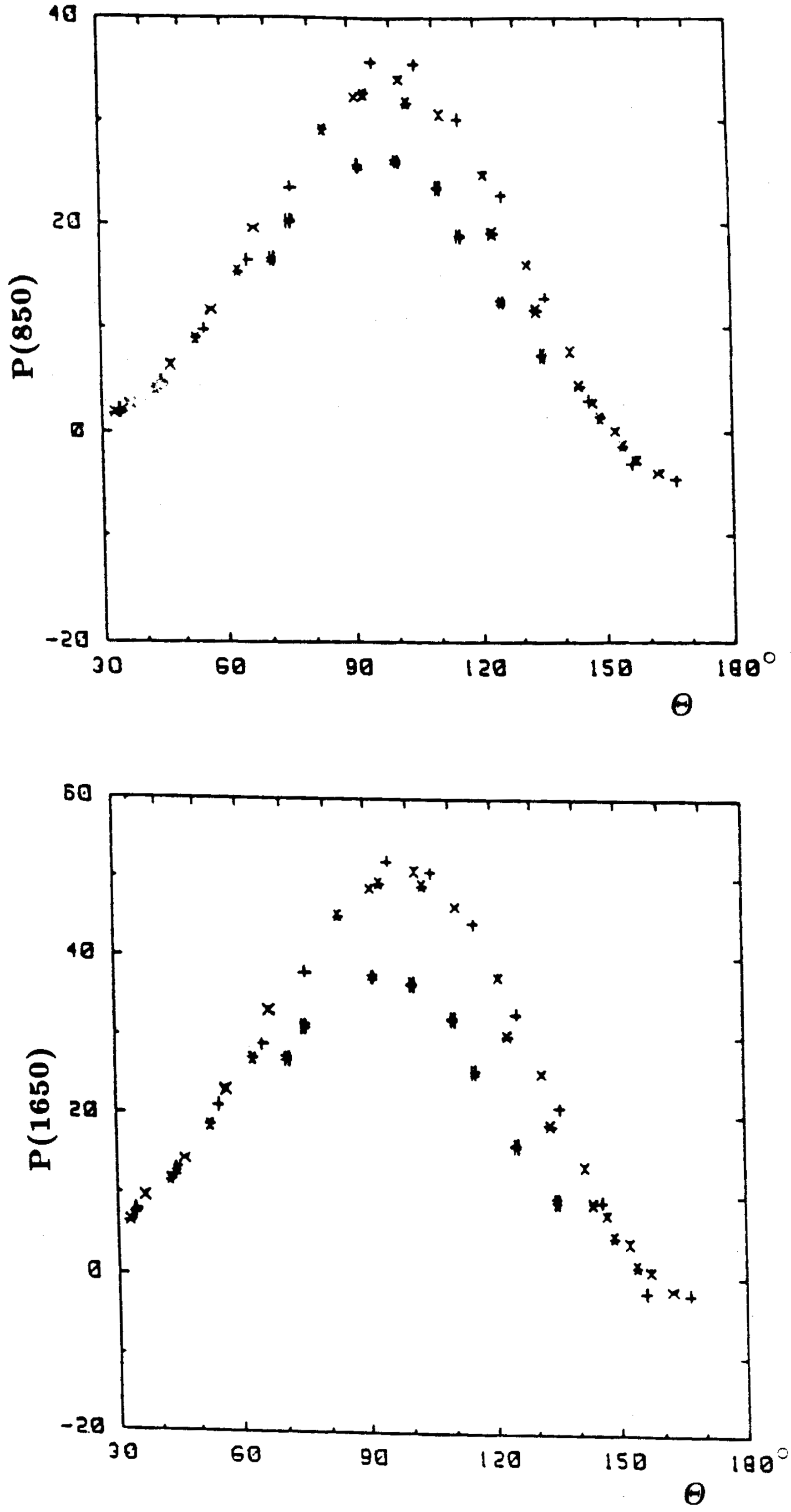

Figure 8 - Ground-based polarization measurements from Le Pic du Midi on May 10 at 7.50 am (✱), May 13 at 5.20 am (+), May 13 at 6 am (x) and May 13 at 6.30 am (*)for the two wavelengths 850 nm and 1650 nm. Measurements correspond to the principal plane and are plotted versus the scattering angle.

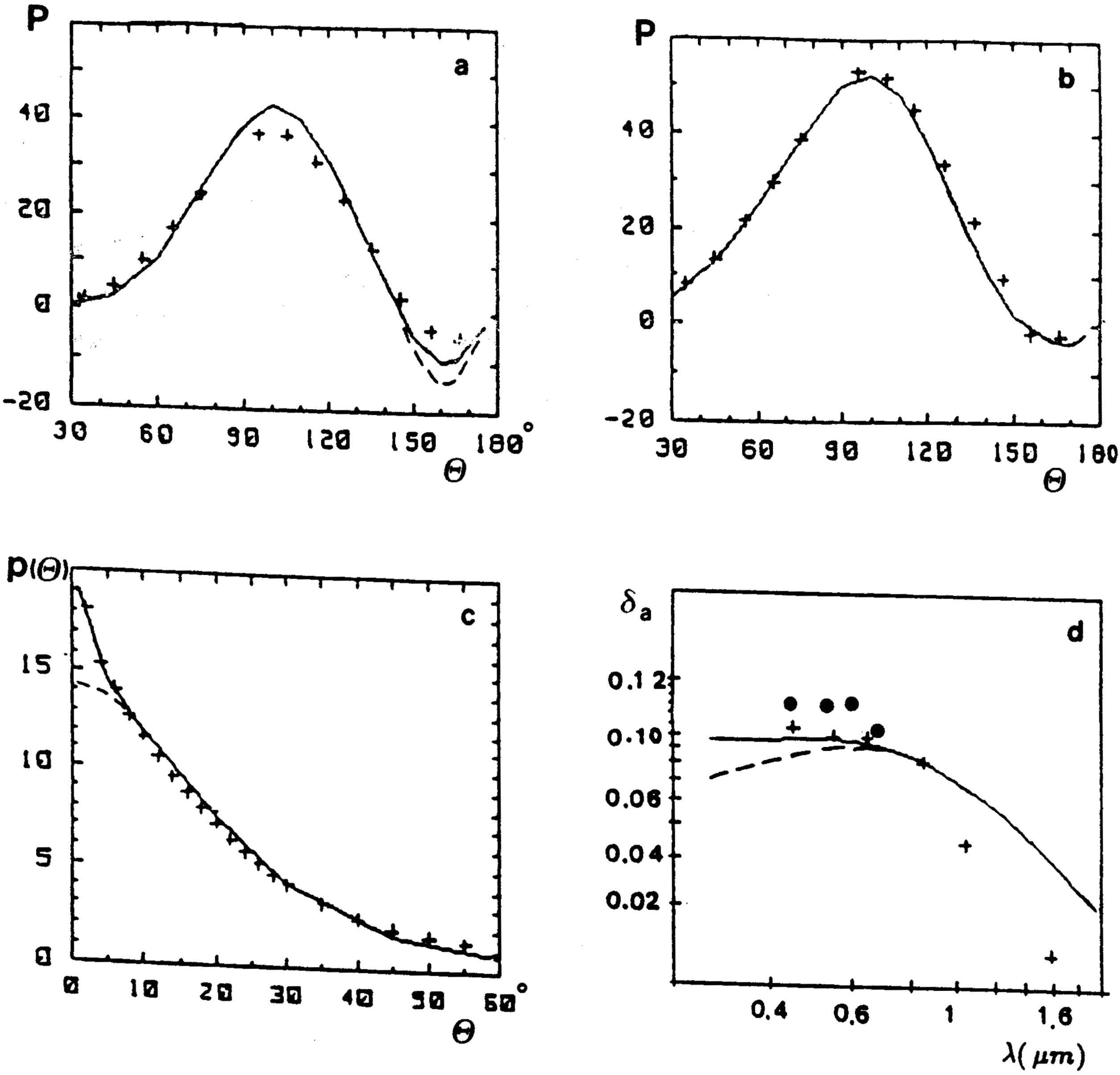

Figure 9 - Restitution of the ground-based measurements on May13 with the aerosol model inverted from the polarization measurements at the two wavelengths for Θ = 90°. Percent polarization measurements (plusses) are drawn versus the scattering angle at λ = 850 nm (a) and λ = 1650 nm (b). The aerosol phase function (+) is plotted in (c) versus the scattering angle. Multispectral measurements of the aerosol optical thicknesses are graphed in (d) for the Si detector (dots) and for the Pbs detector (crosses). Dashed lines are computed for uniform aerosol layer with r_m = 0.33 μm and σ = 0.35. Full lines correspond to a two-layer atmosphere with a standard tropospheric component and a stratospheric layer with r_m = 0.32 μm and σ = 0.34 .

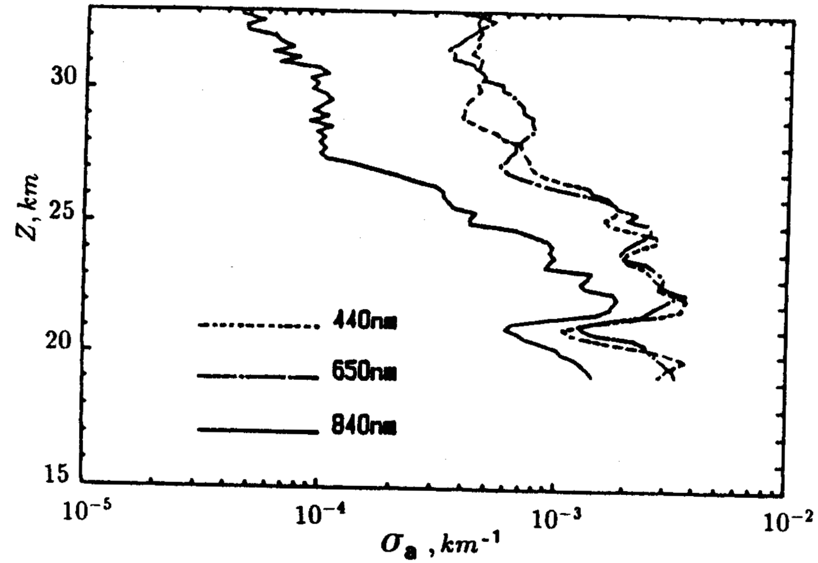

Figure 10 - Vertical profiles of multispectral aerosol extinction coefficients derived from the limb photographies.

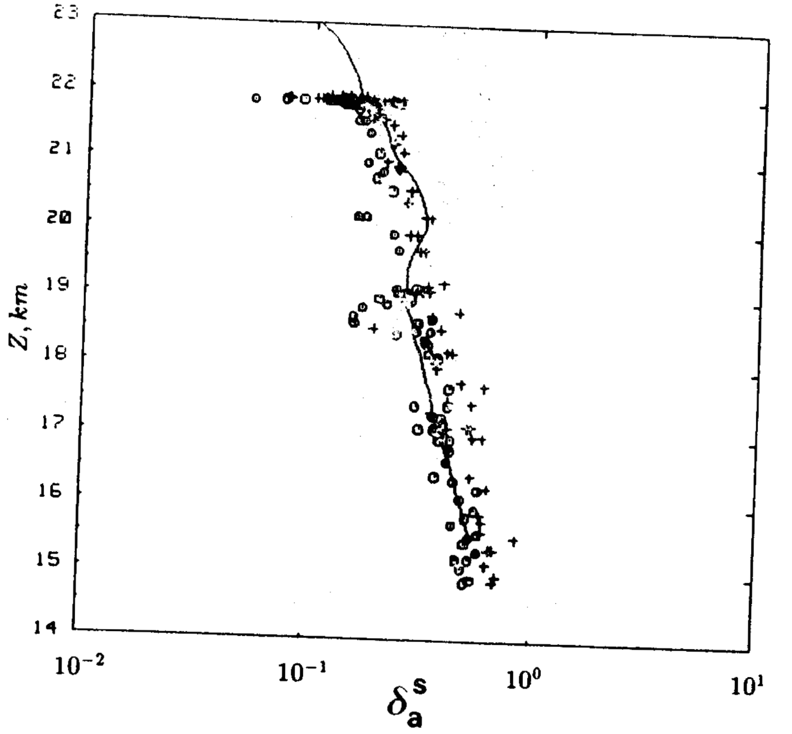

Figure 11 - Comparison of the aerosol slant optical thicknesses at 850 nm, versus the altitude, measured by RADIBAL and the limb experiment.

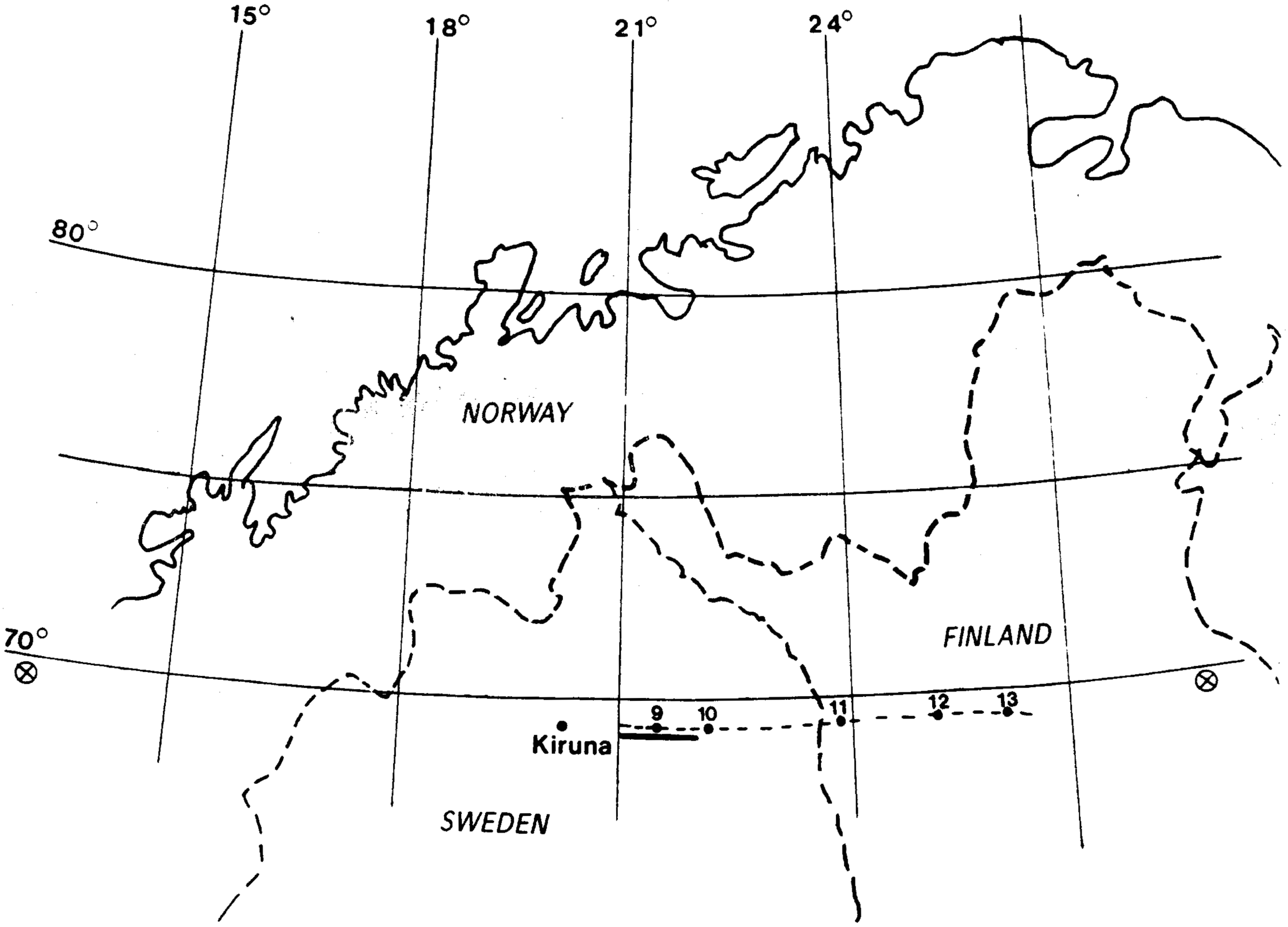

Figure 12 - Map of Scandinavia with the localisation of the joint experiments on January 28, 1988. SAMII tangent points are indicated by crossed circles. The balloon was launch from Kiruna and the dashed line represents the trajectory labelled with time every hour. The full line corresponds to the part of the NASA DC-8 trajectory where the lidar was running.

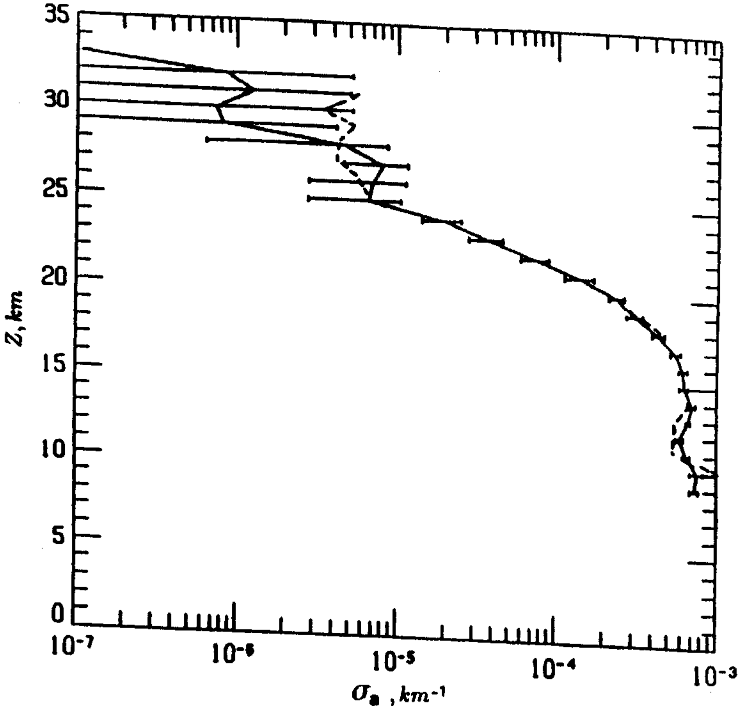

Figure 13 - Vertical profile at $\lambda = 1020$ nm of the aerosol extinction coefficient as measured by SAMII on January 28, 1988. The full line is for the event located at (69°.9N - 13°.8E) with error bars, the dashed line is for (69°.9N - 28°.33E).

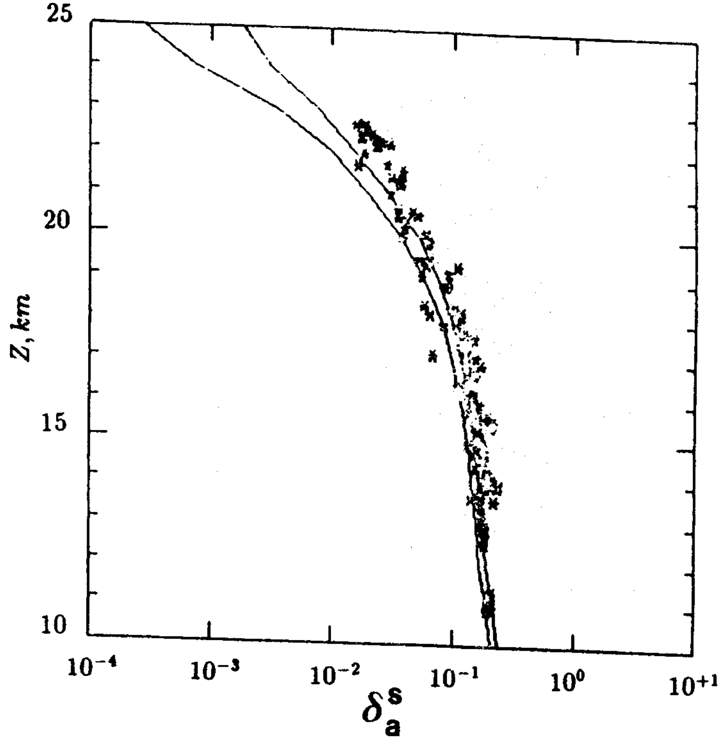

Figure 14 - Comparison of the aerosol slant optical thicknesses at $\lambda = 1020$ nm between RADIBAL (stars) and SAM II (limit full lines).

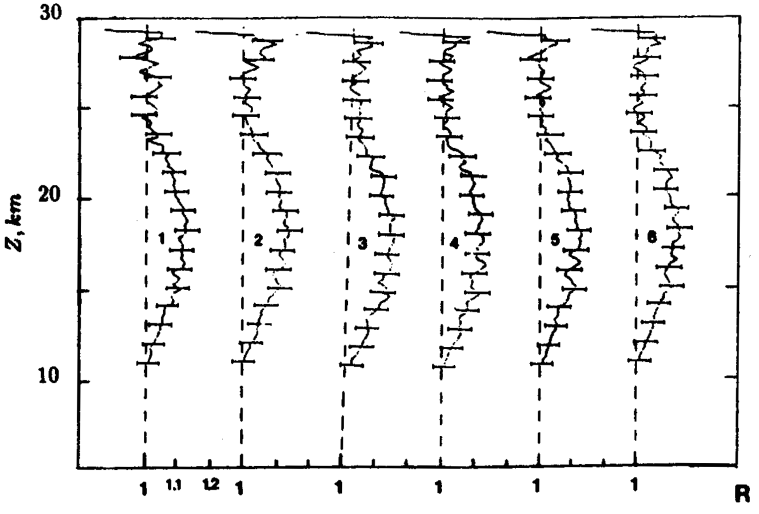

Figure 15 - Lidar backscattering ratio versus altitude measured from the NASA DC-8 in Kiruna on January 28, 1988.

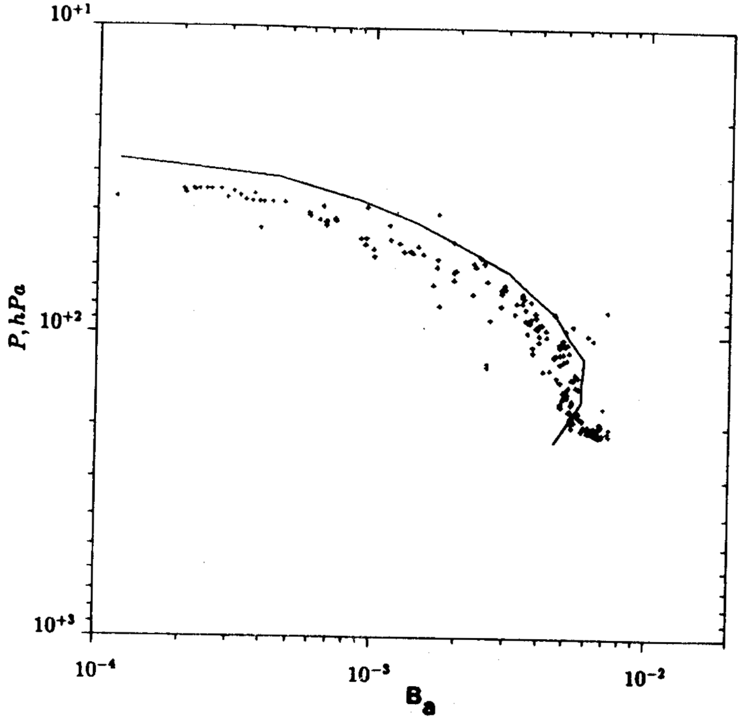

Figure 16 - comparison of the lidar slant backscattering coefficient (full line) to the RADIBAL deduced values (plusses).

Comparative Observations of Stratospheric Aerosols by ground-based Lidar, Balloon-borne Polarimeter and Satellite Solar Occultation.

C. BROGNIEZ, R. SANTER, B.S. DIALLO, M. HERMAN and J. LENOBLE

Laboratoire d'Optique Atmosphérique, Université des Sciences et Techniques de Lille
(U.A. 713 du CNRS) Villeneuve d'Ascq, France

H. JAGER

Fraunhofer-Institute for Atmospheric Environmental Research
Garmisch-Partenkirchen, Federal Republic of Germany

Abstract

The analysis of European correlative experiments of the stratospheric aerosol layer is performed for three periods. These independent experiments are lidar measurements obtained at Garmisch-Partenkirchen, balloon measurements of the reflectance and of the polarization achieved at Aire sur l'Adour with RADIBAL experiment and transmission measurements provided by the SAGE II experiment. Comparisons of the slant optical thicknesses are performed, and the agreement is generally good. Two different schemes are used to retrieve two parameters of the size distribution from the polarization and from the transmission spectral measurements. The discrepancies that appear in few cases for the radius comparison are studied.

1 Introduction

Stratospheric aerosols are studied since years with different and very efficient methods such as lidar measurements (Hamill et al., 1980, Jäger et al., 1984), occultation measurements (McCormick et al. 1979, Mauldin et al., 1985) and also in situ transmission (Ackerman et al., 1981) or polarization (Herman et al., 1986) measurements from balloon.

In Europe, stratospheric lidar measurements are mainly performed at OHP (Observatoire de Haute Provence, France), Frascati, Florence (Italy) and Garmisch-Partenkirchen (FRG). They were used for SAGE II (Stratospheric Aerosol and Gas Experiment) European correlative experiments in conjunction with balloon measurements from the RADIBAL experiment (RADIomètre à BALayage) and from the transmission experiment of IASB (Institut d'Aéronomie Spatiale de Belgique) achieved at Aire sur l'Adour (France).

Some results leading to satisfying comparisons have been already published for few periods : 10-13 November 1984, 26-30 November 1984, April 1985, October 1985 (Ackerman et al., 1989). The goal of this paper is to detail some more correlative experiments that were performed in April 1986, October-November 1987 and April 1989, with particular attention to the error budget of the respective experiments. During April 1986 and October-November 1987 two independent kinds of experiments were achieved (lidar at Garmisch-Partenkirchen and balloon polarization) in near coïncidence with SAGE II occultations, whereas during April 1989 the lidar instrument had to work without ruby fluorescence suppression; therefore, the resulting lidar profiles are limited in height and accuracy and were not used in the intercomparison.

In a first step we will verify the agreement between the vertical profiles of the aerosol optical thicknesses derived from the various experiments. In a second step we will check the procedures used to derive the aerosol size distribution either from the spectral variation of the aerosol extinction coefficient or from the polarization feature.

2 Description of the experiments.

2.1 SAGE II experiment.

Transmittances of the atmosphere at seven wavelengths in the visible and the near infrared are available from solar occultation measurements by SAGE II, and slant optical thicknessess δ are then derived.

The aerosol extinction coefficients σ are deduced after correction of the molecular contribution and, when necessary, of the gaseous contribution, at four channels centered at 1020, 525, 453 and 385 nm. We use here the vertical extinction profiles obtained with the Laboratoire d'Optique Atmosphérique inversion procedure that leads to results similar to those obtained with the NASA Langley Research Center procedure (Chu et al., 1989).

The four wavelength measurements allow to retrieve the aerosol size distribution. Several methods can be used (Yue et al., 1986, Livingston and Russell, 1989). The method used in this paper leads to an effective radius and an effective variance by assuming a log-normal aerosol size distribution (Brogniez and Lenoble, 1988).

Schematically, the spectral variation of the measured extinction coefficient is correctly fitted by adjusting α and β in the analytical two parameter expression

$$ln\ \sigma(\lambda) = ln\ \sigma(1.02) - \alpha\ ln\ (\lambda/1.02) - \beta\ (ln\ (\lambda/1.02))^2 \tag{1}$$

rather than the simple Angström law.

Comparison with similar fits obtained for aerosol models with log-normal size distribution

$$n(r) = \frac{1}{\sqrt{2\pi} r\ ln\ s}\ exp(-\frac{(ln(r/r_m))^2}{2(ln\ s)^2}) \tag{2}$$

(where r_m and s are the modal radius and the variance) lead to identify, from α and β, the two parameters r_m and s, or preferably the effective radius and the effective variance (Hansen and Travis, 1974, Lenoble and Brogniez, 1984) related to r_m and s by

$$r_{eff} = r_m\ exp(2.5\ (ln\ s)^2)\ ,\ \ v_{eff} = exp(ln\ s)^2 - 1 \tag{3}$$

Calculations for the log-normal aerosol models are performed with Mie routines, for spherical particles consisting of aqueous sulfuric acid with 75% H_2SO_4 by mass, as is usually done (Russell and Hamill, 1984, Rosen and Hofmann, 1986), over the whole range of altitudes; the spectral dependance of the refractive index is taken from Palmer and Williams (1975).

2.2 Lidar experiment.

The lidar system consists of a pulsed ruby laser emitting at 694.3 nm and a 52 cm diameter Cassegrain telescope as receiving system. Atmospheric backscatter data are sampled at night time with a height resolution of 600 m by a 64 channel photon counter. Typically, 200 laser returns are averaged to obtain a backscatter profile. The net particle backscattering is obtained by matching the measured total signal with a calculated Rayleigh return (from Munich radiosonde data, 100 km from Garmisch-Partenkirchen) above the aerosol layer, where the particle backscattering is assumed to be negligible. Backscattering profiles are corrected for molecular scattering and transmission losses.

Jäger and Hofman (1991) have demonstrated the good agreement between in situ particle measurements performed at Laramie, Wyoming (41°N), and lidar backscattering measurements performed at Garmisch-Partenkirchen (47.5°N). Consequently, a height and time resolved aerosol model has been derived from the Laramie data to convert midlatitude particle backscattering to extinction. The same model is then used to compute the extinction coefficient at any other wavelength λ.

From each Laramie data set, single mode log-normal size distributions, as defined in section 2.1, have been evaluated with a 1 km height resolution. From Mie calculations of the backscatter and extinction coefficients at appropriate refractive indices, two conversion factors, $\text{extinction}_{694.3}/\text{backscatter}_{694.3}$ and $\text{extinction}_{\lambda}/\text{extinction}_{694.3}$, have been computed. According to the investigations of Russell and Hamill (1984) the range of refractive indices of 1.44 to 1.45 have been used in the Mie calculations, which refer to sulfuric acid/water droplets with a sulfuric acid mass percentage of 65-80. The conversion factors have been then averaged over 5 km intervals and applied to the lidar backscattering data to derive the aerosol extinction coefficients.

2.3 Balloon experiment.

The measurements of the intensity and of the polarization of the sunlight scattered by the stratospheric aerosols are performed at 1650 and 850 nm by a balloon-borne polarimeter, during the balloon ascent and/or descent. At each altitude the rotation of the platform allows us to get measurements at several scattering angles.

The inversion process consists in comparing the reflectance and polarization diagrams with single scattering calculations performed for a set of log-normal size distributions given by equation (2), for spherical 75 % H_2SO_4 droplets, by using the Mie theory. Notice that, because of the absolute calibration of the channels, the reflectance data allow to retrieve the aerosol slant optical thickness.

In fact, in that procedure we have to take into account the molecular contribution which is very important in the 850 nm channel particularly for polarization, the ground reflectance, the multiple scatterings and the parasitic reflectance of the apparatus (Diallo, 1989). A signal modeling accounting for these various effects has been developed (Santer et al. 1988).

The inversion scheme uses first the polarization and the intensity data at 1650 nm, where the molecular influence is lesser, for the particular scattering angle 90° (close to the maximum of polarization). The comparison with theoretical values provides a list of convenient size distributions characterized by their effective radius and variance, with their optical thickness at 1650 nm and their spectral dependance.

Then, the reflectance and polarization diagrams of these models are computed at 850 nm according to the Mie theory, and are compared with the measurements. The solution is the size distribution which gives intensity and polarization diagrams closest to the measurements at that wavelength.

The aerosol slant optical thicknesses are known for this retrieved model at 1650 and

850 nm, and the slant optical thicknesses are then deduced at the SAGE II wavelengths for comparison.

3 Comparisons.

The measurements directly achieved by the various experiments, the used wavelengths, the additionnal required informations for each procedure and the derived data are presented in Table 1.

Table 1. Characteristics of the various experiments.

Experiment	Measurements	λ, nm	Required Informations	Derived Data
SAGE II	transmittances	1020-525	. .	σ_λ
	on slant path	453-385	. .	Aerosol $n(r)$
RADIBAL	intensity, polarization	1650	. .	δ_λ
	diagrams on slant path	850	. .	Aerosol $n(r)$
LIDAR	backscattering at each altitude	694.3	Aerosol models	σ_λ

From SAGE II and RADIBAL inversion a size distribution, defined by two parameters r_m and s, is deduced. The balloon and the occultation measurements give data directly correlated to the slant optical thicknesses, so that, to avoid an additional inversion in deducing the extinction coefficients from RADIBAL optical thicknesses, we will rather compute the slant optical thicknesses from lidar extinction coefficients. The comparisons will be mainly done for the 1020 nm channel, because it is the most accurate for SAGE II experiment (Chu et al., 1989) and because it lies in the RADIBAL range 850-1650 nm.

3.1 Uncertainties.

SAGE II experiment has provided several measurements for the three periods that we will consider. For each extinction value an error bar is obtained (deduced from the quadratic sum of the uncertainty due to the error on transmission measurements, the uncertainty on the Rayleigh contribution and the uncertainty on the gaseous correction). The error on each value is rather large so that, to determine whether the extinction data were valuable or not, we have compared all the extintion values available for a period at one altitude. We have reported in Table 2 at four altitudes for the four wavelengths, the relative dispersion bars RD (95% confidence intervals) on the average extinction profile and the mean relative error bars RE, for the April 86 west profiles.

Table 2. Mean relative error bars RE and relative dispersion bars RD.

z, km	1020 nm		525 nm		453 nm		385 nm	
	RE	RD	RE	RD	RE	RD	RE	RD
15.5	5.7	2.1	22.3	3.6	15.8	4.8	28.9	8.5
18.5	12.4	3.6	26.3	2.4	20.4	1.4	30.4	0.6
21.5	13.8	8.2	37.9	6.0	28.8	4.9	42.8	33.4
24.5	17.7	4.5	100.	3.3	100.	4.7	100.	8.3

The mean relative error is large mainly at high altitudes and small wavelengths. One can see that the dispersion is much weaker than the error bar, that means that the variability of the individual west profiles is not significant and therefore that we can work with an average profile to which we can attribute mean error bars. In fact the examination of these values indicates that the calculated error bars are very probably overestimated as it has been suggested by Chu et al. (1989) and Brogniez and Lenoble (1991). Then errors bars on the slant optical thicknesses are deduced from extinction error bars at each level.

The following uncertainties were considered in the evaluation of the 1020 nm extinction values from 694.3 nm lidar backscatter data : instrumental errors (signal induced noise, multiplier dead time), counting errors, matching errors, radiosonde uncertainties, errors in the computation of the two-way extinction correction (Reiter et al., 1979) and finally errors in the conversion model (Jäger and Hofmann, 1991). The error bars of the extinction coefficient at 1020 nm are computed every 3 km height levels. The error bars on lidar slant optical thicknesses are derived from extinction error bars, assuming the approximate formula

$$\delta = \sigma \sqrt{\frac{\pi R H}{2}} \tag{4}$$

where H is the aerosol scale height and R the distance to the Earth center (Diallo, 1989). For these calculations we have determined H with the lidar extinction profiles.

Finally, to evaluate the uncertainties in the RADIBAL slant optical thicknesses, we have considered the calibration uncertainty of 10%, the error on the pressure of the balloon level ($\simeq$ 2 mb), the influence of the multiple scatterings which have been approximately evaluated, the effect of the parasitic reflectance on the apparatus and the infuence of 10% error in the determination of the ground reflectance at the two wavelengths. Table 3 shows the errors induced by the five contributions and the global uncertainties at few levels for the slant optical thicknesses at 1020 nm, in percent, for the April 1986 flight.

Table 3. Slant optical thickness errors due to various causes.

z, km	calibration error	pressure error	ground reflectance	parasitic reflectance	multiple scattering	resulting total error
15.5	5.	2.	4.	2.	.1	7.
18.5	5.	8.	3.	.1	.1	10.
21.5	8.	6.	3.	5.	.1	12.
24.5	10.	11.	7.	17.	.3	24.

The less important contribution is coming from the multiple scatterings. The uncertainties become very large towards 24 km and above due to the low pressures at higher levels and due to the larger values of the solar elevation.

As for the SAGE II analysis we will limit the study of the balloon results to lower levels.

3.2 Analysis of the results.

3.2.1 April 1986 period.

In April 1986, two lidar backscattering profiles were performed on April 22 and 23 at night. RADIBAL was flown on April 21, in the morning. Covering that period, SAGE II observations were available over Europe at sunset, on April 21, 22, 23 ; that is 6 profiles (3 west profiles and 3 east profiles).

The locations of the SAGE II events are shown in Figure 1 as open squares. Black circles indicate sites of Aire sur l'Adour (A) and Garmisch-Partenkirchen (GP). We have reported in Table 4 the latitude, the longitude of the SAGE II events and their respective distances with the two sites in km.

Table 4. Distances between the various sites in km.

SAGE II events	Aire/Adour 43.4°N - 0.15°E April 21	Garmisch-Partenkirchen 47.5°N - 11°E April 22-23
21/ 48.54°N - 21.38°E	1750	770
21/ 48.34°N - 2.90°W	590	1030
22/ 45.40°N - 17.25°E	1400	560
22/ 45.18°N - 7.03°W	580	1410
23/ 42.01°N - 13.08°E	1090	690
23/ 41.77°N - 11.20°W	920	1870

In Figure 2 are drawn the six SAGE II extinction profiles at 1020 nm. It appears that they are very well gathered within 10-18 km and 22-27 km. In the altitude range 18-22 km a large dispersion appears clearly. Nevertheless one can observe that the 3 east profiles are very close together and that the 3 west profiles are gathered together too.

The dispersion bars separately evaluated for the east and west average profiles (as explained in section 3.1) are weak, so that the difference observed between the east and west measurements could mean that there are two different stratospheric aerosol layers almost stable over three days. Such an hypothesis can be confirmed by studying the winds in the stratospheric layer. An inspection of the 100mb weather chart reveals a transport over central Europe by southwesterly winds during the spring period (European Meteorological Bulletin, German Weather Service, D-6050 Offenbach). From the Munich radiosonde (100 km from Garmisch-Partenkirchen) the average wind directions for the time period April 21, 0000, until April 24, 1200, were derived, they are listed in Table 5.

Table 5. Wind direction at few levels.

pressure mb	average height km	average wind direction degree
200	11.7	237
150	13.5	238
100	16.1	222
70	18.4	200
50	20.6	168
30	23.9	128
20	26.5	107

These data indicate that below about 20 km, southerly to southwesterly winds transported stratospheric airmasses and any aerosol inhomogeneities approximately parallel to the SAGE west or east footprints. Above that altitude, the transport changed to southeasterlies and any inhomogeneities would have been transported across all observing locations.

Taking into account the difference between the east and the west profiles we will compare preferably the lidar profiles with the east SAGE II mean profile because the east events occured closer to Garmisch-Partenkirchen. For the balloon profiles which are mostly deduced from 90° scattering angle measurements, we will compare them with both SAGE II mean profiles.

In Figure 3 are drawn the two lidar extinction coefficient profiles σ at 1020 nm with error bars for the April 22 profile at certain levels. These two profiles exhibit large oscillations which are of the order of the error bars: for example the relative difference between the two profiles is 45% at 15km, 20% at 18 km, 27% at 21 km and 37% at 24 km. The comparison between lidar profiles (Figure 3) and SAGE II east profiles (Figure 2) shows that they are consistent: the lidar values are somewhat larger than SAGE II values above 21 km, but the discrepancy is of the order of magnitude of the lidar uncertainty.

The lidar slant optical thicknesses at 1020 nm are compared in Figure 4 with the mean SAGE II east profile. We have also drawn the two limiting SAGE II profiles, obtained from mean error bars, and some error bars on 22 April lidar values, evaluated as explained in section 3.1. We observe a good agreement especially in the altitude range 12-22 km; at higher altitudes lidar optical thicknesses values are greater than SAGE II mean data by a factor of 1.5-2, but SAGE II values are almost always within the lidar error bars.

Comparison between the two SAGE II mean profiles of slant optical thicknesses and the balloon results at 1020 nm is done in Figure 5. Between 15 and 20 km the polarimetry measurements give slant optical thicknesses nearly 1.5-1.7 times larger than SAGE II mean west values (dashed line), at higher levels the agreement with the west values is good up to nearly 24 km. The east SAGE II measurements (continuous line) match quite well the polarimetry measurements in the whole altitude range proving that Aire sur l'Adour was in the same air mass as Garmisch-Partenkirchen.

Let us now consider the spectral dependance of the aerosol slant optical thickness. SAGE II provides directly measurements at 525, 453 and 385 nm; as explained in section 2.3 the

RADIBAL values at these wavelengths are computed from the retrieved model deduced from 1650 and 850 nm measurements. As for the 1020 nm channel, the SAGE II limiting profiles are deduced from mean uncertainties on aerosol extinction coefficients. The agreement being better for the east SAGE II profile at every wavelength, we show only in Figure 6a-b-c the comparison with the east profile. Below 20-22 km the agreement between the RADIBAL and the SAGE II profiles is good for all wavelengths; above the RADIBAL values are smaller, the differences increasing toward the short wavelengths; the values deduced from polarization measurements are nevertheless within the limiting values for the three channels.

The effective radius and variance deduced from both experiments are shown in Figure 7a-b. In the main aerosol layer, that is to say below $\simeq$20 km the deduced effective radii are of the same order, $\simeq$0.28 μm. Nevertheless, the radius behavior versus altitude is quite different for the two cases : it remains almost constant close to 0.3 μm for the balloon measurements and decreases from $\simeq$ 0.31 μm at 16 km to $\simeq$0.22 μm at 24 km for the SAGE II results corresponding to an extinction increase towards the short wavelengths stronger for SAGE II measurements.

Although the RADIBAL effective variance is strongly variing at lower levels, the values are, in both experiments, very often smaller than 0.1 at altitudes higher than 17 km.

The procedure employed in the SAGE II analysis leads to the retrieval of an "equivalent" size distribution which gives the same spectral variation of extinction as the real one in the SAGE II spectral interval, within the measurement error bars. A very large retrieved variance or the failure of the procedure, i.e. the impossibility of retrieving r_{eff} and v_{eff}, could revealed the presence of a strong second mode. So, it appears that bimodal size distributions can be excluded for the April 1986 SAGE II study. The retrieving procedure from RADIBAL measurements is also based on monomodal models and the possibility to get the polarization measurements with these kind of size distribution leads also to the exclusion of bimodal models.

3.2.2 October-November 1987 period.

During this period the coïncidence in time was poor: three lidar profiles were registered on October 7 and 19 and on November 5. The RADIBAL experiment occured on October 30 in the afternoon. We got six SAGE II east profiles at sunrise in the middle of the month, on October 11, 12, 13, 14, 15 and 16, and three east and three west profiles at sunrise, at the end of the month, on October 29, 30, 31. All the sites, dates and distances in km are listed in Table 6.

Table 6. Distances between the various sites in km.

SAGE II events .	Aire/Adour 43.4°N - 0.15°E October 30	Garmisch-Partenkirchen 47.5°N - 11°E October 7-19, November 5
11/ 42.02°N - 16.54°E		795
12/ 44.98°N - 14.50°E		430
13/ 47.51°N - 12.51°E		125
14/ 49.65°N - 10.57°E		185
15/ 51.46°N - 8.64°E		420
16/ 52.95°N - 6.72°E		625
29/ 48.12°N - 19.78°E	1605	655
29/ 47.85°N - 4.48°W	620	
30/ 45.38°N - 15.69°E	1250	460
30/ 45.18°N - 8.59°W	725	
31/ 42.13°N - 11.39°E	930	660
31/ 41.89°N - 12.90°W	1080	

To evaluate the stability of the stratospheric aerosol layer we have compared the nine east profiles of middle and end of October. They are well gathered in the altitude range 16-21 km and somewhat different at higher levels. For the 1020 nm channel the relative dispersion bars at few levels are : 5.3 % at 15.5 km, 2.1 % at 18.5, 5.6 % at 21.5 and 14.5 % at 24.5 km. The good stability of the aerosol layer is confirmed by the Figure 8 where the three lidar profiles show a rather good gathering between 15-21 km. Above 21 km the November 5 profile is slightly different with extinction coefficients weaker. These remarks show that it seems possible to compare the three lidar profiles with the nine SAGE II east profiles of October.

Figure 9 compares the aerosol slant optical thicknesses at 1020 nm for the lidar data and for the SAGE II average profile of October. The SAGE II limiting profiles deduced from the uncertainties on extinction measurements are reported and some lidar error bars too. We observe an excellent agreement between the different values, the SAGE II slant optical thicknesses being always among the lidar results, and of course within the lidar errors.

The good stability of the layer is also demonstrated when looking to the SAGE II west measurements. The three west profiles of the end of the month are close to the three east previous profiles, a behavior that is different from what was observed in April 1986, so that we will compare the RADIBAL results to the mean SAGE II results computed from the six profiles (three east plus three west) of the end of October.

Figures 10a-b compare the results for λ = 1020 and 385 nm respectively. The balloon measurements, which are well gathered, give slant optical depths 1.2-1.5 times larger than SAGE II mean values for the four channels in the altitude range 15-22 km. Taking into account the estimated error bars one can see that the limiting SAGE II profiles include the balloon values for the shorter channel (that is also true for the 525 and 453 nm channels), the 1020 nm values are always in disagreement meaning that the balloon deduced size distribution compensates the discrepancies towards the short wavelengths. One can remember too that a calibration error exists especially at 1650 nm as said in section 3.1: the assumption of a surestimation of the reflectance measurements could explain some difference.

The effective radius deduced has, this time, the same behavior for the two kinds of experiments: it decreases slightly with altitude but with much larger values for SAGE II experiment especially in the main aerosol layer, that is to say below 21 km (Figure 11); one have a shift of the order of 15 % towards 15- 20 km. The effective variance is again weak, around 0.1 at all altitudes in both cases excluding also bimodal size distribution for the October 1987 study.

3.2.3 April 1989 period.

As it was said previously in the first section this comparison concerns only the SAGE II and the balloon measurements.

The coïncidence was quite good : the balloon experiment took place on April 18 in the evening, and six SAGE II events were available on April 17, 18, 19 at sunset. The distances in km between SAGE II sites and Aire sur l'Adour are listed in Table 7.

Table 7. Distances between the various sites in km.

SAGE II events	Aire/Adour 43.4°N - 0.15°E April 18
17/ 51.18°N - 2.10°E	880
17/ 50.99°N - 22.15°W	1875
18/ 48.46°N - 22.62°E	1820
18/ 48.25°N - 1.65°W	560
19/ 45.31°N - 18.85°E	1500
19/ 45.09°N - 5.40°W	480

The relative dispersion bars in channel 1020 nm at few levels are in : 4.0 % at 15.5 km, 2.2 % at 18.5, 3.5 % at 21.5 and 5.2 % at 24.5 km. They show that the six SAGE II extinction coefficient profiles are very well gathered again so that we will average them and we will compare the average slant optical depth profile to the RADIBAL results.

We have drawn in the Figures 12 the RADIBAL profile, and the SAGE II mean profile with the two limiting profiles deduced from error bars for the 1020 and 385 nm channels. The balloon results are much more dispersed than for 1986 and 1987. To explain this dispersion one can notice that the optical thickness values are somewhat weaker for 1989 than for the two other coïncidences, which took place closer to the El Chichon eruption, so that there was fewer aerosol to detect and the measurements were more difficult to achieve. Nevertheless, owing to the large uncertainties, the SAGE II values are among the RADIBAL values at every wavelength in the altitude range 15-25 km.

The effective radius deduced from polarimetry measurements look much more dispersed than for the other coïncidences (Figure 13). As for 1986 the effective radius varies quite differently for both experiments: it decreases with altitude for SAGE II measurements while it increases slightly for balloon measurements. Below $\simeq$ 20 km the radii are quite similar, as for 1986. The effective variance is weak, around 0.1 as for April 1986 and October 1987.

3.3 Discussion

The three coïncidences have shown some discrepancies between the size distributions retrieved from polarization and from transmission measurements; moreover the parameters of the lidar aerosol model used in 1986 and 1987 to convert the lidar measurements to extinction data are quite different from both polarization and transmission retrieved models, as can be seen in Table 8.

Table 8. Values of the effective radius and variance for the three experiments during the April 1986 coïncidence.

	LIDAR		RADIBAL		SAGE II	
z , km	v_{eff}	r_{eff},μm	v_{eff}	r_{eff},μm	v_{eff}	r_{eff},μm
15	1.75	0.32	0.10	0.29	0.05	0.31
18	1.05	0.31	0.10	0.29	0.06	0.29
21	0.72	0.24	0.06	0.30	0.07	0.25
24	0.80	0.16	0.07	0.30	0.07	0.23

As said in section 3.2.1, the method used in the SAGE II analysis doesn't pretend to lead to the retrieval of the true size distribution; the retrieved parameters of the log-normal model define an "equivalent" size distribution. The procedure employed for the balloon measurements is also based on monomodal models. The log-normal size distributions used in the lidar model are calculated from balloon-borne measurements at Laramie, Wy. The optical counter system in use returns particle concentrations for radii $> 0.01\mu m$ (total number concentration), $> 0.15\mu m$ and $> 0.25\mu m$. So we will compare more precisely the behaviors of the different size distributions.

The two size distribution obtained in April 1986 are drawn in Figure 14 together with the lidar model, at 18 km (a) and 21.4 km (b). The most important features of the Laramie distribution are the relatively large contents of small and large particles which correspond to the large effective variance. The retrieved RADIBAL and SAGE II distributions could indicate that these experiments are unable to detect small and large particles.

In an other way the discrepancies observed between the SAGE II, the balloon and the lidar models can be expressed in spectral variations of the extinction coefficient. We have drawn in Figure 15 the curves for the models obtained in April 1986 at 18 km (a) and 21.4 km (b) and the SAGE II mean east measurements. One can observe that at 18 km the spectral dependances of the extinction deduced from RADIBAL and SAGE II models are similar, as the models are very similar; at 21.4 km the behavior is quite different with especially a stronger spectral variation for the SAGE II smaller particles, that appeared on the 385 nm slant optical thickness curves (Figure 6c). For the lidar large particles there is a smooth spectral variation at the two levels.

We first investigated whether the poor quality of the 385 nm channel SAGE II extinction data could influence the derived aerosol model. The radii deduced by using only the three larger channel data in equation (1), are only slightly different from the radii deduced by using the four channel data. As shown in Figure 16, (case 1986 April 21, east event), the deduced effective radii are always among RADIBAL values in the main aerosol layer and still decrease with increasing altitude; the effective variance, that is not shown, remains of the same order in both cases.

On the other hand we have tested the influence of the aerosol model in the conversion of the lidar data. We calculated the aerosol extinction coefficient at 1020 nm deduced from lidar backscattering measurements by using the SAGE II and the RADIBAL aerosol models instead of the Laramie data. Figure 17 shows the comparison between the three extinction coefficient profiles obtained for the April 22 1986 data. The profiles computed with the RADIBAL and SAGE II models are somewhat different from the profile computed with the lidar model, nevertheless the relative differences are smaller than the relative dispersions or than the error bars of the lidar profile. Both RADIBAL and SAGE II models used together with the lidar data lead to extinction profiles that could also be in agreement with the extinction data obtained from SAGE II measurements (Figure 2). The lidar experiment is then not very sensitive to the aerosol model.

As a final test we computed the reflectance and polarization diagrams at 1650 and 850 nm with the size distributions deduced from SAGE II, and we compared them with the balloon measurements. Figures 18 show the measurements at 18.0 km (squares and triangles) and the curves retrieved with the RADIBAL procedure (18a), in Figure 18b we can see that the reflectance curves are similar in the RADIBAL and SAGE II cases, but the polarization curves are slightly different. Figure 19 shows the same study at 21.4 km altitude : one can notice that the reflectance and polarization diagrams retrieved with the RADIBAL procedure are not so close to the measurements than at 18 km; the SAGE II results show large discrepancies. This analysis means that the polarization measurements are very sensitive to the size distribution and that at higher altitudes it is impossible to get these polarization measurements with the SAGE II aerosol model.

4 Conclusion

Three independant experiments, balloon measurements of the reflectance and of the polarization at 1650 and 850 nm, lidar measurements at 694.3 nm and transmission measurements at 1020, 525, 453 and 385 nm were available for the European correlative analysis of the stratospheric aerosol layer, for three periods.

The 1020 nm channel has been mainly chosen for the comparisons because it is the most accurate for SAGE II experiment and because it is in the RADIBAL spectral range. The aerosol extinction coefficients at 1020 nm have been deduced from lidar data by the means of an aerosol model deduced from balloon-borne measurements achieved at Laramie; the aerosol model derived from balloon measurements at 1650 and 850 nm permits to compute the extinction coefficient at the four SAGE II wavelengths.

The first comparison concerns the slant optical thickness at 1020 nm. The April 1986 results show a good agreement between the three kinds of experiments in the altitude range 12-22 km, that is to say in the main aerosol layer. Above that altitude the lidar optical thicknesses are somewhat larger than the other values, but nevertheless the lidar error bars include the SAGE II and balloon results. For the October 1987 coïncidence the lidar optical thicknesses are in excellent agreement with the SAGE II results, while the RADIBAL values are 1.2-1.5 times larger in the whole altitude range; a calibration error could be partly responsible of these differences. The SAGE II values are inside the balloon results of April 1989 which are much dispersed due to the small number of aerosols, so that this last comparison is poorly satisfying.

The spectral dependance of the extinction coefficient allows us to retrieve the aerosol "equivalent" size distribution, with two different procedures for the RADIBAL and SAGE II experiments. For the coïncidences of April 1986 and 1989 the deduced effective radii are in good agreement in the main aerosol layer while at higher altitudes discrepancies appear with smaller values for SAGE II measurements. The October 1987 comparison shows similar behaviors for the two kinds of derived effective radii, nevertheless the values are quite different. The retrieved effective variances are small and of the same order in all cases; they are very different of the large variance deduced from Laramie data. The conversion of the lidar backscattering coefficient to aerosol extinction coefficient doesn't seem very sensitive to the aerosol model, so that the comparison of the two retrieved size distributions with the model deduced from Laramie measurements doesn't bring any additionnal information.

Concerning the discrepancies appearing between the SAGE II and RADIBAL deduced radii at high altitudes, an important problem has been raised because of the impossibility to retrieve the measured polarization diagrams with the SAGE II parameters or to retrieve the measured SAGE II spectral variations of extinction with the RADIBAL parameters. A more precise study is needed taking into account particularly other size distributions and even bimodal models. The opportunity to test the procedures happened with new correlative experiments performed in early October 1991. These additional measurements may lead to valuable comparisons because of the great abundance of aerosols following the Pinatubo eruption.

ACKNOWLEDGMENTS

We wish to thank the Aerosol Research group at the NASA Langley Research Center which has kindly provided to us the SAGE II data and the Balloon staff of the Centre National d'Etudes Spatiales for the realization of the balloon flights. We are grateful to J.Y. Balois, L. Gonzales, P. Lecomte and C. Verwaerde for the technical assistance in the RADIBAL experiment. H. J. is indebted to D.J. Hofmann for making Laramie balloon data available.

This work has been supported by the CNES and the CNRS within the French Program PAMOY.

REFERENCES

Ackerman, M., C. Lippens and C. Muller, 1981 : Stratospheric Aerosol Properties from Earth Limb Photography. Nature, 292, 587-591.

Ackerman, M., C. Brogniez, B.S. Diallo, G. Fiocco, P. Gobbi, M. Herman, H. Jäger, J. Lenoble, C. Lippens, G. Megie, J. Pelon, R. Reiter and R. Santer, 1989 : European Validation of SAGE II Aerosol profiles. J. Geophys. Res., 94, D6, 8399-8411.

Brogniez, C. and J. Lenoble, 1988 : Size Distribution of Stratospheric Aerosols from SAGE II Multiwavelength Extinction. Aerosols and Climate, edited by P.V. Hobbs and M.P. McCormick, A. Deepak Publishing, Hampton, 305-312.

Brogniez, C. and J. Lenoble, 1991 : Analysis of 5-Year Aerosol Data from the Stratospheric Aerosol and Gas Experiment II. J. Geophys. Res., 96, D8, 15,479-15,497.

Chu,W.P., M.P. McCormick, J. Lenoble, C. Brogniez and P. Pruvost, 1989 : SAGE II Inversion algorithm. J. Geophys. Res., 94, D6, 8339-8351.

Diallo, B.S.,1989 : Utilisation de la Polarisation du Rayonnement Solaire Diffusé par l'Atmosphère pour une caractérisation des Aerosols Stratosphériques; Evolution de la Période Post-El Chichon. Thèse soutenue le 24 mai 1989 pour l'obtention du titre de docteur de l'Université de Lille I.

Hamill, P., T.J. Swissler, M. Osborn and M.P. McCormick, 1980 : Analysis and Interpretation of Lidar Observations of the Stratospheric Aerosol. Remote Sensing of Atmospheres and Oceans, edited by A. Deepak, Academic Press, 149-168.

Hansen, J.E. and L.D. Travis, 1974 : Light Scattering in Planetary Atmospheres. Space Science Reviews 16, 527-610.

Herman, M., J.Y. Balois, L. Gonzales, P. Lecomte, J. Lenoble, R. Santer and C. Verwaerde, 1986 : Stratospheric Aerosol Observations from Balloonborne Polarimetric Experiment. Appl. Opt. 25, 3573-3584.

Jäger, H. and D.J. Hofmann, 1991 : Midlatitude Lidar Backscatter to Mass, Area, and Extinction Conversion Model Based on in situ Aerosol Measurements from 1980 to 1987. Appl. Opt. 30, 127-138.

Jäger, H., R. Reiter,W. Carnuth and W. Funk, 1984 : El Chichon Cloud over Central Europe. Geof. Int., 23 (2), 243-257.

Lenoble, J. and C. Brogniez, 1984 : A Comparative Review of Radiation Aerosol Models. Beitr. Phys. Atmosph. 57, 1, 1-20.

Lenoble, J., P. Pruvost and C. Brogniez, 1984 : SAGE Satellite Observations of Stratospheric Aerosol from Mount St Helens Eruption : A two-wavelength Analysis. J. Geophys. Res., 89, D7, 11,666-11,676.

Livingston, J.M. and P.B. Russell, 1989 : Retrieval of Aerosol Size Distribution Moments from Multiwavelength Particulate Extinction Measurements. J. Geophys. Res., 94, D6, 8425-8434.

McCormick, M.P., P. Hamill, T.J. Pepin, W.P. Chu, T.J. Swissler and L.R. McMaster, 1979 : Satellite Studies of the Stratospheric Aerosol. Bull. Amer. Meteor. Soc., 60, 1038-1046.

Mauldin III, L.E., N.H. Zaun, M.P. McCormick, J.H. Guy and W.R. Vaughn, 1985 : Stratospheric Aerosol and Gas Experiment II Instrument : a Functional Description. Optical Engineering 24, 307-312.

Palmer, K.F and D. Williams, 1975 : Optical Constants of Sulfuric Acid: Application to the Clouds of Venus. App. Opt. 14, 208-219.

Reiter, R., H. Jäger, W. Carnuth and W. Funk, 1979 : The Stratospheric Aerosol Layer Observed by Lidar Since October 1976. A Contribution to the Problem of Hemispheric Climate. Arch. Met. Geoph. Biokl., Ser. B, 27, 121-149.

Rosen, J.M. and D.J. Hofmann, 1986 : Optical Modeling of Stratospheric Aerosol: Present Status. Appl. Opt. 25, 410-419.

Russell, P.B. and P. Hamill, 1984 : Spatial Variation of Stratospheric Aerosol Acidity and Model Refractive Index: Implications of Recent Results. J. Atmos. Sci. 41, 1781-1790.

Santer, R., M. Herman, D. Tanré and J. Lenoble, 1988 : Characterization of Stratospheric Aerosol from Polarization Measurements. J. Geophys. Res., 93, D11, 14,209-14,221.

Yue, G.K., M.P. McCormick and W.P. Chu, 1986 : Retrieval of Composition and Size Distribution of Stratospheric Aerosols with the SAGE II Satellite Experiment. J. Atmos. Ocean. Techn. 3, 371-380.

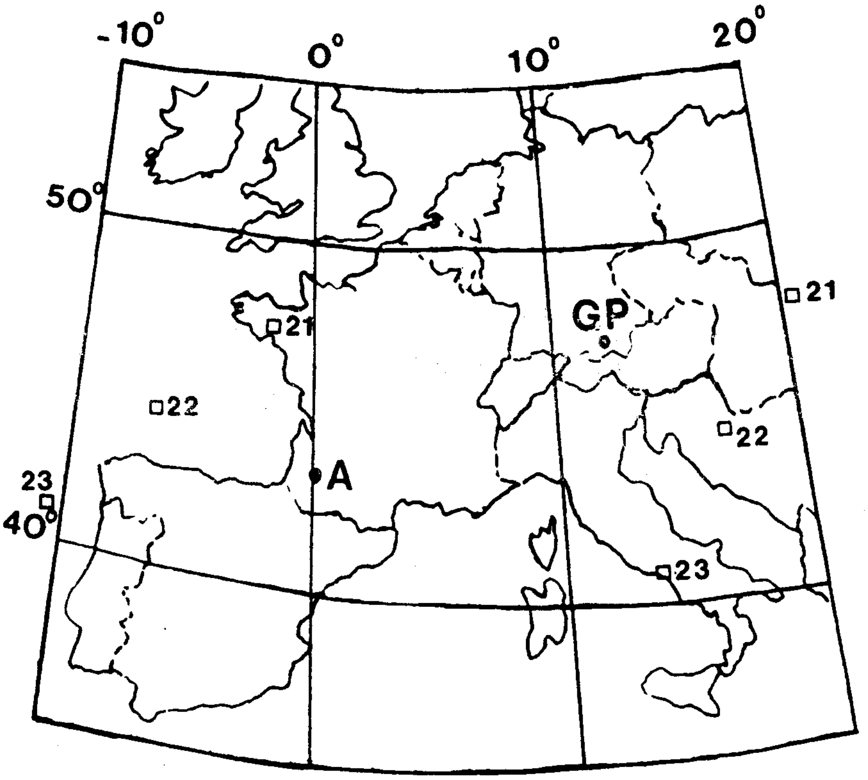

Figure 1. Location of the SAGE II events (squares), for the April 1986 coïncidence, (A) stands for Aire sur l'Adour and (GP) for Garmisch-Partenkirchen.

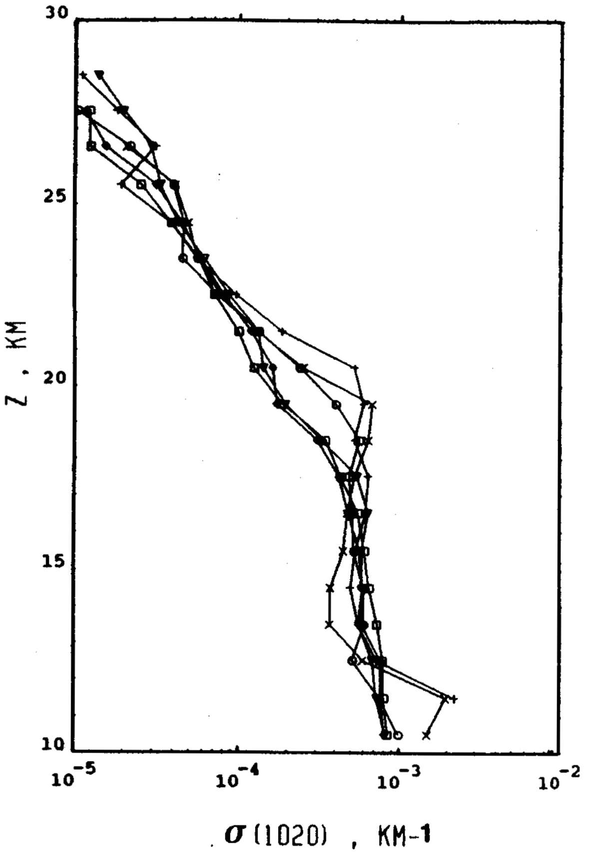

Figure 2. April 1986 SAGE II extinction coefficient profiles at 1020 nm : squares, triangles, diamonds are for west profiles and circles, crosses, plusses are for east profiles.

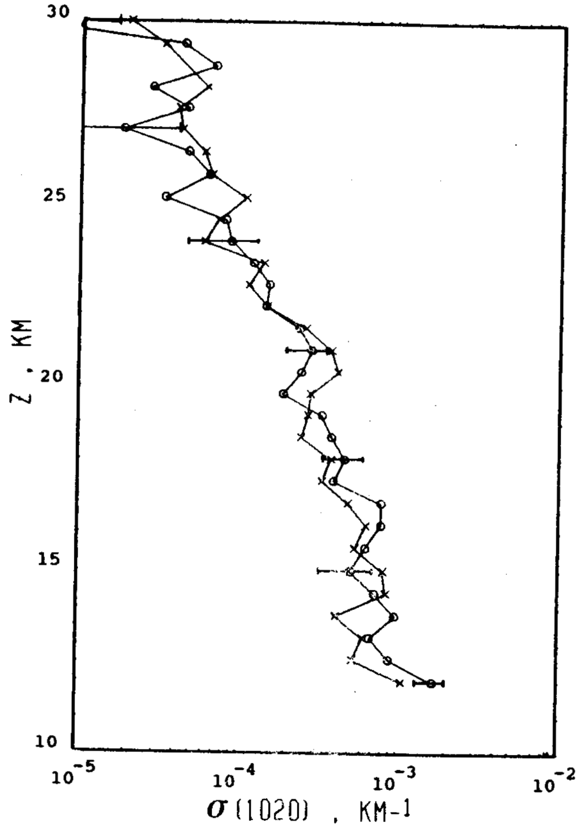

Figure 3. 1986 lidar extinction coefficient at 1020 nm versus altitude : April 22 (open circles) and April 23 (crosses), with some error bars for the April 22 profile.

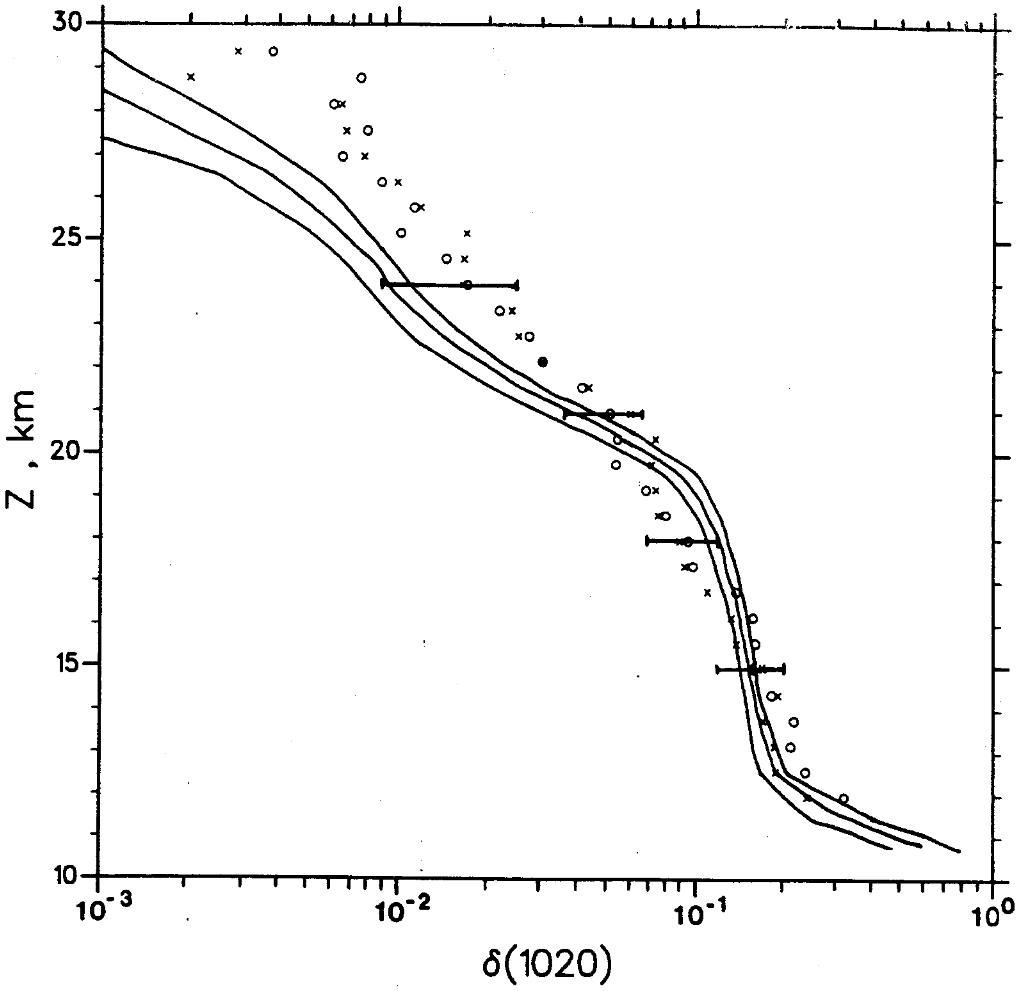

Figure 4. Comparison between the slant optical thickness profiles at 1020 nm computed from lidar measurements (April 22 1986 (open circles) with some error bars and April 23 (crosses)), and the mean SAGE II east profile with its limiting profiles (full lines).

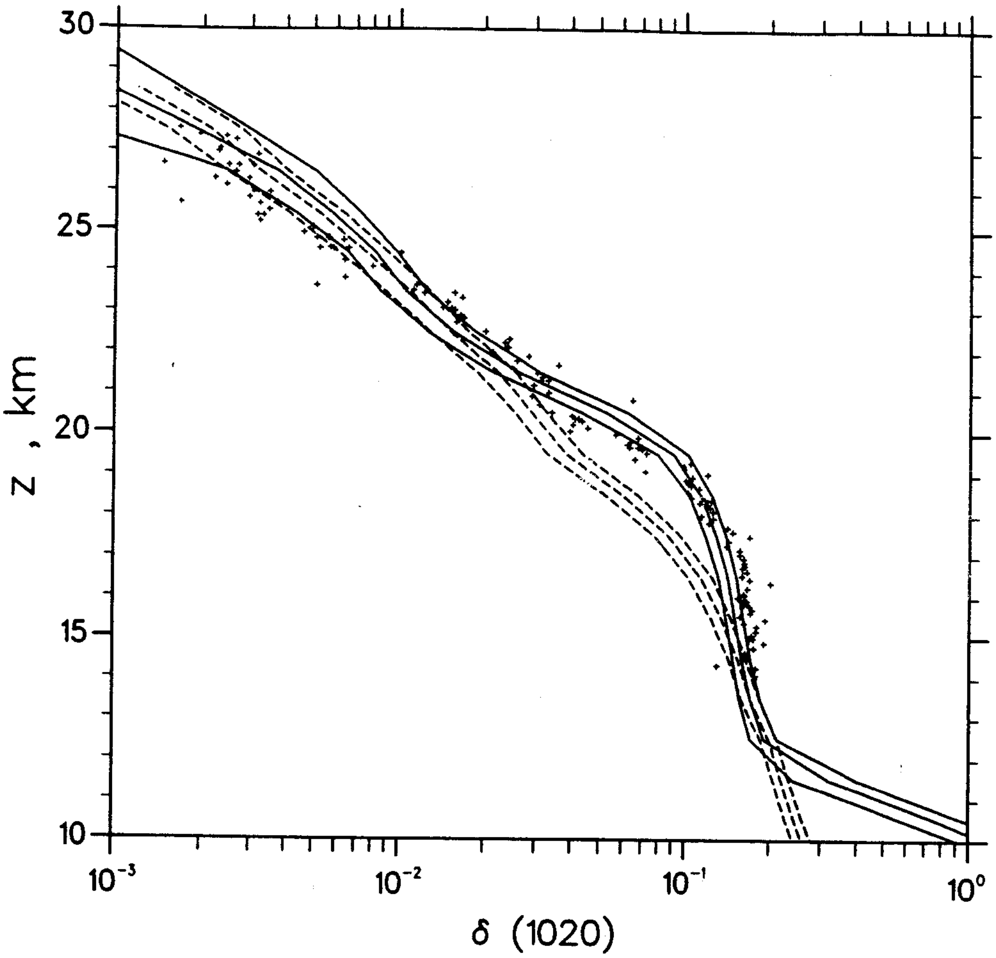

Figure 5. April 1986 balloon slant optical thickness profile at 1020 nm (plusses), compared to the mean SAGE II west profile (dashed lines) and the mean SAGE II east profile (full lines).

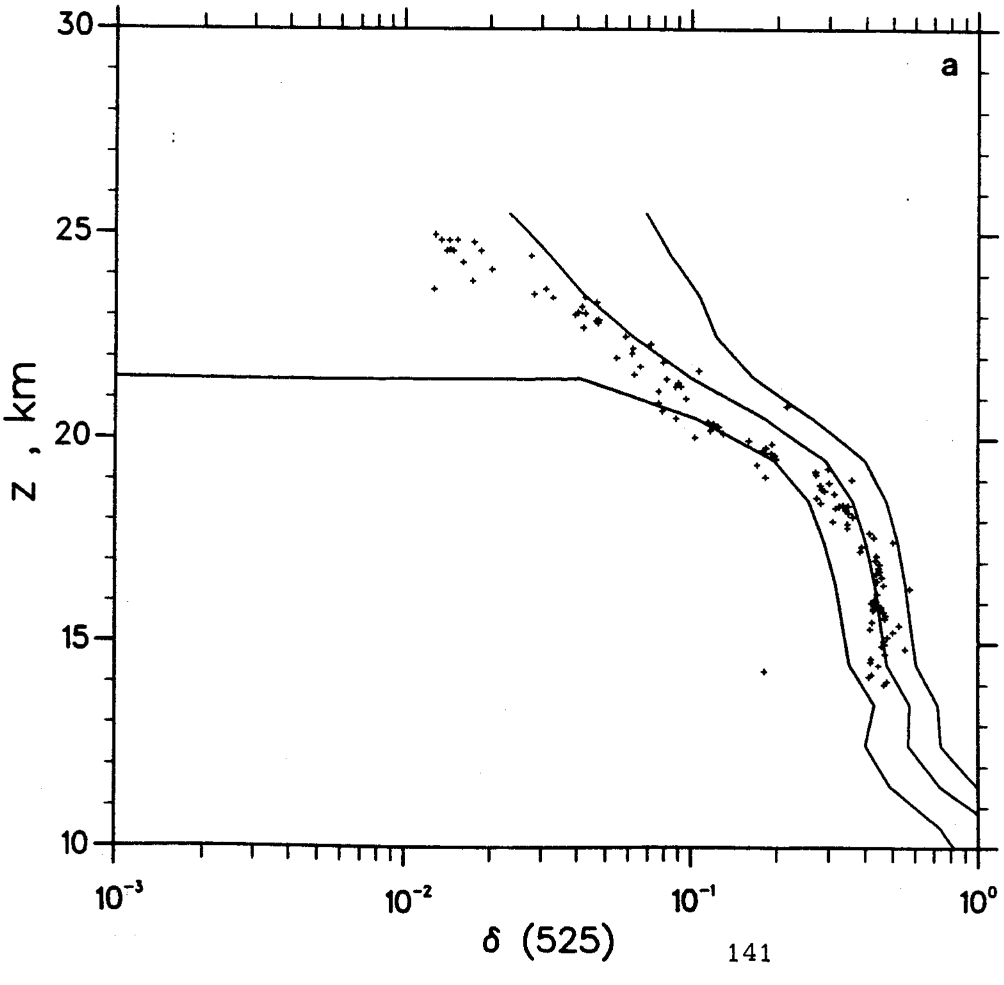

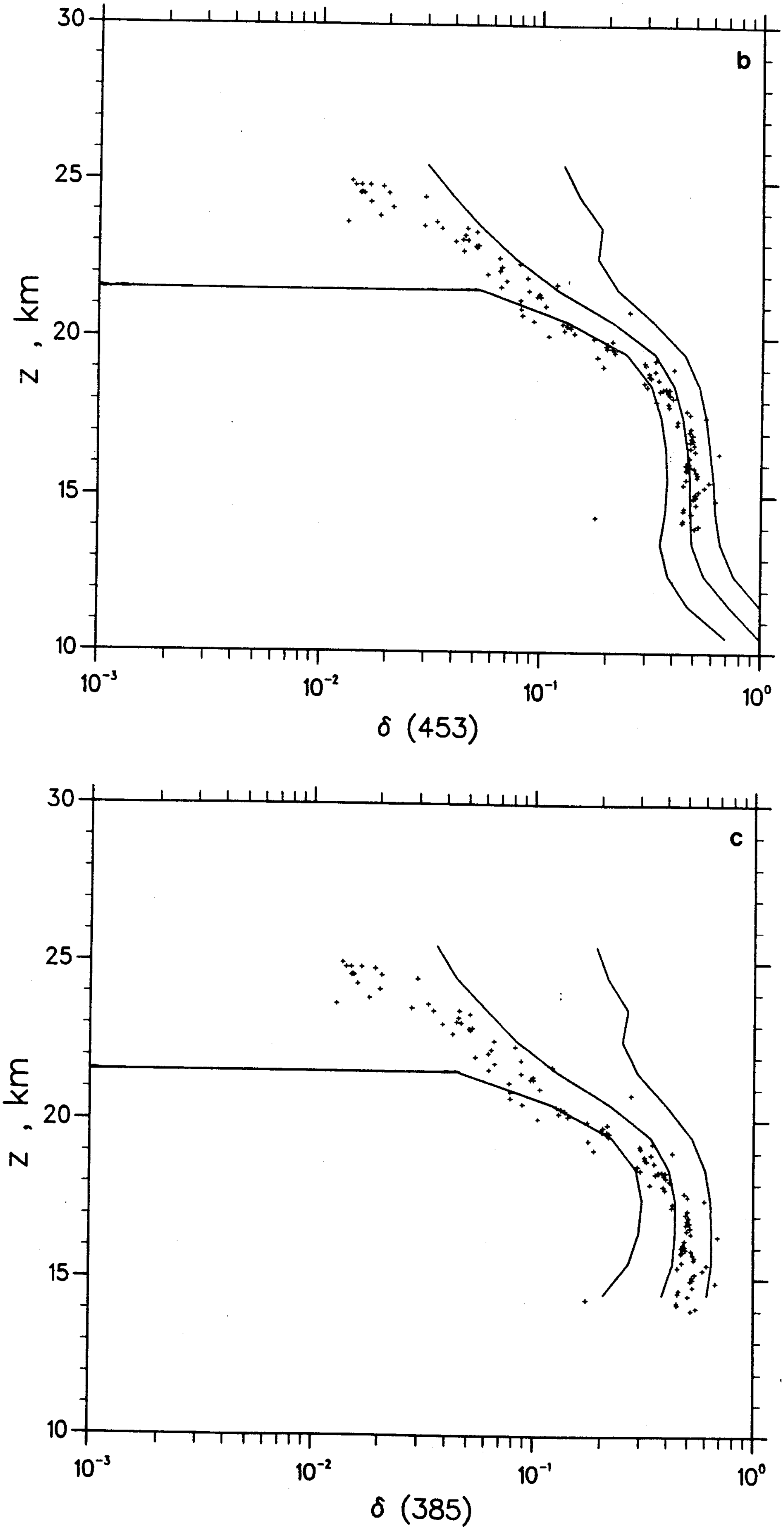

Figure 6. Same as figure 5 but for the 525 (a), 453 (b) and 385 nm (c) wavelengths with only the SAGE II east profile.

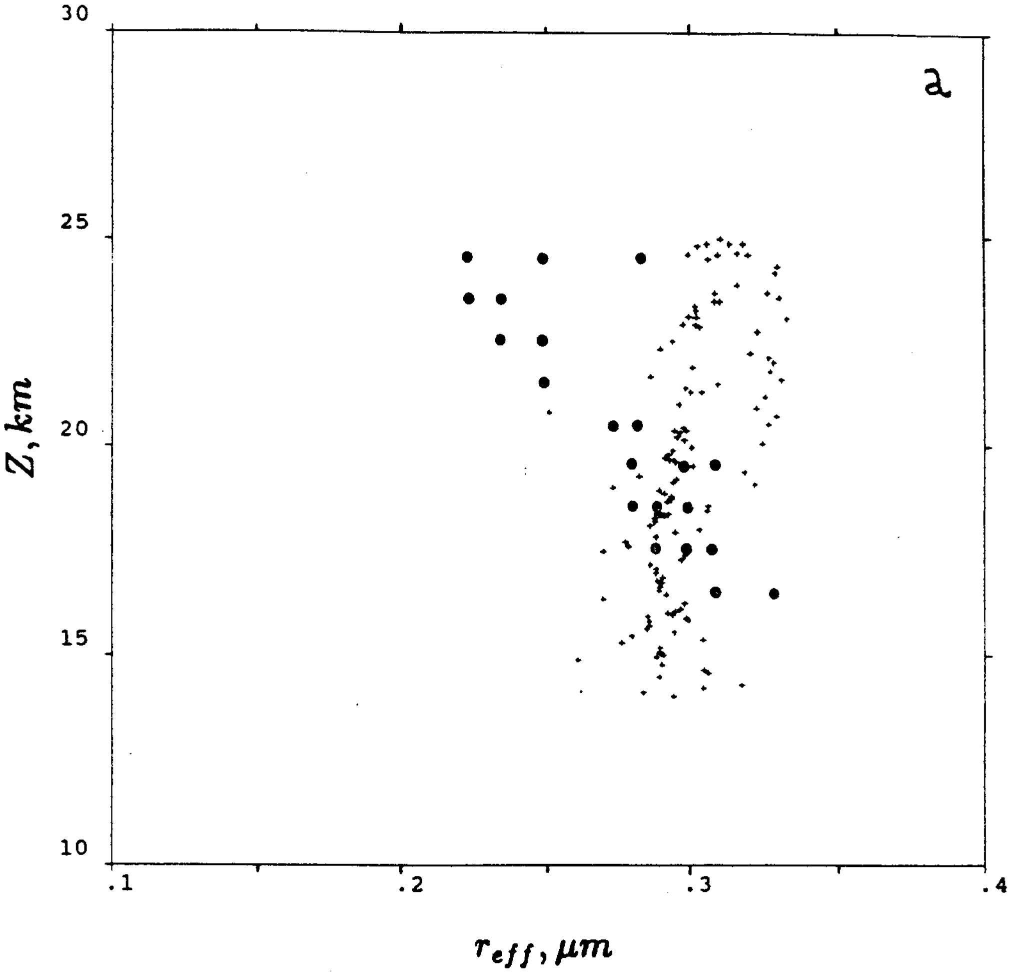

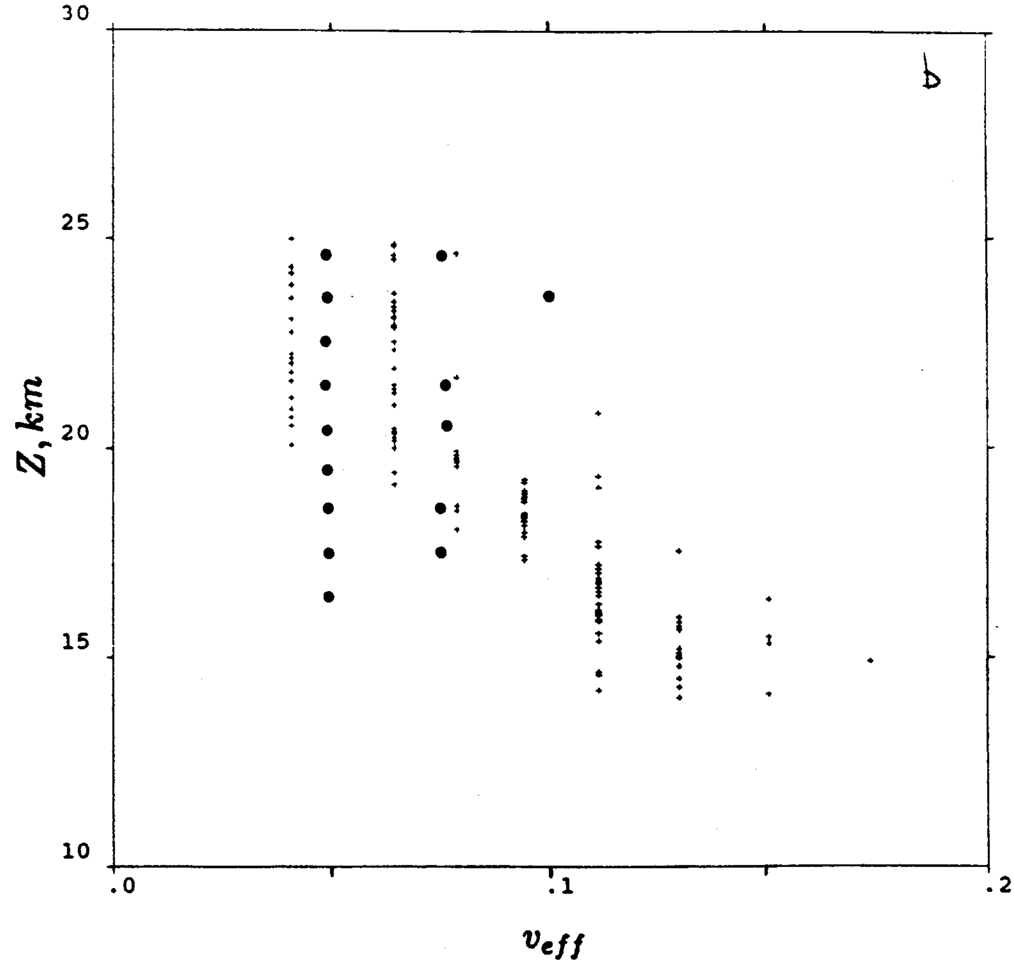

Figure 7. Effective radius (a) and effective variance (b) versus altitude for the April 1986 RADIBAL experiment (plusses) and for the east SAGE II experiment (dots).

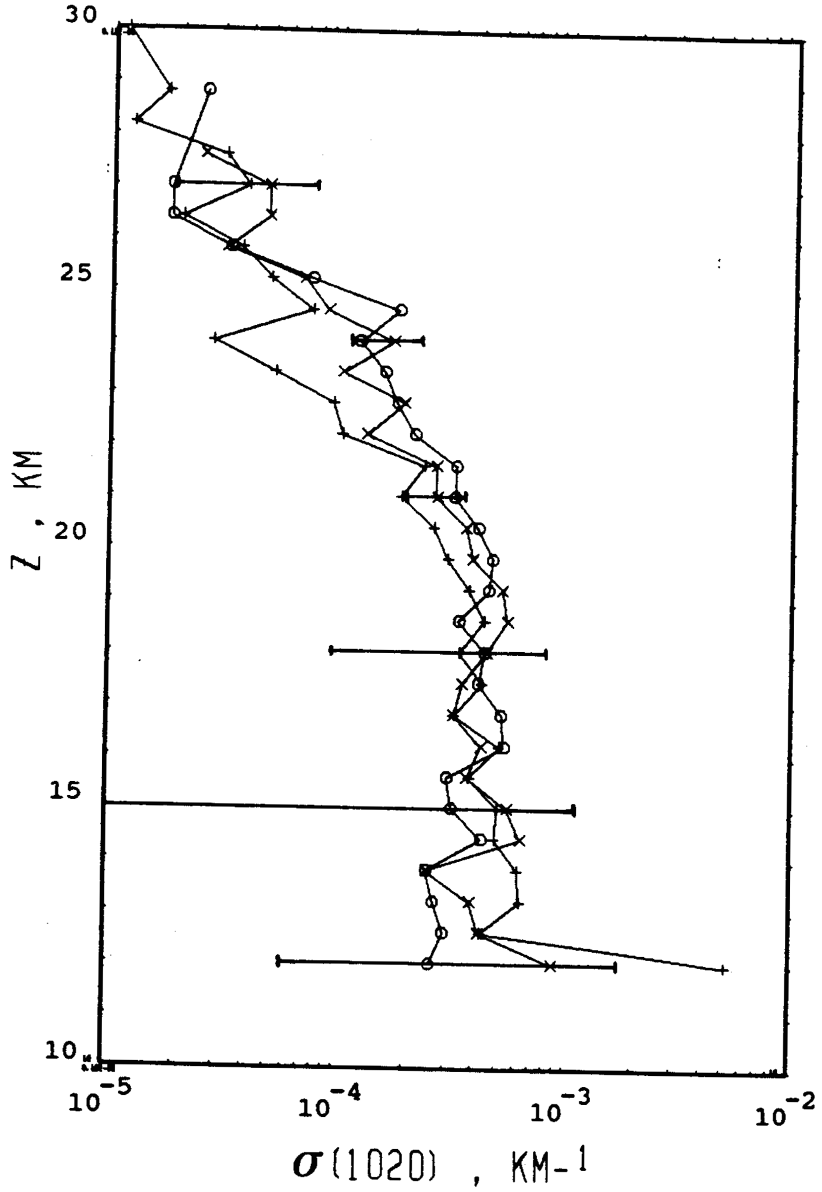

Figure 8. 1987 lidar extinction coefficient at 1020 nm versus altitude : October 7 (open circles), October 19 (crosses) and November 5 (plusses), with some error bars for the October 19 profile.

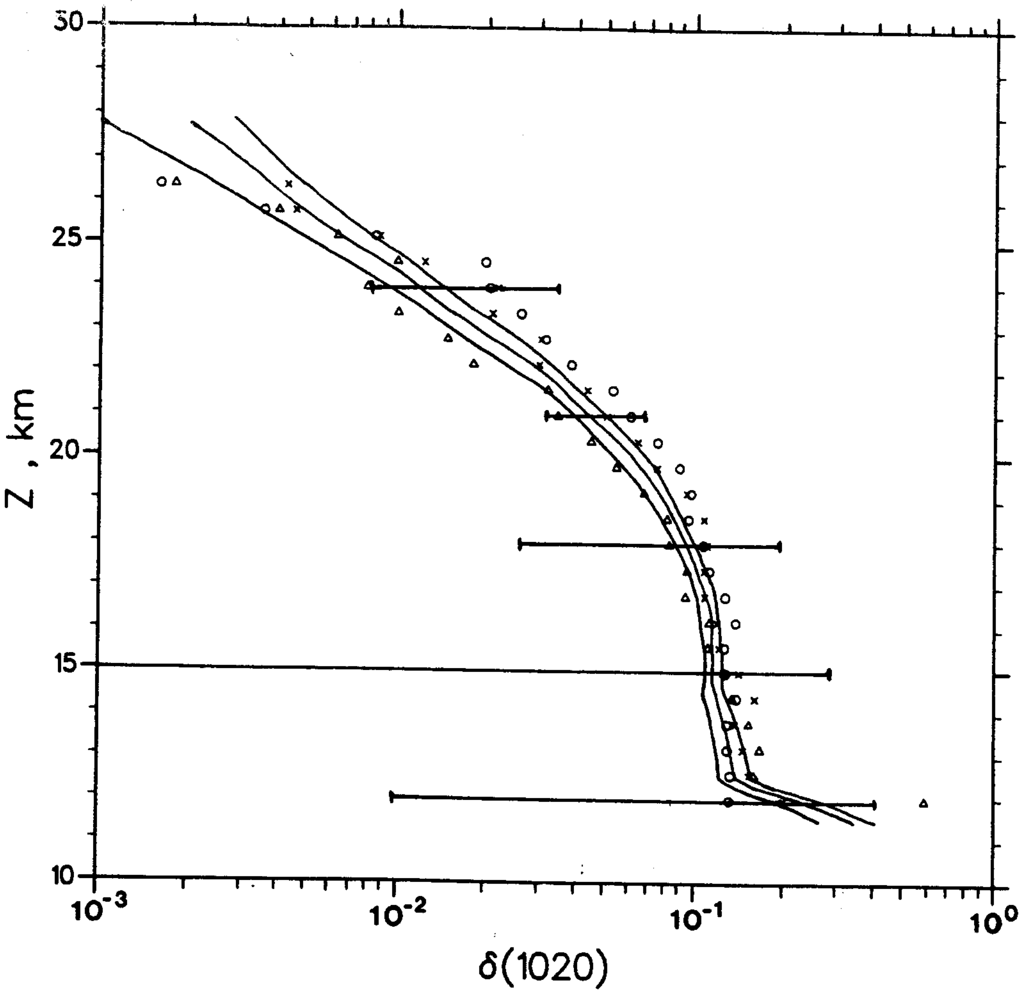

Figure 9. Comparison between the slant optical thickness profiles at 1020 nm computed from lidar measurements (October 7 (open circles), October 19 (crosses) with some error bars and November 5 (triangles)), and the mean SAGE II east profile with its limiting profiles (full lines).

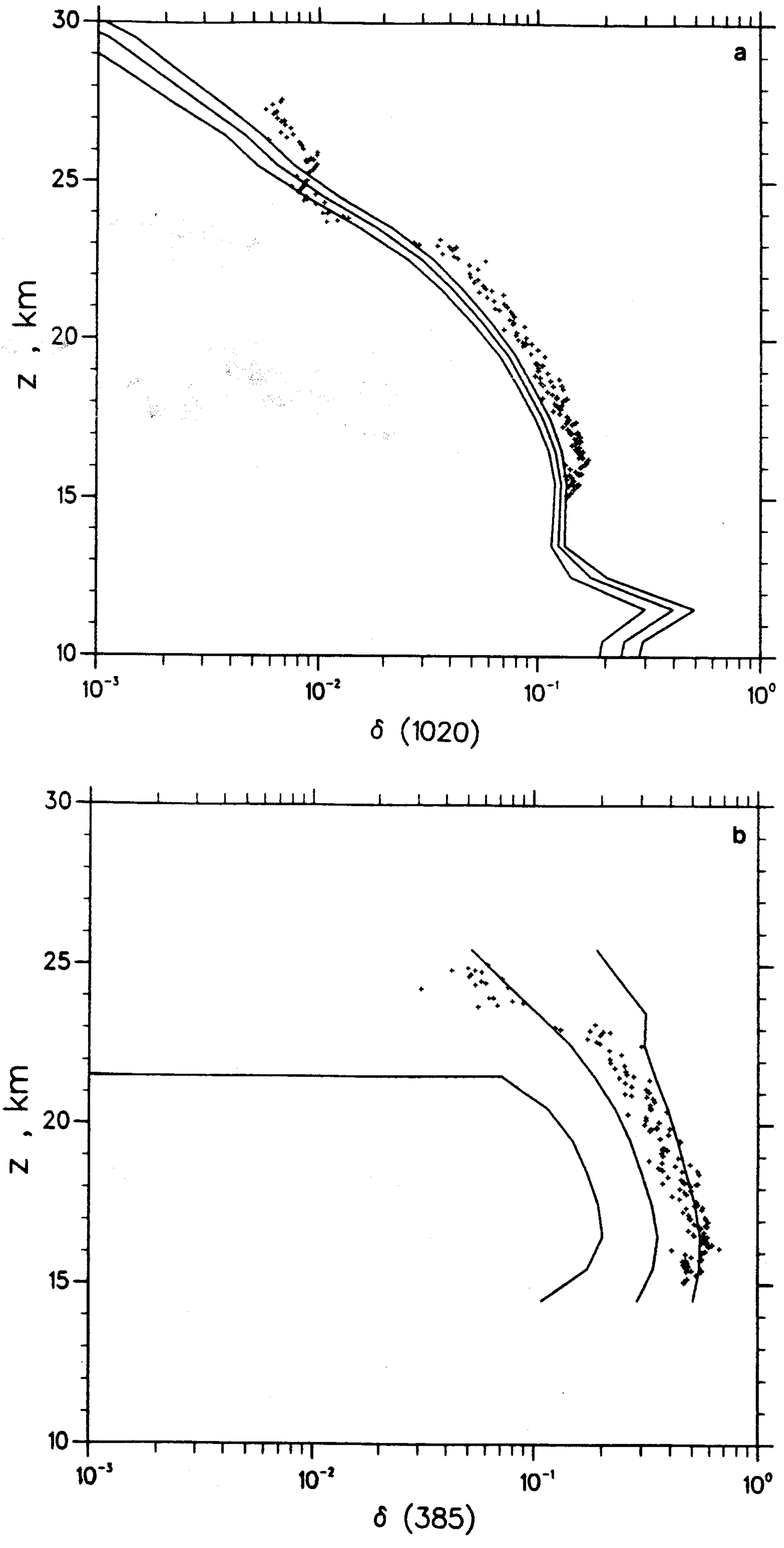

Figure 10. October 1987 balloon slant optical thickness profile (plusses), compared to the mean SAGE II profile (full lines) : at 1020 nm (a) and 385 nm (b).

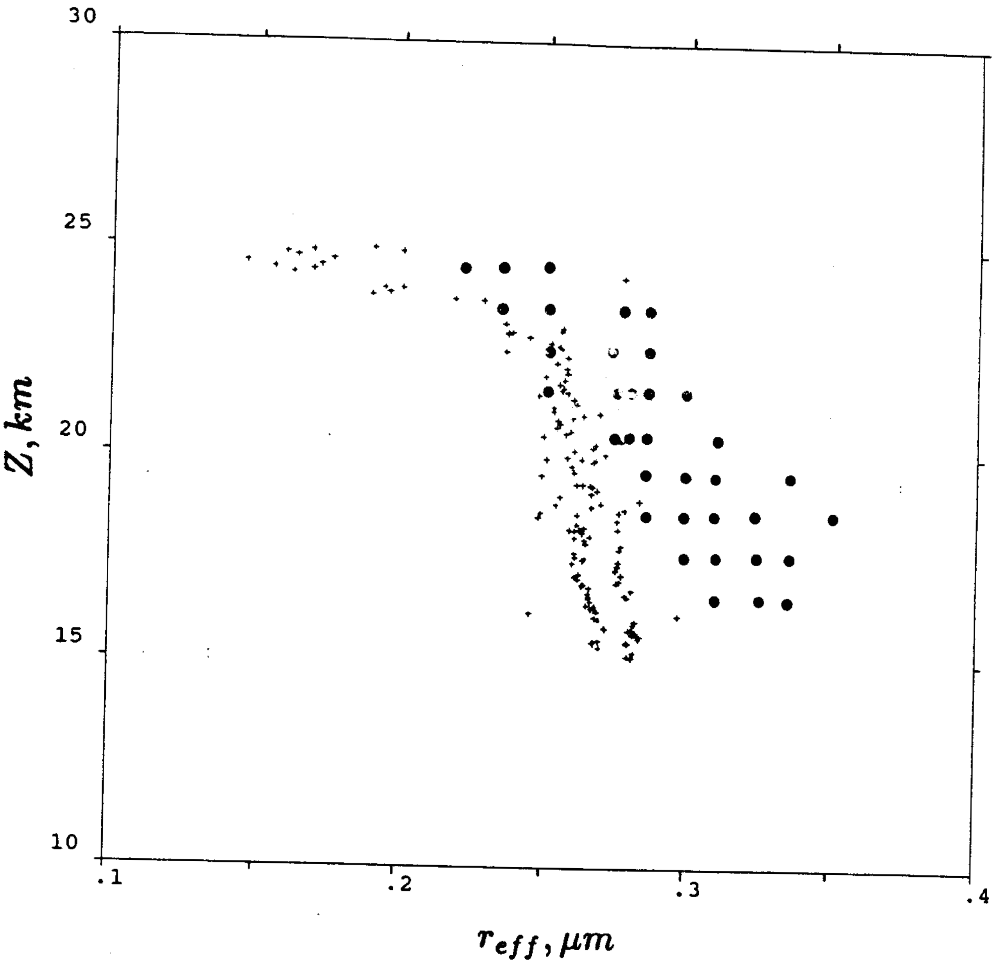

Figure 11. Effective radius versus altitude for the October 1987 RADIBAL experiment (plusses) and for the SAGE II experiment (dots).

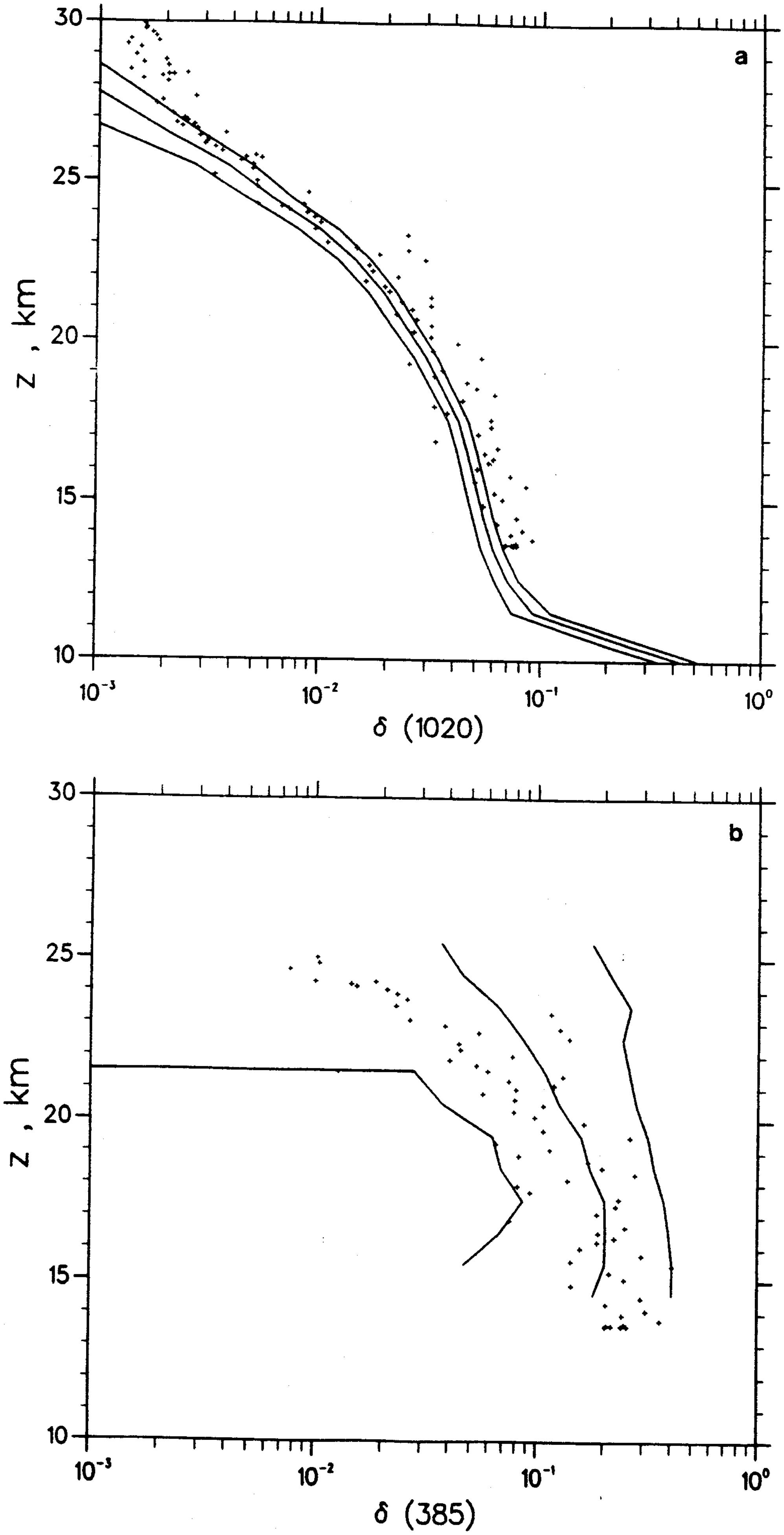

Figure 12. April 1989 balloon slant optical thickness profile (plusses), compared to the mean SAGE II profile (full lines) : at 1020 nm (a) and 385 nm (b).

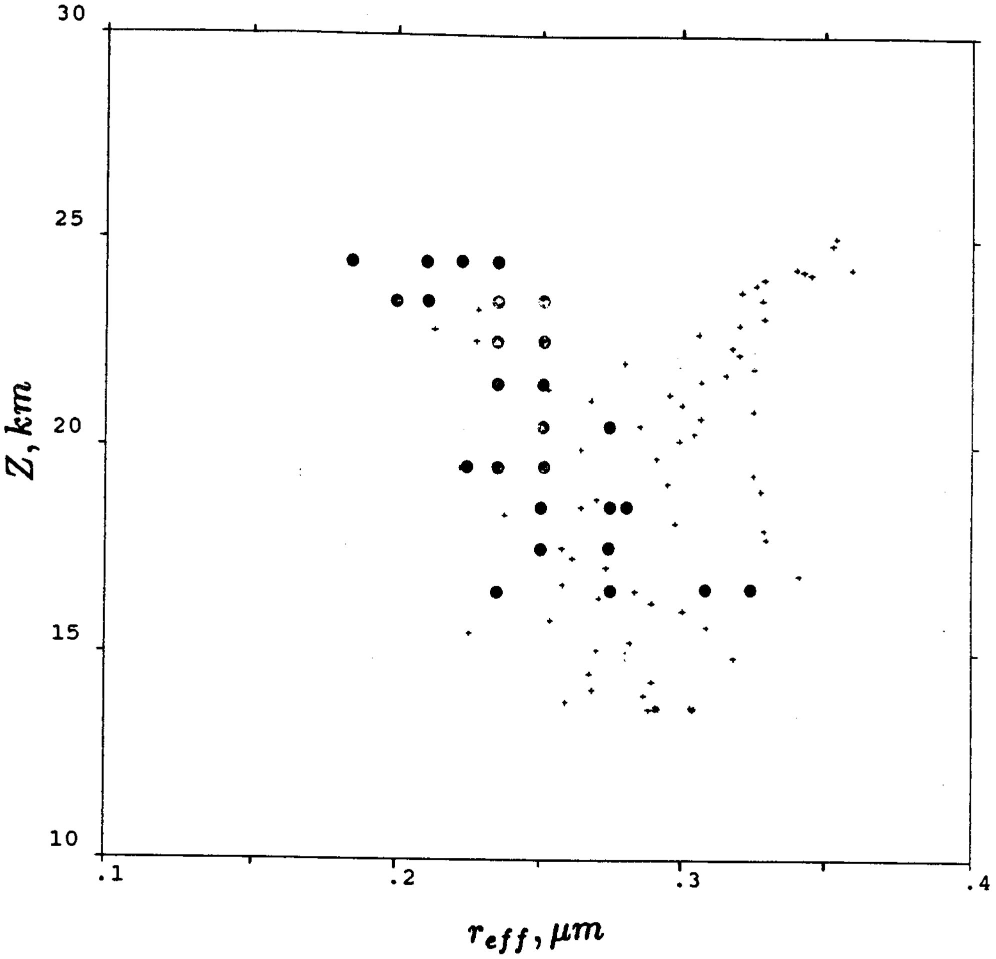

Figure 13. Effective radius versus altitude for the April 1989 RADIBAL experiment (plusses) and for the SAGE II experiment (dots).

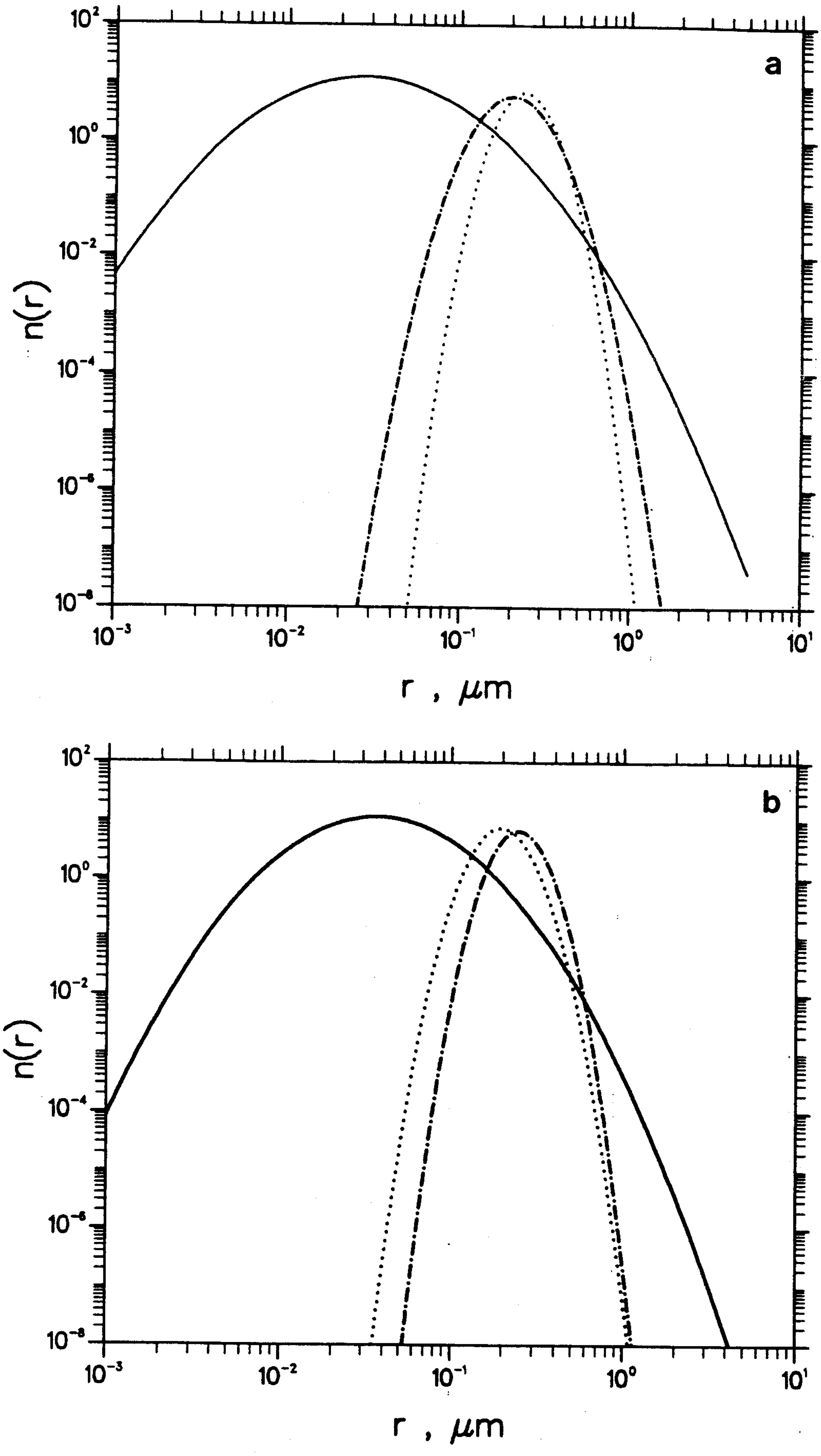

Figure 14. Size distributions deduced from RADIBAL measurements (dashed-dotted), from SAGE II mean east values (dotted) and from Laramie data (full line) in April 1986 at 18 km (a) and 21.4 km (b) altitude.

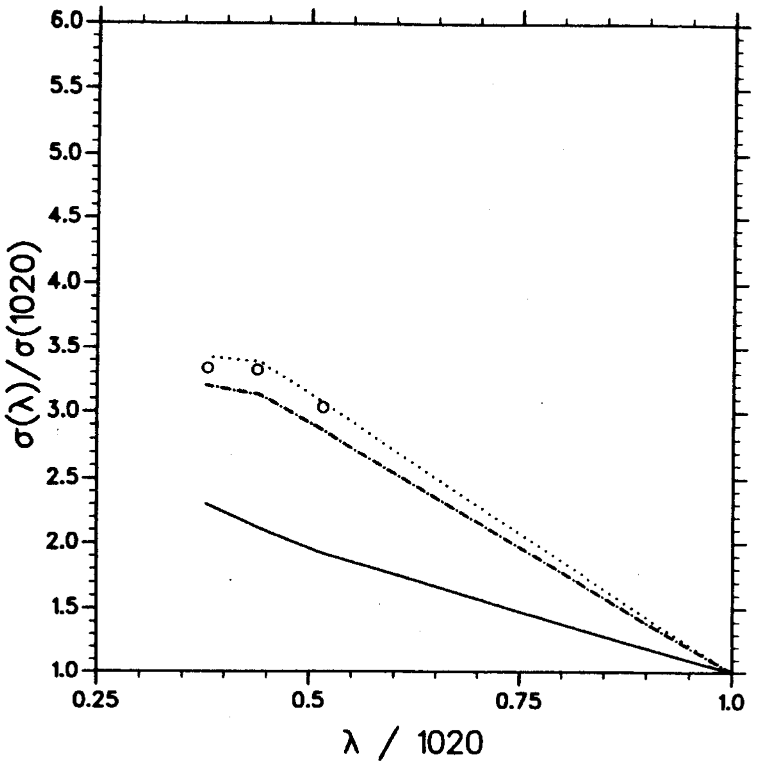

Figure 15a. Spectral dependance of the extinction coefficient derived from RADIBAL model (dashed- dotted), from SAGE II (dotted) and from Laramie data (full line) for April 1986 at 18.0 km altitude. The SAGE II mean east measurements are plotted as circles.

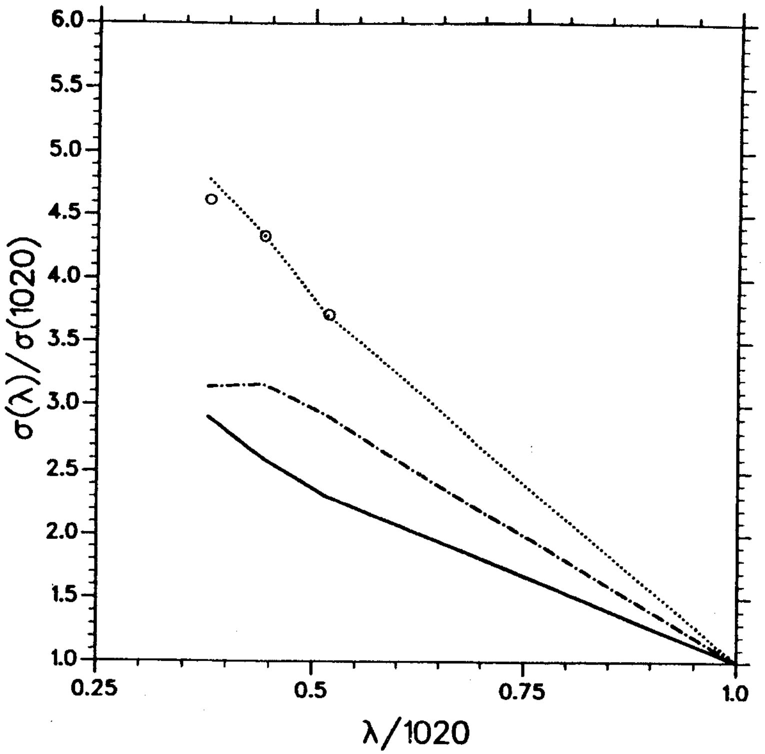

Figure 15b. Same as figure 15a at 21.4 km altitude.

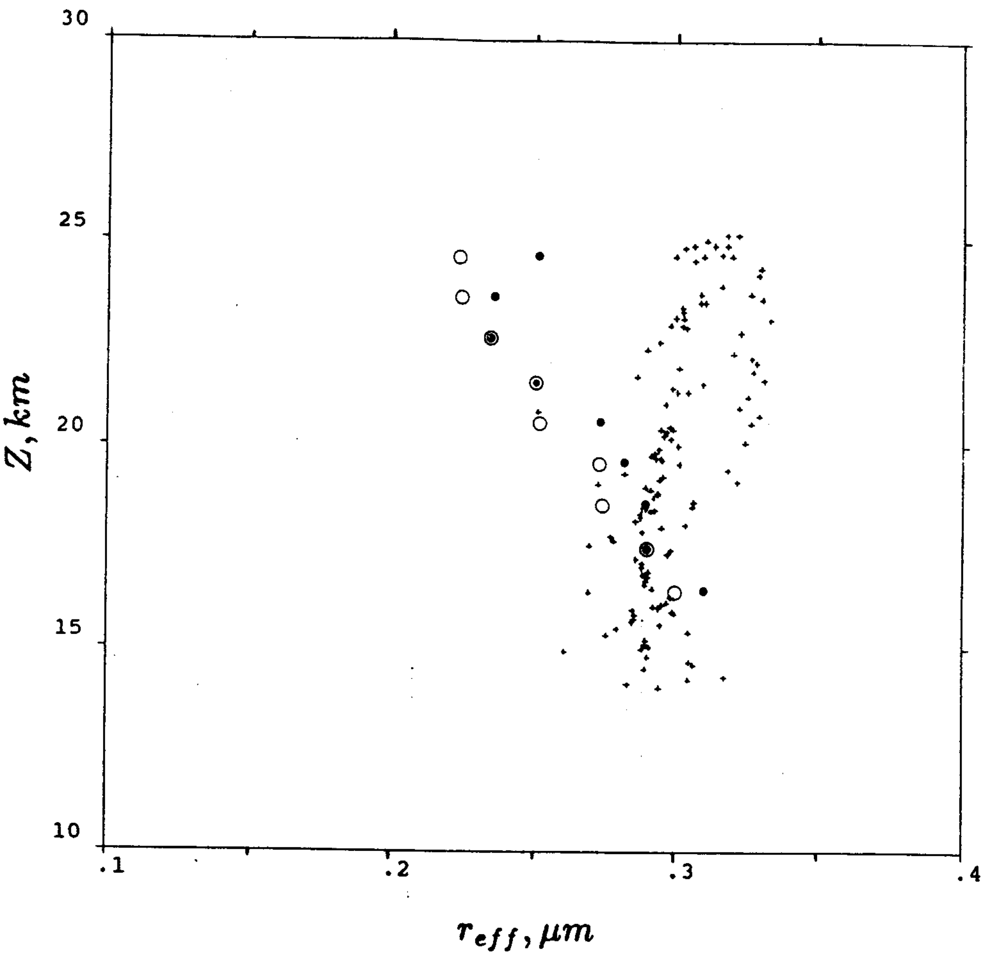

Figure 16. Comparison between the effective radius derived from RADIBAL experiment (plusses), and from SAGE II with a 4 wavelength least squares fit (dots), or a 3 wavelength least squares fit (circles).

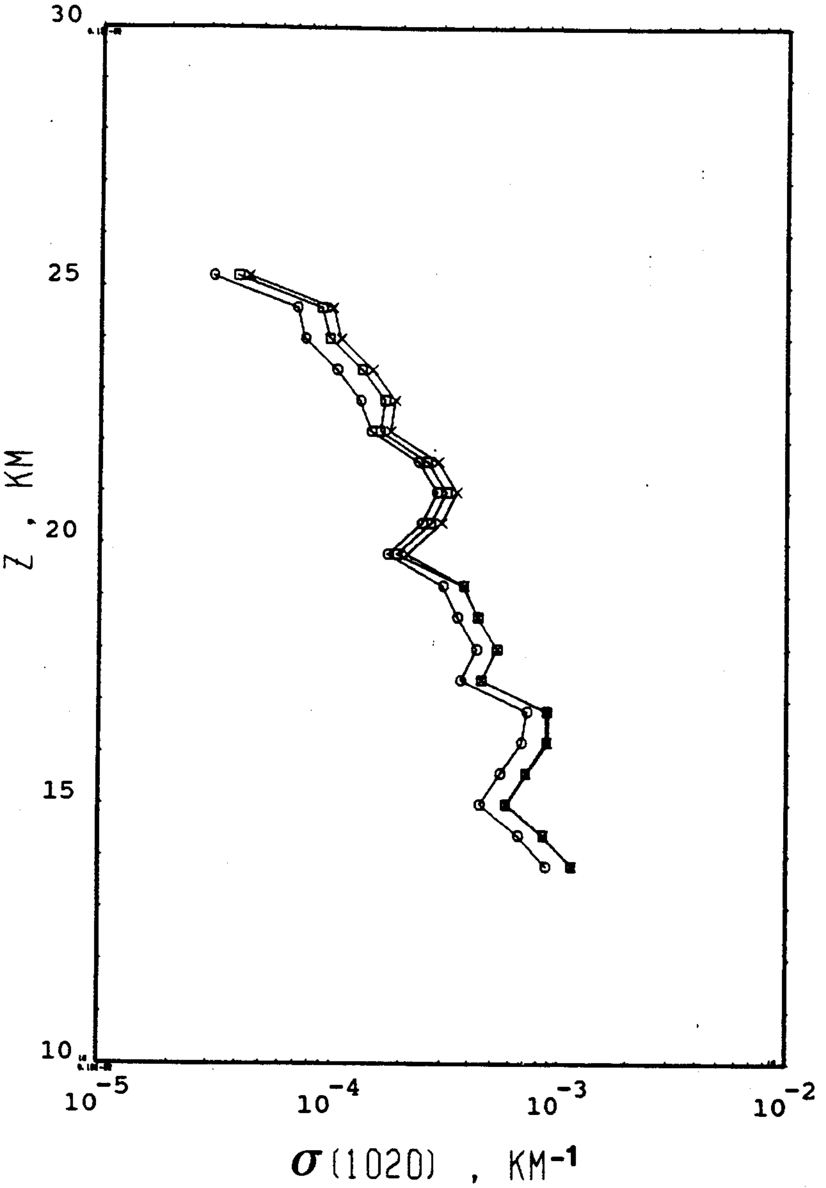

Figure 17. Comparison between the extinction coefficient profiles derived from the lidar data with various size distributions : Laramie (open circles), SAGE II (open squares) and RADIBAL (crosses).

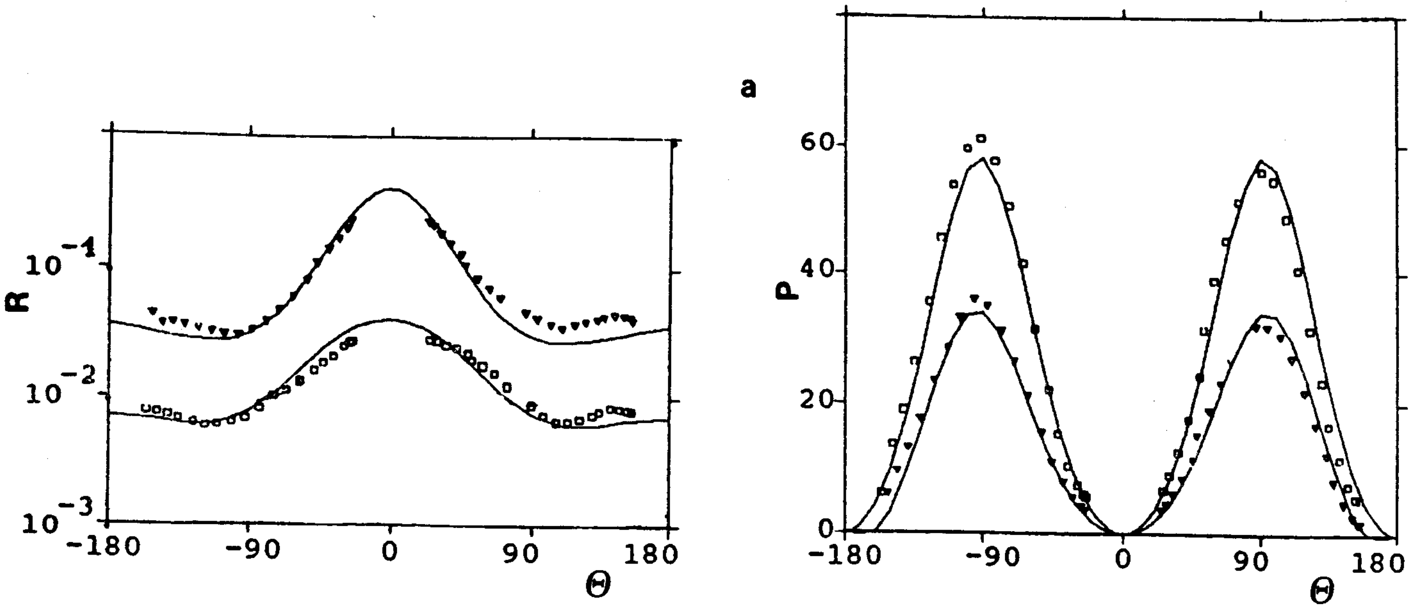

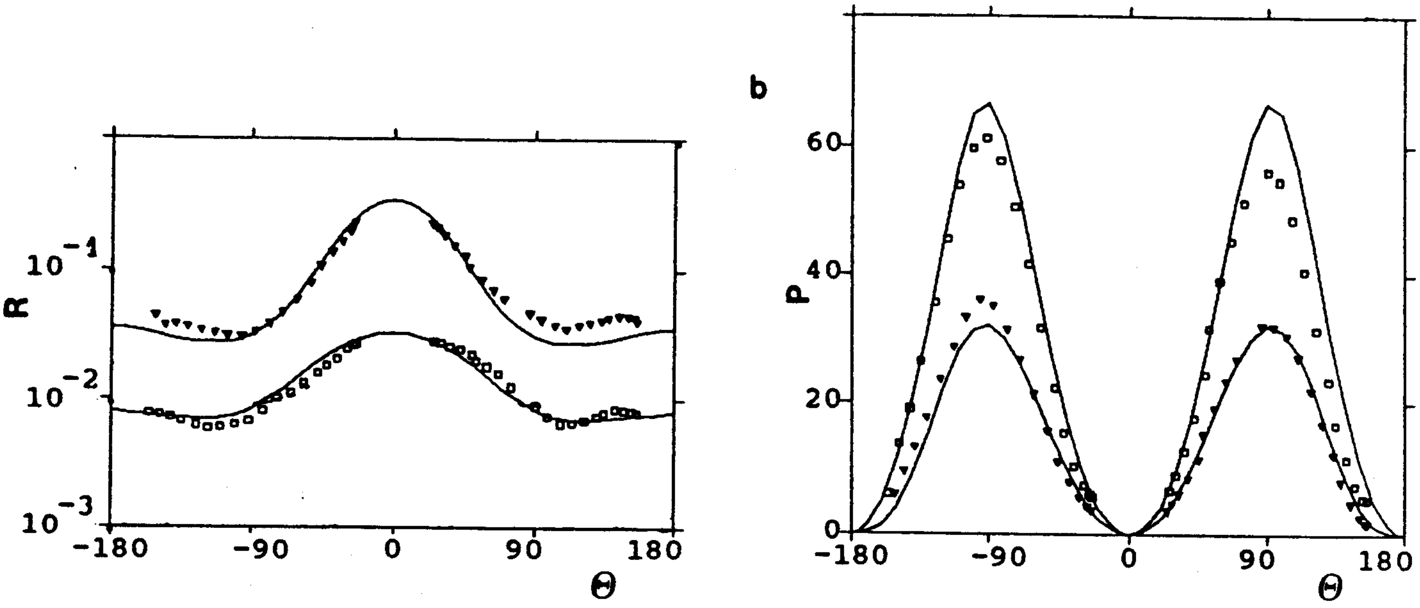

Figure 18a. Measured reflectance (left-hand curves) and polarization ratio in percent (right-hand curves), at 1650 nm (squares) and 850 nm (triangles) versus the scattering angle θ at 18.0 km altitude (the sign of θ is to distinguish observations on both sides of the sun incident plane). The diagrams retrieved with the RADIBAL model are drawn in full lines.

Figure 18b. Same as figure 18a but with the diagrams retrieved with SAGE II model (full lines).

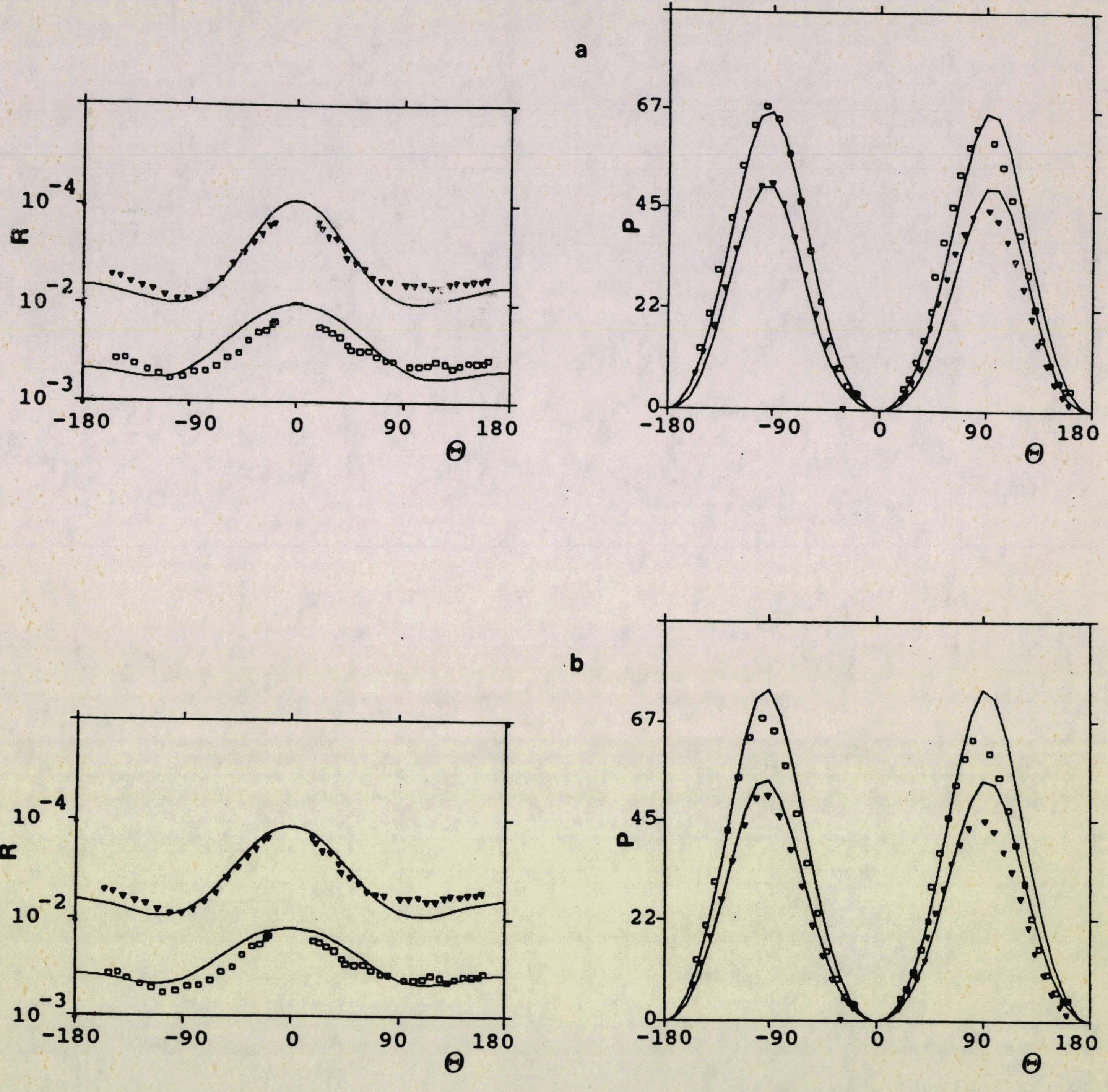

Figure 19. Same as figures 18a-b but at 21.4 km altitude.

3 Moyennes zonales

Pour l'expérience SAGE les profils de coefficient d'extinction moyennés sur des bandes de latitude de 10° pendant des périodes voisines de un mois nous avaient été procurés par la NASA. L'étude de ces moyennes zonales a été entreprise dans le but de proposer un modèle réaliste des aérosols de la stratosphère non perturbée (11). Des résultats particulièrement intéressants ont été obtenus :

- la stratosphère au dessus d'une altitude d'environ 20-25 km (dépendant de l'altitude de la tropopause, c'est à dire du lieu et de la saison) n'est pas influencée par les perturbations existant dans la basse stratosphère et dans la troposphère et on constate, en échelle semi-logarithmique, une décroissance quasi-linéaire du coefficient d'extinction avec l'altitude. Cette décroissance est caractérisée par une échelle de hauteur montrant peu de variations spatio-temporelles.

- l'analyse des coefficients d'extinction moyens m'a permis de mettre en évidence des variations saisonnières aux hautes et moyennes latitudes. J'ai pu montrer que les coefficients d'extinction des périodes estivales, qui étaient plus faibles que ceux des périodes hivernales d'environ un facteur 2, correspondaient à des aérosols plus petits. Les températures stratosphériques moyennes disponibles m'ont permis, moyennant un modèle standard de vapeur d'eau, d'évaluer les variations de taille des particules induites par les changements de température entre les différentes saisons; ces variations vont dans le même sens que les variations observées mais sont insuffisantes pour restituer la totalité des écarts existant et j'en suis arrivée à la conclusion que d'autres explications, chimiques et/ou dynamiques sont à l'origine de ces différences de dimensions.

J'ai bien entendu poursuivi avec SAGE II l'étude des moyennes zonales entreprise pour SAGE. Cette fois nous ne disposions pas des valeurs moyennées fournies par la NASA et j'ai été confrontée à un certain nombre de questions concernant la façon d'évaluer ces moyennes. J'ai dû tout d'abord établir un critère de sélection portant sur la qualité des profils à moyenner et déterminer les périodes sur lesquelles j'allais effectuer ces moyennes, compte tenu de la trajectoire du satellite. Un autre problème plus délicat a surgi : il a fallu décider si la référence était l'altitude vraie ou l'altitude comptée à partir de la tropopause. Après différentes études il s'est avéré que, contrairement à ce qui était admis, la couche d'aérosols ne suit pas les variations saisonnières de l'altitude de la tropopause, mais qu'elle est "liée" à la surface. On note toutefois une étroite relation avec la tropopause pour ce qui est du comportement latitudinal. Ces difficultés étant résolues de façon satisfaisante, j'ai vu apparaître un phénomène intéressant : les intervalles de confiance des coefficients d'extinction sont nettement plus faibles autour de 16-20 km, là où le rapport d'extinction est maximum. Cela signifie que, à ces niveaux, la circulation atmosphérique est telle que la couche d'aérosols est très bien mélangée tout autour du globe. Les barres de dispersion aux plus hautes et plus basses altitudes sont de plus raisonnables ce qui montre qu'il est tout à fait justifié de se limiter à l'étude des moyennes zonales. Lorsqu'on s'éloigne de la couche moyenne (en dessous d'environ 15 km et au dessus d'environ 24 km) la variabilité des mesures devient importante et confirme le modèle unidimensionnel de Toon et al. concernant la formation des aérosols (12). Comme pour l'expérience SAGE on observe une décroissance du coefficient d'extinction avec l'altitude et cette décroissance est corrélée dans la plupart des cas à une décroissance quasi-linéaire du rayon effectif.

Les variations temporelles du coefficient d'extinction moyen étudiées depuis octobre 1984 jusqu'à fin 1990 montrent une décroissance exponentielle, liée à la disparition progressive des aérosols dus à l'éruption du volcan El Chichon (Mars-Avril 1982); les dimensions des particules suivent le même type de variation. A ces décroissances de l'extinction et du rayon des aérosols se superposent des variations saisonnières de période voisine d'un an. Comme pour 1979-1981, le coefficient d'extinction est plus élevé en hiver ce qui correspond ici aussi à des aérosols plus gros On a toute l'année des variances faibles. L'étude des températures stratosphériques fait apparaître cette fois aussi bien des corrélations que des anti-corrélations entre leurs variations et celles des dimensions des particules et ne permet pas de conclure de la même manière que pour SAGE.

L'étude en fonction de la latitude m'a fait apparaître deux autres phénomènes :

- les courbes de variation du coefficient d'extinction présentent un minimum vers 25°- 35° dans les deux hémisphères. Ces minima existent également dans les courbes représentatives du rayon effectif en fonction de la latitude. Les latitudes auxquelles apparaissent ces minima correspondant à des zones où la tropopause est mal définie, j'ai avancé une tentative d'explication faisant intervenir des échanges troposphère-stratosphère.

- le coefficient d'extinction augmente dans la plupart des cas vers les hautes latitudes, au delà de 55° dans les deux hémisphères, mais un accroissement similaire n'apparaît pas de façon aussi nette pour le rayon effectif.

L'analyse de l'ensemble des données aérosol m'a permis de mettre en évidence l'influence de 2 éruptions volcaniques les plus importantes qui s'étaient produites pendant la période couverte par SAGE II. J'ai pu estimer la taille des aérosols injectés dans la stratosphère par le Nevado del Ruiz (novembre 1985) et par l'Etna (septembre 1986) et j'ai pu les différentier par rapport aux aérosols préexistant (13). J'ai présenté ce travail au congrès IUGG (International Union of Geodesy and Geophysics) de Vienne en Août 1991.

JOURNAL OF GEOPHYSICAL RESEARCH, VOL. 92, NO. D3, PAGES 3051-3060, MARCH 20, 1987

Modeling of the Stratospheric Background Aerosols From Zonally Averaged SAGE Profiles

C. BROGNIEZ AND J. LENOBLE

Laboratoire d'Optique Atmosphérique, Université des Sciences et Techniques de Lille, Villeneuve d'Ascq, France

The SAGE (Stratospheric Aerosol and Gas Experiment) satellite aerosol extinction profiles at 1.0 and 0.45 μm, averaged over 10° latitude bands, are used to derive a description of the background stratosphere, which is compared to the Standard Radiation Atmosphere model. At middle and high latitudes a small seasonal variation appears, with larger particles and higher optical depths in winter.

1. INTRODUCTION

Models of the atmospheric structure and its properties are necessary for a better understanding of the major physical processes which influence the climate. The models necessary for global or large-scale climate studies must be supported by experimental observations and are expected to give some realistic description of an "average" atmosphere, leaving out the detailed, local, or transient phenomena.

Models of the stratospheric aerosols have been proposed by different authors [*Pinnick et al.*, 1976; *Toon and Pollack*, 1976] and more recently in the "Standard Radiation Atmosphere" (SRA) defined by the Radiation Commission of the International Association of Meteorology and Atmospheric Physics (IAMAP) [*Radiation Commission*, 1986]. These models were based on several in situ and ground-based observations which, however, were restricted to measurements at a few places at specific times.

The SAGE (Stratospheric Aerosol and Gas Experiment) satellite [*McCormick et al.*, 1979] has provided a global data base of the stratospheric aerosols from February 1979 to November 1981; the available data are the profiles of the aerosol extinction coefficient σ_e at two wavelengths, 1.0 and 0.45 μm. A lot of work has been done with the individual extinction profiles at 1.0 μm. Volcanic eruptions have been observed and the plume transport has been followed [*Newell and Deepak*, 1982]. The ratio between extinctions at 0.45 and 1.0 μm depends on the size distribution of the particles; it provides a method for retrieving one parameter of an assumed general expression of the size distribution as well as the main radiative characteristics [*Yue and Deepak*, 1983, 1984; *Lenoble and Brogniez*, 1984].

In this paper we have used the aerosol extinction profiles, averaged over latitude bands of 10°, for each sweep of the satellite observation between the extreme northern and southern positions, that is, for a little more than a month (about 10 sweeps per year). These average profiles give the general zonally averaged information which is sought for modeling the stratospheric aerosol layer in view of general climate studies. Since a very complete description of the volcanic stratosphere after the Mount St. Helens eruption, including SAGE data, has been given by *Newell and Deepak* [1982] and *Lenoble et al.*, [1984], here we will concentrate on the background, nonperturbed stratosphere.

Copyright 1987 by the American Geophysical Union.

Paper number 6D0665.
0148-0227/87/006D-0665$05.00

In the section 2 we consider the extinction profiles at 1.0 μm and the related optical depth. Section 3 concerns the extinction ratio $\sigma_e(0.45)/\sigma_e(1.0)$, expressed as an average Angström coefficient α deduced from the relation

$$\sigma_e(\lambda) = \sigma_e(1.0)\lambda^{-\alpha} \qquad (1)$$

The Angström coefficient is a convenient indicator of the particle size, decreasing from 4 for molecular sizes to values oscillating around zero for large particles. In section 4 we discuss the seasonal variations in α and how they relate to temperature variations. Finally, section 5 proposes a stratospheric background aerosol model, which is compared to the SRA model, and our conclusions are presented in section 6.

2. EXTINCTION AT 1.0 μm

The profiles, averaged over 10° latitude bands, of the extinction coefficient $\sigma_e(1.0)$ at 1.0 μm, for the period from August 7 to September 13, 1979, are presented in Figure 1*a* for seven latitudes between 55°S to 65°N. The profiles appear quite dependent on the latitude, with larger extinctions for the same altitude at lower latitudes where the tropopause is higher. In Figure 1*b* the same profiles have been redrawn, with the tropopause altitude Z_T as the origin. Figure 1*c* shows one of the profiles (35°S) with the standard deviation of the mean value. As expected from previous observations [*Rosen et al.*, 1975], the structure of the stratospheric aerosol layer is related to the tropopause height. With an altitude scale starting at the tropopause level, all of the profiles present the same general behavior; this has been confirmed for all the periods we have considered except, of course, when a volcanic contribution is present.

2.1. *Temporal Variations*

Figure 2 presents the variation of the average extinction coefficient $\sigma_e(1.0)$ from February 1979 to November 1981 at two altitudes above the tropopause (5 and 15 km) and for three different latitudes (45°N, 5°S, and 35°S). At 5 km above the tropopause in 1979 the extinction coefficient remains quite stable between 1 and 1.5×10^{-4} km^{-1}, which can be considered as typical of the background stratosphere [*Swissler et al.*, 1982]. In 1980 and 1981 the volcanic contributions result in a strong increase in the extinction coefficient, especially in the northern hemisphere (St. Helens on May 18, 1980, at 46°N; Alaid on April 27, 1981, at 51°N; and Pagan on May 15, 1981, at 18°N) and near the equator (Sierra Negra on November 13, 1979, at 0.8°N; and Ulawun on October 7, 1980, at 5°S). The middle and high southern latitudes are only slightly perturbed by the end of 1980 (Ulawun).

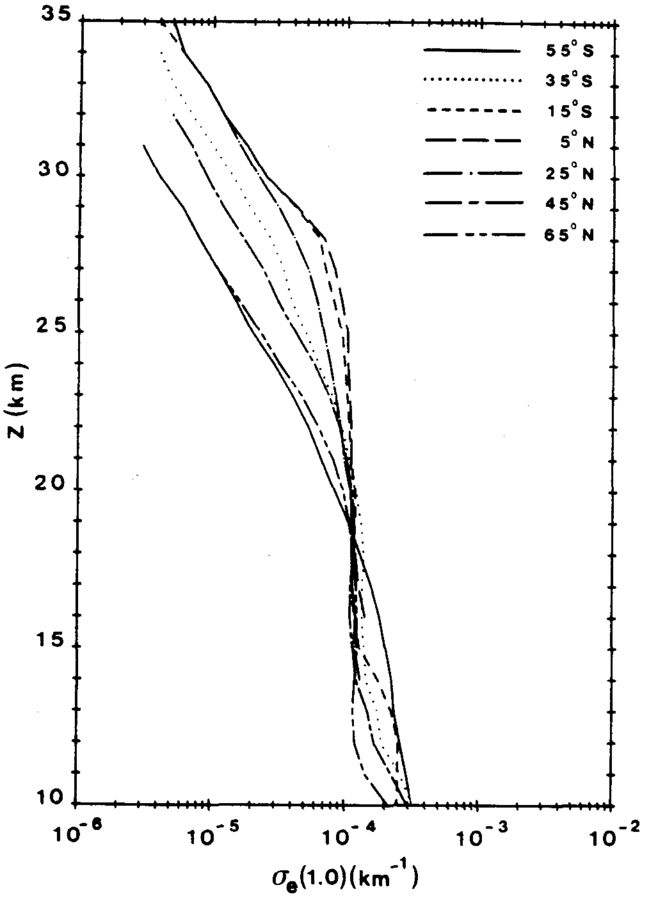

Fig. 1*a*. Aerosol extinction coefficient $\sigma_e(1.0)$ at $\lambda = 1.0$ μm versus altitude Z for the period August 7 to September 13, 1979.

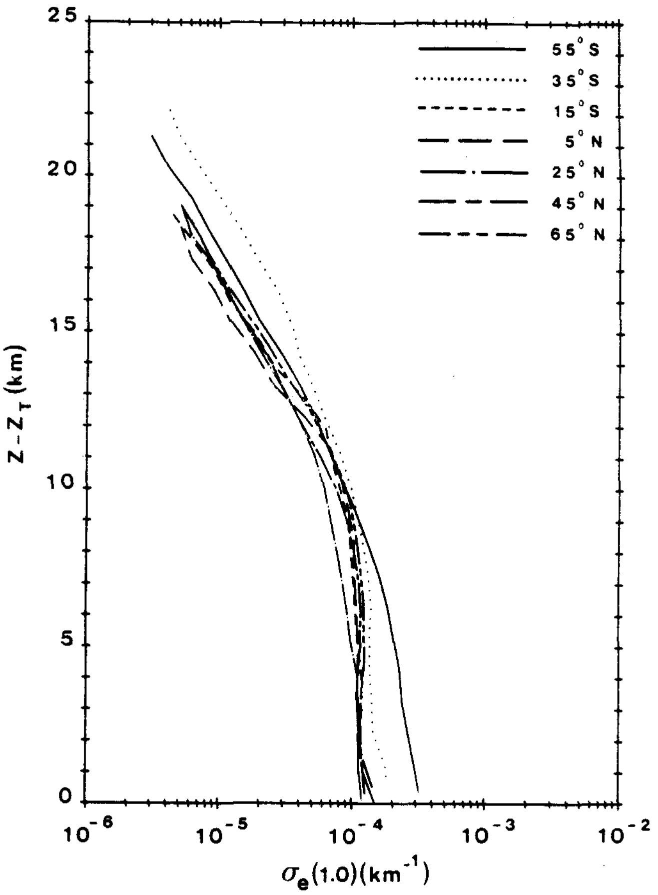

Fig. 1*b*. Same as Figure 1*a* but with the tropopause height Z_T as the origin.

At 15 km above the troposphere there is no visible influence on the extinction coefficient from the volcanic eruptions. For the low latitudes the extinction coefficient remains between 2 and 4 × 10^{-5} km^{-1} during all the considered periods, with somewhat smaller values (1–1.5 × 10^{-5} km^{-1}) at the end of 1979. For the middle and high latitudes the extinction at 15 km exhibits regular seasonal variations, with values between 3 and 5 × 10^{-5} km^{-1} during the local winter and between 1 and 2 × 10^{-5} km^{-1} during the summer.

2.2. *Altitude Variations*

Whatever the perturbations are in the lower stratosphere, the profiles become remarkably similar and almost linear on a logarithmic scale above a fixed level Z_c, which is between 10 and 15 km above the tropopause height Z_T. The profiles can be fitted by the relation

$$\sigma_e(Z) = \sigma_e(Z_c) \exp\left(-\frac{Z - Z_c}{H} \right) \qquad Z \geq Z_c \qquad (2)$$

The scale heights H, obtained by a least squares fit to the profiles, are given in Table 1; they are between 3 and 3.5 km for most cases, with extreme values of 2.4 and 4.6 km. The average value is $\bar{H} = 3.2$ km, with a standard deviation $\Delta H = 0.4$ km. In 1979 the level Z_c where the exponential decrease starts is higher in winter (around Z_T + 16 km) than in summer (around Z_T + 11 km).

In the lower stratosphere we have considered only the profiles corresponding to the nonvolcanic cases described in section 2.1. In most cases the extinction decreases very slightly with altitude. The least squares fit to the profiles points to an exponential decrease, with a scale height between 10 and 100 (i.e., a decrease of the extinction coefficient by a factor of 0.4–0.9 in the first 10 km above the tropopause). In some cases the profile oscillates around a constant value. As mentioned previously, the extinction at 5 km above the tropopause for the unperturbed stratosphere of 1979 remains around 1–1.5 × 10^{-4} km^{-1} for all latitudes.

Finally, note that between the lower stratosphere, with its almost constant extinction, and the higher stratosphere, with its exponential decrease of extinction with a scale height around 3 km, there is a transition layer around Z_c of about 2 km thickness.

2.3. *Latitudinal and Seasonal Variations of Optical Depth*

We have computed the optical depth δ at 1.0 μm above the altitude Z_T + 2 km; the reason for starting 2 km above the tropopause height is to avoid the perturbations close to the tropopause. The same limit has been used in the optical depth computed by *Kent and McCormick* [1984]. Figure 3 shows the variation of δ with the latitude for different periods of 1979, 1980, and 1981. Values as high as 5 × 10^{-3} are found after the volcanic eruptions, confirming the influence on zonal means of the high local values [*Lenoble et al.*, 1984].

For the unperturbed stratosphere of 1979 the optical depth varies between 0.7 and 1.8 × 10^{-3}. For the middle and higher latitudes a small seasonal variation appears, with larger values

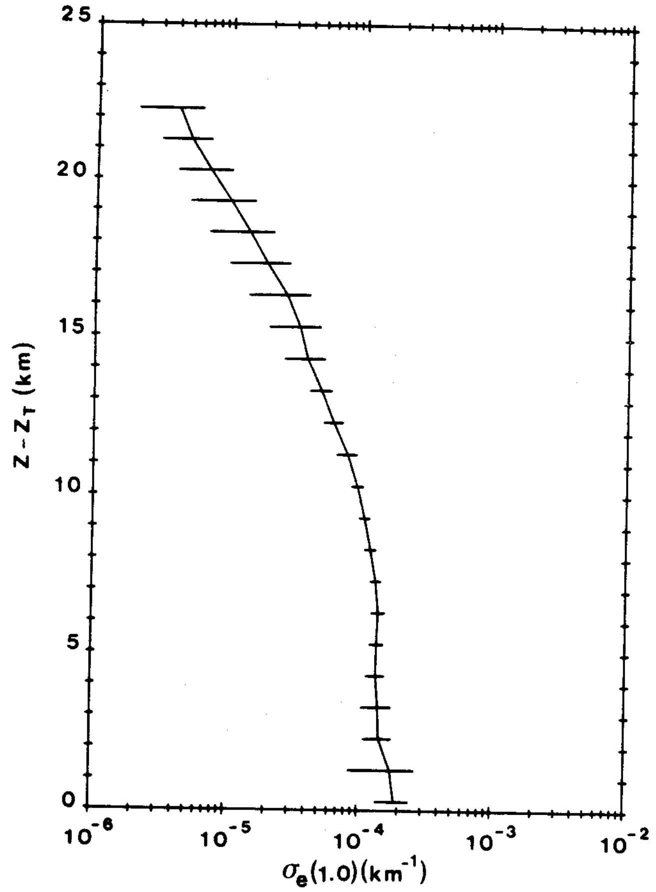

Fig. 1c. Aerosol extinction coefficient $\sigma_e(1.0)$ at 1.0 μm versus the altitude Z with the dispersion bars for latitude 35°S during the period August 7 to September 13, 1979, again with the tropopause height Z_T as the origin.

in winter than in summer. This remains true in the unperturbed or only slightly perturbed zones of the southern hemisphere in 1980 and 1981. It is, of course, related to the seasonal variation of the extinction coefficient discussed previously. Table 2 summarizes these results.

3. ANGSTRÖM COEFFICIENT

The ratio of the extinction coefficients at 0.45 and 1.0 μm is expressed by an Angström coefficient α defined in (1). In order to calculate α from the data the 1.0-μm profiles have been smoothed over 3 km so that they are coherent with the 0.45-μm profiles, which were smoothed during the inversion procedure.

The error on α is mainly due to the error on σ_e (0.45) and has been discussed in detail by *Lenoble and Pruvost* [1983]; they have concluded that there is an upper limit of about 0.5 for the error on the absolute value of α. Two contributions of approximately the same importance lead to this error: the experimental noise on the measured extinction, and the uncertainty on the Rayleigh correction. As a part of the Rayleigh error is systematic along a vertical profile, the relative precision of α is certainly better than 0.5, with a random error of about 0.3. The NO_2 gaseous extinction is corrected using the 0.385-μm channel of SAGE; even if this correction is very crude, it has been shown [*Lenoble and Pruvost*, 1983] that this cannot influence α, at least up to 25 km.

The Angström coefficient has been averaged over 10° latitude bands; the horizontal bars on Figure 5 give the standard deviation from the mean value for some cases. They are due, for one part, to the real variations from one profile to another and, for another part, to the random error on the profiles.

As mentioned previously, if one assumes a mathematical expression for the aerosol size distribution and if one fixes its variance, knowledge of α allows the determination of the mean or effective radius [*Yue and Deepak*, 1983; *Lenoble and Brogniez*, 1984]. In order to avoid any assumptions we have chosen to present here the results directly in terms of the Angström coefficient variations.

The presence of volcanic aerosols leads to irregular profiles, which have been discussed in details in the case of the Mount St. Helens eruption [*Lenoble et al.*, 1984]. We will focus our interest here on the nonperturbed stratosphere and thus consider mainly the data of 1979.

Figure 4 presents the variation of α versus the latitude for six altitudes between 2.5 and 15 km above the tropopause height and for three periods of 1979 (February 21 to March 22; April 29 to May 31; and August 7 to September 13). Examination of data from other periods of 1979 confirms the results discussed in the following sections.

3.1. *Middle and High Latitudes*

Results for the first period presented, February 21 to March 22 (Figure 4*a*), qualitatively confirm most of the conclusions of *Yue and Deepak* [1984], although their results concern the month of March and are averaged over 5° latitude bands; hereinafter, their paper will be referred to as YD.

In the southern hemisphere, at latitudes higher than 35°S, α regularly increases with altitude (from 1.3 to 1.9 at 45°N), indicating that the aerosol particle size decreases with altitude. YD also found a size decrease above 17 km, that is, above approximately $Z_T + 7$ km. However, the increase of size with altitude found by YD below 17 km appears only for lower latitudes on our curves. The size generally increases (i.e., α decreases) with latitude, again in agreement with YD. Between 20°S and 35°S, α first decreases (size increases) with altitude up to $Z_T + 7$ km, then increases (size decreases), as mentioned by YD for higher latitudes. At low levels, α decreases (size increases) when the latitude increases between 20°S and 35°S; at higher levels, α increases (size decreases) with latitude between 20°S and 35°S, in agreement with the size decrease at 22 and 24 km for these latitudes in YD [*Yue and Deepak*, 1984, Figure 2].

In the northern hemisphere, at latitudes higher than 20°N, α is almost constant with altitude (around 1.4 at 45°N), increasing slightly in the first kilometers. When the latitude increases, α decreases, again in agreement with the findings of YD.

The above-described behavior changes gradually with season. For the period from April 29 to May 21 (Figure 4*b*), northern and southern hemisphere values of α are almost identical. At latitudes higher than 35°S or 45°N, α increases regularly from 1.2 to 1.7 with altitude, but it does not reach values as large as those in February–March (1.7 instead of 2.0 at the highest level); α still decreases slightly towards the highest latitudes. The transition zones from the low-latitude behavior are between 20°–35°S and 30°–45°N.

For the period from August 7 to September 13 (Figure 4*c*), the results are almost symmetrical to the results of Figure 4*a*. We find an almost constant value of α with altitude ($\alpha \simeq 1.5$) in the southern hemisphere with an increase of α from 1.2 to 1.8 from the tropopause level up to 15 km above the tropo-

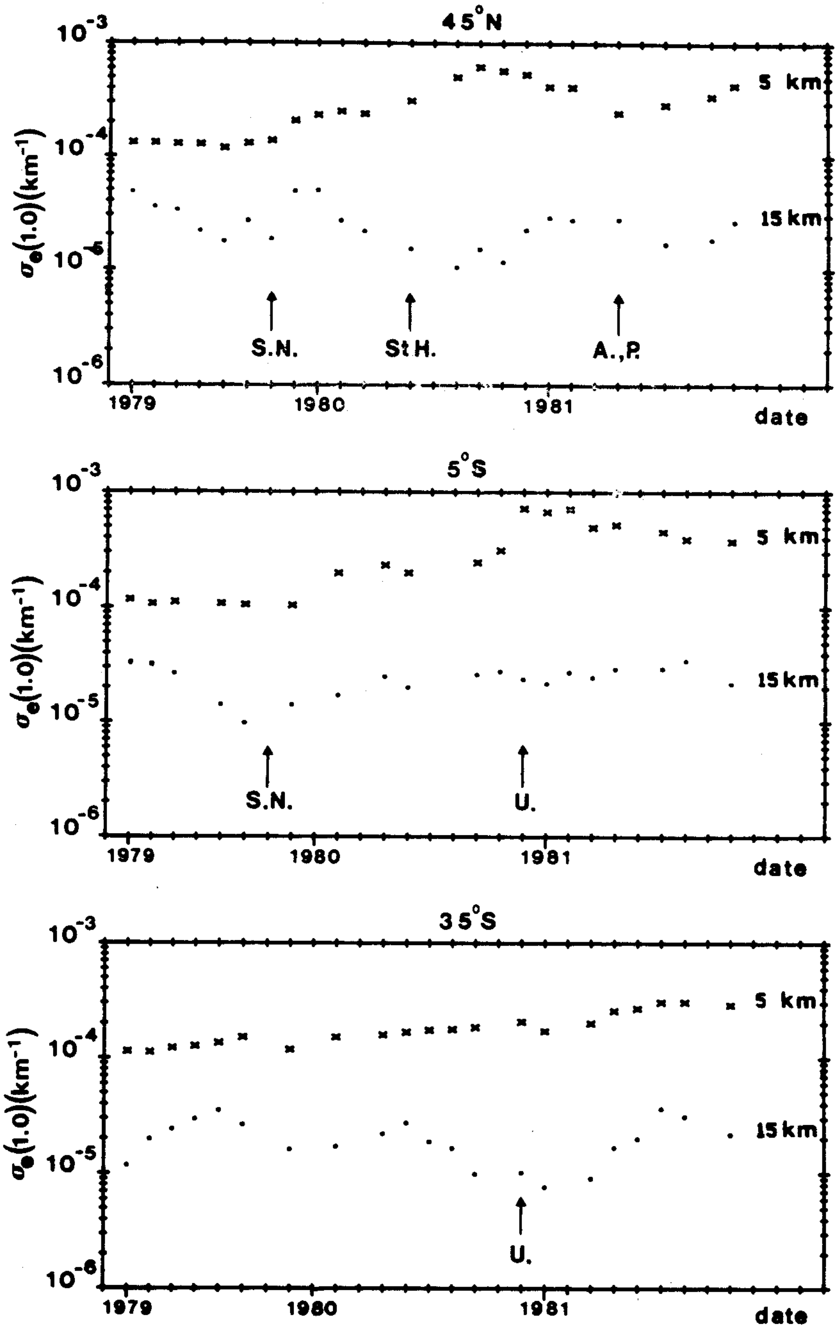

Fig. 2. Aerosol extinction coefficient $\sigma_e(1.0)$ at $\lambda = 1.0$ μm versus the date for two altitudes above the tropopause. Crosses indicate 5 km, and dots indicate 15 km. The arrows show the volcanic eruptions, labeled SN for Sierra Negra, St H for St. Helens, U for Ulawun, A for Alaïd, and P for Pagan.

pause in the northern hemisphere. The transition with the low-latitude behavior is, for both hemispheres, between 20°–35°, with an asymmetry at the level $Z_T + 2.5$ km, where surprisingly high values of α appear in the southern hemisphere.

Figure 5 shows the summer and winter vertical profiles for 55°N (Figure 5*a*) and 45°S (Figure 5*b*). The differences between summer and winter are definitively larger than the error bars.

3.2. *Low Latitudes*

Between 20°S and 20°N the Angström coefficient α, and therefore the aerosol sizes, change very little with latitude and season. The vertical profile shows a decrease (size increase) from values around 1.8 at 2 km above the tropopause to values around 1.5 at 7–10 km, and then an increase (size decrease) up to values of 1.8 or 2 at 15 km above the tropopause. Assuming a tropopause at $Z_T \simeq 16$ km, the decrease of α between $Z_T + 2$ km and $Z_T + 10$ km is in agreement with the increase in particle size found by YD from 18 km to 25 km, which is the highest altitude considered in their curves. For March, YD found a decrease of size from 15 to 18 km, that is, at and just above the tropopause level; this seems confirmed by in situ measurements made in September 1980 in the tropical stratosphere [*Goodman et al.*, 1982]. Of course, it is diffi-

TABLE 1. Values of Scale Heights *H* for All Available Periods and Latitudes

Period	75°S	65°S	55°S	45°S	35°S	25°S	15°S	5°S	5°N	15°N	25°N	35°N	45°N	55°N	65°N	75°N
Feb. 21 to March 21, 1979			3.1	3.2	3.3	3.4	3.1	2.7	2.6	2.7	3.7	3.5	2.9	3.4	3.1	
March 22 to April 28, 1979			3.4	3.3	3.4	2.9	2.8	2.5	2.6	2.8	2.8	3.3	3.0	3.2	3.3	
April 29 to May 31, 1979			3.3	3.4	3.9	3.1	2.6	X					3.4	3.1	3.0	3.0
June 1 to July 6, 1979				4.2	4.2	3.3			2.4	2.7			3.1	3.0	2.9	2.8
Aug. 7 to Sept. 13, 1979			3.2	2.8	3.0	3.1	2.7	2.8	2.8	3.2	3.3	3.4	3.3	2.9	3.0	2.9
Sept. 14 to Oct. 20, 1979		3.3	X	3.4	3.0	2.7	2.6	2.8	2.8	2.6	3.0	3.4	3.3	3.1		
Oct. 21 to Nov. 21, 1979											2.9	3.6	3.3	3.1		
Nov. 22 to Dec. 31, 1979		4.2	4.3	3.8	3.3	3.0	2.9	3.2	3.1	2.7	2.5	2.7	2.8			
Jan. 1 to Jan. 26, 1980										2.6	2.8	2.8	3.1			
Jan. 27 to March 4, 1980	3.3	3.3	3.2	3.2	3.3	3.0	2.9	3.0	3.2	2.8	2.6	2.6	2.6	2.6		
March 5 to April 7, 1980										3.1	2.8	2.7	2.7	2.8		
April 8 to May 8, 1980			3.3	3.2	3.3	3.2	3.0	3.2								
May 11 to June 22, 1980				3.1	3.0	3.1	3.1	3.3	3.4	3.2	3.3	3.1	3.0	3.2	2.8	2.8
June 23 to July 19, 1980				2.9	2.7	3.0	2.9									
July 20 to Aug. 27, 1980			2.8	2.9	3.2	3.2	3.3	3.2	3.4	3.3	3.4	3.3	3.4	2.9	3.0	
Aug. 28 to Sept. 27, 1980			2.9	2.9	2.9	3.0	3.5	3.7	3.9		3.4	3.5	3.3	3.4	2.9	
Sept. 28 to Oct. 30, 1980								3.2	3.7	3.1	3.2	3.4	3.0	3.3	3.0	
Oct. 31 to Dec. 13, 1980	X	3.8	3.3	3.2	3.4	3.4	X	3.8	3.7	X	3.4	3.5	3.5			
Jan. 11 to Feb. 17, 1981		3.4	3.4	3.3	3.4	3.3	3.6	3.9	3.6	3.6	3.8	3.5	3.6	3.5		
Feb. 18 to March 17, 1981		3.1						3.2	3.0	3.0	3.6	3.3	3.5	3.7		
March 18 to April 20, 1981		3.3	3.2	3.2	X	3.7	X	X	X	X						
April 21 to May 30, 1981				4.6	4.1	3.8	3.1	3.1	3.0	3.0	3.1	3.7	4.4	X	3.6	4.1
June 5 to July 2, 1981				X	3.9	3.4									3.1	
July 3 to Aug. 10, 1981			3.0	X	X	3.7	2.8	2.4	2.6	3.0	3.4	3.4	4.1	3.6	3.1	
Aug. 15 to Aug. 27, 1981				3.7	3.9	3.7	3.9	3.5	3.5							
Sept. 4 to Oct. 1, 1981											4.0	3.8	4.3	3.7	3.2	3.0
Oct. 12 to Nov. 18, 1981	X	X	4.6	3.7	3.7	3.5	3.1	2.8	2.4	2.9	4.1	3.9				

Scale heights are given in kilometers. The crosses indicate irregular profiles.

cult to make definitive conclusions from SAGE data because many profiles are perturbed and irregular close to the tropopause level.

3.3. *Seasonal Variations*

As already discussed, the vertical profile of α is almost constant during the winter and increases with altitude in summer for both hemispheres at middle and high latitudes. Figure 5 shows these profiles for the two seasons at 45°S and 55°N. Moreover, it appears that α is larger in summer, at least above $Z_T + 7$ km. We note that the extinction coefficient is smaller in summer (Figure 2), when α is larger. The decrease of the extinction, and therefore of the optical depth, in summer seems to be explained by the presence of smaller particles in this season.

Table 3 summarizes the differences $\delta\alpha$ between α_{summer} and α_{winter} at two levels (12.5 km and 15 km) for the two hemispheres in 1979 and for the southern hemisphere in 1980 and 1981, where the volcanic perturbation is small. Of course, both the imprecision in the measurements of α and the existence of transient phenomena have to be kept in mind. Nevertheless, we have an average $\overline{\delta\alpha} = 0.28$ between summer and winter in 1979 for both hemispheres, $\overline{\delta\alpha} = 0.40$ for the northern hemisphere alone in 1979, and $\overline{\delta\alpha} = 0.20$ for the southern hemi-

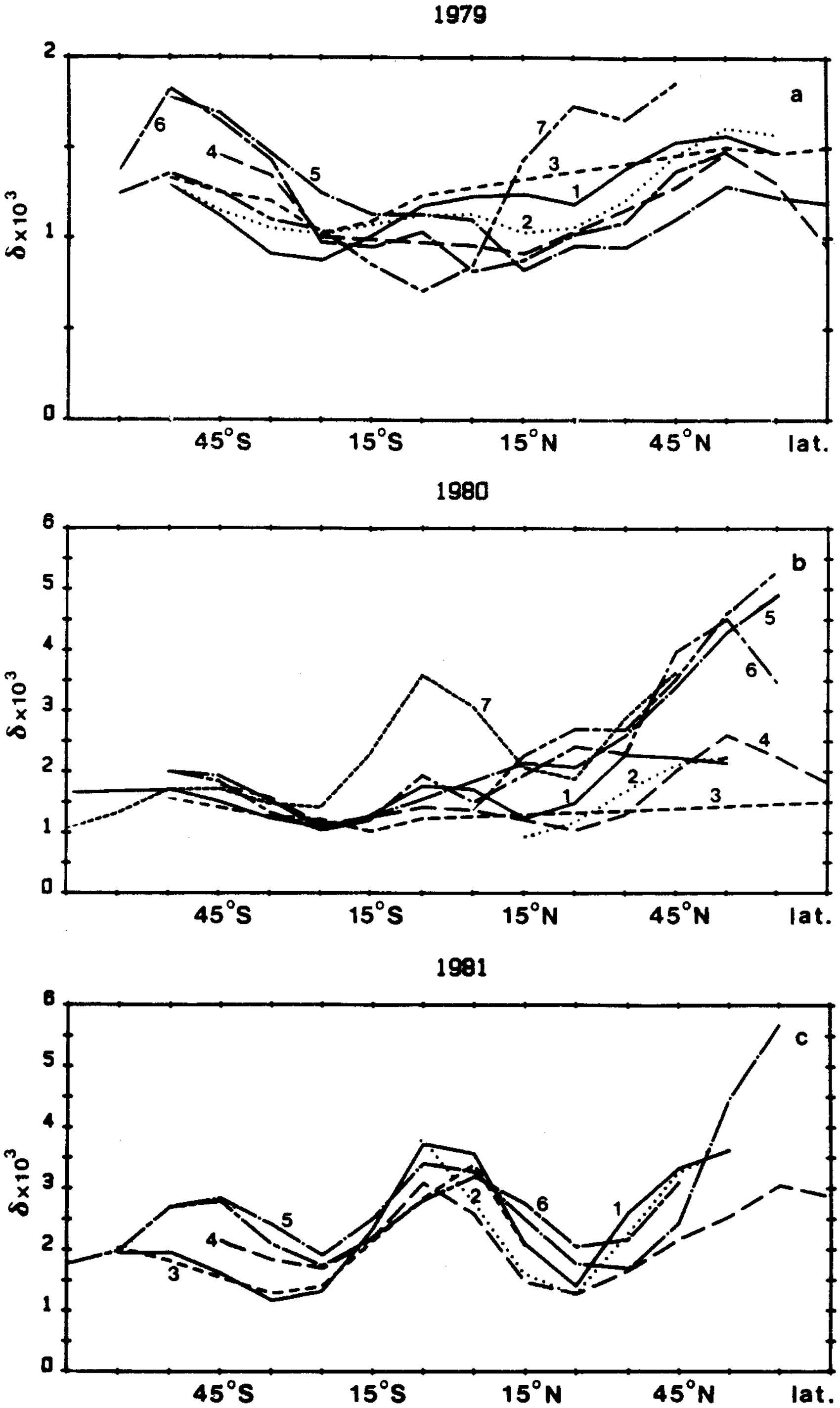

Fig. 3. Optical depth $\delta \times 10^3$ versus latitude for (*a*) 1979: curve 1, February 21 to March 21; curve 2, March 22 to April 28; curve 3, April 29 to May 31; curve 4, June 1 to August 6; curve 5, August 7 to September 13; curve 6, September 14 to October 20; curve 7, November 22 to December 30. (*b*) 1980: curve 1, January 27 to March 4; curve 2, March 5 to April 7; curve 3, April 8 to May 8; curve 4, May 11 to June 22; curve 5, July 20 to August 27; curve 6, August 28 to September 27; curve 7, September 28 to October 30; curve 8, October 31 to December 13. (*c*) 1981: curve 1, January 11 to February 17; curve 2, February 18 to March 17; curve 3, March 18 to April 20; curve 4, April 21 to May 30; curve 5, July 2 to August 10; curve 6, October 12 to November 18.

sphere and the three years; these values, although approximative, point certainly to a real seasonal effect, which we will try to discuss in the next section.

4. DISCUSSION OF THE SEASONAL VARIATIONS

SAM (Stratospheric Aerosol Measurement) II observations have shown very high extinctions related to the very low temperatures in the polar regions [*McCormick et al.*, 1982]. Possibly, this can be explained by an increase in the aerosol sizes when the temperature decreases. Although this is true at all stratospheric temperatures, the aerosol size increase becomes important and has noticeable effects as "polar stratospheric clouds" only below a threshold of about 200 K [*Steele and Hamill*, 1981; *Yue and Deepak*, 1981]. The water vapor pres-

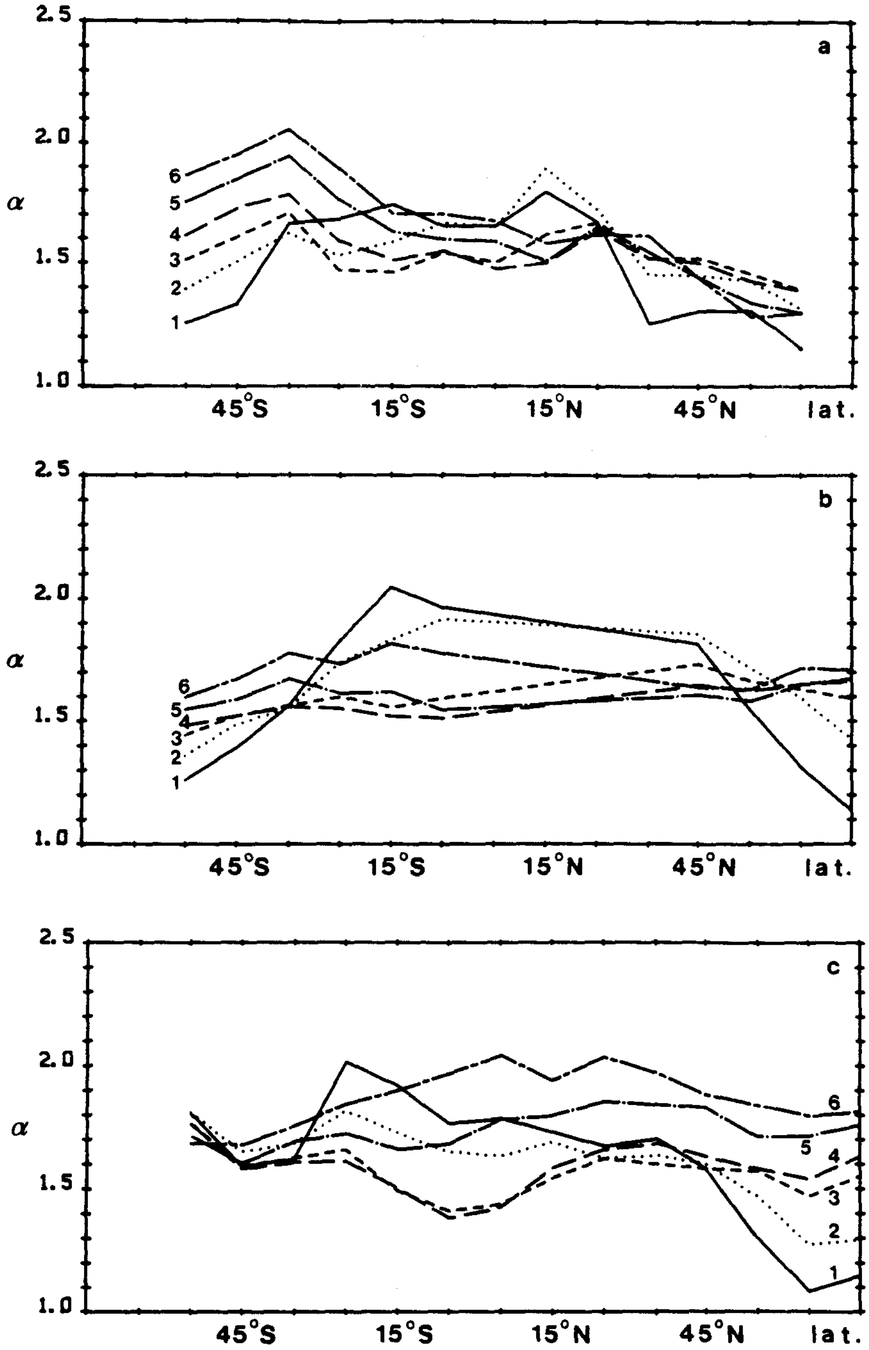

Fig. 4. Angström coefficient α between 0.45 and 1.0 μm versus latitude for various altitudes above the tropopause: curve 1 shows the plot at 2.5 km; curve 2 at 5 km; curve 3 at 7.5 km; curve 4 at 10 km; curve 5 at 12.5 km; and curve 6 at 15 km. (*a*) February 21 to March 21, 1979; (*b*) April 29 to May 31, 1979; and (*c*) August 7 to September 13, 1979.

sure also influences the particle sizes, which increase with the H_2O pressure.

The SAGE data suggest that for the 1979 background stratosphere, the extinction presents a small seasonal variation in the high stratosphere with somewhat larger extinction in winter, which is related to smaller values of α, that is, larger particles in winter. For lognormal (LND) size distributions (see equation (3)) a decrease of α from approximately 1.9 to 1.5 is consistent with an increase of σ_e by a factor around 2.5. In Table 3 the average stratospheric temperatures for both seasons are given from the SAGE tape 1981 meteorological data. One can observe that the temperature is approximately 15 K higher in summer ($T \simeq 230$ K) than in winter ($T \simeq 215$ K). However, the temperature is always above the threshold value needed for a large influence on the particle sizes. The increase of α with altitude in summer also seems related to an increase of temperature, whereas the high stratosphere is almost at constant temperature in winter and with a constant value of α.

We have tried to explain the seasonal variation of the particle sizes by applying the results of *Steele and Hamill* [1981]. Unfortunately, we do not have values of the water vapor pressure; we have used values of 2×10^{-4} mbar for winter and

TABLE 2. Optical Depth δ at 1.0 μm for the Unperturbed Periods

Year	Latitude	Local winter, $\delta \times 10^3$	Local summer, $\delta \times 10^3$	$10^3(\delta_{\text{winter}} - \delta_{\text{summer}})$
		Low Latitudes		
1979	25°S	1.24	0.87	0.37
	15°S	1.12	1.01	0.11
	5°S	1.12	1.18	−0.06
	5°N	1.23	1.09	0.14
	15°N	1.24	0.82	0.42
	25°N	1.19	0.95	0.24
		Middle and High Latitudes		
1979	55°S	1.78	1.28	0.50
	45°S	1.69	1.11	0.58
	35°S	1.46	0.91	0.55
	35°N	1.38	0.95	0.43
	45°N	1.53	1.10	0.43
	55°N	1.56	1.28	0.28
	65°N	1.47	1.22	0.25
1980	55°S	2.00	1.70	0.30
	45°S	1.87	1.50	0.37
	35°S	1.51	1.22	0.29
1981	55°S	2.70	1.95	0.75
	45°S	2.79	1.60	1.19
	35°S	2.37	1.15	1.22

3×10^{-4} mbar for summer from balloon measurements between 20 and 30 km in February and July 1979 [*Fischer et al.*, 1985].

Assuming a lognormal size distribution,

$$n(r) = \frac{1}{(2\pi)^{1/2} r \ln \sigma} \exp\left(-\frac{\ln^2 r/r_m}{2 \ln^2 \sigma}\right) \qquad (3)$$

with a variance $\sigma = 1.60$, an average winter value of $\alpha_{\text{winter}} = 1.55$ gives $r_m^{\text{winter}} = 0.132$ μm. Using the results of *Steele and Hamill* [1981, Table 1] the mode radius should be multiplied by approximately 0.94 to give the summer value $r_m^{\text{summer}} = 0.122$ μm, leading to $\alpha_{\text{summer}} = 1.67$ and $\delta\alpha = 0.12$. This is less than one-half the experimental value.

TABLE 3. Seasonal Effect on α

$Z - Z_T$, km	Latitude	Temperature, K Summer	Temperature, K Winter	$\alpha_{\text{summer}} - \alpha_{\text{winter}}$ 1979	1980	1981
		Southern Latitudes				
12.5	55°S	229	210	0.05	0.15	0.15
12.5	45°S	228	214	0.15	0.33	0.15
12.5	35°S	229	221	0.15	0.15	0.20
12.5	25°S	228	225	−0.05	−0.15	0.15
15	55°S	232	210	0.20	0.15	0.25
15	45°S	232	215	0.25	0.20	0.25
15	35°S	235	224	0.30	0.10	0.30
15	25°S	233	229	0.05	−0.05	0.20
		Northern Latitudes				
12.5	65°N	228	214	0.40		
12.5	55°N	225	218	0.40		
12.5	45°N	227	220	0.40		
12.5	35°N	228	218	0.30		
12.5	25°N	229	223	0.20		
15	65°N	231	213	0.50		
15	55°N	228	220	0.55		
15	45°N	231	222	0.45		
15	35°N	232	222	0.35		
15	25°N	233	228	0.40		

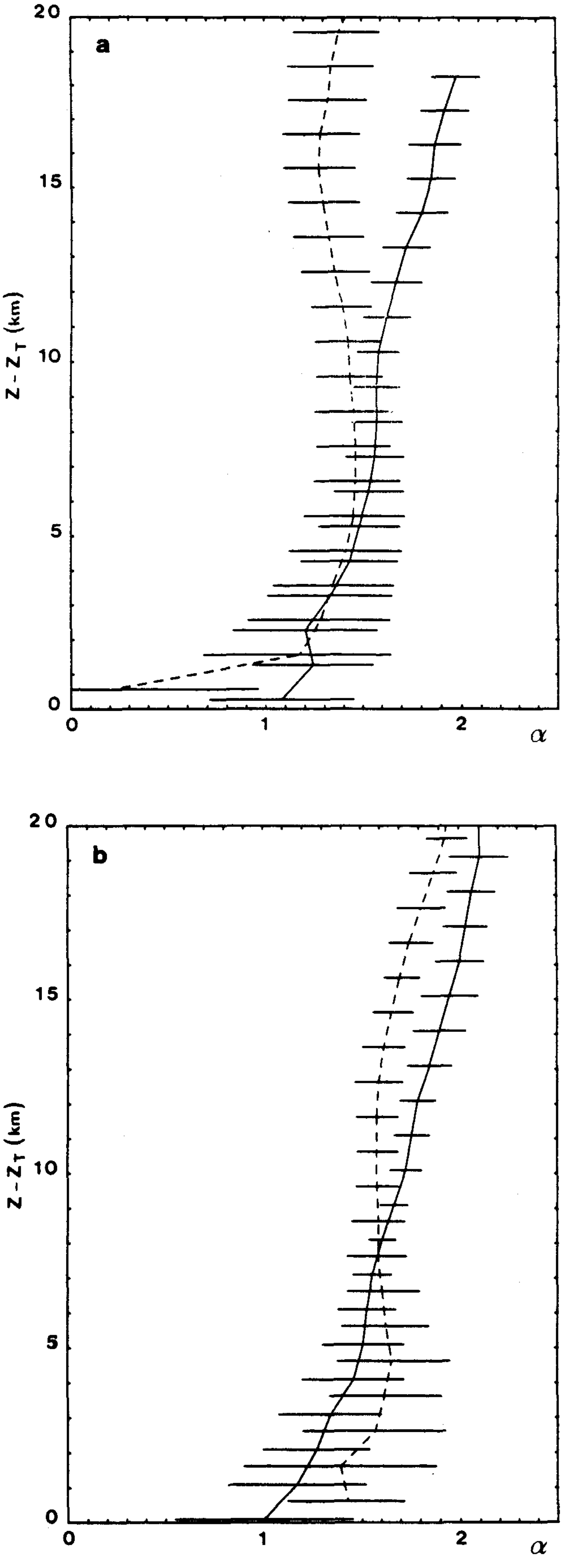

Fig. 5. Angström coefficient α versus altitude Z with the dispersion bars for summer (solid line) and winter (dashed line); the origin is the tropopause height Z_T. (*a*) Latitude 55°N; (*b*) latitude 45°S.

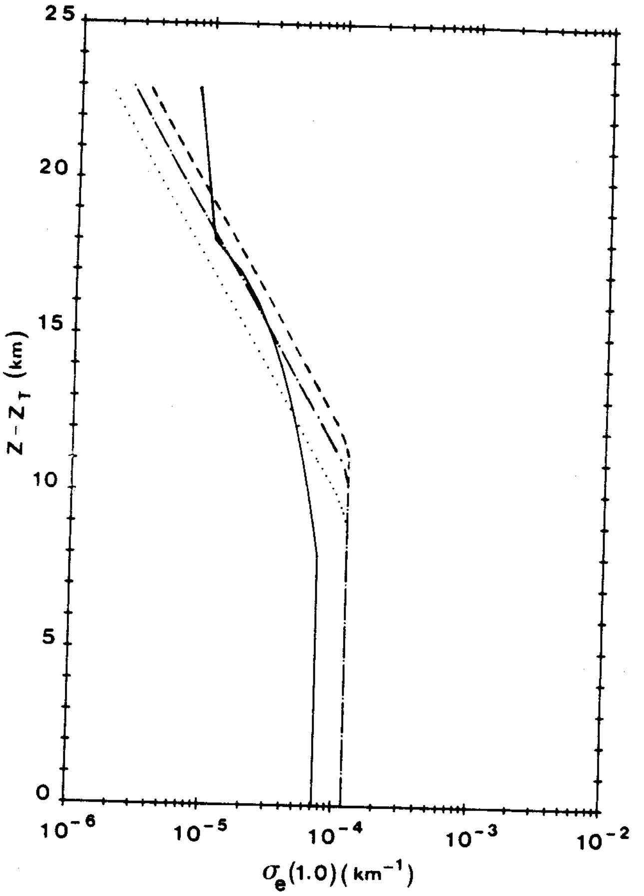

Fig. 6. Comparison between the SRA profile and the SAGE profiles of the aerosol extinction $\sigma_e(1.0)$ at 1.0 μm; Z is the altitude and Z_T is the tropopause height. The solid line indicates the SRA; the dashed line, high-latitude winter; the dotted line, high-latitude summer; and the dot-dashed line, low latitude."

Changing the variance of the size distribution to $\sigma = 1.92$ does not significantly change the above results. The temperature and water vapor variations also affect the refractive index [*Steele and Hamill*, 1981, Table 3]. However, for the variation range which we have to consider, the variations of the refractive index can be neglected. We have assumed a change of H_2O pressure from 2×10^{-4} mbar in winter to 3×10^{-4} mbar in summer, and this change slightly counterbalances the temperature influence. The increase of the mode radius from summer to winter would be slightly larger (1 or 2%), if the water vapor content remained constant or even increased in winter.

In conclusion, it seems that the higher extinction found in winter is due to an increase of the particle sizes. This happens when the temperature is colder, but the theoretical results of *Steele and Hamill* [1981] seem to slightly underestimate the temperature effect. Explanations could be sought in stratospheric chemistry or dynamics; they are beyond the scope of this paper.

5. A MODEL OF THE BACKGROUND STRATOSPHERIC AEROSOL

Summarizing the 1979 zonally averaged SAGE observations that we have described in the previous sections leads to the following rough description of the unperturbed stratospheric aerosol layer. The vertical profile of the stratospheric aerosol extinction is approximately constant in the first 10 km above the tropopause, with $\sigma_e = 1.2 \times 10^{-4}$ km^{-1} at 1.0 μm; in the upper level the decrease is exponential, with a scale height $H \simeq 3.2$ km. Fixing the 1.0-μm extinction coefficient at 15 km above the tropopause at 1.5×10^{-5} km^{-1}, 3×10^{-5} km^{-1}, and 4×10^{-5} km^{-1}, for the high-latitude summer, the low latitudes, and the high-latitude winter, respectively, leads to a transition altitude Z_c equal to 8.4 km, 10.6 km, and 11.5 km above the tropopause for the same cases, respectively. The corresponding optical depths δ from 2 to 18 km above the tropopause are 1.1×10^{-3}, 1.4×10^{-3}, 1.5×10^{-3}, respectively; extrapolation of the same profile at higher altitudes adds a contribution of about 1% to the optical depth.

These profiles are compared to the SRA model [*Radiation Commission*, 1986] in Figure 6. The SRA fixes the tropopause height at $Z_T = 12$ km; the values of extinction and optical depth are given at 0.55 μm, but they can be converted to 1.0 μm using the aerosol size distribution. For 12 km (Z_T) to 20 km ($Z_T + 8$ km) the extinction coefficient is constant with $\sigma_e = 0.68 \times 10^{-4}$ km^{-1} at 1.0 μm, which is a little lower than the average value from SAGE data in 1979. From 20 to 30 km ($Z_T + 8$ to $Z_T + 18$ km) the decrease is linear instead of exponential, as shown from SAGE average profiles, the value of $\sigma_e(1.0)$ at 30 km being fixed at 0.10×10^{-4} km^{-1}. This leads to an optical depth at 1.0 μm from $Z_T + 2$ km to $Z_T + 18$ km of 0.8×10^{-3}. The SRA model then corresponds to a background stratosphere with a minimum aerosol content, even

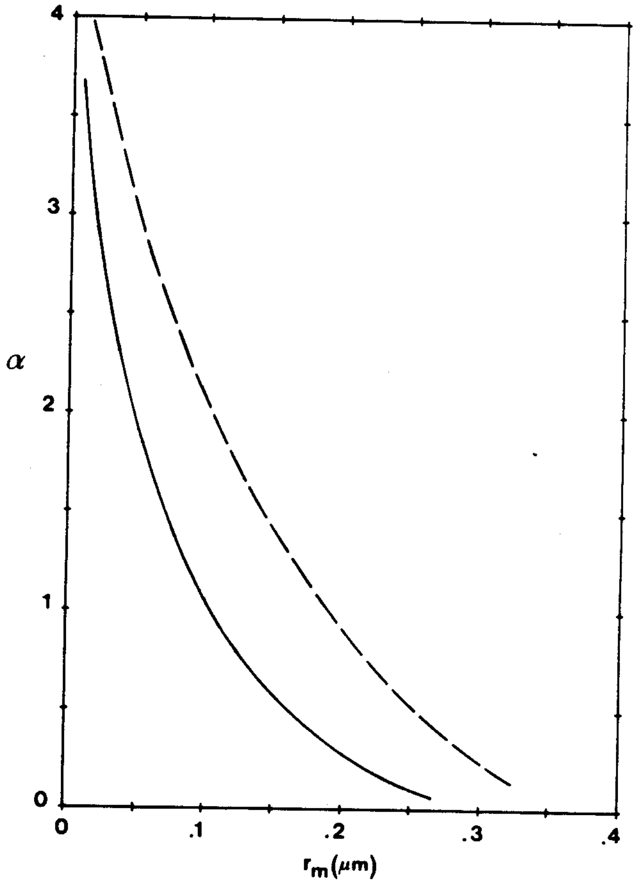

Fig. 7. Angström coefficient α versus mode radius r_m for two log-normal distributions. Solid line indicates $\sigma = 1.60$; the dashed line shows $\sigma = 1.92$.

lower than in 1979. Its main drawbacks are the fixed tropopause altitude and the linear decrease from 8 to 18 km above the tropopause level, which has to be replaced by an exponential decrease.

The size distribution in the SRA model is a modified gamma distribution, which is almost equivalent for the radiative properties in the solar spectrum to a LND size distribution with $\sigma = 1.60$ and $r_m = 0.127$ μm [*Lenoble and Brogniez*, 1984]; it gives an Angström coefficient $\alpha = 1.68$ defined by (1) between 0.45 and 1.0 μm which is reasonable, although a little too high for an average global model. However, a more detailed description should include the variation of the particle sizes found by SAGE. For the middle and high latitudes in winter the average value of α is around 1.55 at all altitudes, while in summer, α increases regularly with the altitude from 1.2, close to the tropopause, to 2.0 at 20 km above the tropopause. Figure 7 shows the relation between α and r_m for two LND models, with $\sigma = 1.60$ and $\sigma = 1.92$. With $\sigma = 1.60$, the values found for α correspond to $r_m = 0.132$ μm in winter and a variation from $r_m = 0.170$ μm to $r_m = 0.104$ μm with altitude for summer, respectively, instead of r_m fixed at 0.127 μm by the SRA. For the low latitudes, α oscillates between approximately 1.5 and 1.8 (r_m between 0.142 and 0.118 μm), with α minimum (r_m maximum) at about 10 km above the tropopause and larger values (r_m smaller) at lower and higher levels.

6. CONCLUSIONS

The SAGE aerosol extinction profiles at 1.0 and 0.45 μm have been averaged over 10° latitude bands and used to give a general description of the background stratosphere which is observed in 1979 before the series of volcanic eruptions of 1980 and 1981; the data of the southern hemisphere, which is perturbed very little, have also been used in 1980–1981.

The extinction profiles at 1.0 μm are directly used to study the vertical, seasonal, and latitudinal variation of the aerosols, whereas the profiles at 0.45 μm are used to compute the ratio σ_e (0.45)/σ_e (1.0) and the related Angström coefficient and to derive additional information about the particle sizes. The vertical profiles of extinction follow the tropopause altitude variations and a model must use the actual tropopause height as an origin for the aerosol profile, instead of a fixed value, as in the Standard Radiation Atmosphere (SRA) model proposed by the *Radiation Commission* [1986].

In approximately the first 10 km above the tropopause, the extinction is almost constant, with a value slightly higher than in the SRA model; above 10–12 km the decrease is exponential instead of linear, as in the SRA model, with an average scale height of 3.2 km; the standard deviation around this value is 0.4 km. The extinction, and therefore the optical depth, are slightly higher in winter than in summer.

The particle size is found almost constant at all altitudes in winter, whereas it decreases when the altitude increases in summer; above 10 km the particles are larger in winter than in summer, which is consistent with the larger extinctions found in winter. An attempt to explain this particle size increase by colder temperatures in winter accounts only for about one-half of the size increase.

Acknowledgments. The SAGE latitude average profiles were kindly provided to us by G. S. Kent and V. O. Farrukh. We are also grateful to C. Deroo for her efficient help in the numerical computations. This work was supported by the Centre National d'Etudes Spatiales under contract 1230.

REFERENCES

Fischer, H., F. Fergg, and D. Rabus, Stratospheric H_2O and HNO_3 profiles derived from solar occultation measurements, *J. Geophys. Res.*, *90*, 3831–3843, 1985.

Goodman, J., K. G. Snetsinger, G. V. Ferry, N. H. Farlow, H. Y. Lem, and D. M. Hayes, Altitude variations in stratospheric aerosols of a tropical region, *Geophys. Res. Lett.*, *9*, 609–612, 1982.

Kent, G. S., and M. P. McCormick, SAGE and SAM II measurements of global stratospheric aerosol optical depth and mass loading, *J. Geophys. Res.*, *89*, 5303–5314, 1984.

Lenoble, J., and C. Brogniez, A comparative review of radiation aerosol models, *Contrib. Atmos. Phys.*, *57*, 1–20, 1984.

Lenoble, J., and P. Pruvost, Inference of the aerosol Angström coefficient from SAGE short-wavelength data, *J. Clim. Appl. Meteorol.*, *22*, 1717–1725, 1983.

Lenoble, J., P. Pruvost, and C. Brogniez, SAGE satellite observations of stratospheric aerosols from Mount St. Helens eruption: A two-wavelength analysis, *J. Geophys. Res.*, *89*, 11,666–11,676, 1984.

McCormick, M. P., P. Hamill, T. J. Pepin, W. P. Chu, T. J. Swissler, and L. R. McMaster, Satellite studies of the stratospheric aerosol, *Bull. Am. Meteorol. Soc.*, *60*, 1038–1046, 1979.

McCormick, M. P., H. M. Steele, P. Hamill, W. P. Chu, and T. J. Swissler, Polar stratospheric cloud sightings by SAM II, *J. Atmos. Sci.*, *39*, 1387–1397, 1982.

Newell, R. E., and A. Deepak (Ed.), Mount St. Helens eruptions of 1980: Atmospheric effects and potential climatic impact, *NASA SP-458*, 119 pp, 1982.

Pinnick, R. G., J. M. Rosen, and D. J. Hofmann, Stratospheric aerosol measurements III: Optical model calculations, *J. Atmos. Sci.*, *33*, 304–314, 1976.

Radiation Commission, A preliminary cloudless standard atmosphere for radiation computation, *WCP-112*, Int. Assoc. of Meteorol. and Atmos. Phys., March 1986. (Available from World Meteorol. Organ., case postale 5, Genève 1211, Suisse).

Rosen, J. M., D. J. Hofmann, and J. Laby, Stratospheric aerosol measurements II: The worldwide distribution, *J. Atmos. Sci.*, *32*, 1457–1462, 1975.

Steele, H. M., and P. Hamill, Effects of temperature and humidity on the growth and optical properties of sulphuric acid water droplets in the stratosphere, *J. Aerosol Sci.* *12*, 517–528, 1981.

Swissler, T. J., P. Hamill, M. Osborn, P. B. Russel, and M. P. McCormick, A comparison of lidar and balloon-borne particle counter measurements of the stratospheric aerosol 1974–1980, *J. Atmos. Sci.*, *39*, 909–916, 1982.

Toon, O. B., and J. B. Pollack, A global average model of atmospheric aerosols for radiative transfer calculations, *J. Appl. Meteorol.*, *15*, 225–246, 1976.

Yue, G. K., and A. Deepak, Modeling of growth and evaporation effects on the extinction of 1.0-μm solar radiation traversing stratospheric sulfuric acid aerosols, *Appl. Opt.*, *20*, 3669–3675, 1981.

Yue, G. K., and A. Deepak, Retrieval of stratospheric aerosol size distribution from atmospheric extinction of solar radiation at two wavelengths, *Appl. Opt.*, *22*, 1639–1645, 1983.

Yue, G. K., and A. Deepak, Latitudinal and altitudinal variation of size distribution of stratospheric aerosols inferred from SAGE aerosol extinction coefficient measurements at two wavelengths, *Geophys. Res. Lett.*, *11*, 999–1002, 1984.

C. Brogniez and J. Lenoble, Laboratoire d'Optique Atmosphérique, UA 713, Université des Sciences et Techniques de Lille, 59655 Villeneuve d'Ascq Cedex, France.

(Received March 6, 1986;
revised October 10, 1986;
accepted November 12, 1986.)

ZONAL DISTRIBUTION OF AEROSOLS FROM SAGE II EXTINCTION PROFILES

C. Brogniez and J. Lenoble
Laboratoire d'Optique Atmosphérique
Université des Sciences et Techniques de Lille
Villeneuve d'Ascq, France

ABSTRACT

The data provided by the Stratospheric Aerosol and Gas Experiment II (SAGE II), at 1.02 μm, are averaged in view of zonal and seasonal study. The profiles of extinction versus altitude reveal a particular behaviour.

1. INTRODUCTION

The Stratospheric Aerosol and Gas Experiment II (Mauldin et al.,1985) has provided daily data of stratospheric aerosol profiles from October 1984 to November 1987 at four wavelengths : 1.02, 0.525, 0.453 and 0.385 μm.

In view of climate studies these profiles are generally zonally averaged to obtain informations on the stratospheric aerosol layer, the so called Junge layer, for allowing zonal and seasonal study of the aerosol distribution (Brogniez and Lenoble, 1987).

We have investigated to what degree it is significant to average these profiles, that is to say to what degree the measurements are distributed around the mean value with a small dispersion. Our study has been done for the aerosol extinction coefficient at 1.02 μm because it is the most accurate aerosol data (Chu et al., 1988).

2. AVERAGED PROFILES AND DISPERSION

The profiles are averaged over latitude bands of 10° for each sweep of the satellite between the North and the South, that is for about one month. Taking into account the trajectory of the satellite, the average for a latitude band is made during a short period of a few days (1 to 5 days). In most of the latitude bands there are generally between 20 and 100 profiles. We have averaged the measurements for each altitude and we have calculated the ratio of the standard deviation to the mean, multiplied by 100, ie :

$$\%SD = 100\frac{\sigma_x}{E(x)}$$

where $E(x)$ is the mean of the extinction measurements x_i and σ_x is the standard deviation.

Figure 1 shows the mean extinction coefficient $E(x)$ at 1.02 μm and the per cent dispersion (% SD) versus altitude above the mean tropopause height for the same period at latitudes 45 N (1-a), and 05 S (1-b) during the spring 1985. We have also noted the number of profiles in the latitude band and the mean tropopause height.

The first noticeable result is that at high and middle latitudes (greater than 15° N and 15° S) the dispersion is small ($\simeq$ 10-15 %) around an altitude of about 4-8 km above the tropopause; at lower and higher levels the % SD increases rapidly. This minimum in the % SD happens where the extinction coefficient is large, about $10^{-3} km^{-1}$, but not an extreme. The altitude where the % SD is minimum varies slightly during the year, but without any obvious seasonal effect (Figure 2).

For low latitudes the % SD is almost constant, smaller than 10 % above the same level of about 5 km up to about 15 km and remains lower than 25 % up to 20 km above the tropopause height.

We observe the same behaviour during the two years 1985 and 1987. For 1986 the % SD profiles are generally more irregular at least for one half of the cases, even at low latitudes, and the % SD is often greater than 20 % (Figure 3).

3. DISCUSSION

The altitude variation of % SD observed at high and middle latitudes, with a strong minimum at a given altitude, could be due either to a better quality of the measurements in this layer, or to a better zonal homogeneity of the aerosol layer at this altitude.

In order to check if the per cent dispersion variation is partly due to the measurement errors we have calculated the mean relative error multiplied by 100, ie :

$$\%RE = \frac{100}{N}\sum_{i=1}^{N}\frac{\Delta x_i}{x_i}$$

where N is the number of measurements and Δx_i is the error on the extinction measurement x_i given on the SAGE II tapes. For comparisons the profile of the per cent mean relative error (% RE) is drawn in Figure 1.

We see that this % RE is rather small (< 15 % and even 10 %) for all levels up to 15 km above the mean tropopause height, that is to say the individual profiles are of good quality at all levels, where the extinction coefficient is larger than nearly 10^{-5} km^{-1}. This is true for the three years, including 1986.

The comparison between the per cent dispersion and the per cent mean relative error proves that the existence of a minimum in the per cent dispersion profile (during 1985 and 1987) is not correlated to a better quality of the measurements. When the dispersion around the mean value is small at about 4-8 km above the tropopause height, that means the measurements have little variability, ie the extinction coefficients are very close

Copyright © 1989 A. DEEPAK Publishing
All rights reserved

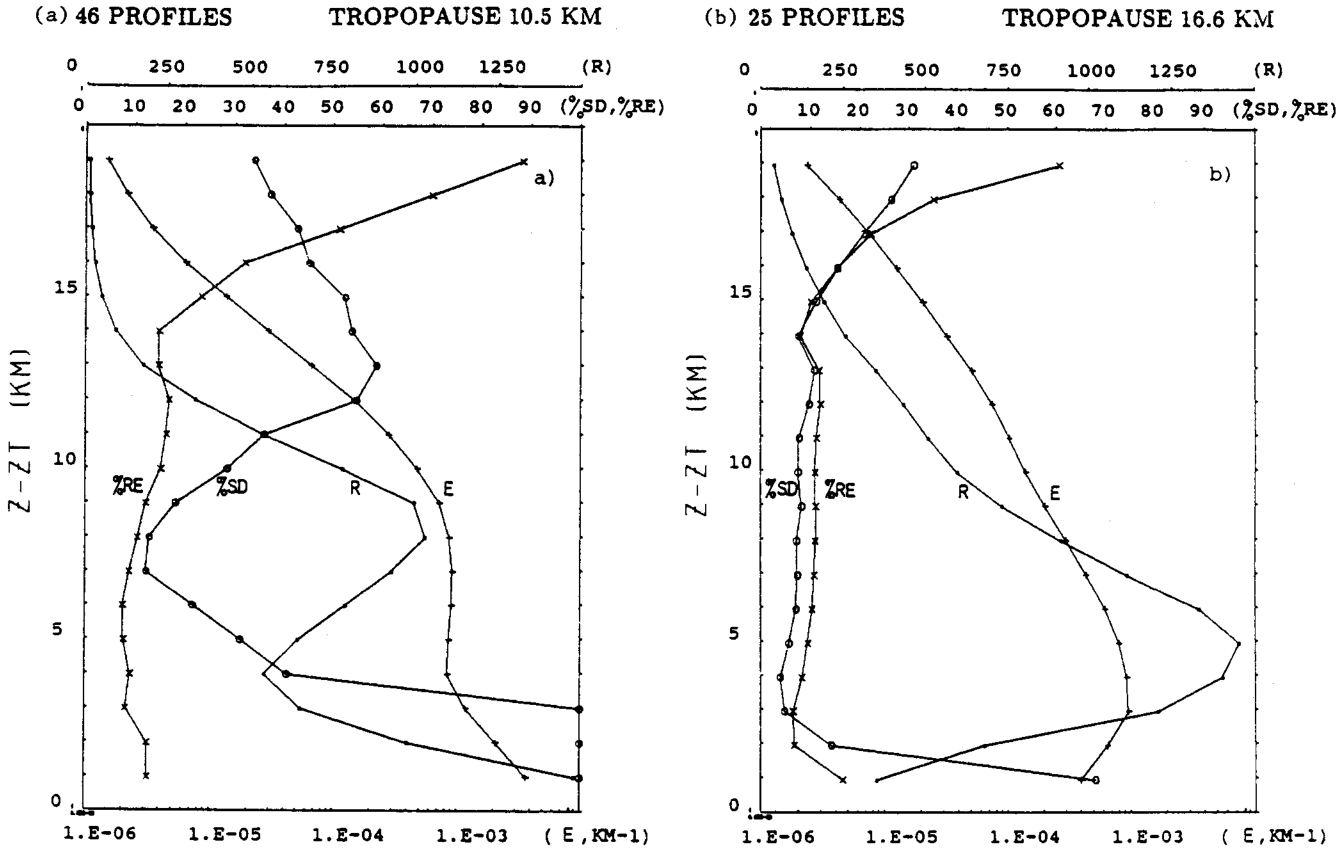

Fig. 1-a. Mean extinction coefficient (E), per cent dispersion (% SD), per cent mean relative error (% RE) and extinction ratio (R) versus altitude above the mean tropopause height at latitude 45 N.

1-b. Same as Figure 1-a, but for the latitude band 5 S.

together for all longitudes in that latitude band.

We have then investigated if the minimum in the per cent dispersion variation was related to the extinction ratio defined by $R = (\sigma_{aer}+\sigma_{Ray})/\sigma_{Ray}$, where σ_{aer} and σ_{Ray} are respectively the aerosol and the molecular extinction coefficients. This extinction ratio profile (R) is drawn on Figures 1-a, 1-b and 2, its maximum being about 5-8 km above the mean tropopause height (7-8 km at high latitudes and 5-6 km at low latitudes). The comparison with the per cent dispersion variations shows that the minimum of the dispersion happens generally a few kilometers (1 to 3) below the maximum of the extinction ratio.

At low latitudes the extinction ratio does not vary between 1985 and 1987. On the contrary at high and middle latitudes it is almost two times greater in 1985 than in 1987, certainly due to the decreasing influence of El Chicon Volcano (March - April 1982, 17°2 N - 93° W). The altitude of the minimum per cent dispersion is the same in 1985 and in 1987 so it is not related to the aerosol abundance.

4. CONCLUSION

For the two years 1985 and 1987, at high and middle latitudes, the stratospheric aerosol layer exhibits a good zonal homogeneity in a layer located between 4 and 8 km above the tropopause height. Above and below this altitude range the dispersion increases rapidly, although the quality of the measurements remains of the same order. The altitude of the minimum of dispersion does not change much with the season and seems to be located slightly below the maximum of the extinction ratio. At lower levels the variation of the aerosol extinction along a latitude band can be due to the variability of the exchanges between the troposphere and the stratosphere. At higher levels no explanation has been found yet.

It is not possible to trace a similar behaviour, neither for ozone nor for nitrogen dioxide profiles, because they are of good quality only at higher levels (15 km and 20 km respectively), i.e. above the main aerosol layer.

For low latitudes on the other hand, the zonal homogeneity is well achieved in the whole stratosphere, as long as the aerosol extinction remains measurable.

ACKNOWLEDGMENTS

The SAGE II data were kindly provided to us by the NASA Langley Research Center. This study has been supported by the Centre National d'Etudes Spatiales (Contrat CNES 1259).

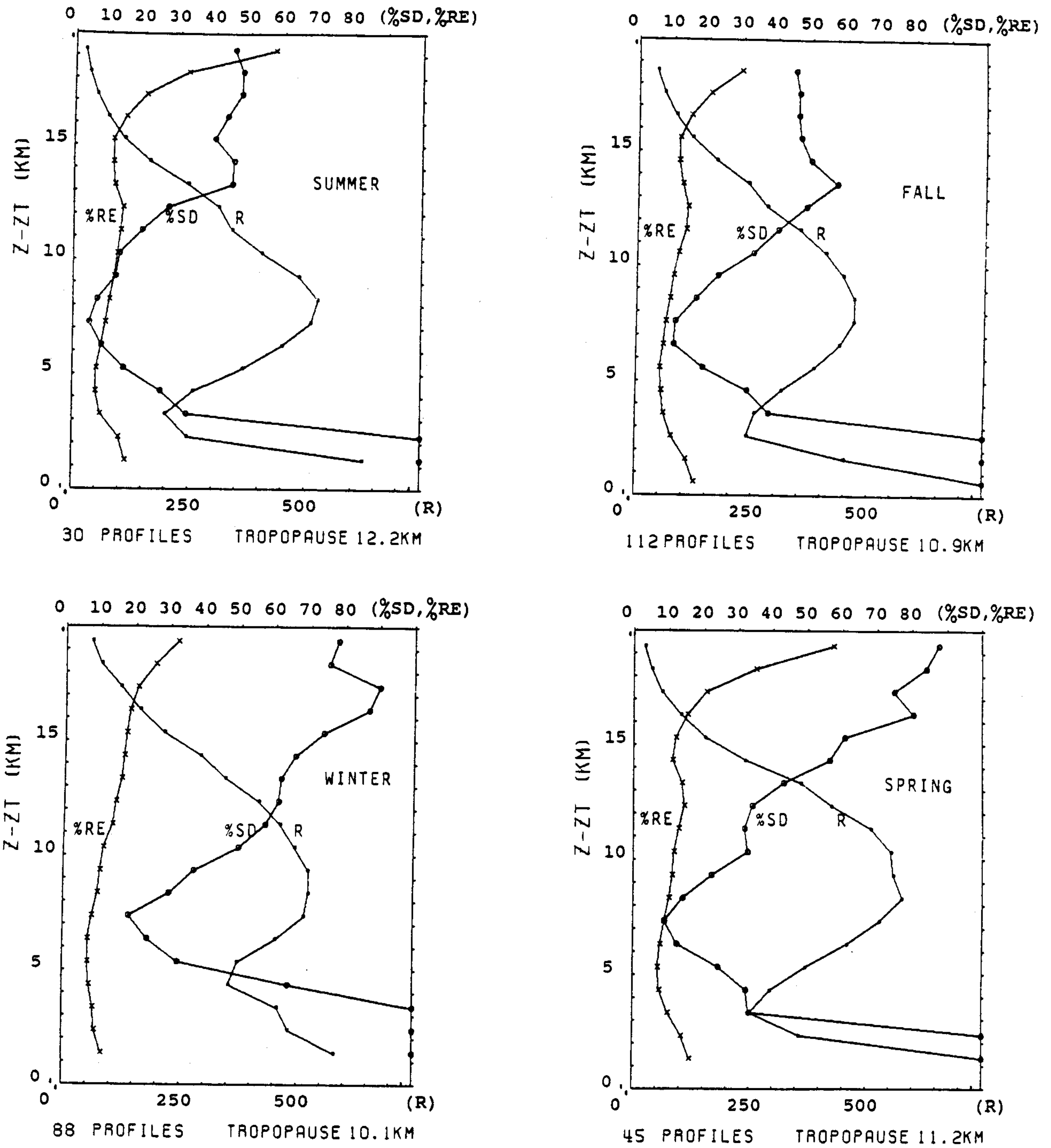

Fig. 2. Per cent dispersion (% SD), per cent mean relative error (% RE) and extinction ratio (R) versus altitude above the mean tropopause height at latitude 45 N for different seasons.

REFERENCES

Brogniez, C., J. Lenoble, 1987 : Modeling of the stratospheric background aerosols from zonally averaged SAGE profiles. J. Geophys. Res. 92, D3, 3051-3060.

Chu,W.P., M.P. McCormick, J. Lenoble, C. Brogniez, P. Pruvost : SAGE II Inversion algorithm. J. Geophys. Res. submitted.

Mauldin III, L.E., N.H. Zaun, M.P. McCormick, J.H. Guy and W.R. Vaughn, 1985 : Stratospheric aerosol and gas experiment II instrument : a functional description. Optical Engineering 24, 307-312.

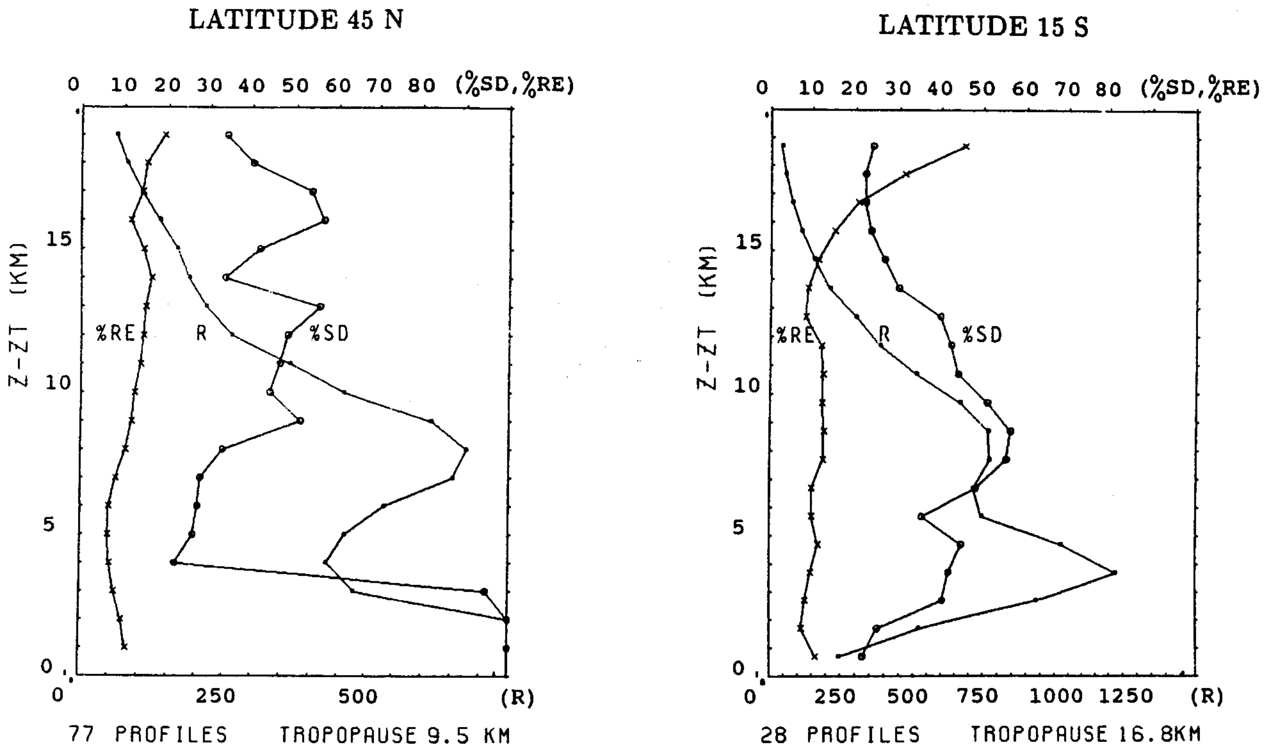

Fig. 3. Per cent dispersion (% SD), per cent mean relative error (% RE) and extinction ratio (R) versus altitude above the mean tropopause height at two latitudes 45 N and 15 S for 1986.

JOURNAL OF GEOPHYSICAL RESEARCH, VOL. 96, NO. D8, PAGES 15,479–15,497, AUGUST 20, 1991

Analysis of 5-Year Aerosol Data From the Stratospheric Aerosol and Gas Experiment II

C. BROGNIEZ AND J. LENOBLE

Laboratoire d'Optique Atmosphérique, Université des Sciences et Techniques de Lille
Villeneuve d'Ascq, France

The Stratospheric Aerosol and Gas Experiment (SAGE) II measured aerosol extinction coefficients at 1.02 μm averaged over a 10° latitude band and over short periods of nearly 5 days are used for latitudinal and seasonal studies. The most evident feature of the time series is the exponential decrease confirming the decay of El Chichon influence; in some latitude bands and at several height levels, small seasonal variations are superimposed. For latitudinal variations, extinction minima at 25°/35° in both hemispheres appear clearly. Using aerosol extinctions at 0.525, 0.453, and 0.385 μm together with the 1.02-μm data permits one to deduce one parameter of the size distribution, the particle effective radius. Seasonal variations of the deduced aerosol radius are not so obvious compared to the extinction data, but latitudinal variations of the radius do exhibit the same behavior as the extinction data, with minima at 25°/35°. This study also shows that SAGE II aerosol data can be used to detect volcanic eruption from extinction variations such as the Nevado del Ruiz and to determine the size of the injected particles.

1. INTRODUCTION

The solar occultation experiments SAM II, SAGE, and SAGE II have provided a continuous monitoring of the stratospheric aerosol layer. The Stratospheric Aerosol Measurement II (SAM II) instrument, which has operated since November 1978 in the high-latitude regions, has first detected the polar stratospheric clouds and followed the decay of the volcanic perturbation after El Chichon eruption [*McCormick and Trepte*, 1986]. The Stratospheric Aerosol and Gas Experiment (SAGE) has provided information on stratospheric aerosols from February 1979 to November 1981 between 70°N and 70°S allowing a first global description of the unperturbed stratosphere and of the distribution of the Mount St. Helens volcanic material [*Brogniez and Lenoble*, 1987]; its measurements of aerosol extinctions at 1.02 μm and 0.45 μm allow the retrieval of an average size of the aerosol particles [*Yue and Deepak*, 1983; *Lenoble et al.*, 1984; *Lenoble and Brogniez*, 1985]. The Stratospheric Aerosol and Gas Experiment II (SAGE II) launched in October 1984 has provided aerosol extinction profiles at four wavelengths over approximately the same latitude zone as SAGE. The validations and the preliminary analysis and utilization of SAGE II data have been presented in several papers published in a special issue of the *Journal of Geophysical Research* (volume 94, 1989).

We present in this paper a first global analysis of 5 years of SAGE II aerosol products, described in section 2. In section 3 we analyze the longitudinal variations in a latitude band, in order to check the usual assumption of uniform distribution around the globe; although SAGE II data generally confirm this assumption, they throw a new light on this problem and the variations of homogeneity with altitude. In section 4 we use the zonally and monthly averaged values of the aerosol extinction coefficient at 1.02 μm to analyze the temporal variations in each latitude band and the latitudinal variations for each period; a major question which is raised is how strongly the stratospheric aerosol layer is linked to the tropopause and how it follows the tropopause height changes. The variations of the 1.02-μm extinction coefficient can be due either to changes in the particle sizes or to a variation of their number, or of course to both. In section 5 we present the data on aerosol effective radius, as it can be deduced from the four SAGE II channels, and we analyze its variations. The period 1984–1989, which has seen the decay of El Chichon volcanic material, has been quiet with only minor volcanic eruptions, the only exception being the Nevado del Ruiz. Section 6 presents the SAGE II data concerning this event.

Copyright 1991 by the American Geophysical Union.

Paper number 91JD01280.
0148-0227/91/91JD-01280$05.00

2. PRESENTATION OF SAGE II AEROSOL DATA

The Stratospheric Aerosol and Gas Experiment II provides daily data of stratospheric aerosol extinction profiles from October 1984 to the present at four wavelengths, 1.02, 0.525, 0.453, and 0.385 μm [*Mauldin et al.*, 1985]. The validations performed, in the United States and Europe [*Russell and McCormick*, 1989; *Ackerman et al.*, 1989], have shown that the 1.02-μm profiles are good, from the local tropopause height up to at least 20 km above the tropopause height, i.e., 30 km in mid-latitude regions, with a precision roughly estimated to be around 10%. From a few kilometers above the ground up to the tropopause height the comparison between the inverted extinction profiles obtained by two different algorithms shows that the extinction data are still credible [*Chu et al.*, 1989].

The three short-wavelength channel aerosol data can be used with confidence only up to 15 km above the tropopause, because the ozone and/or the nitrogen dioxide corrections become too large above this level. The lower height limit of the profiles is due to Rayleigh scattering; it increases from 7 km for 0.525 μm to about 15 km for 0.385 μm. The uncertainties also increase toward the short wavelengths, reaching or exceeding 20% at 0.385 μm. It therefore seems better to use mainly the 1.02-μm data to study the stratospheric aerosol distribution.

However, the three short-wavelength channel data have been validated by field experiments [*Russell and McCormick*, 1989; *Ackerman et al.*, 1989], and the joint usage of the four channels, at altitudes where they are available, brings important supplementary information which concerns the aerosol size distributions. Several approaches can be used to retrieve the size distribution [*Yue et al.*, 1986; *Livingston and Russell*, 1989]; the method used in this paper is based on the work by *Brogniez and Lenoble* [1988]. Although further analysis is needed for a better understanding of the size distribution retrieval problem and for the best choice of retrieval method, the effective radius presented here is a convenient parameter for following the average increase or decrease of the particle sizes.

Five years of SAGE II data are available and are used in this analysis: from October 1984 to November 1989. Global coverage is obtained for each sweep of the SAGE II coverage from north to south, in approximately 1 month. The highest latitudes reached are between 55° and 75° in both hemispheres, depending on the seasons. At each latitude, about 15 profiles are observed at different longitudes separated by 24°, for either sunset or sunrise observations.

3. ZONALLY AVERAGED PROFILES: DISCUSSION OF LONGITUDINAL VARIATIONS

The best method of analyzing such an amount of data is not obvious. The stratospheric aerosols, which have a long lifetime and can have an impact on atmospheric properties and/or on climate [*Pollack et al.*, 1976; *Wang and McCormick*, 1985], are generally assumed to be more or less uniformly distributed over longitude in a latitude band.

This leads to the idea of working with zonally averaged profiles over latitude bands. We have chosen bands of 10° width; this choice of 10° allows us to have enough profiles for a reasonable averaging process at all latitudes. In most of the latitude bands there are generally between 20 and 100 profiles, sometimes less, so we have kept only the mean profiles obtained with at least 10 individual profiles. Taking into account the trajectory of the satellite, the "monthly" average for a latitude band is determined during a relatively short period of a few days (generally 1–5 days). The dates of observation at a given latitude are often different for sunrises and sunsets and moreover often are very far from each other (generally 15–20 days). For a better understanding we will consider an example: in the northern latitude band 30°/40° we have all the profiles between January 19 and January 22, 1985, at sunset and between January 10 and January 13 at sunrise; during the next sweep we get sunset data between February 10 and February 13 and sunrise data between March 3 and March 6, 1985. One period later we have sunset profiles on March 29–30. For January the sunset and sunrise measurements, which are not too far apart from each other in time, could be averaged together, but it is difficult to decide whether the March sunrise profiles have to be associated with the February or with the March sunset profiles. For a better homogeneity of the averaged data it seems more sensible to use only one kind of the sun events.

The analysis presented in this paper concerns the sunset data. A preliminary study has shown that sunrise aerosol data lead to the same conclusions. When both sunset and sunrise occur in the same place, comparisons of the individual extinction profiles confirm the expected absence of diurnal variations.

Before considering the zonally averaged profiles in the next sections, we will analyze here the longitudinal variations of the aerosol 1.02-μm extinction coefficient at a fixed latitude. The objective is to check the assumed uniformity in a latitude band and to clarify the significance of the averaging procedure. Preliminary results have been presented by *Brogniez and Lenoble* [1989] for the 3 years from October 1984 to November 1987, and we have extended this study to the 5 years of available data.

In Figure 1 the extinction coefficient at 1.02 μm is plotted, with its error bars, versus longitude at three altitudes for northern latitudes between 40° and 50° during spring 1985; at around 18.5 km the values are very well gathered, confirming an almost perfect homogeneous distribution of the aerosol layer around the globe. At lower and higher altitudes the homogeneity is not as good, and the aerosols exhibit apparently more or less random longitudinal variations. These variations cannot be explained by larger errors, as will be discussed below; they are therefore true spatial variations of the extinction coefficient along the longitude, which could be analyzed in detail, as has been done for ozone observations by *Cunnold et al.* [1984]. However, longitudinal variations remain small at all levels, and we will further limit our analysis to the zonal means which are meaningful. A similar behavior is observed for most of the time periods at high and middle latitudes, with a few exceptions. In order to analyze more thoroughly this problem of homogeneity of the aerosol distribution in a latitude band, we have considered the vertical profiles of the dispersion of the data around the mean zonal value.

Figure 2 shows altitude distribution of the mean zonal extinction coefficient σ at 1.02 μm and the percent dispersion, $\%SD = 100D/\sigma$, where D is the 95% confidence interval. We present here results for two high- and middle-latitude bands, 40°/50° (referred to as N45 hereafter) during local spring 1985 (same as for Figure 1) and −60°/−50° (referred to as S55 hereafter) during local fall 1988.

Effectively, the noticeable result is that at high and middle latitudes (greater than 20°N and 20°S) the confidence interval is not too large ($\simeq$10–15% in most cases) and often presents minimum values (smaller than 5%) over about 5 km between 15–16 and 20–21 km, confirming the qualitative observation made in Figure 1. This minimum in the $\%SD$ happens in the altitude range where the extinction coefficient is large and coincides nearly with the maximum of the extinction ratio defined by $R = (\sigma_{\text{aer}} + \sigma_{\text{Ray}})/\sigma_{\text{Ray}}$ (where σ_{Ray} is the molecular extinction coefficient), which is also drawn in Figure 2.

We observe this behavior during the 5 years, in almost 70–75% of cases. Nevertheless, for 1986 the $\%SD$ averaged profiles are generally more irregular at least for 35–40% of the cases, and the $\%SD$ is often greater than 15%.

The altitude variation of $\%SD$ observed at high and middle latitudes, with smaller values in a given altitude range, could be due either to a better quality of the measurements in this layer or to a better zonal homogeneity of the aerosol layer at these altitudes. In order to check if the percent dispersion variations depend on the measurement errors, we have calculated the mean relative error in percent, i.e.,

$$\%RE = (100/n) \sum_{i=1}^{n} (\Delta x_i/x_i)$$

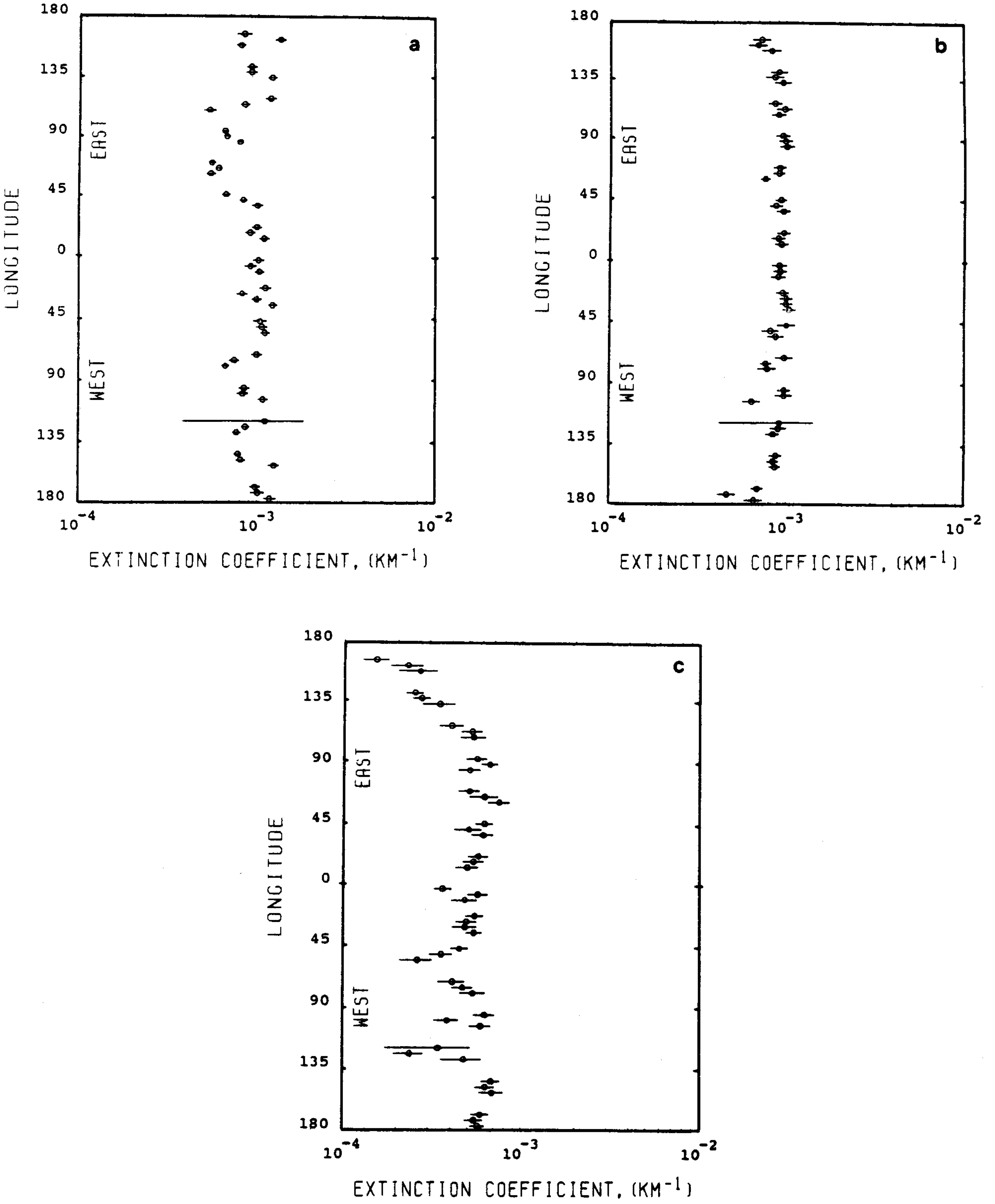

Fig. 1. Extinction coefficient at 1.02 μm, with error bars, versus longitude for N45 latitude band during spring 1985 at three altitudes: (*a*) 16.5 km, (*b*) 18.5 km, and (*c*) 20.5 km.

where Δx_i is the error of the extinction measurement x_i and n is the number of measurements. For comparisons the profiles of the percent mean relative error are drawn in Figure 2. We see that this *%RE* is rather small (<15% and even 10%) for all levels above 12–13 km up to 25 km; that is to say, the individual profiles are of good quality at all levels, where the extinction coefficient is larger than nearly 10^{-5} km^{-1}. This is true for the 5 years, including 1986.

We must also notice that the percent dispersion is often smaller than the percent mean relative error, which could indicate that the errors Δx_i of the extinction measurements x_i are slightly overestimated [*Chu et al.*, 1989]. The compari-

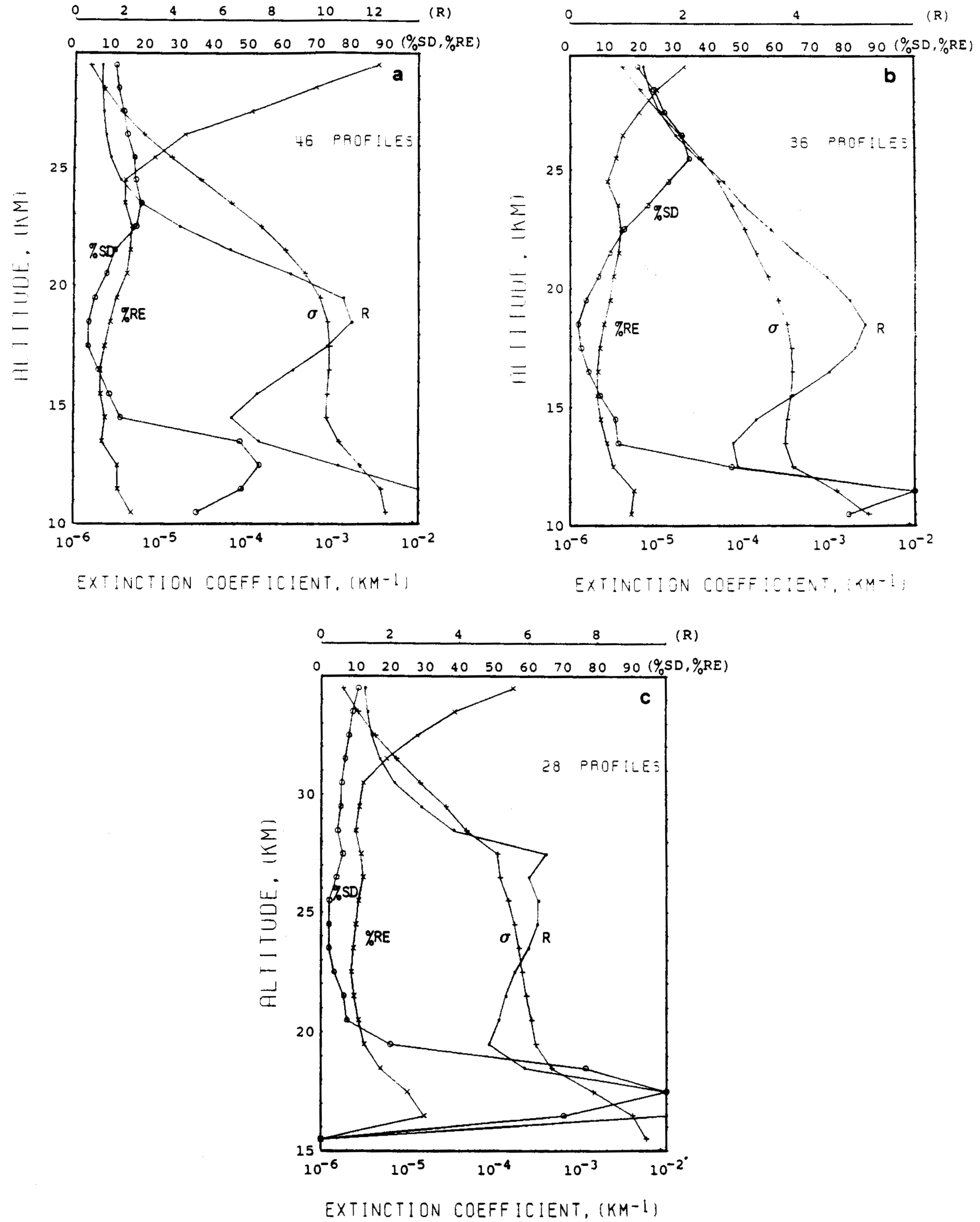

Fig. 2. Mean extinction coefficient (σ) at 1.02 μm, percent dispersion (*%SD*), percent mean relative error (*%RE*), and extinction ratio (*R*) versus altitude for three latitude bands: (*a*) latitude N45, (*b*) latitude S55, and (*c*) latitude N05.

son between the *%SD* and the *%RE* proves that the existence of a minimum in the *%SD* is not correlated with a better quality of the measurements.

At lower latitudes the zonal homogeneity is the same at all altitudes. The *%SD* is less than 10%, is often smaller than 5%, and remains almost constant over 10 km between 18–19 and 29–30 km, except for 1986. The *%RE* is of the order of 10% as for other latitudes, as can be seen in Figure 2*c*, corresponding to latitude band N05 in local winter 1989.

The stratospheric aerosol layer is generally well mixed

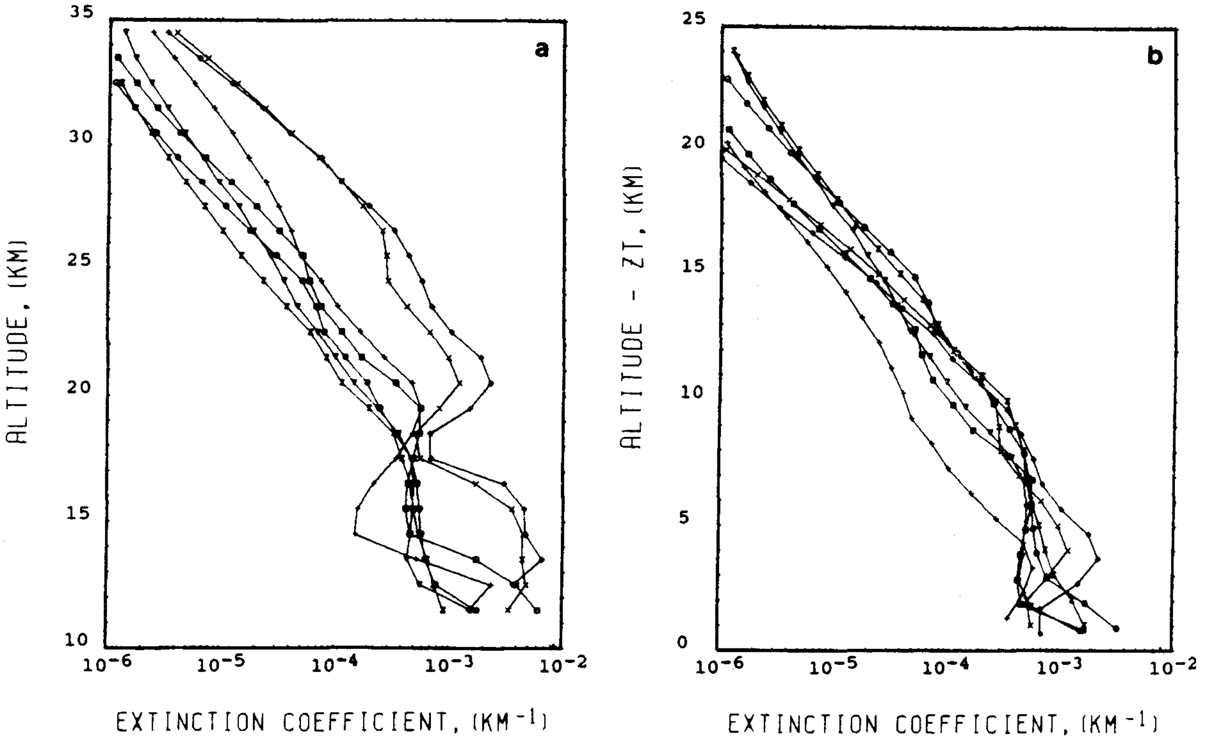

Fig. 3. Mean extinction coefficient at 1.02 μm for several latitude bands (*a*) versus the altitude above the ground and (*b*) versus the altitude above the tropopause height.

around the globe, such that by limiting the following analysis to the zonal means of the extinction coefficient, the results could be physically significant. However, this study has revealed for most cases, at high and middle latitudes, that the best zonal homogeneity is found in a layer of 4–5 km width around the altitude of 18–19 km, i.e., roughly around the level of maximum extinction ratio. No satisfactory explanation of this structure has been found in the stratospheric circulation or in the aerosol formation processes.

4. CHOICE OF THE REFERENCE LEVEL: ANALYSIS OF TEMPORAL AND LATITUDINAL VARIATIONS

In this section we will analyze the zonally averaged 1.02-μm extinction coefficient profiles for the 5 years of SAGE II data, looking for temporal and latitudinal variations. The first problem to solve is as follows. Shall we compare directly the vertical profiles, i.e., consider extinction coefficients at a given level above the ground for different latitudes or seasons, or is it more sensible to choose the tropopause height as a reference level, i.e., to compare extinction coefficients always at the same altitude above the tropopause which varies strongly with latitude and season?

A first look at articles about stratospheric aerosols shows that their profiles at various latitudes are dependent on the tropopause height [*Rosen et al.*, 1975; *Brogniez and Lenoble*, 1987]. SAGE II data, during free volcanic period, follow the same behavior, i.e., averaged extinction profiles at different latitudes compare closely when the height is starting at tropopause level. Zonal mean profiles at seven latitude bands are shown in Figure 3 for the period from October 5 to November 18, 1988; Figure 3*a* compares directly the vertical profiles versus the altitude above the ground, whereas in Figure 3*b* the profiles have been shifted, according to the variations of the tropopause height, and are shown versus the altitude above the tropopause level, ZT. We note the closer agreement in the second case and a similar exponential decay with altitude for all profiles. This observed good gathering is confirmed when relative dispersion (standard deviation divided by the mean value) is drawn in percent versus altitude (Figure 4). In the same manner most of the analyses of SAGE I, SAGE II, and SAM II data use the stratospheric optical depth integrated from 2 km above the tropopause level [*Kent and McCormick*, 1984].

However, things are probably not always so simple, as can be observed both from the temporal variations and from the latitude behavior of the extinction coefficient or of the optical depth. This problem will be discussed in detail in the following sections.

4.1. *Temporal Variations*

Several authors have noticed a seasonal variation, with a winter maximum, of the stratospheric aerosol optical depth integrated from 2 km above the tropopause level, from SAGE I data [*Brogniez and Lenoble*, 1987] and from SAGE II data [*Yue et al.*, 1991]. From SAGE I data analysis these seasonal variations, more noticeable at middle latitudes, had been related to the seasonal variations of the extinction coefficients at high levels above the tropopause. Nevertheless, local temperature variations had not been sufficient to explain the entire difference between the summer and the winter values [*Brogniez and Lenoble*, 1987]. For SAGE II data analysis, *Yue et al.* [1991] reached a similar conclusion, that a microphysical model relating the particle sizes to the

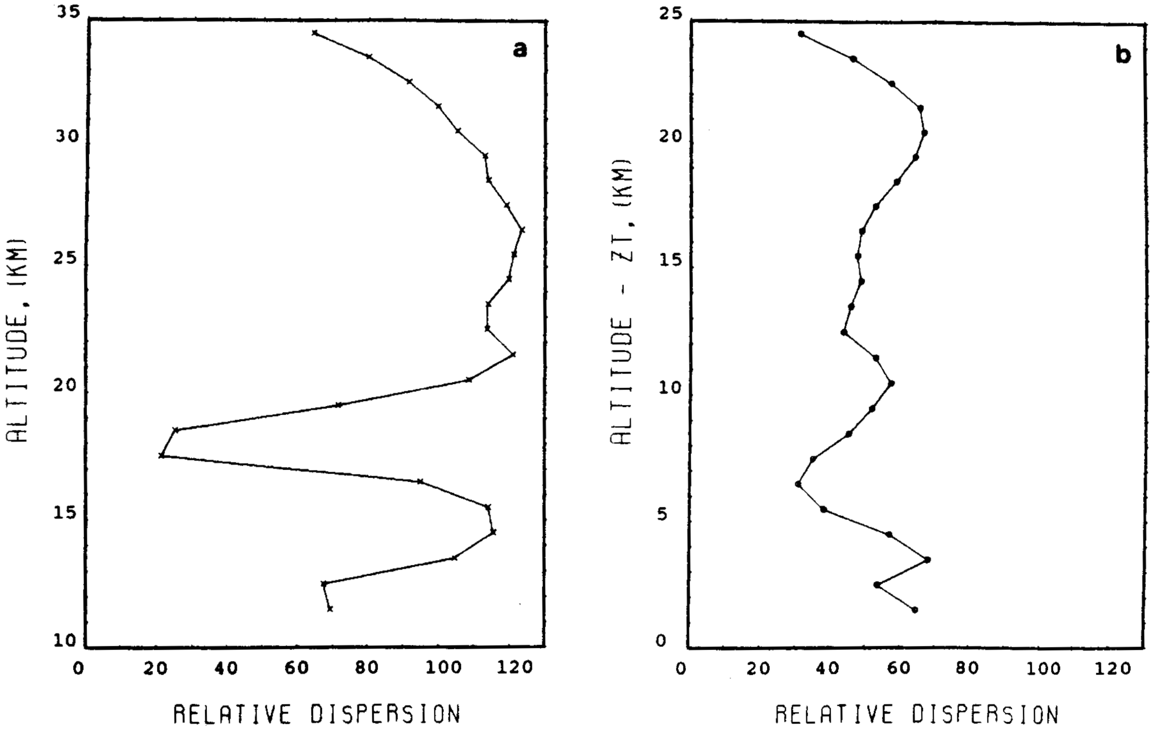

Fig. 4. Relative dispersion (percent) (*a*) versus the altitude above the ground and (*b*) versus the altitude above the tropopause height.

temperature was not able to explain the seasonal variations of the optical depth.

Figure 5 shows the variations of the extinction coefficient versus time for two altitudes above the tropopause height and for the N45 and S45 latitude bands. We have also added the tropopause altitude fluctuations and indications of local winter. We limit the present study to high and middle latitudes because of the perturbation due to Nevado del Ruiz at low latitudes, which will be studied further in section 6. As will be seen also in section 6, the Etna located at middle latitude had a weak influence on the following results.

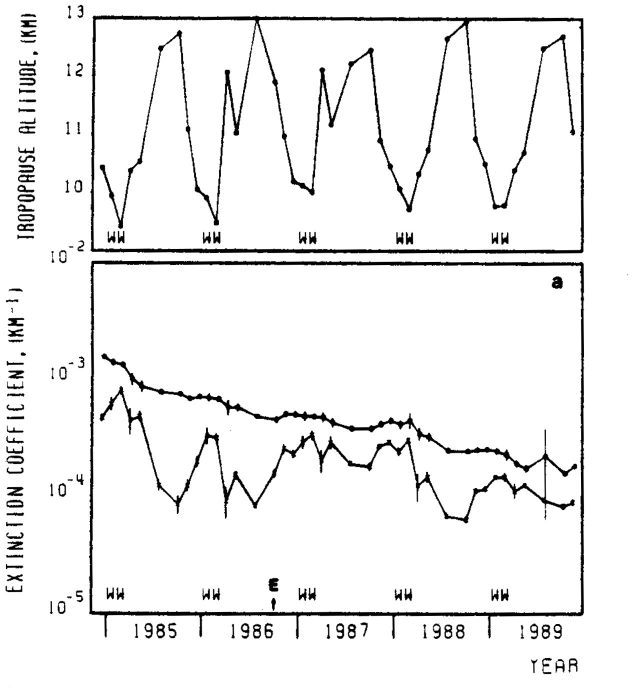

Fig. 5*a*. Mean extinction coefficient at 1.02 μm, with 95% confidence intervals, versus time for the N45 latitude band at two levels above the tropopause height: 5 km (open circles) and 10 km (crosses). The arrow indicates the Etna eruption, and WW stands for local winter. The top curve shows the tropopause height variations.

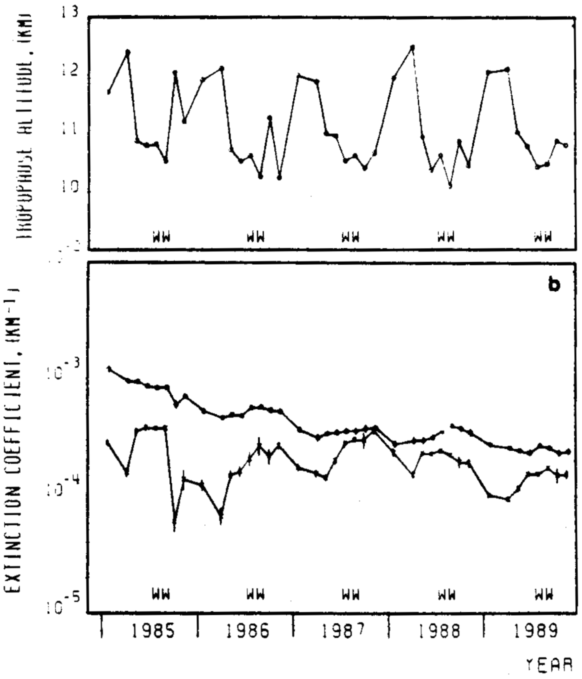

Fig. 5*b*. Same as Figure 5*a* but for the S45 latitude band.

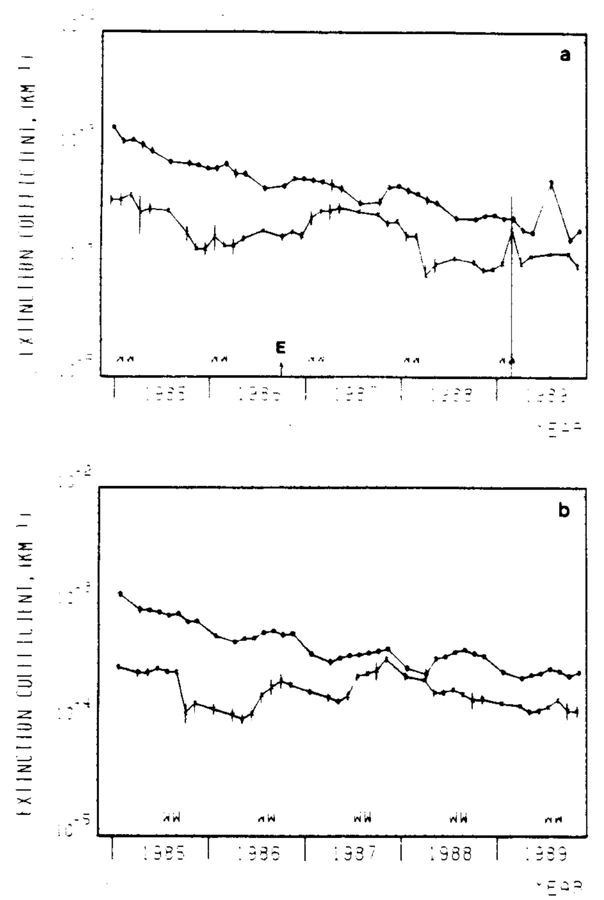

Fig. 6. Mean extinction coefficient at 1.02 μm, with 95% confidence intervals, versus time for (*a*) N45 and (*b*) S45 latitude bands at two altitudes above a mean tropopause height of 11 km; 5 km (open circles) and 10 km (crosses).

First, it appears that the extinction is about 3–7 times greater in early 1985 than by the end of 1989, depending on the level, because of the decreasing influence of the El Chichon volcano (March–April 1982, 17.2°N, 93°W). With values of about 2×10^{-4} km^{-1} at 5 km above the tropopause by the end of 1989, the background state ($1.–1.5 \times 10^{-4}$ km^{-1}) is almost recovered [*Swissler et al.*, 1982].

Independently of this regular decrease, the winter maxima appear clearly as noted previously. However, if we consider the seasonal variations of the tropopause altitude, it also appears that the highest winter extinction values at a given altitude are related to the lowest tropopause levels, i.e., these winter maxima are observed at true altitudes lower than the altitudes of the summer minima. As the extinction coefficient generally decreases with increasing altitude, we could expect that the seasonal variations would disappear (or be strongly reduced) when the extinction is observed at a fixed altitude; this has also been noticed by *Yue et al.* [1991]. In other words the "aerosol layer" does not seem to follow the tropopause height seasonal variations, and a better analysis of the data is probably achieved by referring the profiles in each latitude band to the annual mean tropopause level than by referring them to the tropopause level for each period. This has been done in Figure 6, where we have drawn the extinction coefficient versus time for the same latitude bands, but now with a mean tropopause height, averaged all over the 5 years, as a reference.

These curves clearly show that the aerosol extinction coefficients seem to decrease almost regularly at a constant altitude above the ground. However, in addition to the slow decay of the extinction (due to the decrease in the El Chichon contribution) we can see that at several levels, slight seasonal variations remain, which are more obvious in the southern hemisphere.

We have tried to fit these temporal variations with the following formula:

$$\sigma(1.02) = \left[P_1 + P_2 \sin\left(\frac{2\pi}{T} n\right)\right] \exp(-P_3 n^k) \qquad (1)$$

where n is the reference number of the period, counted from the first period of the measurements. P_1, P_2, and P_3 are coefficients deduced from a least squares fit. The values T and k have been adjusted after a few trials. T varies between 9.5 and 10., and k is within 0.5–0.6 depending on the latitude and on the altitude; this last value gives a better fit to the data than a pure exponential function of n. As suggested by *Hofmann and Rosen* [1987], this departure from an exponential may be due to an unknown volcanic eruption for southern latitudes and to the Etna eruption for northern latitudes.

The exponential term takes into account the decay of the El Chichon perturbation, and the sinusoidal term describes the seasonal oscillations. This expression (equation (1)) agrees well with the experimental data at all the latitude bands (northern or southern mid-latitude), but only for a small range of altitudes (about 2–3 km) a few kilometers above the tropopause level where the seasonal oscillations are noticeable. At high latitudes the measurements are not numerous enough to perform any curve fitting. Figure 7 shows the fit for two altitudes where the oscillations exist. A quick look at other wavelengths shows that the behavior is the same as at 1.02 μm.

Figure 8 shows the optical depths calculated from the tropopause height plus 2 km as is usually done and from the mean tropopause height averaged over the 5 years plus 2 km. We can observe again the decreasing influence of El Chichon with an optical depth about 4 times greater in 1985 than in 1989. The curves obtained for the optical depth above the tropopause height plus 2 km exhibit great seasonal variations. As expected, the variations are almost completely suppressed, at least in the northern hemisphere, when the averaged tropopause height is chosen as a reference level, and this is true for most of the latitude bands. This result is quite evident because seasonal variations of the extinction coefficient are only observed in a small altitude range, so the summation all over the stratosphere will smooth out these oscillations. However, a small seasonal variation of the optical depth can be observed in the southern hemisphere (Figure 9 is for the S45 band) where (1) is fitted with the same parameter values, T and k, as for the extinction coefficient.

A similar analysis has been made by *Yue et al.* [1991] for the 0.525-μm optical depth calculated from SAGE II data for the period of December 1984 to December 1987. In their work, Yue et al. have tried an analytical expression, somewhat similar to (1), for the optical depth variations, integrated from the tropopause level plus 2 km, for latitude bands higher than 20° in both hemispheres. They noticed that

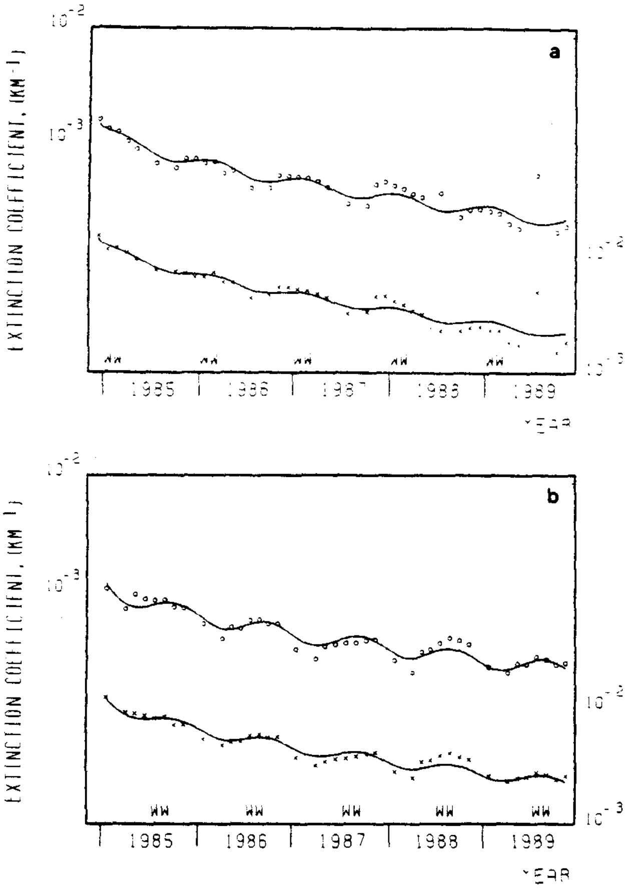

Fig. 7. Mean extinction coefficient at 1.02 μm versus time for (*a*) N45 and (*b*) S45 latitude bands at two levels (4 km (open circles) and 5 km (crosses) above a mean tropopause height of 11 km) and their fits obtained from (1) (solid curves).

the seasonal oscillations of the tropopause height were partially responsible of those variations and that a small sinusoidal component remained after correction, but they did not analyze this remaining signal. We will try to explain the remaining seasonal variations in section 5 by the variations of the particle sizes.

4.2. *Latitudinal Variations*

We will consider in this section the latitudinal variations of the 1.02-μm extinction coefficient for each period of observation. As discussed in section 3, the observations at a given latitude are acquired only during a few days, and the whole latitude range is scanned in about 1 month; however, the temporal variations over 1 month are slow and should not modify the following analysis. As shown in Figure 3, the extinction profiles at various latitudes compare much better when referred to the tropopause height than when referred to the ground level. The tropopause level varies strongly from about 9 km to 17 km from high to low latitudes, and the aerosol layer seems to follow more or less these height variations. It seems to be sensible, for a given period, to study the latitude variations of the aerosol extinction coefficient at a fixed altitude above the tropopause height.

Figure 10 shows the extinction coefficient at 1.02 μm, with 95% confidence intervals, versus latitude for two altitudes

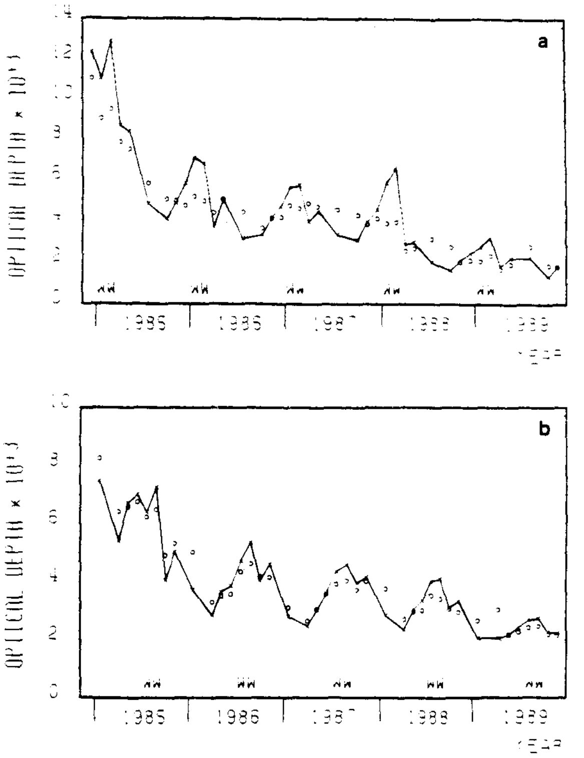

Fig. 8. Optical depth at 1.02 μm counted from the tropopause height plus 2 km (crosses) and from the mean tropopause height plus 2 km (open circles) versus time for (*a*) N45 and (*b*) S45 latitude bands.

above the tropopause and for four periods, far from the Nevado del Ruiz volcanic event; we have also drawn for comparison the tropopause altitude variations. More or less pronounced for the different periods is a minimum of $\sigma(1.02)$ which appears clearly in the latitude bands 25°/35° in both hemispheres and exists whatever the altitude is, although it is stronger at high levels. To characterize this minimum, we have evaluated the ratio between the extinction coefficient at 45° and the minimum $\sigma(45°)/\sigma\text{min}$ for the southern and the northern latitudes. At 5 km above the tropopause we get values of 1–1.5 for this ratio, and at 10 km we have generally values greater than 2.

The latitude ranges 25°/35° correspond to latitudes where

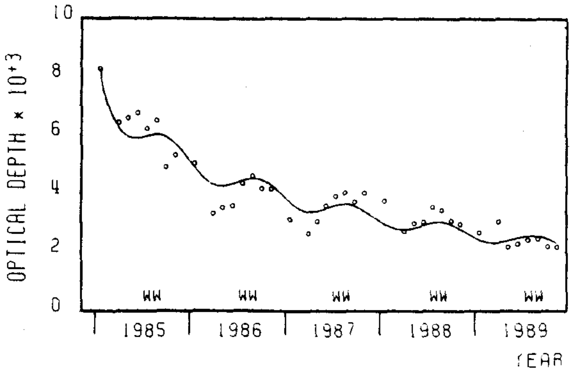

Fig. 9. Optical depth at 1.02 μm counted from the mean tropopause height plus 2 km (open circles) versus time for the S45 latitude band and the fit obtained from (1).

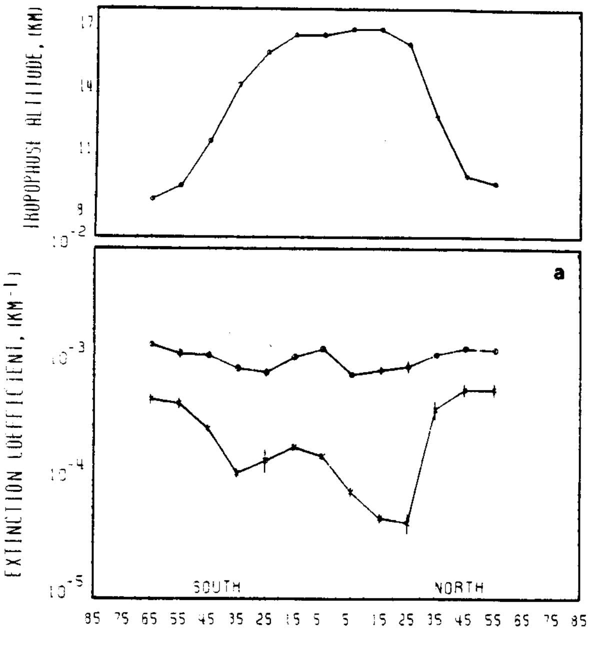

Fig. 10*a*. Mean extinction coefficient at 1.02 μm, with 95% confidence intervals, versus latitude during the 1985 northern winter period at two levels above the tropopause height: 5 km (open circles) and 10 km (crosses). The top curve shows the tropopause height variations.

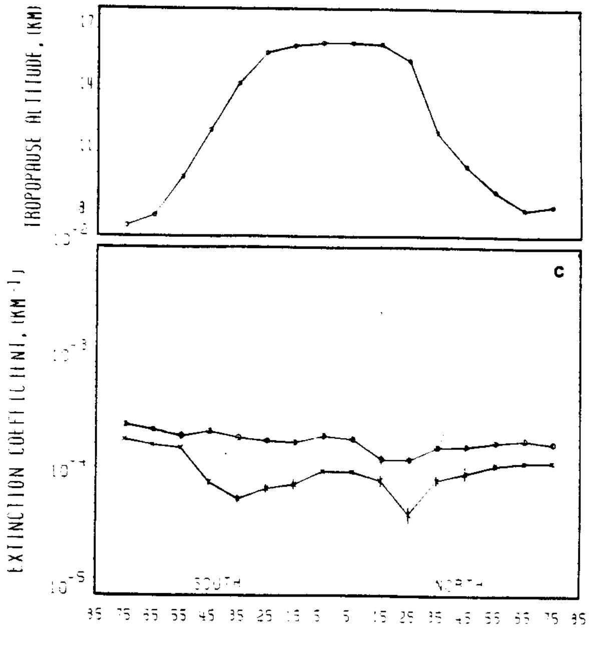

Fig. 10*c*. Same as Figure 10*a* but during the 1989 northern spring period.

the tropopause level breaks, leading to troposphere-stratosphere exchanges [*Rosen et al.*, 1975]. Figure 3 has shown that the extinction coefficient decreases with increasing altitude, so the low values of this coefficient could be explained by downwelling of stratospheric air.

The extinctions at 45°/55° are similar to the extinction values at low latitudes (between 15°N and 15°S). Nearby the tropopause, the extinctions at 45° and at 55° are almost the same; at higher altitudes the extinction at S55 is nearly 1.5–1.8 times the S45 value, while the N55 extinction is only 1.2–1.5 times the N45 extinction value. Toward the higher latitudes, S65/S75 and N65/N75, the increase is weaker: 1–1.3.

Most exceptions appear at 65°/75°, in the southern hemi-

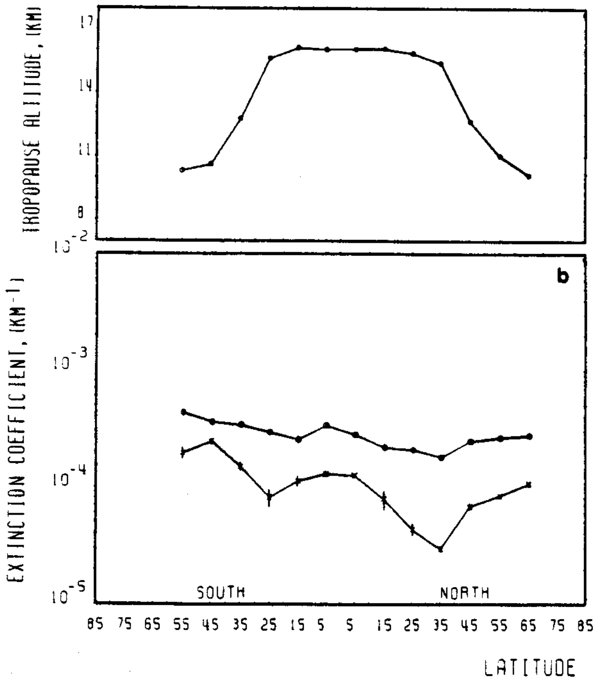

Fig. 10*b*. Same as Figure 10*a* but during the 1988 northern summer period.

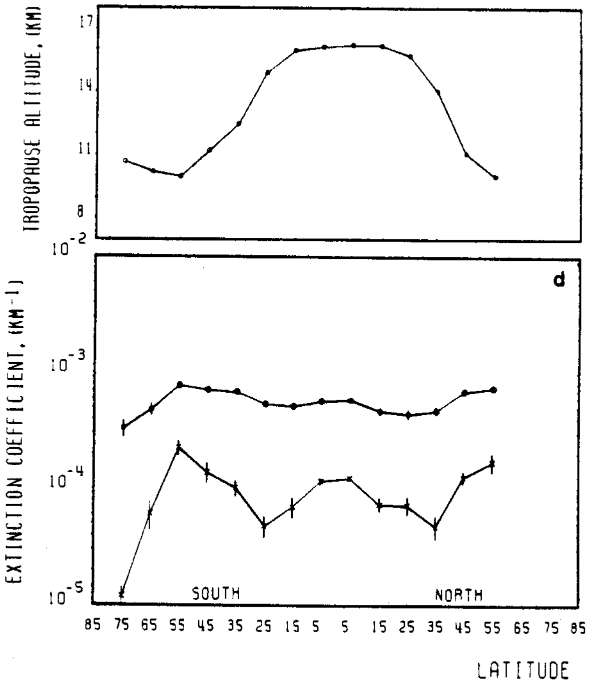

Fig. 10*d*. Same as Figure 10*a* but during 1985 southern spring period.

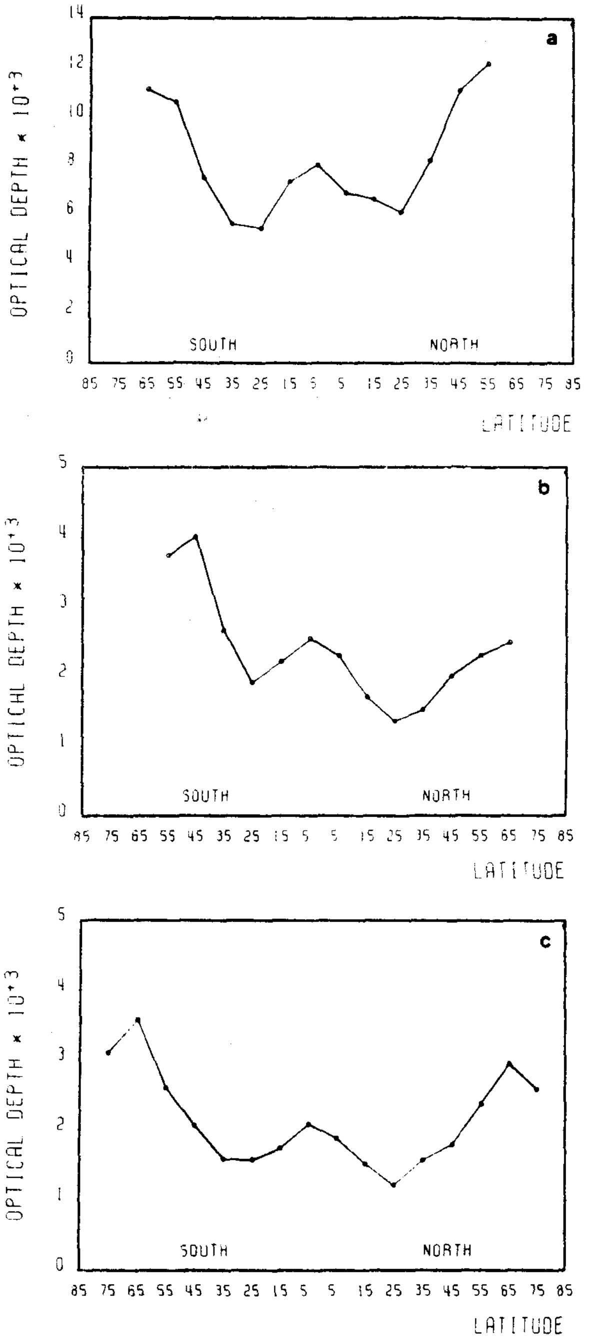

Fig. 11. Optical depth at 1.02 μm counted from the tropopause height plus 2 km versus latitude for the same periods as in Figures 10*a*–10*c*.

sphere for all the local winter–spring periods, where the measurements strongly decrease. The S65 extinction values are nearly 2–3 times weaker than the S55 values, and the S75 values are also 1.5–2 times weaker than the S65 values (Figure 10*d*).

The optical depth calculated at 1.02 μm from the tropopause height plus 2 km exhibits, of course, the same kind of variations with minimum values at about 25°/35° as shown in Figure 11, confirming the behavior observed previously in SAGE I data [*Brogniez and Lenoble*, 1987]. The ratio between the optical depth at the 45° latitude band and the minimum value is of the order of 1.5–2. As for the extinction coefficient, the 55° latitude band optical depth values are larger than the 45° values in both hemispheres, almost 1.3–1.5 times larger. Toward the 65°/75° latitude bands the optical depth follows the same kind of variations as the extinction coefficient: it increases generally a little except during the southern local winter–spring periods, where the optical depth decreases strongly.

5. Aerosol Size Distribution and Concentration

As mentioned in section 2 of this paper, the extinction coefficients at 0.525, 0.453, and 0.385 μm used together with the 1.02-μm data allow us to retrieve some information on the aerosol size distribution at each altitude of each individual profile. The method has been described by *Brogniez and Lenoble* [1988] and is briefly recalled here.

The spectral variations of the extinction coefficient are fitted using an analytical expression,

$$\ln \sigma(\lambda) = \ln \sigma(1.02) - \alpha \ln (\lambda/1.02) - \beta[\ln (\lambda/1.02)]^2 \qquad (2)$$

rather than the simple Angström law.

Comparisons with similar fits obtained for aerosol models with lognormal size distribution,

$$n(r) = \frac{1}{(2\pi)^{1/2}\, r \ln s} \exp\left\{-\frac{[\ln (r/r_m)]^2}{2(\ln s)^2}\right\} \qquad (3)$$

(where r_m and s are the modal radius and the variance), lead to the identification, from α and β, of the two parameters r_m and s, or preferably the effective radius and the effective variance [*Hansen and Travis*, 1974], which are defined by [*Lenoble and Brogniez*, 1984]

$$\begin{aligned} r_{eff} &= r_m \exp [2.5 \ (\ln s)^2] \\ v_{eff} &= \exp (\ln s)^2 - 1 \end{aligned} \qquad (4)$$

Calculations for the lognormal aerosol models have been performed with Mie routines for spherical particles consisting of aqueous sulfuric acid with 75% H_2SO_4 by mass, as is usually done [*Rosen and Hofmann*, 1986]. This procedure leads to the retrieval of an "equivalent" size distribution, in the sense that this size distribution may not be the real one, but may give the same spectral variation of extinction as the real one in the SAGE II spectral interval within the measurement error bars.

Some experimental observations have found two modes in the stratospheric aerosol size distribution [*Knollenberg and Huffman*, 1983; *Hofmann and Rosen*, 1987]. However, there is no hope of retrieving a bimodal size distribution from the SAGE II four-channel data. Actually, our analysis has proved that only an effective radius can be obtained with a reasonable accuracy, associated with rough information about the variance. The presence of a strong second mode could be revealed in our procedure, either by a very large retrieved variance or by the failure of the procedure, i.e., the impossibility of retrieving r_{eff} and v_{eff}.

Zonal means of the effective radius (and of the effective variance) and 95% confidence intervals have been evaluated as for the extinction data. The 0.385-μm channel, for which the extinction measurements are credible only above the

15-km level up to 25 km in the high- and mid-latitude bands, limits the altitude range in which we can obtain these size parameters.

5.1. *Vertical Profiles of the Aerosol Effective Radius and Variance*

Figure 12 shows the effective radius, with 95% confidence intervals, versus altitude above the ground for three latitudes (high-, middle-, and low-latitude bands) at some quiet periods. The major characteristic of the averaged profiles at high and middle latitudes in both hemispheres is that r_{eff} decreases almost linearly when the altitude increases from 15 km to 25 km, whatever the time period is. Typically, we have, for latitude band N45, 0.35 µm at 15 km and 0.2 µm at 25 km in early 1985.

The validity of the derived effective radius has been estimated by comparing it with correlative measurements. For example, for the lidar experiment, *Jäger et al.* [1988] obtained at the same time (in early 1985), at Garmisch-Partenkirchen (47.5°N, 11°E) with a bimodal distribution, a modal radius of 0.1 µm for the first mode and 0.4 µm for the second mode between 18 and 21 km, with a number concentration of 10% for large particles; that leads to an effective radius of 0.29 µm. Several infrared balloon polarimetry measurements [*Herman et al.*, 1986] have been performed and have given aerosol size distributions which agree reasonably with ours [*Brogniez and Lenoble*, 1988; *Diallo et al.*, 1989]. Comparative studies between SAGE II, lidar, and polarization measurements have also been achieved and have led to satisfying results [*Ackerman et al.*, 1989]; other comparisons are presently in progress.

At low latitudes a transition period appears by the end of 1987 at N15, and slightly later, by August 1988, at other low-latitude bands. Before that date the radius decreases with altitude, as it decreases at middle and high latitudes; after that the behavior is somewhat different: from ≈18 km up to ≈21 km it slightly increases, remains constant over 5–6 km, and then decreases (Figure 13). These last results, obtained after mid-1988, confirm previous studies made by *Yue and Deepak* [1984] on March 1979 SAGE data and by *Brogniez and Lenoble* [1987] on February 1979 to November 1981 SAGE data.

The second parameter retrieved with our method is the effective variance. As can be seen in Figure 12, it is often almost constant (around 0.05–0.1, i.e., s = 1.25–1.35) between 15 and 23 km whatever the latitude band is; above 23 km it generally increases up to 0.4–0.5. Moreover, a few profiles present a great increase (v_{eff} ≈ 0.4, i.e., s ≈ 1.8) toward 16–17 km. For comparison the effective variances retrieved from infrared balloon polarimetry measurements made in October 1985 and April 1986 are in good agreement with ours; in November 1984 the values are somewhat larger than ours [*Diallo et al.*, 1989].

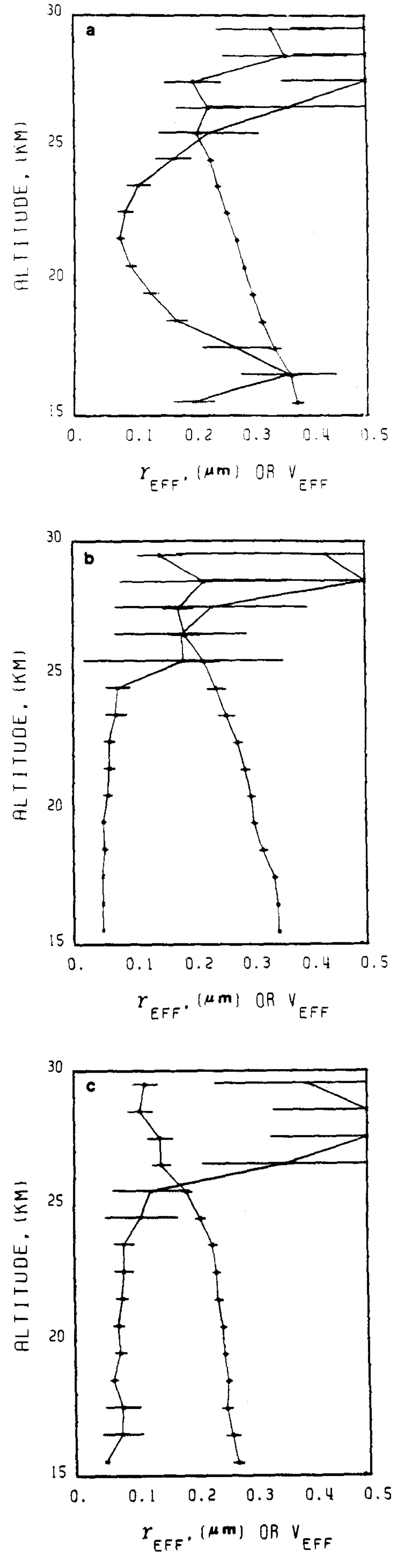

Fig. 12. (Opposite) Effective radius (open circles) and effective variance (crosses), with 95% confidence intervals, versus altitude for three latitude bands at three different periods: (*a*) S45 latitude during 1985 local summer, (*b*) S25 latitude during 1986 local spring, and (*c*) N65 latitude during 1989 local summer.

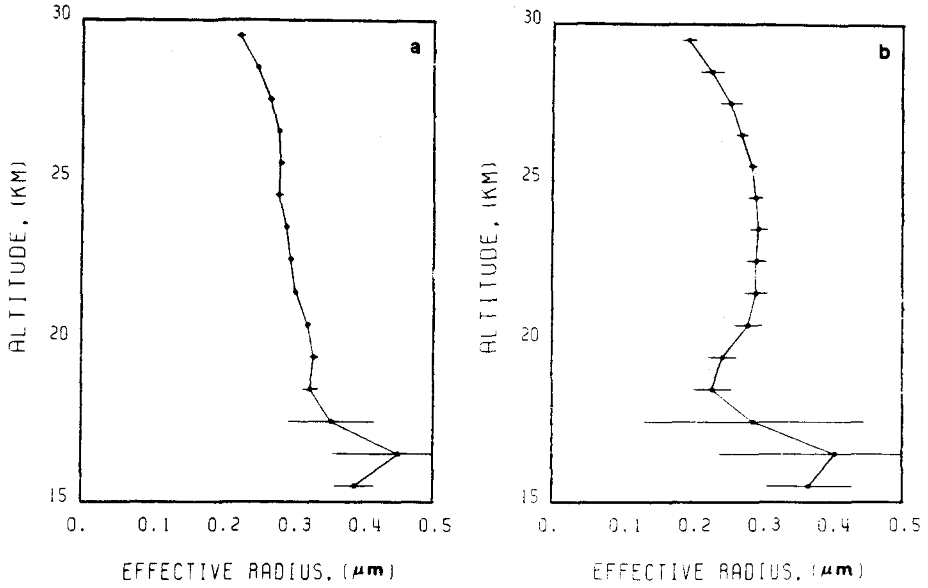

Fig. 13. Effective radius, with 95% confidence intervals, versus altitude at N15 for two periods: (*a*) June–July 1986 and (*b*) November–December 1988.

5.2. *Temporal Variations of the Aerosol Effective Radius and Variance*

Variations of the effective radius versus time are shown in Figure 14 at two altitudes above the mean tropopause height for the same latitude bands (N45 and S45) chosen in the extinction study. We observe again a slight decrease throughout the 5 years, which is more or less important depending on the altitude; the decay of the extinction coefficient after the El Chichon eruption is then correlated with a decrease in the effective radius.

We have, for example, at the level 5 km for the latitude N45, $r_{\mathrm{eff}} = 0.35$ μm by the end of 1984 and $r_{\mathrm{eff}} = 0.28$ μm by the end of 1989, that is to say, a decrease of 20%. (For comparison, just before the Mount St. Helens eruption, on May 18, 1980, the effective radius was 0.22 μm with an effective variance of 0.25; it had grown up to 0.45 μm after this event [*Lenoble et al.*, 1984]).

A least squares fit leads to an exponential decrease with the same value for k as used previously in (1). This kind of decrease exists whatever the latitude band is (high-latitude or mid-latitude band) in both hemispheres.

Although some oscillations exist, there is no evidence of seasonal variations, with the maxima happening not in winter but sometimes shifted. Nevertheless, the 95% confidence intervals are weak, meaning that most of the fluctuations are significant. For southern latitudes a small seasonal effect still appears on r_{eff} at some altitudes with local winter maxima as for extinction variations (Figure 14*b*), and an equation similar to (1) fits almost as well. We can conclude that the aerosols are larger in winter in those bands, as had been found from SAGE I data analysis [*Brogniez and Lenoble*, 1987]. In that work it was shown that the radius maxima occurred when the local temperature was at a minimum. For comparison we have studied the local temperature variations over time for SAGE II data. Unfortunately, these temperature variations are not always correlated with the radius variations: radius maxima do not occur at the same time as the temperature minima, except for the S55 latitude band (Figure 15*a*), and one can observe sometimes a shift and sometimes an anticorrelation as shown in Figure 15*b* for the S35 latitude band. We have not found a satisfactory explanation for these radius variations, which are most likely due to the interaction of various causes.

The effective variance at 10 km above the mean tropopause height for the N45 latitude band is drawn in Figure 16. One can see that it has great oscillations and large confidence intervals, so its variations will not be discussed here. We will only keep in mind that it is always lower than 0.2 (around 0.1), which could mean that the size distribution is monomodal.

The effective variance at 5 km above the mean tropopause height has not been represented because of its greater oscillations and larger confidence intervals. It is slightly higher, up to 0.4, confirming the large values observed sometimes at low altitudes in the vertical profiles.

5.3. *Latitudinal Variations of the Aerosol Effective Radius*

For time periods free of volcanic event, the latitudinal variations of the effective radius show the same kind of behavior as the extinction coefficients do, with minimum values at 25°/35° (Figure 17). We have only shown the variations at 7 and 10 km above the tropopause level because at 5 km, for high-latitude bands such as 75° and 65°, this level is at an altitude of ≃12–13 km, and the results must be considered with care because of the lack of the 0.385-μm channel data (cf. section 2). For the 12-km level the altitude at low latitudes is ≃28–29 km so that at the lowest-latitude bands, the results are less credible, because the uncertainties on the individual profiles become very large.

As was done for the extinction coefficient and for the optical depth, we have compared the effective radius at 45° and at the minimum. The ratio $r_{\mathrm{eff}}(45°)/r_{\mathrm{eff}}\mathrm{min}$ is 1.1–1.2 depending on the level; that is to say, it increases nearly 10–20% between 25°/35° and the mid-latitudes.

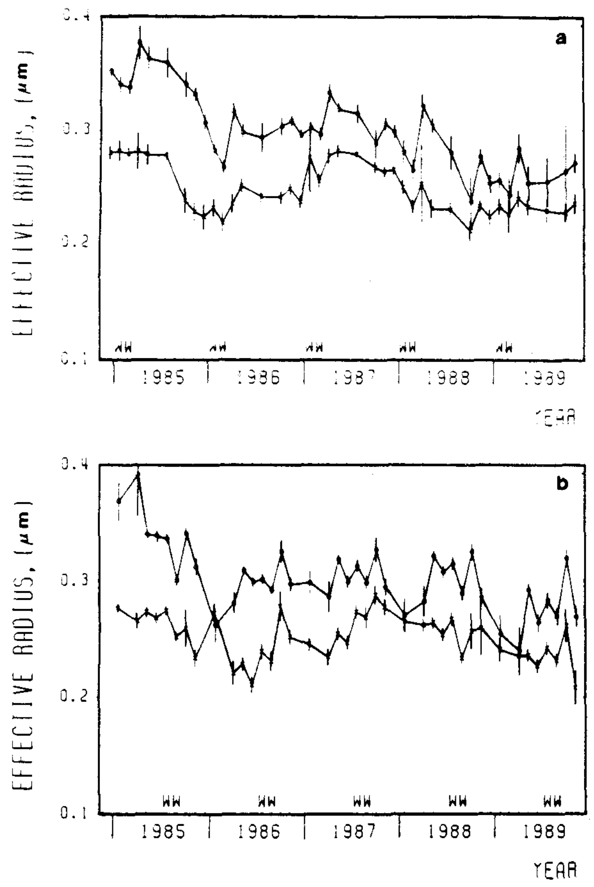

Fig. 14. Effective radius, with 95% confidence intervals, versus time for (*a*) N45 and (*b*) S45 latitude bands at two levels above a mean tropopause height of 11 km: 5 km (open circles) and 10 km (crosses).

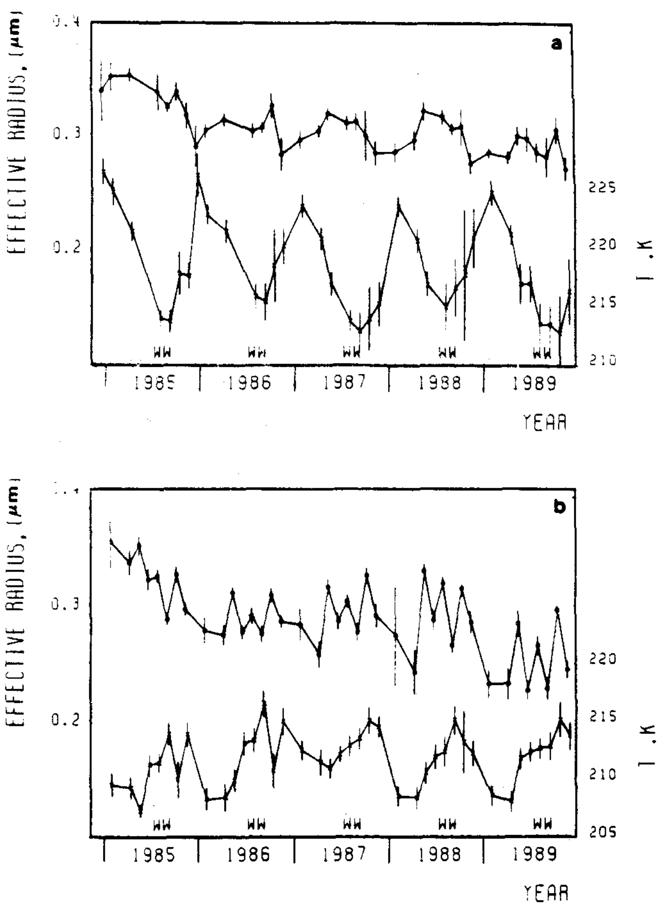

Fig. 15. Local temperature (crosses) and effective radius (open circles), both with 95% confidence intervals, versus time for (*a*) S55 and (*b*) S35 latitude bands at 5 km above the mean tropopause height.

As found previously, the temperature is unable to explain the radius time variations. The latitudinal fluctuations of the local temperature do not exhibit typical phenomena allowing us to understand the minimum values of the radius at 25°/35°.

As the vertical profiles of the radius (Figure 18) show that it is decreasing with increasing altitude, the hypothesis of downwelling air, near the latitudes 25°/35°, made in section 4.2 to explain the minimum values in the latitudinal extinction variations, is strengthened because smaller particles could be injected at low levels in a downward air motion.

The increase of the radius is going on toward the 55° latitude band and more weakly toward the higher latitudes. During the local winter-spring season of the southern hemisphere the calculated radius at 65° and 75° exhibits large confidence intervals, so that it is difficult to say if the strong decrease of the extinction coefficient seen in section 4.2 is due to a decrease of the effective radius.

In most cases we can conclude that the effective radius presents the same variations as the extinction coefficient (or the optical depth) does, with similar values at middle (around 45°/55° north and south) and at low latitudes (between 15°N and 15°S) and with minimum values at 25°/35°.

5.4. *Aerosol Concentration*

As stated in the introduction, if the aerosol extinction coefficient is greater at one time or location, then either the particles are larger with the same concentration, or they are of the same size but ina higher concentration, and of course both possibilities can occur simultaneously. We have found that the extinction coefficient and the effective radius were generally both decreasing or increasing together, and we

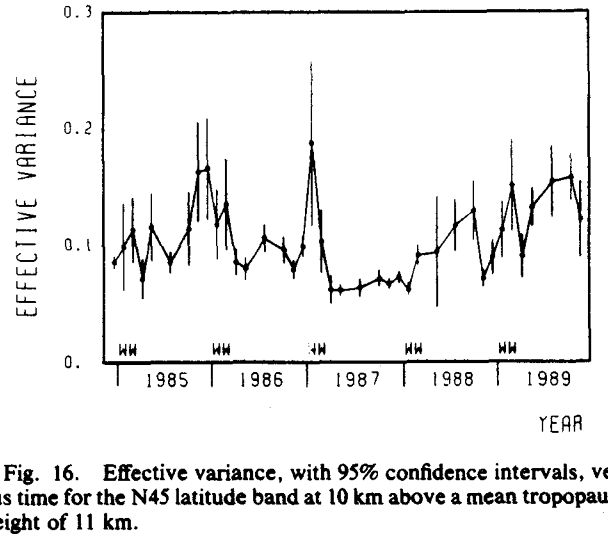

Fig. 16. Effective variance, with 95% confidence intervals, versus time for the N45 latitude band at 10 km above a mean tropopause height of 11 km.

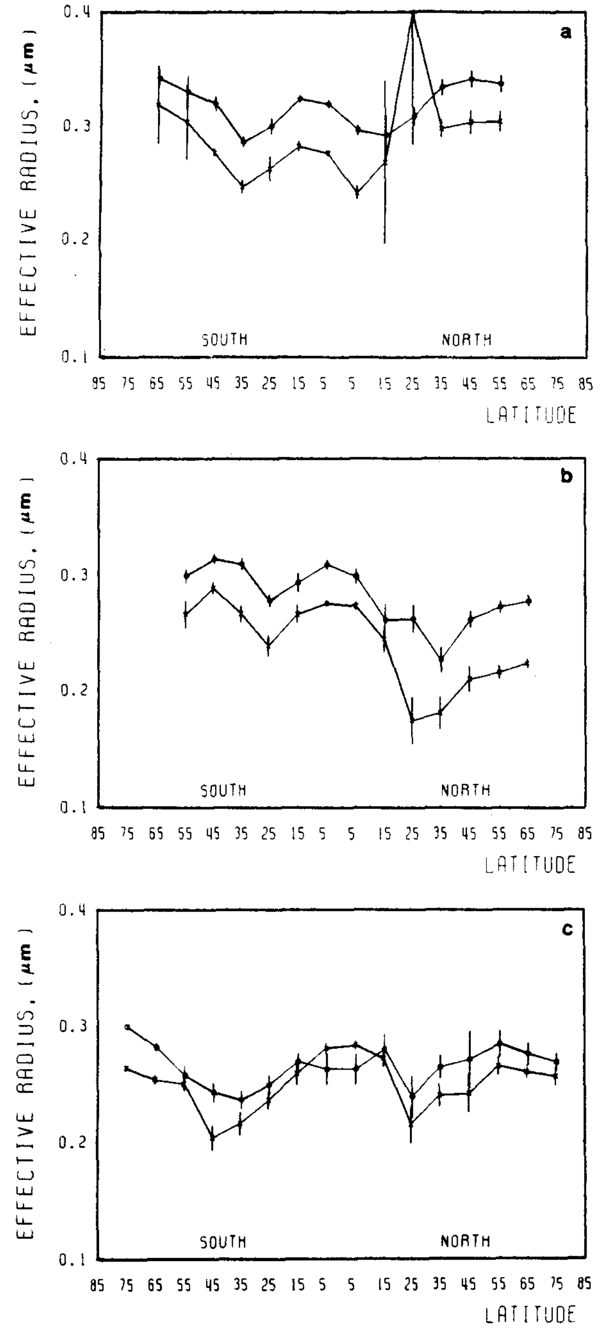

Fig. 17. Effective radius with 95% confidence intervals, at two levels above the tropopause height (7 km (open circles) and 10 km (crosses)) versus latitude for the same three periods as Figure 10*a*–10*c* and 11: (*a*) 1985 northern winter period, (*b*) 1988 northern summer period, and (*c*) 1989 northern spring period.

have investigated whether the concentration could also be partly responsible for the extinction variations.

We have therefore evaluated the aerosol concentration from the extinction coefficient at 1.02 μm using a LND aerosol model with effective radius and variance determined previously from the spectral variations of extinction. In fact, we have taken a mean value for the effective variance to avoid unrealistic fluctuations due to the great oscillations of the effective variance (after having, of course, verified that the results were not too sensitive to such changes in variance).

Figure 19 compares the time variations of the extinction coefficient, of the effective radius, and of the concentration at 5 km above the mean tropopause for the N45 and S45 latitude bands. One can see, among the oscillations, an obvious decrease of the concentration which is nearly 3 particles/cm^3 by the end of 1984 and 1 particle/cm^3 by the end of 1989. For some latitude bands, slight seasonal variations of the concentration are superimposed; for example, in the N45 band where the winter maxima of the extinction were not correlated with the radius maxima, winter maxima of the concentration appear, and in the S45 band where the winter maxima of the extinction were quite well correlated with the radius maxima, the variations of the concentration are sometimes anticorrelated with the extinction variations. (Note that we have suppressed a value of the concentration because it has a large error of 100%.)

For the decay of El Chichon perturbation we have seen that it corresponds to an important decrease of the particle size (of almost 20% at 5 km for N45). The aerosol concentration also decreases strongly (by almost 60%).

In the northern hemisphere the winter maxima of the extinction coefficient seem to correspond to larger concentrations of almost the same kind of particles as for the summer minima. In the southern hemisphere the winter maxima of the extinction correspond to larger aerosols than for the summer, and in a weaker or almost identical concentration.

Latitudinal variations of the concentration have been calculated, but no particular behavior appears; especially, there is no evidence of a weaker concentration at 25°/35°. Some changes occur depending on the season or/and on the level, changes that can be attributed to the large errors.

Estimation of the concentration errors from possible retrieval bias errors shows that they are important (of the order of 15–20%, sometimes 30%). So, especially for small variations, these results must be taken with care, and we will not discuss the weak concentration variations further.

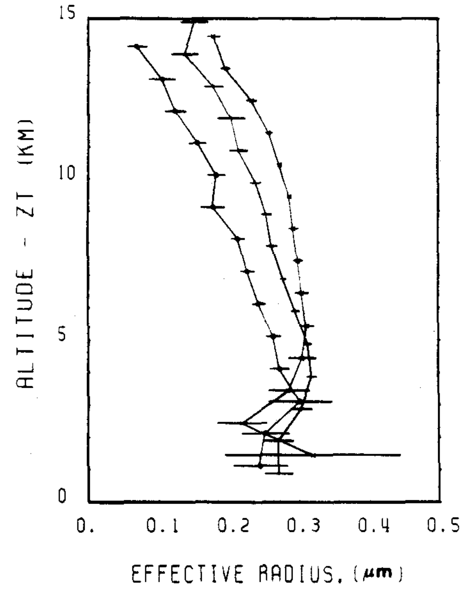

Fig. 18. Effective radius, with 95% confidence intervals, versus altitude above the tropopause height, during 1988 northern summer period for three latitude bands: N35 (open circles), N05 (crosses), and S25 (plus signs).

6. VOLCANIC EVENTS

In the previous sections we have only considered high- and middle-latitude bands for temporal study and quiet periods for latitudinal study, because of the perturbation due to the Nevado del Ruiz volcano eruption, referred as NDR hereafter, which occurred on November 13, 1985 (4.9°N, 75.4°W).

Zonally averaged vertical profiles of the extinction coefficient have been drawn in Figure 20 for the N05 latitude band just before the eruption and just after. During the month of January the zonal homogeneity has not been achieved, as can be seen from the large confidence intervals (Figure 20*b*). One month later the volcanic material is distributed at all longitudes, and the averaged profile is again very significant (Figure 20*c*). The large values of the extinction coefficient indicate that the aerosol layer is located above the tropopause, between around 19 and 27 km, with a maximum at 20–21 km.

Temporal variations of the extinction coefficient at the same latitude show a rapid and strong increase at 5 km above the tropopause ($\sigma(1.02)$ being 5–6 times larger), with diminishing effects at higher levels ($\sigma(1.02)$ being 3–4 times larger) (Figure 21*a*). The previous value of the extinction is recovered slowly after roughly 1 year at 5 km and after slightly more than 1 year at higher altitudes. Latitude bands N15, S05, and S15 were also perturbed but in a weaker extent; for

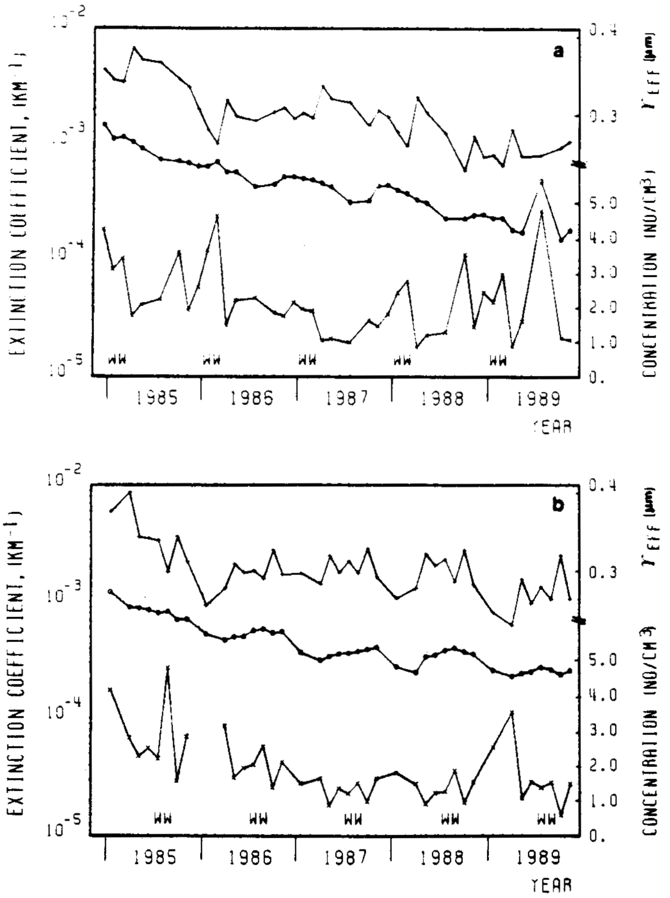

Fig. 19. Mean extinction coefficient at 1.02 µm (open circles), effective radius (plus signs), and concentration (crosses) versus time at 5 km above a mean tropopause height of 11 km for (*a*) N45 and (*b*) S45 latitude bands.

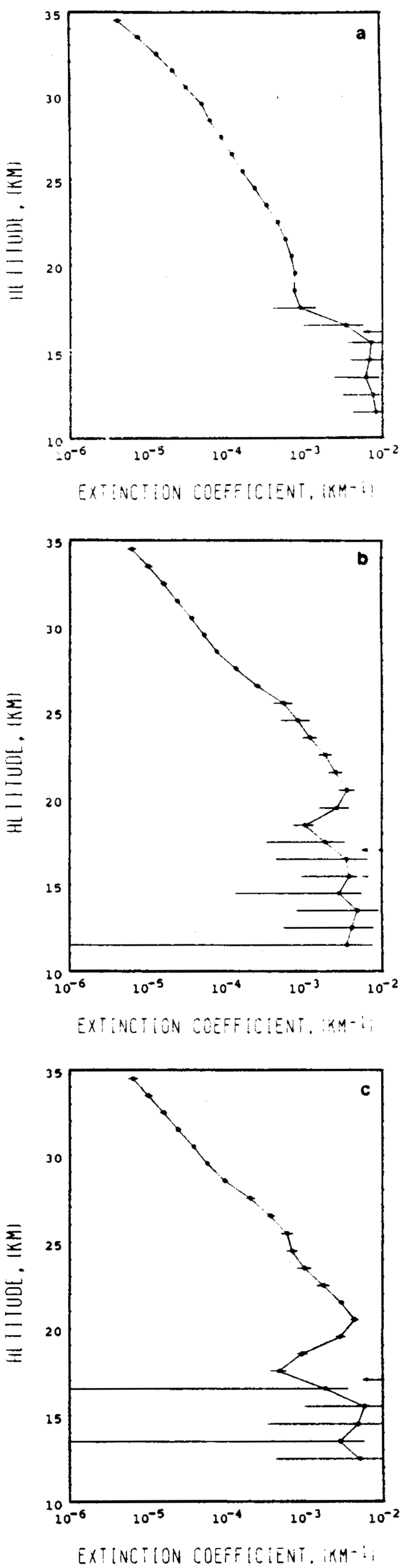

Fig. 20. Mean extinction coefficient at 1.02 µm, with 95% confidence intervals, versus the altitude above the ground for the N05 latitude band during three periods: (*a*) by the end of October 1985, (*b*) by middle of January, and (*c*) by middle of February 1986. The arrows indicate the tropopause heights.

the N25 and S25 latitudes the El Chichon decay was just compensated by the NDR increase.

One can see that optical depth calculated from mean tropopause height plus 2 km (i.e., 18 km) exhibits a great enhancement, with values 4 times larger after the event (Figure 21*b*). Profiles of effective radius versus altitude show the same quasi-linear decrease in the altitude range 20–30 km, whatever the period is, before or after the eruption (Figure 22).

Effective radius variations versus time at N05, drawn in Figure 23, show that there are some changes in the particle size due to the NDR eruption. However, the variations depend on the level: at a level close to 5 km above the mean tropopause height the radius decreases just after the eruption (by about 7%) and then increases, while it increases immediately after the eruption at a level close to 10 km (by almost 4%).

Yue et al. [1991] have found, after the NDR eruption, an increase in the "averaged" size of aerosol particles from a study of the optical depth ratio (at 0.525 and 1.02 µm); the term averaged employed by Yue et al. signifies that the size has been calculated from optical depths (integrated from the local tropopause plus 2 km). To get a good understanding of their results, we have calculated the optical depth ratio with optical depths integrated from a mean tropopause height of 16 km plus 2 km and from the local tropopause plus 2 km, as Yue et al. have done. We observe no significant difference between the two curves, but if we calculate the optical depth ratio with optical depths integrated from 18 plus 2 km instead of 16 plus 2 km, the results are completely different. In Figure 24 we note that after the NDR eruption the optical depth ratio increases (that is to say the averaged size decreases) when the optical depth is counted from 16 plus 2 km (Figure 24*a*), while the optical depth ratio decreases (the averaged size increases) when the optical depth is counted from 18 plus 2 km (Figure 24*b*), according to the observed radius variations over time.

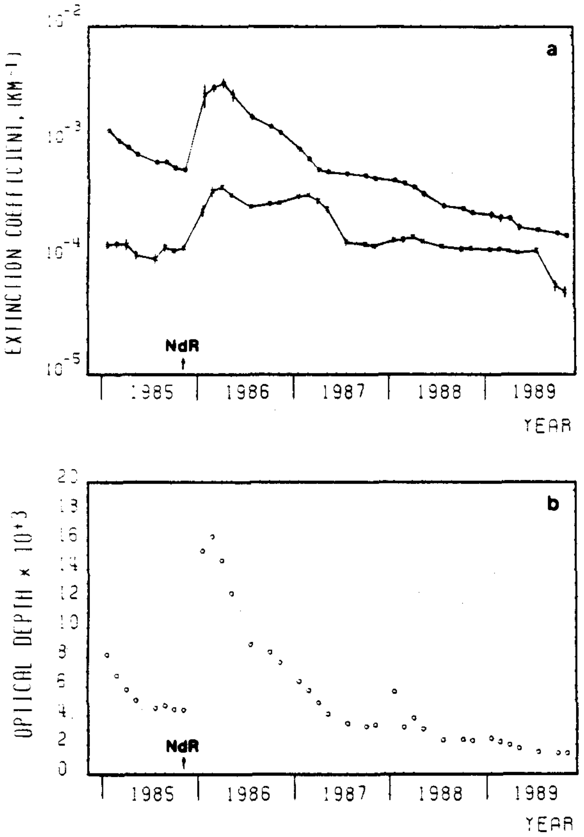

Fig. 21. (*a*) Mean extinction coefficient at 1.02 µm, with 95% confidence intervals, versus time for the N05 latitude band at two levels above the tropopause height: 5 km (open circles) and 10 km (crosses). The arrow indicates the NDR eruption. (*b*) The optical depth at 1.02 µm counted from the mean tropopause height (16 km) plus 2 km versus time for the N05 latitude band is also shown.

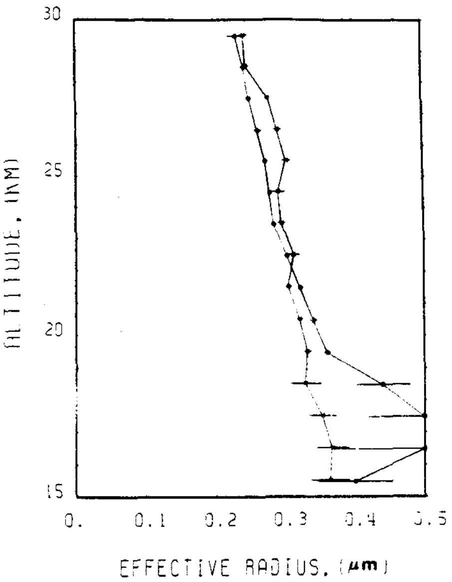

Fig. 22. Effective radius, with 95% confidence intervals, versus altitude for the N05 latitude band by the end of October 1985 (open circles) and by the middle of February 1986 (crosses).

As can be seen in Figure 25, the increase in the extinction coefficient seems mostly correlated to an increase in the concentration, which, for example, becomes 3–4 times greater at the 5-km level. The Nevado del Ruiz eruption has then injected into the stratosphere a great quantity of aerosols not very different from those left there 3 years after the El Chichon event.

An eruption of the Etna volcano occurs in September 1986

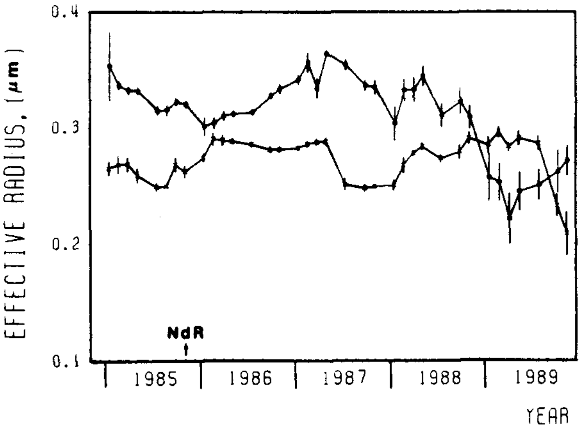

Fig. 23. Effective radius, with 95% confidence intervals, versus time for the N05 latitude band at two levels above a mean tropopause height of 16 km: 5 km (open circles) and 10 km (crosses).

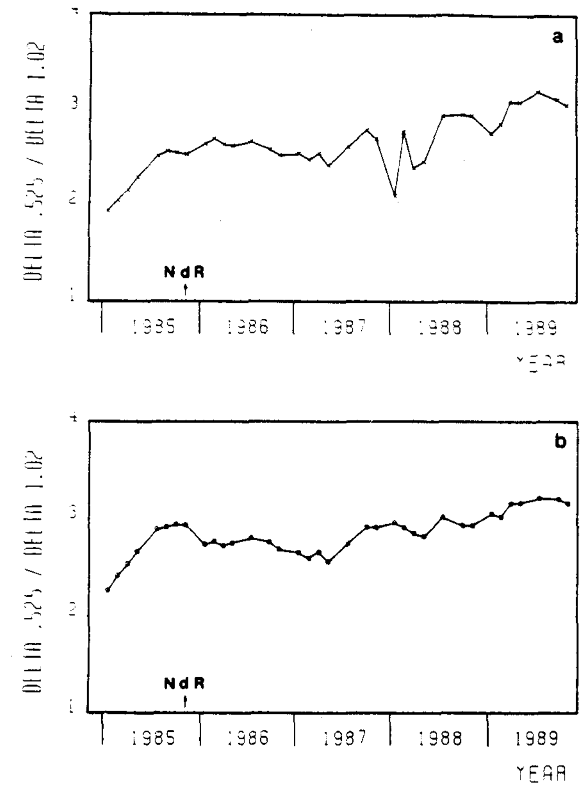

Fig. 24. Optical depth ratio (between 0.525 μm and 1.02 μm) versus time for optical depths calculated from a mean tropopause height of (*a*) 16 km plus 2 km or (*b*) 18 km plus 2 km.

(37.7°N, 15°E). The curves of extinction coefficients versus time exhibit some perturbations at high levels ($\sigma(1.02)$ being 2 times larger than before the eruption) (Figure 26*a*), but they are not as strong as the ones due to NDR (Figure 21*a*). At 5 km above the mean tropopause, no change appears. In other latitude bands the influence is weaker, as can be seen in Figure 6*a*. Confirming these observations, the optical depth also shows little enhancement, but the enhancement is again much weaker than the one due to NDR.

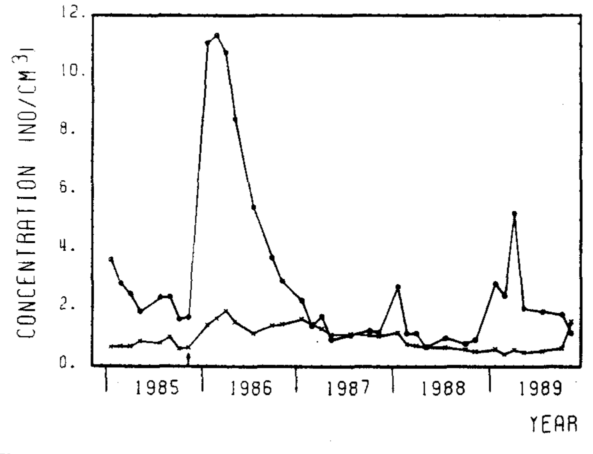

Fig. 25. Concentration versus time for the N05 latitude band at two levels above a mean tropopause height of 16 km; 5 km (open circles) and 10 km (crosses).

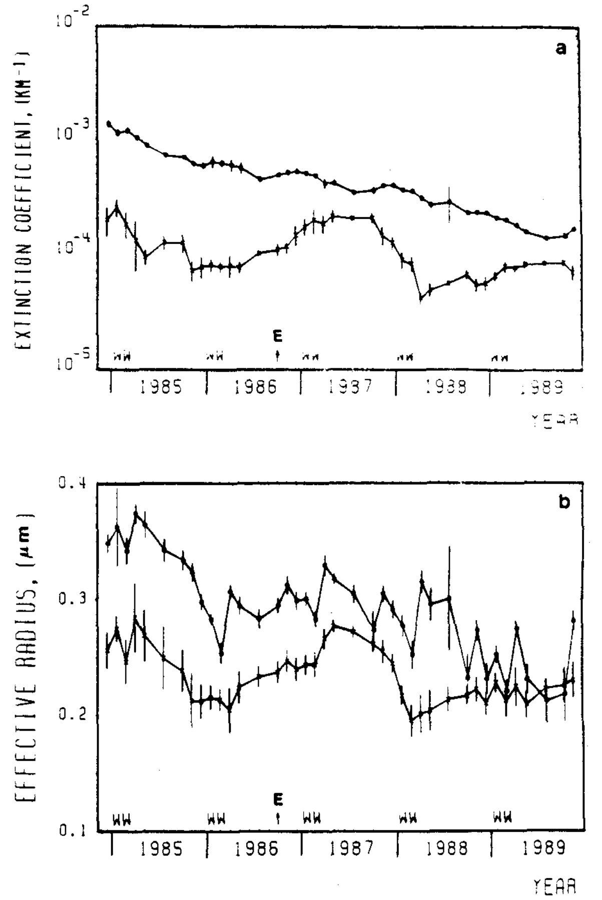

Fig. 26. (*a*) Mean extinction coefficient at 1.02 μm, with 95% confidence intervals, versus time for the N35 latitude band at two altitudes above a mean tropopause height of 13 km: 5 km (open circles) and 10 km (crosses). (*b*) The effective radius, with 95% confidence intervals, versus time for the N35 latitude band at two levels above a mean tropopause height of 13 km (5 km (open circles) and 10 km (crosses)) is also shown.

The time variations of the effective radius show that it increases after the event, especially at 10 km above the tropopause; at 5 km the effect is not as obvious because the fluctuations are important (Figure 26*b*). The vertical profile of the effective radius presents some changes with larger values at all altitudes after the eruption; for example, r_{eff} increases from 0.22 μm to 0.28 μm near 22 km altitude (Figure 27). By comparing this to the NDR radius profile (Figure 22), we can conclude that the aerosols were of similar size in both cases.

Because of the oscillations of the concentration one cannot see in its variations any important change, although it was announced that the Etna volcano eruption had sent aerosols over Europe, Japan, and the United States [*Page and Fuis*, 1986]. Therefore the only conclusion we can draw is that the Etna volcano has not sent a great number of aerosols into the stratosphere.

7. CONCLUSION

The analysis of 5 years of the SAGE II aerosol data provides a good description of the post El Chichon stratospheric aerosol layer. It has been performed by means of zonally, monthly averaged values of the aerosol extinction coefficients.

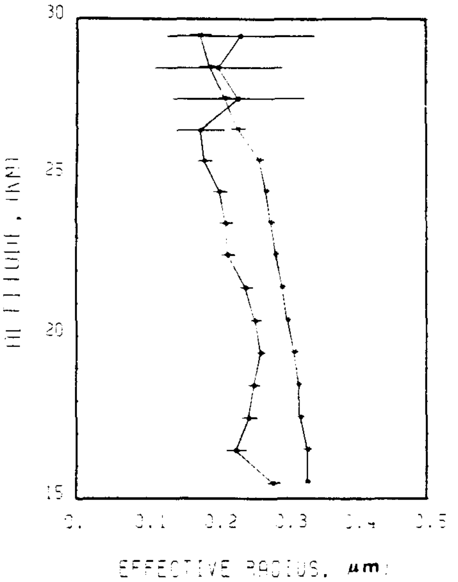

Fig. 27. Effective radius, with 95% confidence intervals, versus altitude for the N35 latitude band by the middle of February 1986 (open circles) and by the end of April 1987 (crosses).

At low latitudes the aerosols present a very homogeneous distribution all over the globe, with a dispersion around the zonal mean which is of the order of or even smaller than the experimental error, at all altitudes. At high and middle latitudes a similar behavior is observed but only within the 16- to 21-km altitude range, and with an altitude of the minimum dispersion close to that of the maximum of the extinction ratio; below and above this well-mixed layer the distribution is less homogeneous. No explanation has been found for this structure, but it should be justified by detailed stratospheric models.

The zonally, monthly averaged profiles of the 1.02-μm extinction coefficients have been analyzed for temporal and latitudinal variations. The first problem we have raised is a reference level problem; it appears that the best reference level is the ground level for temporal study in a latitude band and the tropopause level for latitudinal study of a given period. That is to say, the stratospheric aerosol layer does not follow the seasonal variations of the tropopause level, and on the contrary follows more or less the latitudinal variations of this level.

From the SAGE II four-channel extinction data we have retrieved an effective radius and compared its variations with the variations of the 1.02-μm extinction coefficient. On the time series the most obvious feature is the exponential decrease of extinction over the whole period due to the decay of El Chichon volcanic material. During the same period the effective radius decreases, for example, from 0.35 to 0.28 μm at the altitude 5 km above the mean tropopause height at N45. However, the decrease in the extinction is also due to the decrease in the particle number of the order of 60%.

The usually observed winter maxima, superposed on the general decrease, are strongly reduced when data are analyzed with respect to the mean tropopause level. However, they can still be observed, at mid-latitudes, especially in the southern hemisphere. These winter maxima exist only in a small altitude range, and this seasonal effect is less pronounced in the optical depth except in the southern latitude. The winter maxima are generally accompanied by an increase of the effective radius which cannot be explained by temperature variations.

The latitudinal variations of the extinction coefficient typically exhibit a minimum around 25°/35° in both hemispheres, which is related to smaller values of the effective radius. As the effective radius generally decreases with altitude, we may tentatively explain the decrease of the extinction and particle size in the tropical regions by an intrusion of aerosols coming from high levels toward low levels, where the tropopause is not well defined.

The major volcanic event observed during the period of this study is the Nevado del Ruiz, but the Etna eruption can also be detected in SAGE II data. From this study one can deduce that the Nevado del Ruiz has injected into the stratosphere a great number of aerosols similar to those existing before the eruption. On the contrary, following the radius decay the Etna has sent larger particles than preeruption aerosols, and these Etna aerosols were identical in size to the NDR aerosols.

Acknowledgments. The SAGE II data were kindly provided to us by the Aerosol Research Group at the NASA Langley Research Center. We are grateful to C. Deroo for her efficient help in the numerical computations and to G. K. Yue, M. P. McCormick, and E. Chiou, who provided us with their manuscript prior to publication. This study has been supported by the Centre National d'Etudes Spatiales (contract 88/CNES/1260).

REFERENCES

Ackerman, M., et al., European validation of SAGE II aerosol profiles, *J. Geophys. Res.*, *94*, 8399–8411, 1989.

Brogniez, C., and J. Lenoble, Modeling of the stratospheric background aerosols from zonally averaged SAGE profiles, *J. Geophys. Res.*, *92*, 3051–3060, 1987.

Brogniez, C., and J. Lenoble, Size distribution of stratospheric aerosols from SAGE II multiwavelength extinction, in *Aerosols and Climate*, edited by P. V. Hobbs and M. P. McCormick, pp. 305–312, A. Deepak, Hampton, Va., 1988.

Brogniez, C., and J. Lenoble, Zonal distribution of aerosols from SAGE II extinction profiles, in *IRS'88: Current Problems in Atmospheric Radiation*, edited by J. Lenoble and J. F. Geleyn, pp. 593–596, A. Deepak, Hampton, Va., 1989.

Chu, W. P., M. P. McCormick, J. Lenoble, C. Brogniez, and P. Pruvost, SAGE II inversion algorithm, *J. Geophys. Res.*, *94*, 8339–8351, 1989.

Cunnold, D. M., M. C. Pitts, and C. R. Trepte, An intercomparison of SAGE and SBUV ozone observations for March and April 1979, *J. Geophys. Res.*, *89*, 5249–5262, 1984.

Diallo, B. S., C. Brogniez, M. Herman, R. Santer, and J. Lenoble, Characterization of the stratospheric aerosols from polarization measurements: Comparison with SAGE II observations, in *IRS'88: Current Problems in Atmospheric Radiation*, edited by J. Lenoble and J. F. Geleyn, pp. 564–567, A. Deepak, Hampton, Va., 1989.

Hansen, J. E., and L. D. Travis, Light scattering in planetary atmospheres, *Space Sci. Rev. 16*, 527–610, 1974.

Herman, M., J. Y. Balois, L. Gonzales, P. Lecomte, J. Lenoble, R. Santer, and C. Verwaerde, Stratospheric aerosol observations from Balloonborne Polarimetric Experiment, *Appl. Opt.*, *25*, 3573–3584, 1986.

Hofmann, D. J., and J. M. Rosen, On the prolonged lifetime of the El Chichon sulfuric acid aerosol cloud, *J. Geophys. Res.*, *92*, 9825–9830, 1987.

Jäger, H., M. Littfass, D. J. Hofmann, and J. M. Rosen, Stratospheric extinction and mass variations after a major volcanic eruption, derived from lidar measurements at northern midlatitudes, in *Aerosols and Climate*, edited by P. V. Hobbs and M. P. McCormick, pp. 215–222, A. Deepak, Hampton, Va., 1988.

Kent, G. S., and M. P. McCormick, SAGE and SAM II measurements of global stratospheric aerosol optical depth and mass loading, *J. Geophys. Res.*, *89*, 5303–5314, 1984.

Knollenberg, R. G., and D. Huffman, Measurements of the aerosol size distributions in the El Chichon cloud, *Geophys. Res. Lett.*, *10*, 1025–1028, 1983.

Lenoble, J., and C. Brogniez, A comparative review of radiation aerosol models, *Beitr. Phys. Atmos.*, *57*(1), 1–20, 1984.

Lenoble, J., and C. Brogniez, Information on stratospheric aerosol characteristics contained in the SAGE satellite multiwavelength extinction measurements, *Appl. Opt.*, *24*, 1054–1063, 1985.

Lenoble, J., P. Pruvost, and C. Brogniez, SAGE satellite observations of stratospheric aerosol from Mount St. Helens eruption: a two-wavelength analysis, *J. Geophys. Res.*, *89*, 11,666–11,676, 1984.

Livingston, J. M., and P. B. Russell, Retrieval of aerosol size distribution moments from multiwavelength particulate extinction measurements, *J. Geophys. Res.*, *94*, 8425–8434, 1989.

Mauldin, L. E., III, N. H. Zaun, M. P. McCormick, J. H. Guy, and W. R. Vaughn, Stratospheric Aerosol and Gas Experiment II instrument: A functional description, *Opt. Eng.*, *24*, 307–312, 1985.

McCormick, M. P., and C. R. Trepte, SAM II measurements of Antartic PSC's and Aerosols, *Geophys. Res. Lett.*, *13*, 1276–1279, 1986.

Page, R. A., and G. Fuis, Profile data made available, more collected, *Eos Trans. AGU*, *67*, 1311–1312, 1986.

Pollack, J. B., O. B. Toon, C. Sagan, A. Summers, B. Baldwin, and W. Van Camp, Stratospheric aerosols and climate change, *Nature*, *263*, 551–555, 1976.

Rosen, J. M., and D. J. Hofmann, Optical modeling of stratospheric aerosol: Present status, *Appl. Opt.*, *25*, 410–419, 1986.

Rosen, J. M., D. J. Hofmann, and J. Laby, Stratospheric aerosol measurements, II, The worldwide distribution, *J. Atmos. Sci.*, *32*, 1457–1462, 1975.

Russell, P. B., and M. P. McCormick, SAGE II aerosol data validation and initial data use: An introduction and overview, *J. Geophys. Res.*, *94*, 8335–8338, 1989.

Swissler, T. J., P. Hamill, M. Osborn, P. B. Russell, and M. P. McCormick, A comparison of lidar and balloon-borne particle counter measurements of the stratospheric aerosol 1974–1980, *J. Atmos. Sci.*, *39*, 909–916, 1982.

Wang, P., and M. P. McCormick, Behavior of zonal mean aerosol extinction ratio and its relationship with zonal mean temperature during the winter 1978–1979 stratospheric warming, *J. Geophys. Res.*, *90*, 2360–2364, 1985.

Yue, G. K., and A. Deepak, Retrieval of stratospheric aerosol size distribution from atmospheric extinction of solar radiation at two wavelengths, *Appl. Opt.*, *22*, 1639–1645, 1983.

Yue, G. K., and A. Deepak, Latitudinal and altitudinal variation of size distribution of stratospheric aerosols inferred from SAGE aerosol extinction measurements at two wavelengths, *Geophys. Res. Lett.*, *11*, 999–1002, 1984.

Yue, G. K., M. P. McCormick, and W. P. Chu, Retrieval of composition and size distribution of stratospheric aerosols with the SAGE II satellite experiment, *J. Atmos. Oceanic Technol.*, *3*, 371–380, 1986.

Yue, G. K., M. P. McCormick, and E. Chiou, Stratospheric aerosols optical depth observed by the SAGE II experiment: Decay of the El Chichon and Ruiz volcanic perturbations, *J. Geophys. Res.*, *96*, 5209–5219, 1991.

C. Brogniez and J. Lenoble, Laboratoire d'Optique Atmosphérique, Université des Sciences et Techniques de Lille, Batiment 5, 59655 Villeneuve d'Ascq, Cedex, France.

(Received November 19, 1990;
revised May 6, 1991;
accepted May 7, 1991.)

Conclusion

Le problème de la restitution du spectre dimensionnel des aérosols stratosphériques reste ouvert. En effet la comparaison entre les paramètres du spectre dimensionnel obtenus avec l'inversion des mesures polarimétriques ballon, et ceux déduits des mesures SAGE II montre que les résultats sont parfois en désaccord ce qui nécessite une étude plus complète de l'inversion. En particulier il importe d'améliorer les algorithmes utilisés par les expériences RADIBAL et SAGE II de façon à pouvoir restituer des granulométries bimodales.

L'éruption catastrophique du Pinatubo (Philippines) qui a eu lieu au début de l'été 1991 a été parfaitement suivie par SAGE II et j'attends les données afin de pouvoir étudier la progression du nuage volcanique et de caractériser les nouveaux aérosols. Début Octobre 1991 un vol ballon a été effectué ainsi que des tirs lidar à l'Observatoire de Haute Provence et à Garmisch-Partenkirchen, des mesures SAGE II sont également disponibles; le dépouillement des mesures est en cours.

J'approfondis actuellement l'étude de l'inversion dans le cadre de la nouvelle expérience d'occultation SAGE III dont le lancement est prévu pour 1997, et pour laquelle nous disposerons de deux canaux aérosols supplémentaires (0,760 et 1,550 μm), ce qui va permettre de préciser les variations spectrales du coefficient d'extinction des particules.

En ce qui concerne les variations saisonnières de la taille des particules, qui ne semblent pas corrélées de manière claire aux variations de la température stratosphérique, j'envisage de tenir compte simultanément des données de température et de vapeur d'eau disponibles pour chaque évènement et dont l'inversion à partir des mesures SAGE II est actuellement opérationnelle (P. Pruvost), pour étudier l'évolution des aérosols stratosphériques .

BIBLIOTHÈQUE INTERUNIVERSITAIRE
SECTION DE SCIENCES
LILLE